Sena FERAH

DEPARTMENT OF MEDICAL BIOLOGY MASTER OF THESIS

2023

T.C.
BURSA ULUDAG UNIVERSITY
INSTITUTE OF HEALTH SCIENCES
FACULTY OF MEDICINE
DEPARTMENT OF MEDICAL BIOLOGY

INVESTIGATION OF THE EFFECTS OF SUPPLEMENTARY THERAPY CANDIDATE MOLECULES IN BREAKING CHEMOTHERAPY RESISTANCE IN GLIOBLASTOMA CELLS AND RETROSPECTIVELY SUPPORTING THE FINDINGS WITH PRIMARY TUMORS

SENA FERAH

MASTER OF THESIS

BURSA-2023

T.C.
BURSA ULUDAG UNIVERSITY
INSTITUTE OF HEALTH SCIENCES
FACULTY OF MEDICINE
DEPARTMENT OF
MEDICAL BIOLOGY

INVESTIGATION OF THE EFFECTS OF SUPPLEMENTARY THERAPY CANDIDATE MOLECULES IN BREAKING CHEMOTHERAPY RESISTANCE IN GLIOBLASTOMA CELLS AND RETROSPECTIVELY SUPPORTING THE FINDINGS WITH PRIMARY TUMORS

Sena FERAH

MASTER OF THESIS

THESIS SUPERVISOR:
Prof. Dr. Berrin TUNCA

THIZ-2021-747 & TYL-2023-1365
Bursa Uludag University Scientific Research Projects Coordination Unit

BURSA-2023

T.C.
BURSA ULUDAĞ ÜNİVERSİTESİ
SAĞLIK BİLİMLERİ ENSTİTÜSÜ

ETİK BEYANI

Yüksek Lisans tezi olarak sunduğum "Investigation Of The Effects Of Supplementary Therapy Candidate Molecules In Breaking Chemotherapy Resistance In Glioblastoma Cells And Retrospectively Supporting The Findings With Primary Tumors" adlı çalışmanın, proje safhasından sonuçlanmasına kadar geçen bütün süreçlerde bilimsel etik kurallarına uygun bir şekilde hazırlandığını ve yararlandığım eserlerin kaynaklar bölümünde gösterilenlerden oluştuğunu belirtir ve beyan ederim.

Adı Soyadı
Sena FERAH

Tarih ve İmza

TEZ KONTROL ve BEYAN FORMU

20/07/2023

Adı Soyadı: Sena Ferah

Anabilim Dalı: Tıbbi Biyoloji

Tez Konusu: Investigation Of The Effects Of Supplementary Therapy Candidate Molecules In Breaking Chemotherapy Resistance In Glioblastoma Cells And Retrospectively Supporting The Findings With Primary Tumors

ÖZELLİKLER	**UYGUNDUR**	**UYGUN DEĞİLDİR**	**AÇIKLAMA**
Tezin Boyutları	■	❑	
Dış Kapak Sayfası	■	❑	
İç Kapak Sayfası	■	❑	
Kabul Onay Sayfası	■	❑	
Sayfa Düzeni	■	❑	
İçindekiler Sayfası	■	❑	
Yazı Karakteri	■	❑	
Satır Aralıkları	■	❑	
Başlıklar	■	❑	
Sayfa Numaraları	■	❑	
Eklerin Yerleştirilmesi	■	❑	
Tabloların Yerleştirilmesi	■	❑	
Kaynaklar	■	❑	

DANIŞMAN ONAYI

Unvanı Adı Soyadı: Prof. Dr. Berrin Tunca

İmza:

TABLE OF CONTENTS

TURKISH ABSTRACT

Glioblastoma Hücrelerinde Kemoterapi Direncinin Kırılmasında Tamamlayıcı Tedavi Adayı Moleküllerin Etkilerinin Araştırılarak Bulguların Retrospektif Olarak Primer Tümörler İle Desteklenmesi

Mevcut projede, tamamlayıcı tedavi potansiyeli olabileceği öngörülen doğal bileşiklerden fisetin ve berberinin temozolomide (TMZ) ile kombin olarak dirençsiz, doğal ve kazanılmış dirençli glioblastoma (GBM) hücrelerinin tedavisinde ilaç direncini kırma ve TMZ başarısını arttırma potansiyeli üzerine etkilerinin hem normoksik hem de kanser mikroçevresine daha uyumlu olan hipoksik ortam şartlarında incelenmesi ve yapılan çalışmadaki bulguların primer beyin tümörü hücrelerinde de valide edilebilmesi amaçlanmıştır. Amaç doğrultusunda ilk olarak terapötik etkinliği değerlendirilen flavonodilerden fisetin ve berberinin tek başlarına ve TMZ ile kombinasyon halinde hücre proliferasyonu üzerine etkinliği xCELLigence yöntemi ile, hücre döngüsü ve apoptoz üzerine etkinliği flow sitometrik yöntem ile, hücre agresifliği üzerine etkinliği normoksik koşullarda yara iyileşmesi, koloni testi ve 3B kültür modeli ile ve hipoksik koşullarda yara iyileşme testi ile belirlenmiştir. Daha sonra bu çalışmada, GBM tedavisi için daha düşük dozda daha etkili olduğu belirlenen fisetinin TMZ ile kombine tedavisindeki etkinliğinin TMZ'ye dirençli ve duyarlı hücre hatları arasındaki MSH2 ve ZEB1 gen ekspresyon düzeyleri araştırılmış ve farklı karaktere sahip primer beyin tümörlerinde valide edilmiştir. Mevcut çalışmanın bulguları özellikle fisetinin fonksiyonel analizlerle hem normoksik hem de hipoksik ortamda anti-tümör etkinliği olduğunu göstermiş ve özellikle TMZ ile kombinasyonunda dirençli hücrelerde de TMZ'nin etkinliğini arttırdığını göstermiştir. Ayrıca, TMZ+Fisetin tedavisinin MSH2 seviyelerini arttırmada ve ZEB1 seviyelerini düşürmede hem hücre hattı hem de GBM primer hastalarında etkili olduğu belirlenmiştir. TMZ+Fisetin kombin tedavisinin etkinliğini destekleyen mevcut bulgular, GBM'de yeni tedavi stratejilerinin geliştirilmesinde farklı mekanizmalarda bile direnci kırmada etkili olabilen fisetinin anti-kanser ajanı olarak kullanılabilme potansiyeline sahip olabileceğini göstermektedir.

Anahtar kelimeler: Glioblastoma, temozolomide, fisetin, berberin, ilaç direnci

ENGLISH ABSTRACT

In the current study, it was aimed to examine the effects of fisetin and berberine, which are predicted to have prospects of complementary therapy, on the potential to elucidate drug resistance and increase the success of temozolomide (TMZ) in the treatment of non-resistant, natural, and acquired resistant glioblastoma (GBM) cells in combination with TMZ in both normoxic and hypoxic environment conditions that are more compatible with the cancer microenvironment, and to validate the findings in the study in primary brain tumor cells. For this purpose, initially, the therapeutic efficacy of fisetin and berberine, alone or in combination with TMZ, on cell proliferation was determined by the xCELLigence method, their effectiveness on cell cycle and apoptosis by flow cytometric method, their effectiveness on cell aggressiveness was determined by wound healing under normoxic conditions, colony test and 3D culture model, and wound healing test in hypoxic conditions. Furthermore, the efficacy of fisetin, which was determined to be more effective at a lower dose for GBM treatment, in combination with TMZ, the MSH2 and ZEB1 gene expression levels between TMZ-resistant and sensitive cell lines were investigated and validated in primary brain tumors with different characteristics. Hence, the findings of the current study showed that fisetin had anti-tumor activity in both normoxic and hypoxic environments by functional analysis and showed that it increased the activity of TMZ in resistant cells, especially in combination with TMZ. Consonantly, TMZ+Fisetin treatment was found to be effective in increasing MSH2 levels and decreasing ZEB1 levels in both cell lines and GBM primary patients. Consequently, current findings supporting the efficacy of TMZ+Fisetin combination therapy indicate that fisetin, which can be effective in breaking resistance even in different mechanisms, may have the potential to be used as an anti-cancer agent in the development of new treatment strategies in GBM.

Keywords: Glioblastoma, temozolomide, fisetin, berberine, drug resistance

1. INTRODUCTION

Glioblastoma (GBM) is the most common and aggressive malignant brain tumor (Wen, & Kesari, 2008). The World Health Organization (WHO) defines GBM as a group of stage IV tumors characterized as malignant, mitotically active, and prone to necrosis. GBM has a 5-year survival rate of 4-5% and has a rather grim prognosis (McLendon, & Halperin, 2003). Standard treatment of GBM consists of surgical resection, radiotherapy, and chemotherapy. Despite this treatment protocol, patients have a median survival of only 12.6 months (Van Gool et al., 2022). Maximum surgical resection is an effective treatment method that prolongs the survival of this disease. However, due to the invasive nature of GBM and the location of the tumor in the brain, maximum resection cannot be performed in many cases, which is primarily associated with recurrence (Stupp et al., 2009). There are also factors such as the limited ability of drugs to cross the blood-brain barrier (BBB), the inability of drugs to reach sufficient concentration on the tumor site due to early spread to the cerebrospinal fluid, the short half-life of drugs, the inability to remove all of the tumor cells, the presence of GBM stem cells (GSCs), and therapy resistance in GBM treatment failure and relapse. The effect of MGMT, one of the repair mechanisms, on drug resistance is known (Butler et al., 2020). In addition to MGMT, plausible mechanisms, including decreased activity of mismatch repair (MMR) genes (such as mutS homologue 2 (MSH2) (Caccese et al., 2020)), GBM stem cells, hypoxia, and dysregulation of other effectors, are also involved in drug resistance (Garnier et al., 2018). Moreover, the involvement of ZEB1 in the PI3K/Akt pathways, vital in the epithelial-mesenchymal process, helps to drive tumorigenesis and metastasis (Wu et al., 2012). Temozolomide (TMZ), an alkylating agent, is a chemotherapy drug commonly used to treat GBM, which can exceed the BBB and is effective in oral use (Schreck, & Grossman, 2018). In addition to the limited use of the chemotherapy drug, the severe side effects of the drug and the resistance of the patients to the drug over time are the most critical factors that complicate the treatment. In this context, effective treatment options, development of new techniques, and improvement of existing technologies are required for GBMs.

Recently, natural compounds have been frequently used to determine new

treatment methods in many cancer types, and efforts have been made to make existing treatments more effective and reduce the resulting cytotoxic effects (Kammerud et al., 2021). In addition, the combined use of natural compounds with pharmaceutical and therapeutic properties and chemotherapeutic agents increases the effectiveness and reduces the dose and side effects of the chemotherapeutic agent (Cragg, & Newman, 2005; Li et al., 2010). Flavonoids are natural compounds from the class of polyphenolic secondary metabolites found mainly in fruits and vegetables. With the use of flavonoids, which have been determined to have neuroprotective and anti-tumor effects in studies, with the drug, the most important goals are to reduce the effective dose of the drug, reduce the side effects, and increase the effectiveness of the drug, and also to delay the resistance gained against the drug. Therefore, there is a fundamental need to develop new therapeutic strategies for GBM treatment. In this context, fisetin, evaluated in this study, is a flavonoid that exhibits various bioactivities, including anti-oxidant, anti-inflammatory and anti-cancer, and is found in strawberries, apples, onions, wine, and tea (Imran et al., 2020). Berberine (5,6-dihydro-9,10-dimethoxybenzo[g]-1,3-benzodiocolo[5,6-a]quinolizinium) is a natural compound traditionally used in Chinese medicine and also has anti-inflammatory and anti-cancer properties (Neag et al., 2018). It is known that both natural compounds are used as supplements (Neag et al., 2018). Based on these results, it is argued that flavonoids can serve as the basis for future *in-vitro* and *in-vivo* studies, with their apoptotic effect on GBM cells (Pak, & Vatan, 2019). In addition, parameters such as MSH2, ZEB1, p53, PI3K, and Bax/Bcl2, which are of great importance in TMZ resistance in GBM cells, are also targeted by fisetin and berberine (Singh, Miner, Hennis, & Mittal, 2021; Zhang, & Jia, 2016). Due to the presence of common pathways involved in TMZ resistance and targeted by selected flavonoids (Kammerud et al., 2021), flavonoids are predicted to be a guide for obtaining positive results in TMZ activity and resistance. Since commercial cell lines do not fully reflect the diversity in human materials and are insufficient in developing personalized treatment methods (Grube, Freitag, Kalff, Ewald, & Walter, 2021), in the current study, it was aimed to determine the characteristics of the resistance-related mechanisms in acquired resistant and primary brain tumor cells and to examine the effectiveness of the selected flavonoid on TMZ treatment in order to validate the study in cell lines.

Flavonoids, a natural compound, exhibit various bioactivities, primarily anti-cancer, in GBM cells in studies. However, like many flavonoids, fisetin and berberine, combined with the chemotherapy drug TMZ, have a synergistic, additive or antagonistic effect on the biological processes in GBM cells and the aggressiveness of the tumor is unknown. There needs to be more literature on the combined activity of TMZ and flavonoids in GBM cells, innate and acquired resistant cell lines, and primary brain tumor cells and their respective mechanisms of action. In the current project, it is aimed to examine the effects of flavonoids on cell viability, migration and colony formation ability associated with tumor aggressiveness by examining the interactions of flavonoids in combination with TMZ. Additionally, it is aimed to determine the effectiveness of the migration ability of fisetin and berberine in TMZ-sensitive, natural, and acquired resistant cells under normoxia and hypoxia and to reveal their usability for *in-vivo* studies and their potential to be evaluated in advanced projects.

Aim 1: The synergistic, additive, or antagonistic effects of the combination of fisetin and berberine with the chemotherapy agent TMZ, determining the effective doses of flavonoids in combination with TMZ and their effects on cell proliferation, and its possible effects on suppression of cell death mechanisms and aggressiveness in the *in-vitro* tumor environment, and the relationship between functional invasion and colony formation ability are aimed.

Aim 2: It is aimed to examine the genetic levels of MSH2, which is one of the DNA repair mechanisms, and ZEB1, which is involved in EMT, the mechanisms related to the effect of the combination of fisetin and berberine with the chemotherapy agent TMZ on drug resistance.

Aim 3: It is aimed to determine the characteristics of primary brain tumor cells in terms of resistance-related mechanisms and to examine the effectiveness of an effective selected flavonoid on TMZ treatment.

As a result of the successful completion of the planned project, the effects of fisetin and berberine, which are widely used natural compounds, on biological processes associated with GBM tumors and their anti-cancer activity will be better understood. With the findings to be obtained, it will be possible to contribute developing more effective and economical treatment protocols with less side-effects in the treatment of GBM, and comprehensive projects will be structured.

2. BACKGROUND

2.1. Brain tumors

Brain tumors are defined as the uncontrolled proliferation of cells as a result of the regeneration of brain cells, their transformation into a different structure, and the formation of a mass of abnormal cells that fail to die off, and their growth over time and putting pressure on the inside of the head as the mass grows. Cancer is a complex disease to treat, and brain tumors are particularly challenging and can cause symptoms such as neurological dysfunction, seizures, and headaches (Chandana, Movva, Arora, & Singh, 2008). More than 100 histologically different subtypes of brain and other central nervous systems (CNS) tumors comprise a varied group with varying descriptive epidemiology, clinical traits, therapies, and prognosis (Figure 1). Primary and secondary brain tumors are the two main subtypes of brain tumors. The main leading of primary cancers are radiation, infections, and genetics (Wrensch, Minn, Chew, Bondy, & Berger, 2002). Secondary tumors originate from metastatic cancer, which can be from a different type of cancer than the brain like breast cancer that has metastasized to the brain (Ohgaki, & Kleihues, 2012). Rather than the type of origin precursor, primary and secondary glioblastomas (GBMs) may be difficult to distinguish histologically from each other; however, they still have different genetic and epigenetic features Figure 1 (see 2.1.3.1).

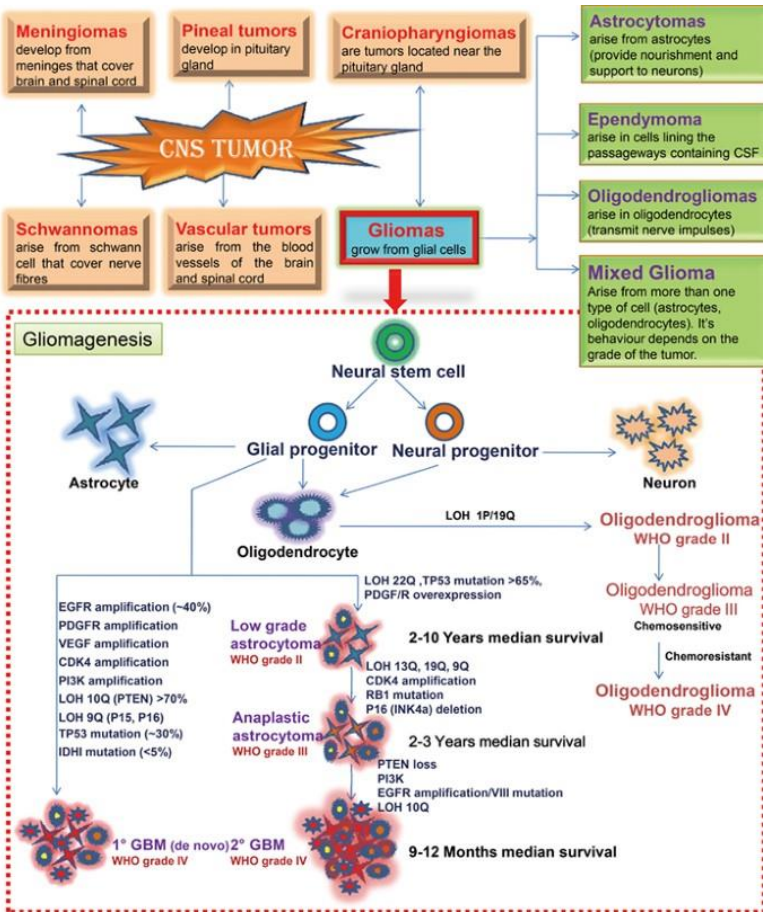

Figure 1. Presence of molecular and genetic alterations in the classification of CNS tumors, particularly gliomas (Rajesh et al., 2017).

Currently, diagnosis of brain tumors is typically made through neuroimaging techniques and examination of conditions. Magnetic Resonance Images (MRIs) are one of the best imaging methods for detecting these tumors, as it allows medical staff to see the tissue and identify if cells are developing abnormally (Figure 2). Once the tumor has been identified, physicians must assess which type of cancer it is and decide on a course of treatment (Chandana et al., 2008).

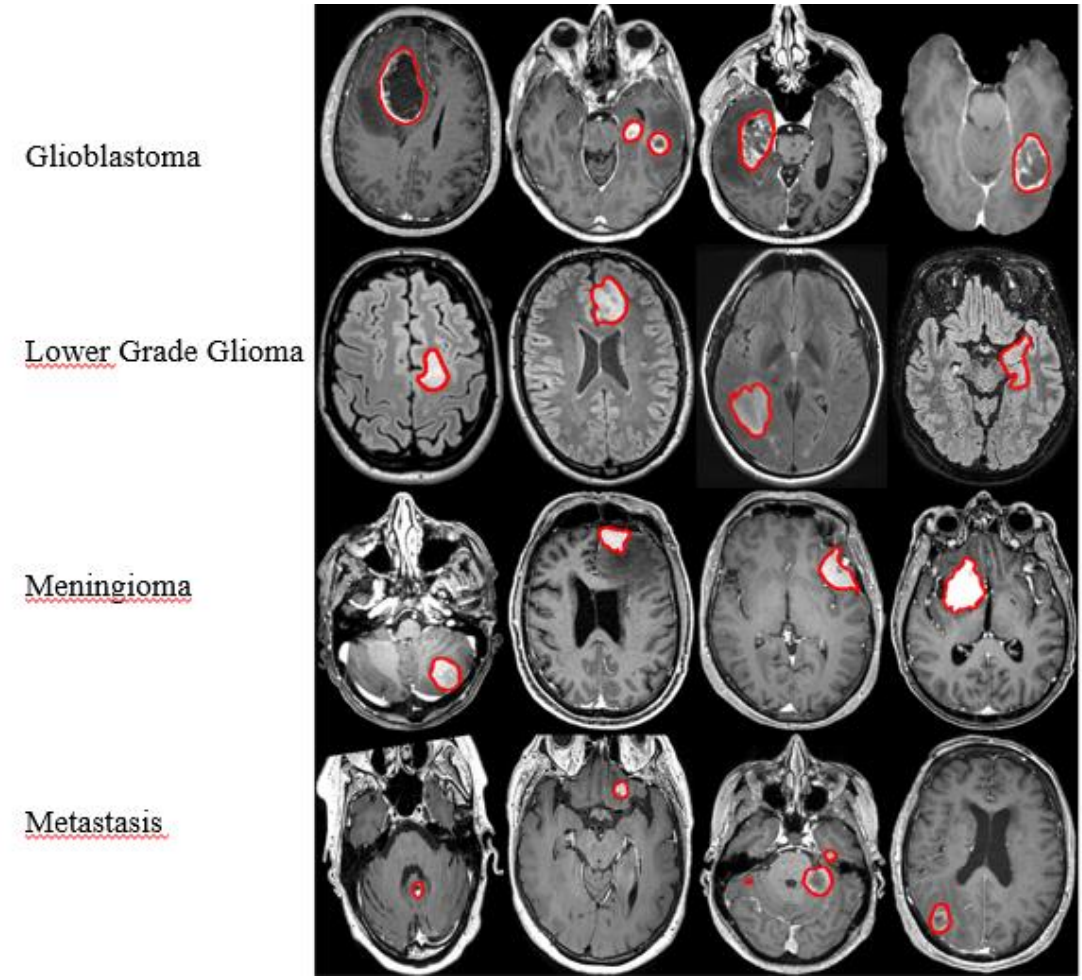

Figure 2. Magnetic resonance imaging (MRI) representation of different brain tumors before surgical operation (Bouget et al., 2022).

2.1.1. Brain Tumor Epidemiology

Brain tumors are one of the leading causes of mortality worldwide, and it has been estimated that the incidence of brain tumors has been rising over the past several years. In addition, adults have the highest overall incidence (5.57/100000) (95% CI = 5.55–5.60) of malignant brain tumors compared to other ages (Leece et al., 2017). The World Health Organization (WHO) projects that there were 308,102 new cases of brain tumors in 2020, which made up around 1,6% of all cancers and the cancer-related fatalities stated as 2,5% globally (Figure 3. a) (Sung et al., 2021). Also, the numbers were concerningly high in Turkiye, standing at 2,6% of new cases (6,102), and the death rate rose further to 4.0%, covering 5.070 of the patients in 2020. In conclusion, in Turkiye, The survival rates were ranked 12th while the death rates were in 8th rank

as an upward trend of all cancers in 2020 (Figure 3. b) (Globocan, 2021). Since the survival rates for brain tumors, especially in Turkiye, have not risen, with a recent study published in 2022 also proves it, with the survival rates in Turkiye being less than 40% (Girardi et al., 2023), there is an emergency need for improvements in the detection, diagnosis, and treatment modalities of brain tumors in worldwide and in developing countries such as Turkiye, where the brain tumor death rate is still exceptionally high.

a)

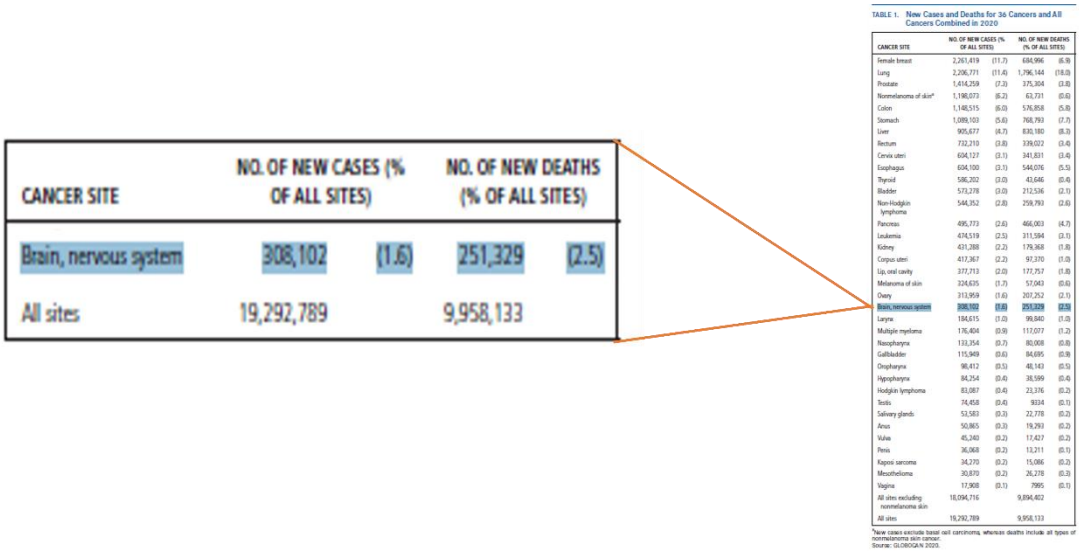

CANCER SITE	NO. OF NEW CASES (% OF ALL SITES)		NO. OF NEW DEATHS (% OF ALL SITES)	
Brain, nervous system	308,102	(1.6)	251,329	(2.5)
All sites	19,292,789		9,958,133	

b)

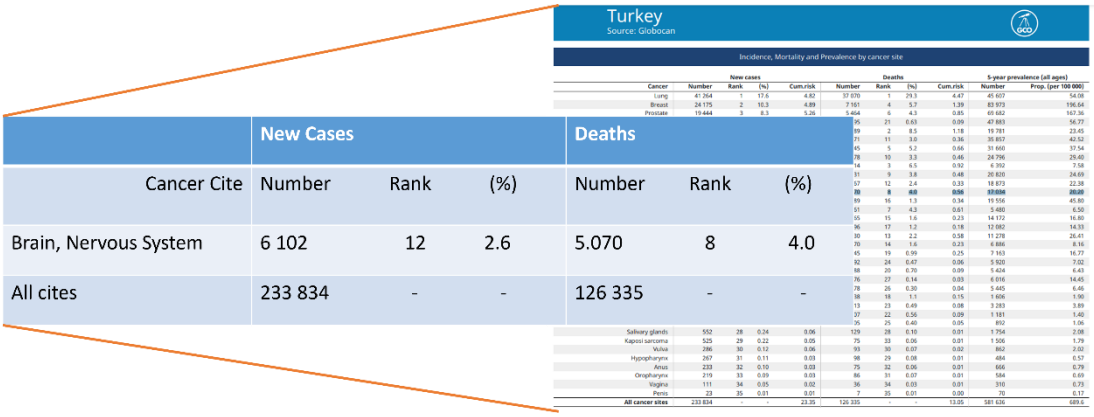

Turkey
Source: Globocan

Incidence, Mortality and Prevalence by cancer site

	New Cases			Deaths		
Cancer Cite	Number	Rank	(%)	Number	Rank	(%)
Brain, Nervous System	6 102	12	2.6	5.070	8	4.0
All cites	233 834	-	-	126 335	-	-

Figure 3. The epidemiology of brain and nervous system cancers in 2020 a) in the world b) in Turkiye (Globocan, 2021).

2.1.2. Gliomas and Classification of Gliomas

Gliomas, a kind of heterogenous brain tumors that develop in glial cells, are the most frequent brain tumors in adults (Mesfin, & Al-Dhahir, 2023). The classification of gliomas is based on the information obtained from histological evaluation and molecular and genetic abnormalities but the proper categorization of glioma presents major difficulties. The classification of gliomas is challenging when it comes to distinguishing between different subtypes, such as astrocytomas, oligodendrogliomas, and GBMs (McDonald, Aw, & Kleihues, 2013). The subtypes of gliomas are typically named based on where they arise from, but there are a variety of factors affecting the complexity of glioma classification. The subjective and variable nature of histological and molecular markers present main significant difficulties. The grades (I to IV) and the degree of tumor involvement are shown by histopathology. The main reason for challenging features in histology is because of the fact that it relies on the microscopic interpretation of independent neuropathologists who differ from one another. In addition, the identification of genetic changes that might be clinically significant is provided by molecular profiling, and some of these molecular markers related to glioma classification are changing in a time-dependent manner with discoveries. Thus, understanding the genesis of glioma and its current molecular profile is crucial for gliomas to be classified, graded, and treated (Mesfin, & Al-Dhahir, 2023). The international standard for classifying brains is known as the WHO Classification of Tumors of the CNS, which is the up-to-date version of classifications from 1979, 1993, 2000, 2007, and 2016.

According to histological characteristics and clinical behavior, the WHO grading approach gives a tumor grade from I-IV. Grade I tumors are the least malignant, with a more indolent course, and are mainly found in children and young adults. Grade II tumors grow more slowly but might recur if not entirely removed. In grade III tumors, there is vigorous growth and quick tissue-surrounding spread, while grade IV gliomas, including GBM, are the most malignant (Kleihues et al., 2002). Once the histological classification is done, several more features must be considered such as IDH status, molecular alterations, DNA methylation phenotype (Figure 4).

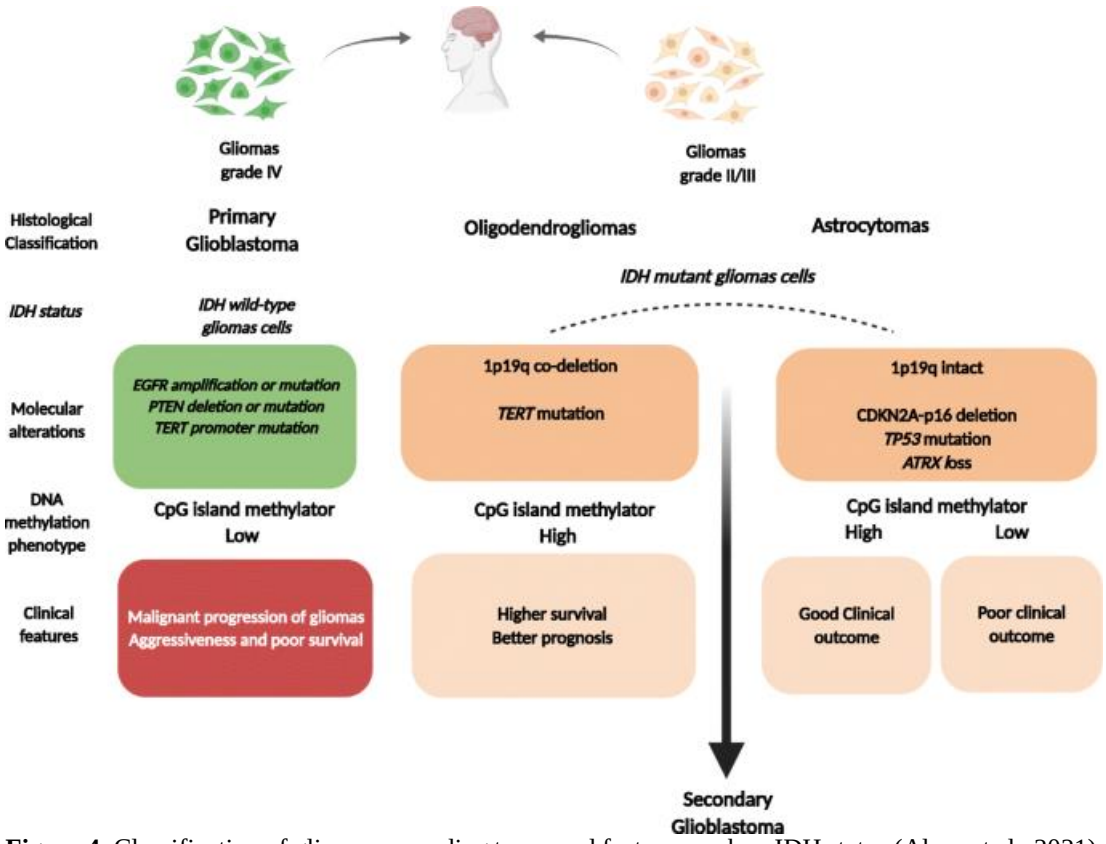

Figure 4. Classification of gliomas according to several features such as IDH status (Alves et al., 2021).

Gliomas can be categorized taking into account genetic and epigenetic markers using the WHO's seven-layer integrated grading system such as isocitrate dehydrogenase (IDH) mutations, α-thalassemia/mental-retardation-syndrome-X-linked gene (ATRX) expression, 1p/19q codeletion, cyclin-dependent kinase inhibitor 2A/B (CDKN2A/B) homozygous deletion, telomerase reverse transcriptase (TERT) promoter mutation/ epidermal growth factor receptor (EGFR) gene amplification and/or chromosomes 7 gain and 10 loss (+7/-10), Histone H3 G34R/V mutations, Histone H3 K27M/ mutations (Louis et al., 2021).

Primary and secondary gliomas are divided into two considering several molecular pathogenesis (Wen, & Kesari, 2008). IDH mutations are examined for the distinction between primary and secondary and are essential markers for prognosis estimation. IDH wild-type status is correlated with primary GBM, while IDH mutations are found in secondary GBM, oligodendroglioma, and astrocytoma. Also, 1p/19q codeletions characterize different grades of gliomas. Oligodendrogliomas have 1p/19q codeletion, and secondary GBM has an allelic loss of chromosomes 19q (Kleihues et al., 2002) in contrast to astrocytomas with intact 1p/19q. IDH-wild type

(WT), non-codeleted (1p/19q) tumors are more prone to bad prognosis than IDH-mutant, codeleted counterparts. In addition, oligodendrogliomas include TERT mutations, and their CpG island methylator is high and correlated with higher survival. Astrocytomas have CDKN2A-p16 deletion, ATRX loss, and tumor protein 53 (TP53) mutation (Figure 4). However, their clinical outcome depends on the DNA methylation status, which is good when the CpG island methylator is high and poor when the CpG island methylator is low. On the other hand, grade IV primary GBMs consist of EGFR amplification or mutation, phosphatase, and tensin homolog (PTEN) deletion or mutation, or TERT promoter mutation, which results in malignant progression of gliomas and relatively low survival rates (Alves et al., 2021). These findings pave a path for guiding personalized treatments and patient outcomes.

Given the complexity of the disease and the wide range of tumor phenotypes observed in gliomas, molecular parameters have now been added as biomarkers of grading and as a means of determining the prognosis of various tumor forms. This implies that a single glioma tumor may simultaneously belong to several classifications, necessitating a combination of therapies for effective treatment. In summary, the latest version of the aforementioned markers from the WHO classification of CNS is crucial for comprehending accurate tumor cellular structure, deciding tumor grading, typing, and treatment cascades. Further investigation into the genetic, epigenetic, and other markers involved in carcinogenesis is required in light of the growing complexity of glioma categorization.

2.1.3. Glioblastoma (GBM)

Glioblastoma (GBM) (grade IV) is the most common, aggressive, and deadliest variant in the broad spectrum of intrinsic glial brain tumors, which is approximately 70% of malignant gliomas (Wen, & Kesari, 2008). In addition, a particularly devastating type of brain cancer, GBM, has a dismal prognosis and can spread rapidly without severe symptoms (McLendon, & Halperin, 2003). Although the pathogenesis of GBM is still not fully known, it has been shown in recent studies that GBM cells form the connection between microtubules and also invade the entire brain environment, including normal neuron development (Venkataramani et al., 2022). The tumor heterogeneity of GBM, which consists of differentiated tumor cell populations,

mesenchymal cells, glioma stem cells (GSC), and tumor microenvironment (fibroblasts, microglia, astrocyte), is one of the principal causes of the aggressiveness and even, resistance and recurrence of the disease (Figure 5).

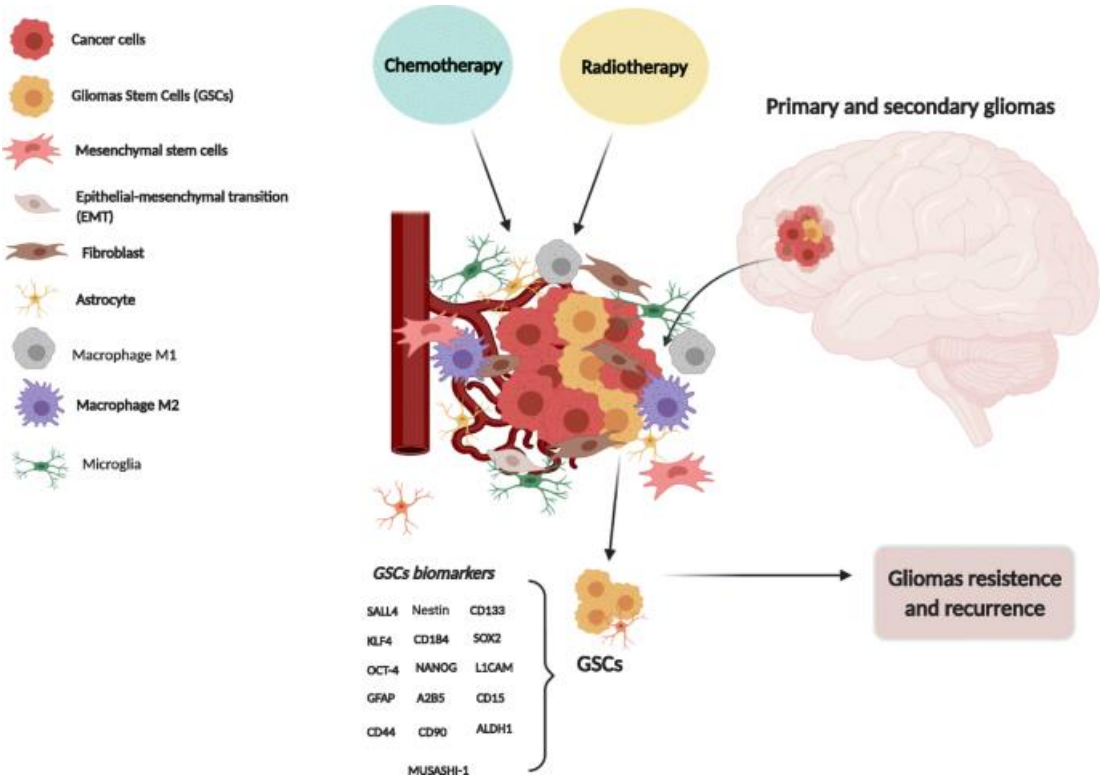

Figure 5. Representation of glioma tumor heteregonity including GSC, mesenchymal stem cells, stromal cells (fibroblasts, microglia, astrocyte) and several markers of GSCs related to glioma resistance and recurrence (Alves et al., 2021).

2.1.3.1. Genetic and Epigenetic Features in GBM

Genetic and epigenetic factors are crucial for the accurate diagnosis and subgrouping of brain tumors, and many molecular analyses can be performed on tumor cells, such as cell lines and resected tissue from patients.

2.1.3.1.1. Genetic Biomarkers

Researchers have been focusing on predictive biomarkers that can predict whether to diagnose GBM or respond to the treatment. Given contexts like the heterogeneity of GBM, this procedure has been challenging. In this regard, the Tumor Cancer Genome Atlas (TCGA) is a valuable tool for resolving the pathways affected

by many mutations that are activated in most GBM tumors and play a part in forming GBM, such as EGFR. Additionally, there is a program called ProfiLER that uses either next-generation sequencing or comparative genomic hybridization to provide tumor genomic profiles from patients with fresh or paraffin-embedded, primary or recurrent tumors and biopsies, which is a significant step for personalized medicine (Bonneville-Levard et al., 2021). Further, commonly used biomarkers in GBM are listed below.

The most important genetic mechanisms in brain tumors are IDH mutations, which are examined for primary and secondary differentiation of gliomas, as mentioned above in 2.1.2. section. IDH-WT is the disease type that accounts for 90% of GBM cases clinically defined as primary GBM. The diagnosis of the patient is made directly as stage IV and is associated with aggressiveness and a poor prognosis. Mutations of IDH, an enzyme involved in the citric acid cycle, are observed in all secondary GBMs that develop from the lower stage (Alves et al., 2021). When the IDH1/2 mutation occurs, it catalyzes the formation of 2-hydroxyglutarate (2–HG), which has oncogenic activity, from α-ketoglutarate (α-KG) by replacing the 2-ketone group (Figure 6). It is associated chiefly with epigenetic instability, cancer cell differentiation, and good prognosis (Yang, Ye, Guan, & Xiong, 2012).

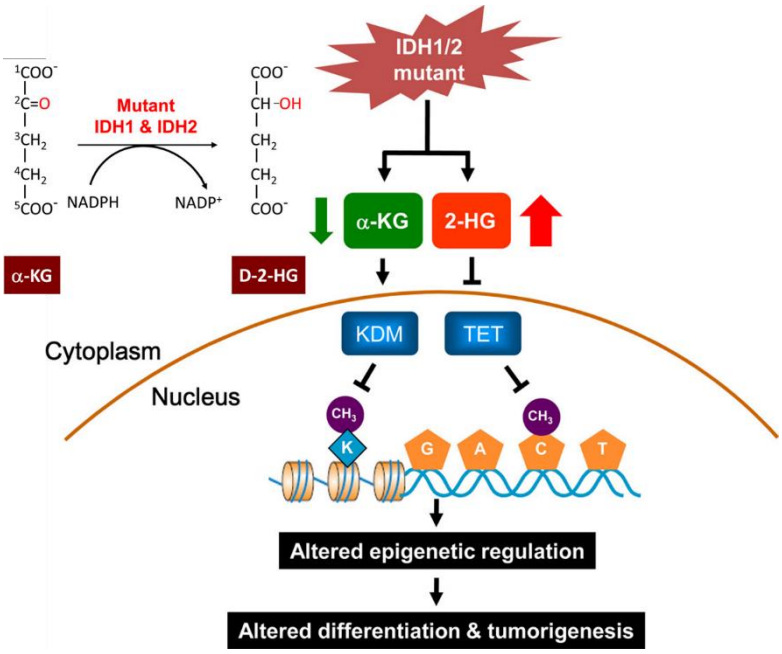

Figure 6. IDH1 mutation promotes high expression of 2-HG levels and alters epigenetic regulation which results in cell differentiation (Yang et al., 2012).

The well-known tumor suppressor TP53 produces the protein p53, essential for controlling cell division and apoptosis (Zhang et al., 2018). According to prior research, TP53 mutations were present in roughly 50% of the glioma, and it has been demonstrated that mutant TP53 and p53 depletion can hasten cell proliferation with uncontrollable cell division while supporting cancer cell metastasis (Guo et al., 2020). The TP53 mutation, which is usually linked to tumor malignancy of GBM, is connected to a worse prognosis and effectiveness of standard treatments (Lee et al., 2020). On the other hand, the transcription repressor named promyelocytic leukemia zinc finger (PLZF), which is excessively expressed in GBM, can reduce p53's acetylation, promote its ubiquitination, and regulate the expression of TP53. This states that by preventing p53 from functioning, PLZF may contribute to the emergence and spread of GBM (Choi et al., 2014).

The active EGFR signaling pathway observed in other cancer types is also very important for GBM. Increased EGFR amplification and overexpression and, additionally, the epidermal growth factor receptor variant III (EGFRvIII) mutation promote the aggressive character and overgrowth of GBM cells (Tini et al., 2015). In the literature, EGFR and EGFRvIII are symbolized as partners in crime, and it is also found that the activation of this EGFRvIII receptor results in the uptake of phosphoinositide 3-kinase (PI3K) into the cell membrane and affects many molecular mechanisms (Zadeh, Bhat, & Aldape, 2013) (Figure 7). A recently published paper hypothesized that there was altered gene expression in the EGFR pathway in patients newly diagnosed with EGFR-amplified GBM but not in patients with GBM recurrence. These findings suggested EGFR overexpression as a potential mechanism for understanding GBM recurrence (Dhawan, Manem, Yeaney, Lathia, & Ahluwalia, 2023). Different research focusing on the association between EGFR expression and patient prognosis demonstrated no variation in patient survival according to EGFR expression (Amirpour, Bahari, Nafisi, Rahmani, Taghipour Zahir, 2020). Another study also investigated that the knockdown of EGFR decreases the binding of tumor suppressive gene p53 to DNA-dependent protein kinase catalytic subunit (DNA-PKcs), which promotes the transcriptional activity of p53 (Ding et al., 2022).

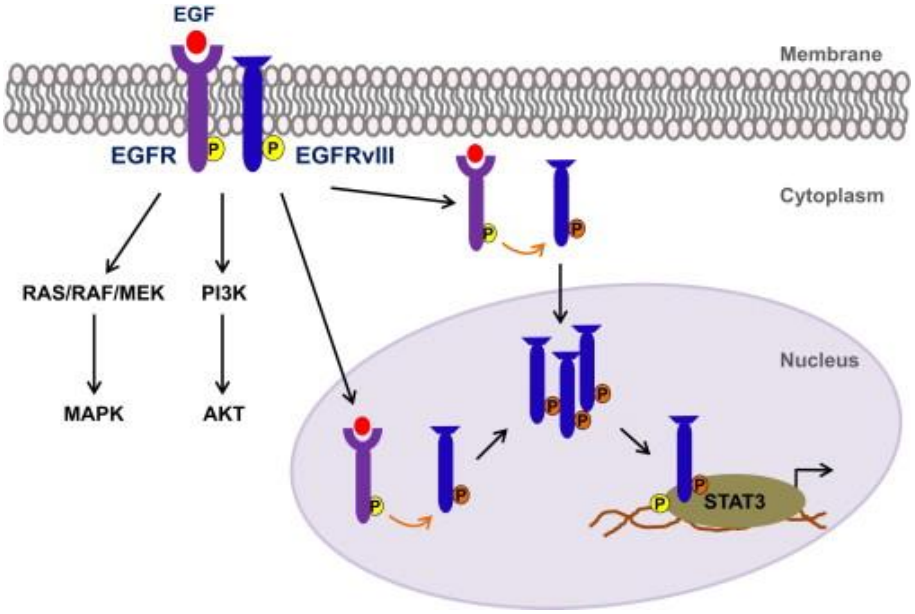

Figure 7. Activation of several pathways with EGFR and EGFRvIII interaction (Zadeh et al., 2013).

PI3K/Akt signaling is correlated with oncogenic pathways (Hashemi et al., 2023), and it is regulated by non-coding RNAs such as miR-579 (Ghaffarian Zirak, Tajik, Asadi, Hashemian, & Javid, 2022). Numerous GBM treatments focus on targeting PI3K/Akt. The PI3K/AKT/mTOR signaling system can be inhibited with AKT inhibitors, which have shown promise in preclinical research (Sami, & Karsy, 2013). Another strategy to increase the effectiveness of therapy is to integrate PI3K inhibition with additional medicines, such as an enhancer of zeste homolog 2 (EZH2) blocking (Mishra, Kumar, Raza, & Sehrawat, 2020). Additionally, the isoform of PI3K (p110) has been selectively targeted by a new peptide medicine known as Selectide-18, which has demonstrated the potential to reduce cancer growth *in-vitro* (Hutchings Pridham, Liu, & Sheng, 2022). Deactivation of Akt, inhibition of SIRT1, and enhancement of apoptotic cell death can also be facilitated by Cotinus coggygria flavonoid nanoliposomes (CCF-NLs) (Wang, Wang, To, Zhao, & Wang, 2015).

The PTEN tumor suppressor gene interacts with pathways such as PI3K/Akt, and in the case of PTEN mutation, cancer aggressiveness, proliferation, and survival are not suppressed. It is also associated with this treatment resistance in GBM (Fan et al., 2002; Hashemi et al., 2023).

There are recurrent mutations in the histone chaperone protein ATRX in GBM. The ATRX protein plays an important epigenetic role by depositing histones in

repetitive DNA regions (Ratnakumar, & Bernstein, 2013). ATRX mutation causes loss of function of the ATRX gene, and tumor cells escape telomere length degradation (Koschmann, Lowenstein, & Castro, 2016). Loss of ATRX also impairs the mechanism involved in DNA repair and mutations, thus accumulating and playing an essential role in treatment sensitivity (Koschmann et al., 2016; Qin et al., 2022). It has been found that cell proliferation and cell migration have been inhibited, and cell death has been increased *in-vitro* analysis by the knockdown of ATRX with ATRX small interfering RNA (siRNA) 590i transfection (Cai et al., 2015).

Telomerases prevent telomeres from shortening and entering apoptosis as the cell divides. Telomerase is abnormally active in GBM cells, and mutations in the TERT gene can impair telomere repair and cause DNA damage (Fernandes et al., 2020). TERT promoter mutations, most commonly C228T and C250T (Killela et al., 2013), which are detected between 60–75% of GBM, are associated with poor disease prediction by contributing to the cancer cell invasive character (Vuong et al., 2020).

Vascular endothelial growth factor (VEGF) is one of the most important biomarkers for tumor angiogenesis, and it is essential for GBM to achieve nutrients through new blood vessels and survive its inhibition through many methods that have been driven attention for years (Cheng et al., 1996; Reardon et al., 2011). It is overexpressed in GBM, proving it also with 1.56 pg/dL increased levels of VEGF in the patient's serum (Seyedmirzaei, Shobeiri, Turgut, Hanaei, & Rezaei, 2021) and mostly correlated with dismal prognosis (Wagle et al., 2020) (Figure 8).

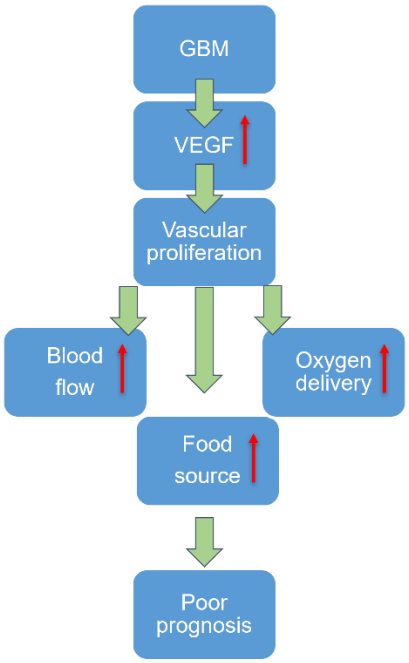

Figure 8. The effect of VEGF levels in GBM (Generated from: Wagle et al., 2020).

2.1.3.1.2. Epigenetics Biomarkers

Genetic changes in brain tumors have a very important relationship with epigenetic changes. Epigenetic mechanisms are divided into two as DNA and RNA based epigenetic mechanisms. DNA-based epigenetic mechanisms include DNA methylation and histone modifications, while RNA-based epigenetic mechanisms include non-coding RNAs.

2.1.3.1.2.1. DNA Methylation

One of the epigenetic mechanisms is methylation, and the very first discovered example is a DNA repair protein O6-Methylguanine-DNA Methyltransferase (MGMT), the determinant of the response to the chemotherapy drug temozolomide (TMZ) used in GBM treatment (Butler et al., 2020). In clinical studies, patients with MGMT overexpression may be recommended to undergo an alternative treatment option. The methylation added to lead the cancerous cell to apoptosis with TMZ treatment is removed by demethylation of MGMT. As the DNA is repaired, the cancerous cell escapes death, continues dividing, and develops resistance to the TMZ drug (Figure 9. a). It also happens when the promoter region of MGMT is not

methylated (Figure 9. b-middle). The expression of MGMT decreases when the MGMT promoter region is methylated, so the new methylation does not bind to MGMT, and TMZ works efficiently (Figure 9. b-top). However, if the mechanism of MGMT is expressed despite methylation in this promoter region, it can be associated with non-coding RNAs (Figure 9. b-bottom).

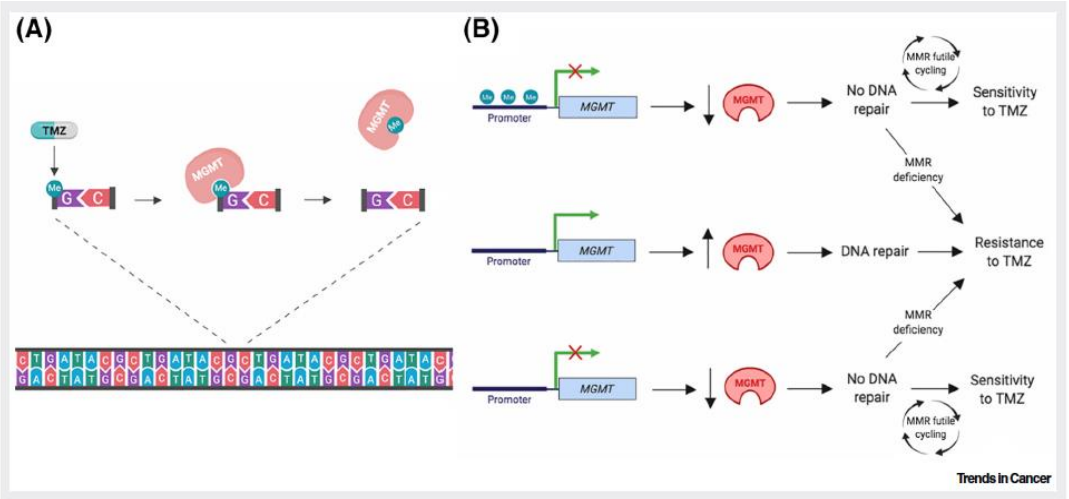

Figure 9. Metyhlation status of MGMT affecting chemotherapy drug TMZ treatment response (Butler et al., 2020).

2.1.3.1.2.2. Histone modification

Histone modification is a prominent epigenetic mechanism that has ability to change gene expression without alteration to the genomic DNA. Histone modifications can include histone acetylation, histone methylation, histone phosphorylation, and histone ubiquitination (Figure 10).

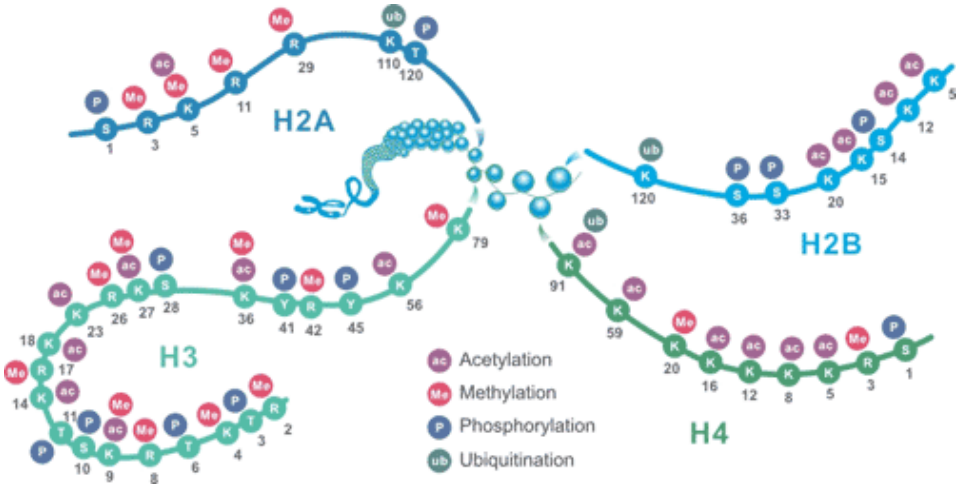

Figure 10. Schematic representation of histone modifications (Taken from: Cusabio.com).

Methylation of lysine 27 on histone 3 (H3K27me) is the most important of the histone modifications, determining the differentiation between pediatric brain tumors and adult brain tumors (Chan et al., 2013). There is also an investigated program, STOPHIM, for revealing the STOchastic Process of HIstone Modification and used to understand H3K27 methylation in a better way (Harutyunyan et al., 2020). Furthermore, it has been proved that GBM tumor cells develop more quickly in the presence of histone lysine-specific demethylase (LSD1). When it is inhibited, the senescence response is brought on (Saccà et al., 2019). Although not yet applied to routine treatment, epigenetic-based treatments have recently been the focus of treatment strategies. To illustrate, the effects of histone deacetylase (HDAC) directed inhibitors, which are involved in histone modifications from DNA-based epigenetic mechanisms related to chromatin regulation, have been demonstrated in the treatment of GBM in a very recent article (Figure 11) (Everix, Seane, Ebenhan, Goethals, & Bolcaen, 2023).

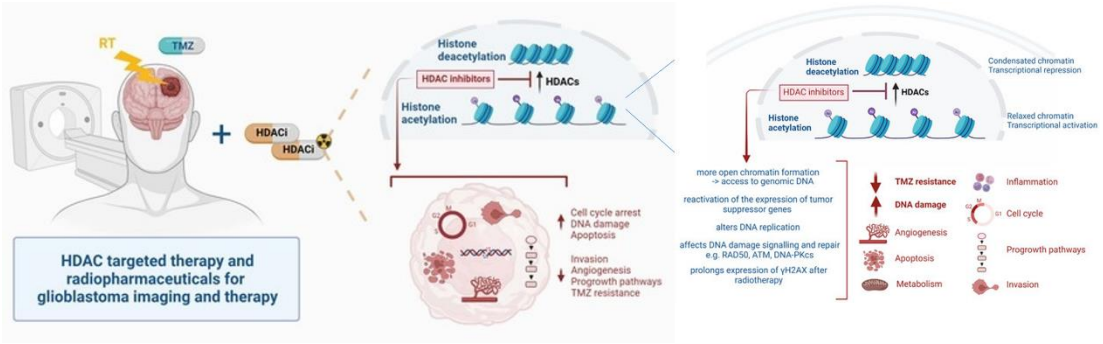

Figure 11. The use of HDAC inhibitors (HDACi) in addition of the treatment of GBM (Everix et al., 2023).

2.1.3.1.2.3. Non-coding RNAs

Non-coding RNAs, including short non-coding RNAs such as microRNAs (miRNAs), long non-coding RNAs (lncRNAs), and circular RNAs (circRNAs), are of great importance in GBM. The non-coding part of DNA corresponds to 98% of the DNA, which is considered “junk” DNA. However, the importance of this part, thanks to its functions such as regulating DNA, has been understood recently with the help of the Encyclopedia of DNA Elements (ENCODE) project (Do, & Kim, 2018).

miRNAs are short non-coding RNAs that consist of 19 to 25 nucleotides that control gene expression post-transcriptionally (Ranganathan, & Sivasankar, 2014).

More than 3,000 human miRNAs have been identified to date, according to miRbase (http://mirbase.org/). A miRNA can bind to several different mRNAs or genes, but above 50% of miRNA genes are localized in fragile sites or genomic regions favorable to cancer (Calin et al., 2004). One can also say that expression levels of miRNA, as well as changes in miRNA sequence such as single nucleotide polymorphism (SNP), may serve as important biomarkers in cancer. miRNA profiling can be done by extracting RNA from specific tissue and using Real-Time Quantitative Reverse Transcription PCR (RT-qPCR), microarray, or RNA sequencing (Pritchard, Cheng, & Tewari, 2012). miRNAs regulate GBM malignancy parameters such as cell proliferation and survival, and since these miRNAs can be shed by GBM cells, they can be preserved in the patient's cerebrospinal fluid (Figure 12) (Zhang et al., 2017). miRNAs can be present as oncogene or tumor suppressors; hence, the level of miRNAs associated with tumor suppressors decreases, and the level of oncogene-associated miRNAs increases in GBM (Matsuzaki, & Suzuki, 2014). Last but not least, some miRNAs are also associated with therapy resistance (Banno et al., 2014) and often deregulated in GBM (Table 1).

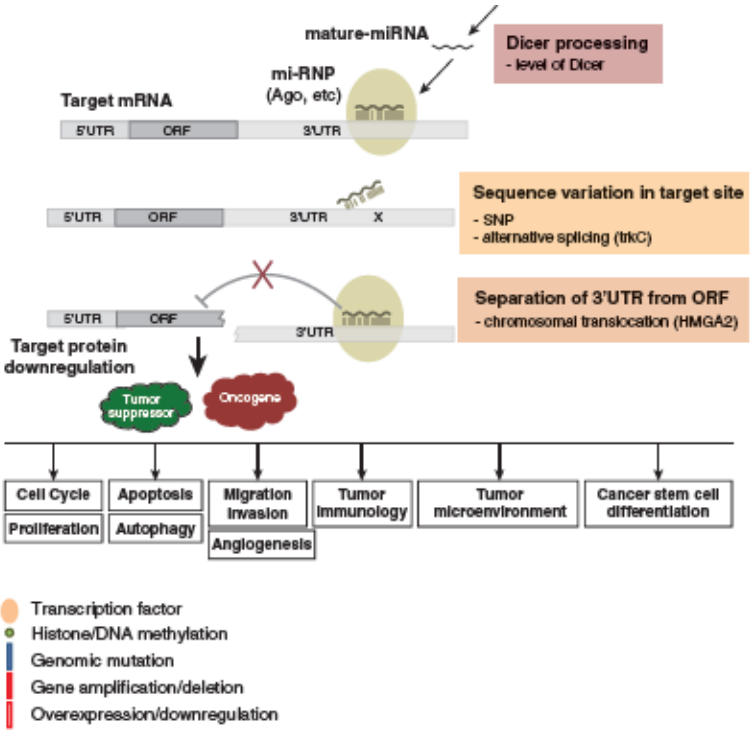

Figure 12. Deregulation of miRNAs in cancer (Zhang et al., 2017).

Table 1. Some deregulated miRNAs in GBM and their functions (Modified from: Zhang et al., 2017).

miRNA	Expression in GBM	Survival correlation	Targets	Function	
				Overexpression	Anti-miR
Let-7	Down		KRAS	Migration↓, Proliferation↓, In vivo tumor growth↓	
Hsa-miR-21	Up (Up in high-grade tumor)	Y	RECK, TIMP3, APAF1, NP32A, SMARCA4, Spry2, Caspases, PTEN, Cdc25A, HNRPK, TAp63, RRFIP1, PDCD4, p53	Invasiveness↑	Invasiveness↓, Apoptosis↑, Viability↓, Proliferation↓, *In vivo* tumor volume↓, Chemosensitivity↑, Radiosensitizes↑
Hsa-miR-10ab	Up (Up in TMZ-resistant tumor)	Y	HOXD10		
Hsa-miR-181abc	Down		Bcl-2	Proliferation↓, Apoptosis↑, Invasiveness↓, Chemosensitivity and Radiosensitivity↑	
Hsa-miR-218	Down (Down in mesenchymal subtype)		IKK-β, HIF2α	Invasiveness↓	
Hsa-miR-221/222	Up (Up in high-grade tumor, CD133+ cells)	Y	P27, Akt, PUMA, P57, PTPμ BIRC1, NIAP, ICAM-1	Proliferation↑, Invasiveness↑, *In vivo* tumor growth ↑, Apoptosis↓, Migration↑	Proliferation↓, Apoptosis↑, *In vivo* tumor volume↓ STAT1/2 upregulation
Hsa-miR-195	(Up in TMZ resistant)		CCND3, E2F3, CCND1	Proliferation↓, Invasiveness↓	Chemosensitivity, Viability↓

One of the first oncogenic miRNAs (oncomirs) associated with glioma malignancy, miR-21 increases invasiveness by targeting pathways such as PTEN (Chai, Song, Han, Li, & Li, 2018). Clinically higher expression of mir-21 is associated with worse survival in patients (Pan, Mao, Deng, Li, & Geng, 2014). Hence, inhibiting oncomirs by methods such as miRNA inhibitors, siRNA is crucial for targeted therapy. For instance, silencing miR-21 has been shown to reduce invasion and increase apoptosis (Zhang et al., 2017). Silencing miR-21 may increase the chemosensitivity of human GBM cells since it can inhibit apoptosis by activating the PI3K/AKT pathway, which is critical in the mechanism of TMZ resistance (Figure 13) (Ma, Zhou, Chang, & Xue, 2019).

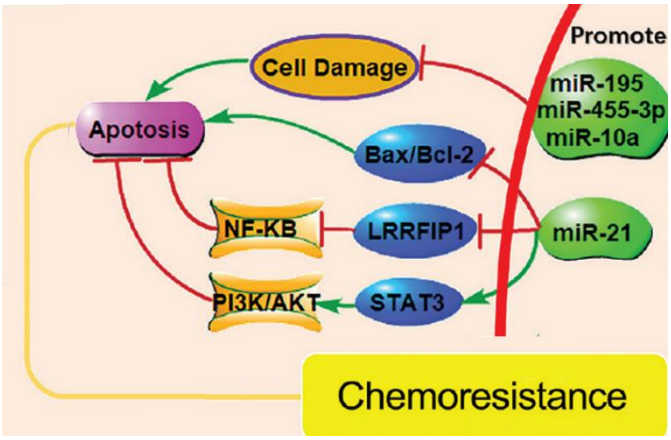

Figure 13. Correlation of miR-21 and apoptosis via several pathways (modified from: Ma, Zhou, Chang, & Xue, 2019).

To give another example, miR-218, a tumor suppressor miRNA with low expression levels in GBM, prevents cell survival and angiogenesis by affecting hypoxia-related factors. In *in-vivo* experiments, it is found that miR-218 expression (in Tum-3691–218-TMZ ve U87-218-TMZ) can reduce tumor size and increase sensitivity to TMZ treatment acting upon pathways such as EGFR shown in Figure 14 (Mathew et al., 2014).

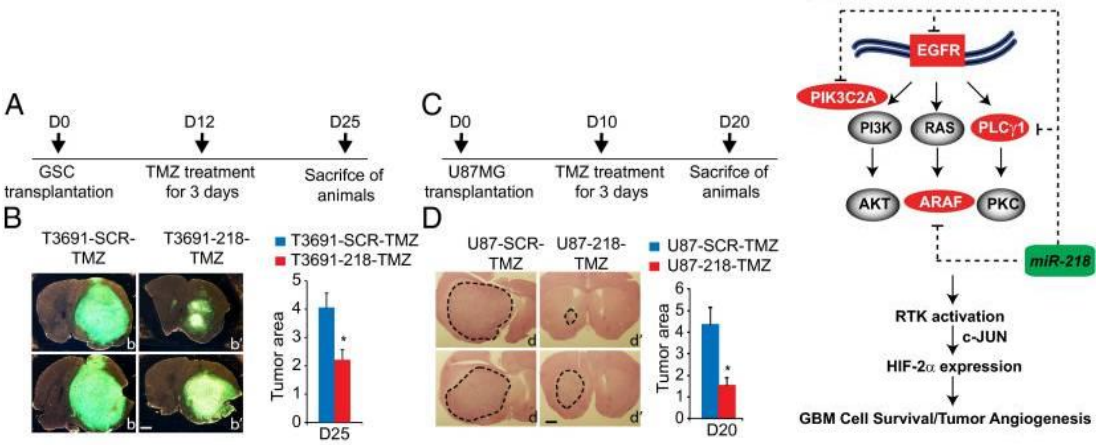

Figure 14. miR-218 functions as tumor suppressor and its elevated levels are correlated with reduction in tumor size and TMZ resistance *in-vivo* (Mathew et al., 2014).

In treatments targeting miRNAs, methods such as anti-miR oligonucleotides, miRNA sponges, miRNA inhibitors, and miRNA mimicry have been developed, and many delivery systems such as nanoparticles, antibodies, and viral vectors are used in such methods (Bernardo et al., 2015; McDermott et al., 2011). There is also a recent clinical trial that focuses on oncomiR levels (miR-10b) and specific treatment (anti-mir-10b) that can be applied to glioma patients (ClinicalTrials.gov ID NCT01849952).

Furthermore, lncRNAs, classified as epigenetic mechanisms, hold the potential as biomarkers for diagnosing, predicting outcomes and responding to treatment. With a length exceeding 200 nucleotides, lncRNAs constitute a group of non-coding RNAs, and The ENCODE Project has identified over 50,000 lncRNAs in the human genome (Huarte, 2015). These lncRNAs possess diverse features, including chromatin remodeling, functioning as sponges, and activating or repressing transcription (Figure 15). Moreover, lncRNAs, unlike miRNAs, can directly interact with proteins and thus regulate their stability (Figure 15) (Huarte, 2015). Additionally,

epigenetic variations have emerged as significant mediators of targeted therapies and resistance to traditional cytotoxic agents.

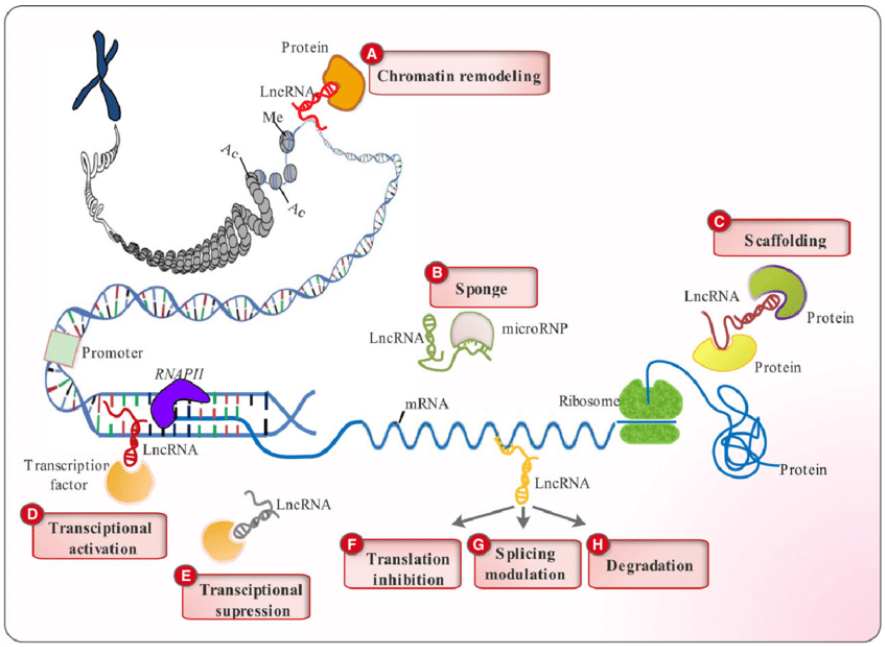

Figure 15. Different roles of lncRNAs (Salehi, Taheri, Azarpira, Zare, & Behzad-Behbahani, 2015).

There are many lncRNAs that are deregulated in GBM. One of the most studied of these, Metastasis Associated Lung Adenocarcinoma Transcript 1 (MALAT1), Nuclear Paraspeckle Assembly Transcript 1 (NEAT1), HOX transcript antisense RNA (HOTAIR) and Colorectal Neoplasia Differentially Expressed (CRNDE) have been overexpressed in GBM while Tumor Suppressor Candidate 7 (TUSC7) have been underexpressed. MALAT1 can target pathways such as MGMT and zinc-finger E-box-binding homeobox factor 1 (ZEB1) and interact with miRNAs such as miR-101. Silencing of MALAT1, which is also related to TMZ resistance, is found to abrogate TMZ resistance in GBM cells and lead to apoptosis (Rezaei, Tamizkar, Sharifi, Taheri, & Ghafouri-Fard, 2021).

NEAT1 can show oncogenic effects by functioning as a sponge directly interacting with miRNAs like miR-449b-5p (Zhen, Yun-Hui, Hong-Yu, Jun, & Yi-Long, 2016). Suppression of NEAT1 results in a decrease in the proliferation, invasion, and migration of GBM cells (Rezaei et al., 2021). Knockdown of HOTAIR or EZH2 leads to cell cycle arrest in GBM cells, and inhibition of HOTAIR suppresses GBM tumor migration (Rezaei et al., 2021). CRNDE, also an oncogenic lncRNA, is associated with TMZ resistance and poor disease prediction in GBM. A recent study

has developed siRNAs that specifically target CRNDE. The knockdown of CRNDE through siRNAs has been found to successfully enhance the effectiveness of TMZ treatment and apoptosis while reducing cell viability and colony formation (Zhao et al., 2021). The tumor suppressor lncRNA, known as TUSC7, cooperates with mir-10a, and its reduced expression is linked to resistance to TMZ in GBM (Rezaei et al., 2021). Together with the lncRNA examples above, numerous lncRNAs influence the various parameters of GBM malignity and treatment (Table 2).

Table 2. A comprehensive examination of lncRNAs indicating a) increased expression in GBM. b) reduced expression in GBM (Rezaei et al., 2021).

a)

lncRNA	Patients' specimens	Cell line	Targets/ Regulators	Signaling pathways	Functional impact
MIR22HG	18 gliomas and 5 NBT	U87MG, LN229, and LN18	b-catenin, miR-22-3p, SFRP2, PCDH15	Wnt	MIR22HG is over-expressed in glioma and glioma stem-like cells. Its silencing constrains the Wnt/b-catenin axis *via* loss of miR-22-3p and -5p. This diminishes proliferation, invasion and tumor growth.
SNHG5	–	U251, U87, LN229 and HEB	ELK1, caspase-3, STAT1, p-p38/ YY1, TNF-a	p38/MAPK	SNHG5 enhances GBM proliferation and suppresses apoptosis in GBM. YY1 is the activator of SNHG5 transcription in GBM.
SNHG9	–	U87 and U251	miR-199a-5p and Wnt2	Wnt/b-catenin	SNHG9 enhances aerobic glycolysis and cell proliferation, which can be weakened by miR-199a-5p.
SAMMSON	56 patients with GBM, 34 patients with diffuse neurosarcoidosis and 35 healthy controls	U87, U-373	miR-622	–	SAMMSON overexpression down-regulates miR-622 and increases proliferation rate.
DLEU1	10 GBM tissues and 10 adjacent NBT	SHG-44, U251	TRA F4	–	Over-expression of DLEU enhances viability and cell proliferation.
TRG-AS1	51 glioma tissues and 51 NBTs	U251, U87, A172, LN229, NHAs	miR-877-5p	–	TRG-AS1 inhibits miR-877-5p while miR-877-5p inhibits SUZ12 expression.
LINC01579	51 patients with GBM	U251, U87, U87MG, LN229, NHA	miR-139-5p	–	LINC01579 regulates cell proliferation and apoptosis through binding with miR-139-5p.
AGAP2-AS1	58 GBM patients	A172, U87/MG, U251/ MG, LN229, SHG44, NHA	EZH2 and LSD1	–	Up-regulation of AGAP2-AS1 enhances cell proliferation and apoptosis.
lnc-TALC	79 GBM patients	LN229, U251, 551W, HG7, 229R, 251R, 551WR, HG7R	miR-20b-3p/ phosphorylated AKT/FOXO3 axis	c-MET	lnc-TALC is associated with TMZ resistance through interacting with miR-20b-3p to enhance c-Met expression.
LncSBF2-AS1	20 primary and their corresponding recurrent GBM specimens (each pair from the same patient who was under TMZ treatment)	U87, LN229, A172, T98, U251, HEK293T, N3 primary culture cell	miR-151a-3p/ ZEB1	–	SBF2-AS1 is up-regulated in TMZ-resistant GBM cells and tissues.
SNHG20	78 pairs of human glioblastoma tissues and adjacent tissues	U87MG, U343, U251, LN215, NHA	Cyclin D1, CDK4, caspase 9, PI3K, Akt and mTOR	PI3K/Akt/ mTOR	SNHG20 overexpression enhanced cell proliferation, decreased apoptosis and increased stem properties.

b)

lncRNA	Patients' specimens	Cell line	Targets/ Regulators	Signaling pathways	Functional role
AC016405.3	3 GBM samples and paired NBTs, 64 FFPE GBM specimens	U87MG, U251MG	miR-19a-5p, TET2	–	AC016405.3 inhibits proliferation and metastasis *via* affecting expression of TET2.
LINC00657	40 pairs of GBM tissues and adjacent normal tissues	HA1800, U-87, LN-18, and U-118 MG	miR-190a-3p	pTEN	LINC00657 suppresses viability and colony formation in through increasing cell apoptosis.
AC003092.1	108 human glioma tissue samples (75 grade IV, 5 grade III, 13 grade II, and 15 grade I astrocytoma cases)	U87, U251 and their TMZ-resistant lines, U87TR and U251TR	TFPI-2, miR-195	–	Down-regulation of AC003092.1 correlates with TMZ resistance, higher risk of relapse, and poor outcome.
GAS5	50 FFPE GB specimens and 10 NBTs	–	miR-34a	–	GAS5 level in reduced in GBM.
RNCR3	–	U87, U251, U373, A172	miR-185-5p, KLF16	–	RNCR3 overexpression suppresses cell survival and proliferation, enhances cell apoptosis and activity of caspase-3/7.
NBAT1	48 cases of GBM (two groups of low=24 and high=24 expression of NBAT1) and 30 cases of normal brain tissues	SVGP12, U251, U87, U373, T98, and LZ229	Akt	–	NBAT1 down-regulation correlates with proliferation ability, tumor size, degree of malignancy and cell viability.
TUSC7	116 GBM specimens, 72 insensitive and 44 sensitive to TMZ treatment	U87	miR-10a	–	Under-expression of TUSC7 confers resistant to TMZ.
RAMP2-AS1	20 GBM patients and adjacent normal tissue	U87 and U251	NOTCH3, P21, DHC10	NOTCH	RAMP2-AS1 suppresses GBM cell growth and enhances cell cycle progression.
RP11-838N2.4	53 patients: 38 GBM cases, 3 grade III astrocytoma cases, 10 grade II astrocytoma cases, 2 grade I astrocytoma cases	U87TR, U251TR, U87, U251	miR-10a, EphA8	TGF-β	Down-regulation of RP11-838N2.4 was correlated with higher probability of tumor relapse.

GBM, glioblastoma multiform; TMZ, temozolomide; OS, overall survival; GSC, glioblastoma stem cell; FFPE, formalin-fixed, paraffin paraffin-embedded.

2.1.3.2. Standard GBM Treatment and Clinical Application

In GBM, surgical resection, radiotherapy, and concomitant chemotherapy applications are defined as standard treatments (Figure 16. a). Despite this treatment protocol that has been applied for years, the median life expectancy of GBM patients is only 12.6 months, and the 5-year survival is limited to approximately 4-5% (Van Gool, Makalowski, Schirrmacher, & Stuecker, 2022).

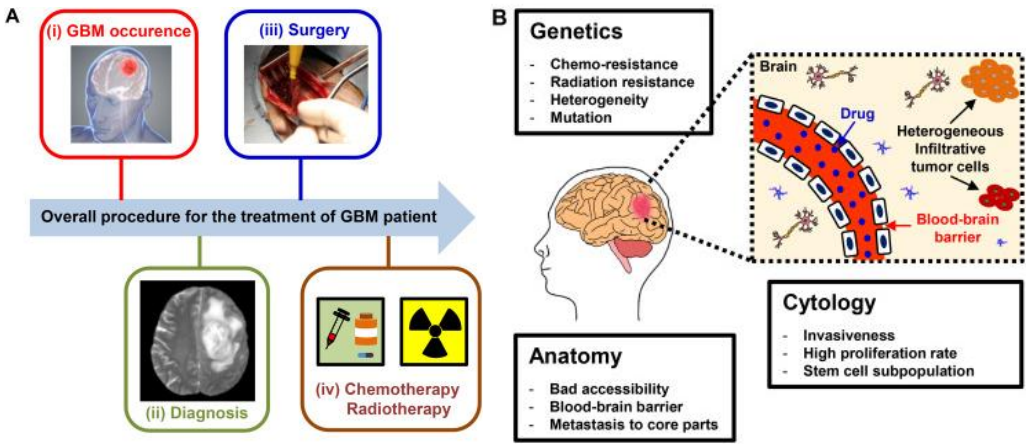

Figure 16. a) Steps of treatment for GBM patients b) Challenges in GBM treatment (Cha et al., 2020).

Difficulties that limit the survival of patients may be encountered at several steps of the standard treatment procedure. In GBM treatment, initially, it is aimed to

achieve maximum resection in order to prevent tumor recurrence. However, GBM can be particularly difficult to treat due to its complex origin, and it can be inoperable due to its location and prevalence in areas where brain surgery would cause too much neural damage. Hence, the risk of recurrence of the patient continues (Stupp et al., 2009). In addition, the inability to remove all of the tumor cells, the presence of GSCs, the limited number of the drugs that have ability to cross the blood-brain barrier (BBB), the inability of drugs to reach sufficient concentration on the tumor site due to early spread to the cerebrospinal fluid, short half-life of drugs, and resistance to therapy and many more parameters may lead to failure of GBM treatment and recurrence of the tumor as well (Figure 16. b). Surgery can ultimately reduce symptoms and provide more stabilization, while chemo-radiation therapy targets and destroys cancerous cells. Standard treatment consists of 6 weeks of 60 Gy radiation in total (2Gy every day, every 5 days in a week) and 6 weeks of adjuvant TMZ treatment (daily uptake in amounts calculated according to the body-surface area) with following 6 cycles of TMZ therapy (5 days out of 28 days of each cycle) (Figure 17). The Stupp Protocol has been accepted as the primary standard treatment since 2005, as the simultaneous use of temozolomide with radiotherapy causes radiosensitivity (Kil et al., 2008) and can prolong the survival induced by radiotherapy alone, albeit by approximately 2.5 months (Russo et al., 2009). However, the vast majority of patients receiving chemo-radiotherapy treatment experience deteriorating side effects, such as hematological problems with each consecutive cycle of treatment (Bae et al., 2014). Up to now, the only way to prolong patient survival more is the addition of tumor-treating fields, a device approved by The Food and Drug Administration (FDA) (Koehler et al., 2021) that disturbs cancer cells by electrical conduction together with chemotherapy (Stupp et al., 2017). Nevertheless, it still has difficulties, such as having a device on the patient's scalp for a long time, that must be overcome.

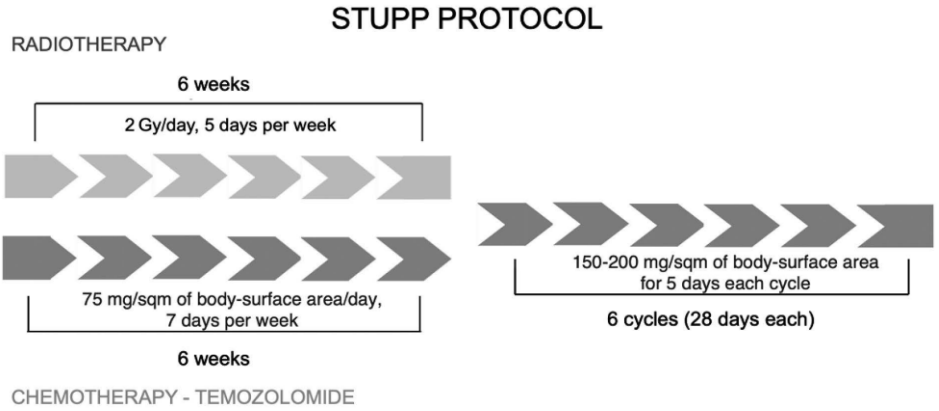

Figure 17. A standard therapy for GBM patients: Stupp Protocol (Bilicki, Zbrożek, Fudalej, Deptała, & Badowska-Kozakiewicz, 2022).

Developing and using a new drug for disease in the clinic can take many years. Therefore, discovering specific combination therapies on approved treatment has driven recent attention by scientists. First, it has been approved that "checkmating" cancer with combination therapy rather than mono is more effective since lower doses of each drug may diminish both drug resistance and drug toxicity in both tumor and healthy cells if the combination therapy is not antagonistic (Ghosh, Nandi, & Bhattacharjee, 2018). Subsequently, there are newly discovered specific combination therapies in clinical trials applied for GBM patients by targeting different biomarkers shown in Table 3. Despite drugs, there is also a brain tumor vaccine named rindopepimut designed to target EGFRvIII amplification (Jain, 2018).

Table 3. Clinical trials targeting several pathways with combination therapy for GBM patients (Ghosh et al., 2018).

Target	Molecule	GBM type	Stage of testing	References
Alkylation mediated DNA damage	Temozolomide (TMZ) + radiotherapy (RT)	GBM	Phase IV	NCT00686725
αvβ3 and αvβ5 integrin inhibitor+	Cilengitide + TMZ + RT	Newly diagnosed GBM patients with methylated MGMT promoter	Phase III	NCT00689221
Tyrosine kinase inhibitor	Imatinib mesylate + hydroxyurea	TMZ resistant progressive GBM	Phase III	NCT00154375
Pan-VEGFR tyrosine kinase inhibitor	Cediranib + lomustine chemotherapy	Recurrent GBM	Phase III	NCT00777153
VEGF-A	Bevacizumab (Avastin®) + TMZ + RT	Newly diagnosed GBM	Phase III	NCT00943826
Immunostimulant	TMZ + RT + poly ICLC	Newly diagnosed GBM	Phase II	NCT00262730
Multiple kinase inhibitor	TMZ + RT + sorafenib	GBM	Phase II	NCT00544817
Tubulin inhibitor	TMZ + PPX (CT2103)	GBM without MGMT methylation	Phase II	NCT01402063
mTOR inhibitor	TMZ + RT + bevacizumab + everolimus	GBM	Phase II	NCT00805961
VEGF-A + topoisomerase I inhibitor	TMZ + avastin + irinotecan	Unresectable/Multifocal GBM	Phase II	NCT00979017
EGFR inhibitor	TMZ + bevacizumab + tarceva	GBM	Phase II	NCT005255525

Ultimately, with clinical challenges and limited, extremely challenging treatments available, GBMs are still severe medical conditions. Therefore, recent

studies continue to emphasize the significance of developing efficient treatment approaches to enhance both the survival rates and quality of life for GBM patients highlighting the importance of biomarkers for individual therapy. It encourages us to explore more individualized and disease-adaptive GBM treatment paradigms to address each patient's unique type of cancer in a personalized way over time. According to that, there has been a principal intention to find natural products that can be possibly used in combination new therapeutics and vaccines to improve the treatment (Rong, Li, & Zhang, 2022).

2.1.3.2.1. Temozolomide (TMZ)

Temozolomide (TMZ) (or Temodar®), a compound of triazene, a widely used oral chemotherapy drug in treating GBM after tumor resection, is an effective alkylating agent. TMZ can exceed BBB due to its lipophilic feature and small size (194 kb) (Schreck, & Grossman, 2018). TMZ undergoes spontaneous hydrolysis in the body, converting it into its active compound, 5-(3-methyltriazol-1-yl) imidazole-4-carboxamide (MTIC), under physiological pH conditions. MTIC is further hydrolyzed inside the nucleus, giving rise to 5-amino-imidazole-4-methyl Amide (AIC) and methyl diazolium in 24 hours (Figure 18). These compounds are then transported to the nucleus, where methyl diazo ions transfer methyl groups onto guanine or adenine. As a consequence of this process, N7 methylguanine (N7MG), N3 methyl adenine (N3MA), and O6 methylguanine (O6MG) are formed, resulting in mismatched base pairs during DNA replication (Figure 19).

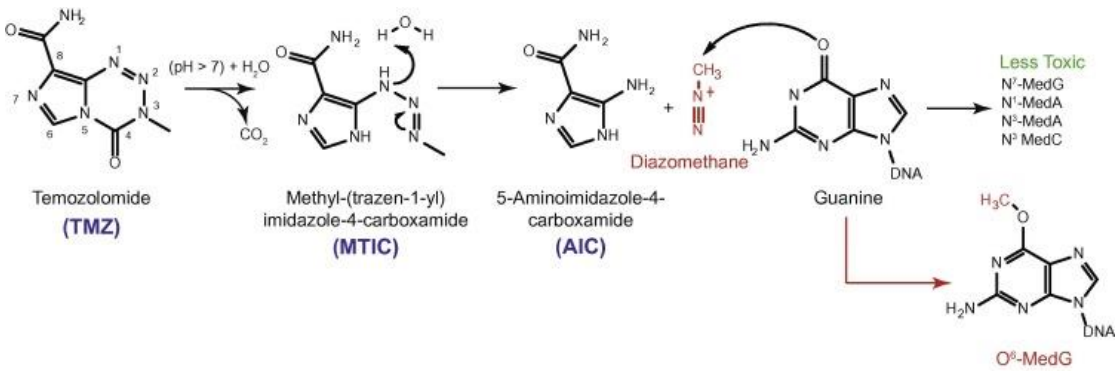

Figure 18. Conversion of TMZ to MTIC, AIC and methyl diazonium ion once its entering body (Rai et al., 2016).

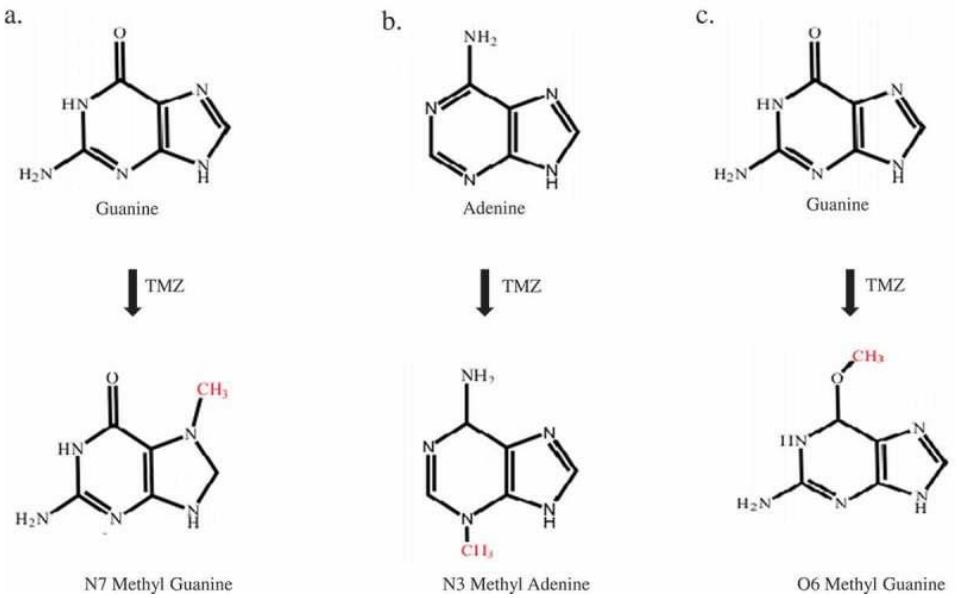

Figure 19. Compounds formed after methylation added by TMZ (Arora, & Somasundaram, 2019).

The main mechanism of TMZ is that it works as an alkylating agent by damaging the DNA of cancerous cells, thereby triggering the DNA repair pathway, inhibiting their ability to divide, leading to cell cycle arrest and apoptosis, a programmed cell death (Figure 20) (Willey, Yang, & Bonner, 2016). Although it is accepted as standard therapy, this increment in survival rate caused by TMZ can be illusive because many GBM tumors develop resistance to TMZ, leading to treatment failure and poor prognosis (Arora, & Somasundaram, 2019). Additionally, various delivery systems, such as nanoparticles and nanogel, are being developed to facilitate the delivery and controlled release of TMZ alone or with a combination of natural substances (Liang et al., 2023).

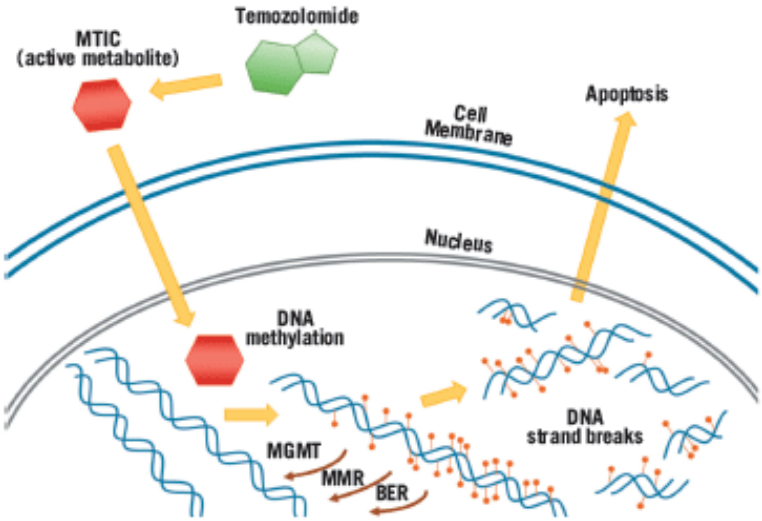

Figure 20. Mode of action of TMZ entering inside nucleus in form of MTIC, triggering MGMT, mismatch repair (MMR) and base excision repair (BER) and causing DNA strand breaks and apoptosis (Schreck, & Grossman, 2018).

2.1.3.2.2. TMZ drug resistance

TMZ is a commonly used chemotherapy drug for GBM; however, its limited effectiveness by developing resistance, as mentioned above, remains an important obstacle to overcome. Aside from the limited selection and use of chemotherapy medications, the most critical variables that complicate and lead to treatment failure are the severe side effects of the drug and the patient's resistance to the drug over time owing to congenital or long-term drug use. Approximately 70% of GBM cells reoccur de novo or with acquired resistance, and recurrence of GBM that has become more aggressive with the development of treatment resistance is still one of the leading causes of cancer-related deaths (Dymova, Kuligina, & Richter, 2021). A clinical trial combines TMZ with a PARP inhibitor in patients with recurrent GBM to enhance the therapeutic response to TMZ (Yoshimoto et al., 2012). Additionally, several mechanisms have been proposed to explain TMZ resistance, including the upregulation of drug efflux pumps (P-glycoprotein 1 (P-gp1)), which can pump out drugs and reduce effectiveness, stem cell presence, alterations in drug metabolism, and the activation of DNA repair pathways (Ortiz et al., 2021).

Furthermore, since there are significant differences between innately resistant cancer cells and cancer cells that acquire resistance over time (Meena et al., 2013), it is preferable to develop chemoresistant cell lines that acquire resistance through long-term exposure to TMZ from a well-characterized standard TMZ-susceptible parent cell line to develop the most effective therapeutic approaches. In this context, developing new treatments, improving existing treatment possibilities for effective treatment options, and prolonging current patient survival for GBMs are necessary.

2.1.3.2.3. Factors affecting TMZ resistance

The mechanisms of TMZ resistance in GBM are complex and multifactorial. They include cancer stem cells (CSC), DNA repair mechanisms, cell cycle checkpoints, drug efflux pumps, immune evasion, the Warburg effect, and alterations in signaling pathways and gene expression patterns. Also, the molecular heterogeneity of GBM contributes to resistance and recurrence (Figure 21).

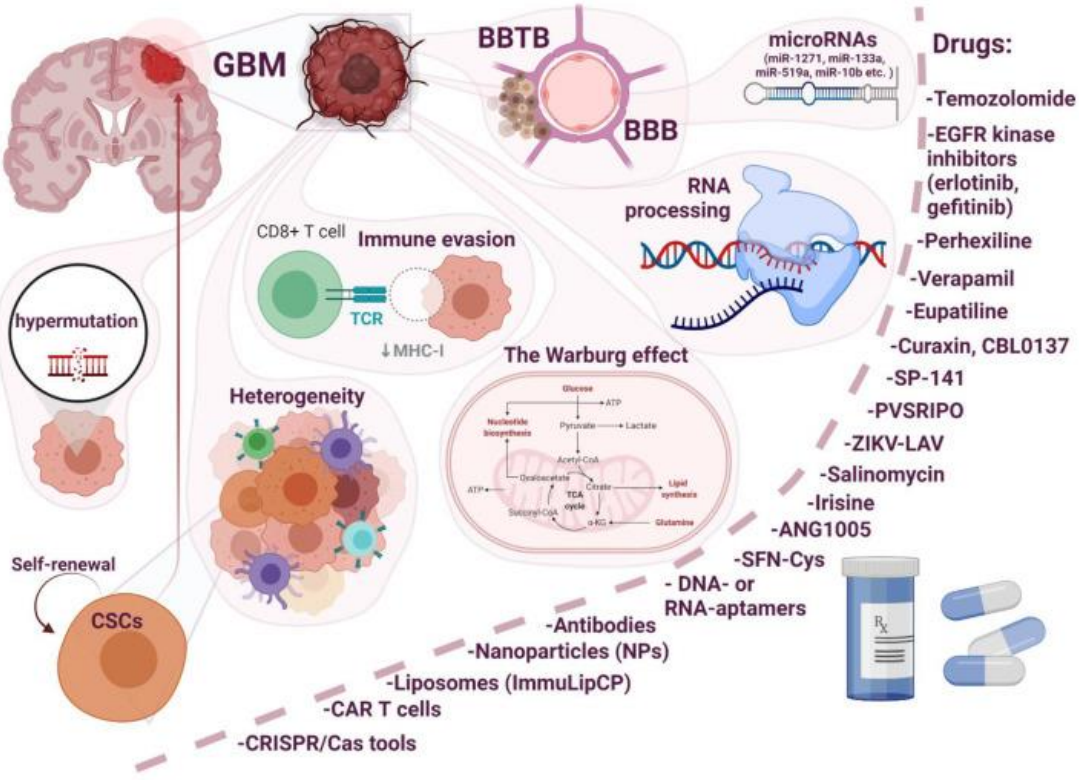

Figure 21. Factors affecting drug resistance in GBM (Dymova et al., 2021).

As mentioned earlier, the way TMZ therapy kills rapidly proliferating cancer cells is to induce DNA damage to lead cells to apoptosis, but the increased expression

of MGMT repairs DNA damage by TMZ, leading to treatment resistance, resulting in ineffective therapy (Figure 9) (Butler et al., 2020). MGMT have been used in a clinical trial over the last two decades to estimate the treatment cascade and response of GBM patients (Hegi et al., 2004). It is also proven that MGMT-expressed patients have quite shorter overall survival of up to 20 months compared to MGMT-unexpressed patients in terms of TMZ treatment (Spiegl-Kreinecker et al., 2010). Consequently, it is recommended to apply another and more effective treatment to patients found to have overexpression of MGMT in clinical practice in order not to cause unnecessary cytotoxicity. However, since GBM is a heterogeneous cancer, it is not expected that the same treatment will affect every patient in the same way because it contains many different parameters besides MGMT, which varies from patient to patient. There is also a clinical trial that aims to sensitize TMZ resistance by targeting base excision repair (Sorribes, Handelman, & Jain, 2020). Recently, it has been highlighted that increased and/or decreased gene expression of another repair mechanism, MMR, (such as mutS homologue 2 (MSH2) (Caccese et al., 2020)) may lead to drug resistance (Dong, Jiang, Kang, & Guan, 2023). However, further investigation is needed in order to understand this subject comprehensively. Additionally, drug resistance has been linked to various factors such as epithelial-mesenchymal transition (EMT) and hypoxia that have been found to play an important role in the efficacy of TMZ and the crosstalk between pathways, especially with p53, in response to factors such as hypoxia play a prominent role in drug resistance (Figure 22). In this study, the various factors and their possible relation with each other that can affect TMZ drug resistance in GBM cells was discussed.

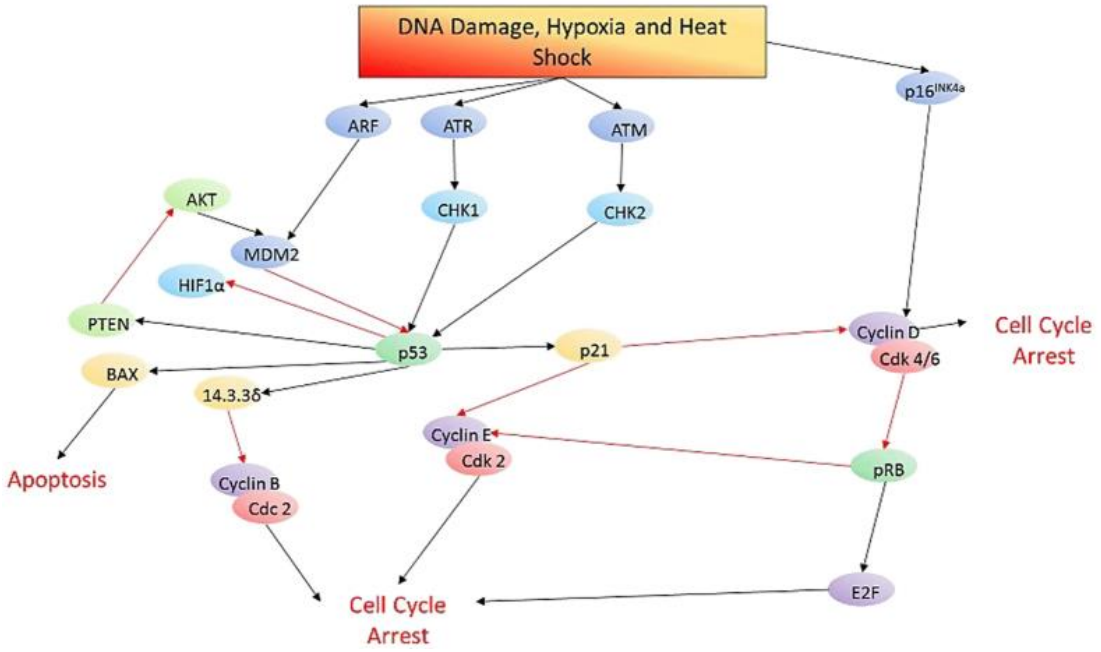

Figure 22. The crosstalk between several pathways in response to stress, hypoxia, and drug resistance (Pearson, & Regad, 2017).

2.1.3.2.3.1. Glioma Stem Cells (GSC)

GBM is a highly heterogenic tumor, meaning that various genetic and molecular subtypes can be established within a single tumor, and glioma stem cells (GSC) are mainly responsible for this heterogeneity (Figure 5). GSCs, capable of self-renewal and invading adjacent tissue cells, can differentiate into different cell types in a tumor. These particular cells, known as GSCs, are believed to originate from the normal stem cells present in the brain. However, certain factors, such as genetic mutations and environmental triggers, can cause these normal cells to transform into GSCs. The presence of GSC biomarkers such as CD133, SOX-2, NANOG, and OCT4 contributes to tumor heterogeneity, leading to cancer treatment failure, drug resistance, and tumor recurrence. The tumor recurrence is due to the GSCs resisting the therapy and repopulating (Garnier et al., 2018). In this respect, MMR inactivation and the presence of GSC can also cause tumor recurrence by promoting drug resistance in GBM cells by mechanisms including dysregulation of other post-transcriptional effectors (Figure 5). Thus, GSCs are one of contributing factors to possessing TMZ resistance in GBM (Singh et al., 2021).

The CD133 gene, which serves as a marker for GSCs, is highly expressed in TMZ-resistant tumors, indicating their ability to resist the effects of the chemotherapy drug (Liu et al., 2006). Moreover, the accumulation of GSCs in TMZ-resistant tumors leads to various molecular and genetic changes, ultimately resulting in increased resistance. In addition, cancer cells that enter the EMT process gain features like CSCs with enhanced anti-apoptotic properties and elevated expression of drug efflux pumps (Du & Shim 2016). Additionally, transcription factors such as ZEB1 in EMT and CSC are used functionally similar or in common (see 2.1.3.2.3.2).

Overall, the regenerative properties and drug resistance of GSCs, along with the alteration of surrounding tissues, contribute significantly to treatment failure, drug resistance, and tumor recurrence. Their specific role in TMZ resistance in GBM is an area of intensive research that requires more attention.

2.1.3.2.3.2. Epithelial-Mesenchymal Transition (EMT)

Epithelial-Mesenchymal Transition (EMT) is a key mechanism that happens during embryonic development, wound healing, and cancer growth. It includes the change of polygonal-shaped epithelial cells, which line the surfaces of organs, into spindle-shaped mesenchymal cells (Maier, Wirth, & Beug, 2010). Despite the morphological change, the transformation of epithelial to mesenchymal results in changes in several patterns (Figure 23). EMT encompasses a dynamic process that can be reversed by the mesenchymal-epithelial transition (MET) (Lamouille, Xu, & Derynck, 2014). In the mesenchymal state, cells have different gene expression levels and more aggressive and invasive behavior contributing to tumor progression (Rocha, & Morgado-Diaz, 2021). Within the process, mesenchymal-like cells acquire anterior-posterior polarity traits rather than apical-basal polarity, characterized by epithelial cells. Hence, the acquisition of mesenchymal phenotype results in metastasis, inability to have strong cell-to-cell adhesion, all of which agree with the aggressive hallmarks of the tumor. One can also say that EMT exhibits a strong relationship with chemotherapy resistance in cancer, particularly TMZ resistance in GBM (Tang et al., 2016). EMT also potentiates chemo-radiotherapy resistance by decreasing the sensitivity of cancer cells to DNA damage and apoptosis (Debaugnies et al., 2023). Several factors such as hypoxia (Figure 23), oxidative stress, and inflammation in the

tumor microenvironment strongly induce EMT, and it can be regulated with various signaling pathways (transforming growth factor-beta (TGF-β) pathway) and transcriptional factors (Snail, Slug, Twist, and ZEB1). Snail, Twist, and ZEB1 are the most common transcriptional factors in EMT, and their functions are also connected to CSC (Mladinich, Ruan, & Chan, 2016). ZEB1 has also been found to provide stem cell-like features in breast and prostate cancer (Pérez et al., 2021; Zhou et al., 2017), which can be disrupted with ZEB1 knockdown (Pérez et al., 2021).

ZEB1 participates in tumor formation and metastasis development (Wu et al., 2012) by taking part in the PI3K/Akt signaling pathway, which is of great importance in drug resistance. It is a direct target of TGF-β and other EMT inducers and inhibits interleukin-2 (IL-2) gene expression (William et al., 1991). ZEB1 promotes the downregulation of epithelial markers, such as E-cadherin, and the upregulation of mesenchymal markers, such as N-cadherin, vimentin, and fibronectin. Recent studies have shown that ZEB1 functions as an E-cadherin repressor in EMT and induces chemoresistance (Drápela, Bouchal, Jolly, Culig, & Souček, 2020). Developing strategies to overcome TMZ resistance in GBM is a major challenge in cancer therapy. Recent studies have focused on targeting EMT and its associated pathways as a novel strategy to overcome TMZ resistance in GBM. These approaches include the use of EMT inhibitors, such as TGF-β inhibitors, Snail inhibitors, and ZEB1 inhibitors. They also include the use of miRNAs, small molecules, and nanoparticles that can block EMT and enhance the sensitivity of GBM cells to TMZ. Most importantly, since the overexpression of ZEB1 is associated with poor prognosis and resistance to TMZ in GBM, it has been demonstrated that its knockdown sensitizes these cells to TMZ treatment and reduces the migration and invasion of GBM cells (Siebzehnrubl et al., 2013).

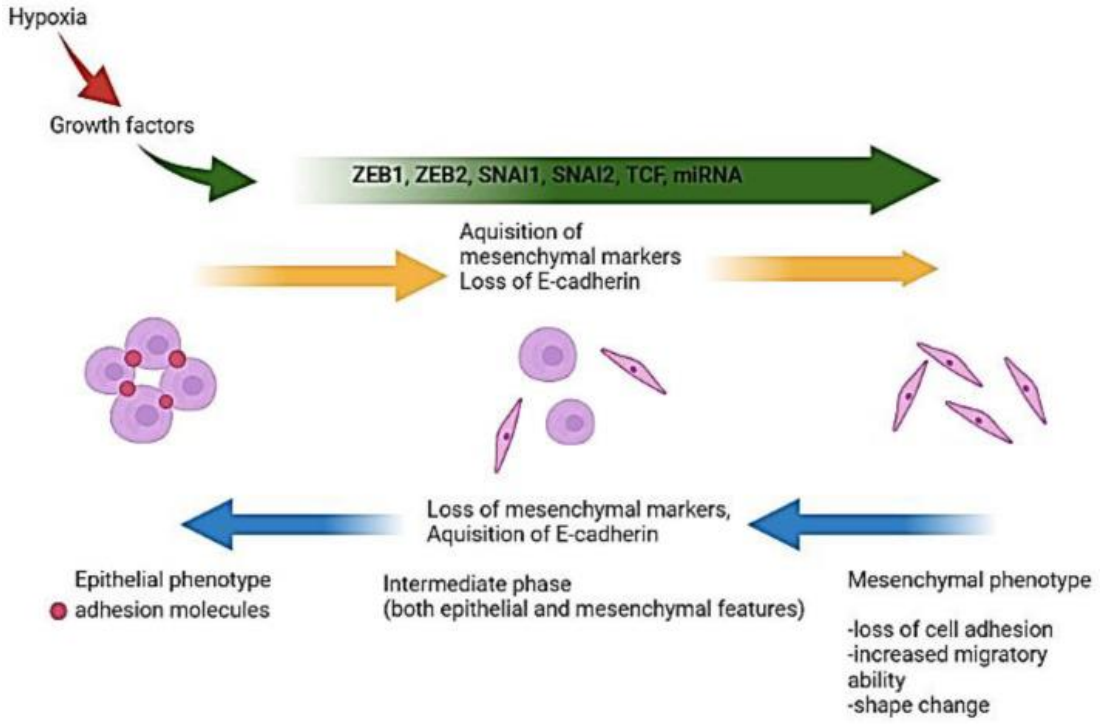

Figure 23. The hypoxia-related epithelial and mesenchymal phenotype and change of biomarkers such as ZEB1 involved in the process (Crivii et al., 2022).

The EMT process is modulated not only genetically but also epigenetically. MALAT1 LncRNA, which has received one of the most attention in GBM, is related to EMT. MALAT1 appears to regulate the EMT process by pathways such as ZEB1 and PI3K/Akt (Luo et al., 2019).

Scientists aim to identify new therapeutic targets and biomarkers for treating TMZ-resistant GBM. Understanding EMT and its role in TMZ resistance in GBM is still evolving. Additionally, more studies are needed to understand the relationship between EMT and other mechanisms of TMZ resistance, such as DNA repair pathways.

2.1.3.2.3.3. Mismatch Repair Mechanisms (MMR)

Mismatch repair mechanisms (MMR) are essential for maintaining genomic stability and preventing the accumulation of mutations that lead to cancer. MMR is a complex process that recognizes and repairs errors during DNA replication, such as misincorporated nucleotides and small insertions or deletions. In addition, it also

functions in the repair of cytotoxic lesions caused by DNA alkylators (Li, Pearlman, & Hsieh, 2016). In humans, several molecular markers are used to identify the MMR system, including MutS homologs (MSH) and post-meiotic segregation increased 1 (PMS1), that work together to detect and correct these errors. The MMR mechanism targets thymine, which tries to bind to O6-MeG formed by TMZ treatment and creates a single-strand break in DNA by forming a futile DNA repair cycle (Figure 24). Given MMR system functionally works in the cells lacking MGMT (Tancredi et al., 2022). This leads the cancerous cell to cell cycle arrest and apoptosis (Jiapaer, Furuta, Tanaka, Kitabayashi, & Nakada, 2018). Several MMR markers have been identified that are associated with apoptosis, cell cycle arrest, and drug resistance (Kuang, Wang, & Zhou, 2013). Also, dysfunctions in MMR lead to TMZ resistance in GBM (Zhang, Stevens, & Bradshaw, 2012). If MGMT expression is high in TMZ-resistant cells, the activity of the MMR mechanism decreases, and MMR markers such as MSH2/6 are expected to be at low levels. Because the MMR mechanism does not work and the mutated part cannot be cut by DNA repair, the TMZ-resistant cell cannot be directed to apoptosis and continues proliferating. A study comparing GBM cells that received and did not receive TMZ treatment for a long time shows decreased cell cycle arrest and MSH6 levels in TMZ-resistant cells (Yamashiro, Nakao, Ohba, & Hirose, 2020). In gliomas, silencing MSH 2/6 and PMS2 further increased TMZ resistance and was linked to a poor response to the drug (Happold et al., 2012). In the immunohistochemical (IHC) analysis performed on 355 glioma patients, MMR protein loss was found in 12.1% of the patients, and 55.8% of them belonged to MSH2 (Caccese et al., 2020). In particular, the MSH2 gene is located on chromosome 2 and encodes the MSH2 protein. MSH2 is a critical component of the MMR system that recognizes and binds to mispaired nucleotides. Wherefore, in GBM, mutations in this gene are generally correlated with TMZ resistance (McFaline-Figueroa et al., 2015). Decreased MSH2 expression via mir21 and mir155 contributes to 5-fluorouracil drug resistance, which means that the gene is turned off by epigenetic modifications to the DNA that do not change the underlying sequence (Deng, Wang, Lei, Lei, & Xiong, 2017).

Future research in this area focuses on further elucidating the mechanisms of MMR-mediated TMZ resistance and identifying new targets for intervention.

Developing strategies to overcome TMZ resistance is an active area of research, and one approach could be to develop combinational therapy with drugs and natural products that can modulate MMR pathways. Advances in genomics and epigenomics may lead to the development of personalized therapies that take into account the specific genetic and epigenetic alterations present in individual tumors.

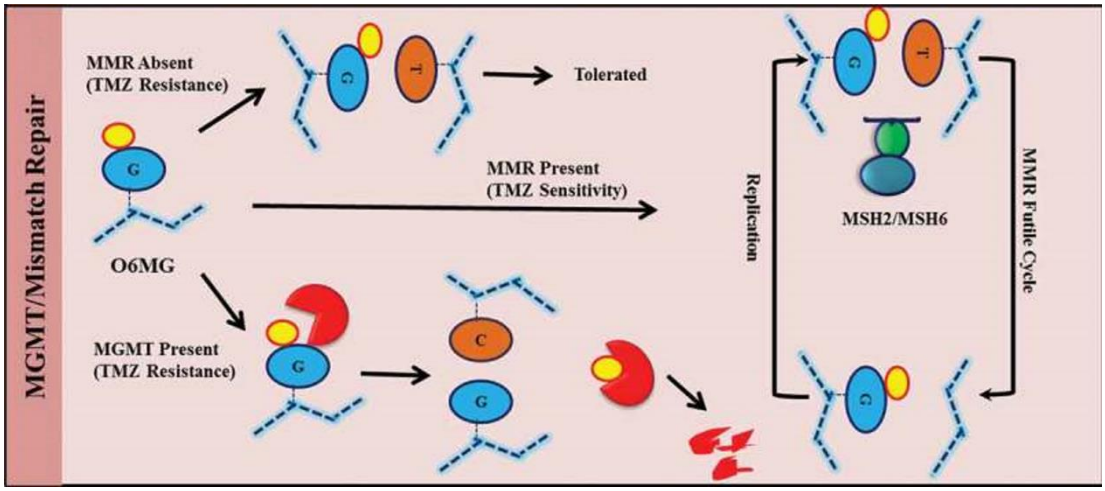

Figure 24. The response of MGMT and MMR to TMZ-induced O6MG and their related mechanism to TMZ resistance. When MMR is present, MSH2/6 prevent the replication of mismatched pair with futile cycle and leading single strand breaks and eventually, apoptosis (Arora, & Somasundaram, 2019).

2.1.3.2.3.4. Hypoxia

In *in-vitro* cancer research, the reliability of the obtained data is important to imitate the environment as close as possible to the cancer microenvironment. One of the most convenient ways to create this environment in GBM cell culture is to create a hypoxia environment with relatively low oxygen levels (1-5% O_2). As the tumor grows, the need for oxygen increases, and the sensation of this situation by vascularization results in enhancement of vascularization around the tumor. In conformity with the expected outcome under deprived oxygen levels, the vascular endothelial growth factor (VEGF) level is upregulated (Semenza, 2010). Strengthened angiogenesis also supports the increase in invasion, leading to faster tumor growth and spread. Thereupon, the blood vessels are unable to reach the entire tumor, and the tumor areas remaining in the center are exposed to insufficient oxygen. Tumor cells remaining in the hypoxic environment continue to survive and multiply by changing

their behavior. For cancer cells to provide a food source in a hypoxic environment, mitochondrial respiration is inhibited, and glycolysis is increased by the Warburg effect (Marchiq, & Pouysségur, 2016). This condition is also mediated by hypoxia-inducible factor 1 (HIF-1), which can regulate the responses in hypoxic environments (Marchiq, & Pouysségur, 2016). The ability to mimic the hypoxia, often preferred by the tumor, can provide an environment closer to the tumor microenvironment.

Studies have revealed that tumor cells whose metabolism is altered in a hypoxic environment can lead to more robust metastatic behavior, migration, and remodeling of the extracellular matrix by stimulation of EMT (Spill, Reynolds, Kamm, & Zaman, 2016). Hypoxia, frequently observed in GBM tumors, leads to the aggressive development of the brain tumor, the emergence of the GSC phenotype, invasion into healthy tissues, and drug resistance (Musah-Eroje, & Watson, 2019).

Hypoxia can suppress E-cadherin by increased ZEB1 (Chu, Boley, Moraes, Barsky, & Robertson, 2013) or direct cells to the extravasation process, EMT, through increasing levels of the GSC marker SOX2 and plasticity (Sun et al., 2020). It may cause GBM cells to pass into mesenchymal structures, acquire metastatic and invasive features, and even have therapy resistance (Figure 25). HIF can also lead to increased tumor malignancies and therapy strain, with increased genetic instability and mutations triggered by decreased MMR levels (Mihaylova et al., 2003). It has been shown that HIF-1α also causes an increase in ZEB1 in colorectal cancers (Zhang et al., 2015). In addition, it has been shown that changes in lncRNA expression level mediate the formation of resistance to targeted therapies and traditional cytotoxic agents (Huang et al., 2019). In particular, HOTAIR (Weng et al., 2022), a lncRNA mediating hypoxia-induced drug resistance involved in epigenetic mechanisms, and MALAT1 (Shih et al., 2021), a hypoxia-induced lncRNA, are both associated with hypoxia, and both commonly contributes to drug resistance by acting on the ZEB1 protein which is highly expressed in brain tumors (Feng et al., 2019; Weng et al., 2022). For these reasons, in the present study, potential differences in GBM cell behavior arising from the oxygen level difference in the hypoxic tumor microenvironment were determined regarding tumor migration and invasion. They provided preliminary data for future studies that could better represent *in-vivo* environments. The anti-cancer effect of bioactive molecules (fisetin and berberine) included in the current study was evaluated

comparatively in TMZ-resistant and non-resistant GBM cell lines using normoxia and hypoxia conditions.

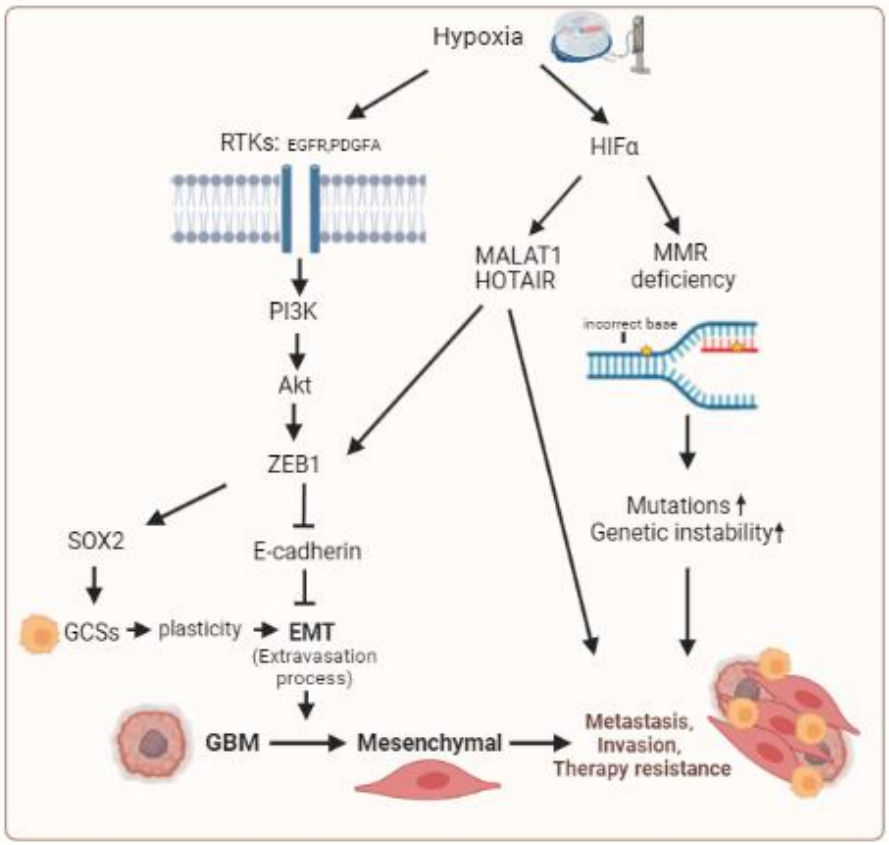

Figure 25. Some possible pathways induced by hypoxia resulting in therapy resistance in GBM cells (Created with Biorender.com).

2.2. The use of bioactive molecules in overcoming drug resistance

Nowadays, natural compounds are often preferred in determining new treatments for many types of cancer. Efforts are being made to minimize the cytotoxic effects of these compounds, widely used as food supplements, and to make existing treatments more effective (Kammerud et al., 2021). Studies show that using natural substances with specific therapeutic properties together with chemotherapeutic agents can synergistically increase the effectiveness of chemotherapeutic agents, reducing the appropriate drug dose and possible side effects (Cragg, & Newman, 2005; Li et al., 2010). In this context, flavonoids and their subcategories, such as flavonols and catechins, are often associated with the treatment of cancer (Hollman, & Katan, 1999).

2.2.1. Flavonoids

Flavonoids are natural constituents of the polyphenolic secondary metabolite class, mainly found in fruits and vegetables (Panche, Diwan, & Chandra, 2016). Flavonoids, which have been determined to have neuroprotective and anti-tumor effects by research, are classified within themselves. The most abundantly used flavonoid subgroup in human food intake is a flavonol, a 3-hydroxy derivative of another subgroup, flavanones (Panche et al., 2016). Studies carried out in independent laboratories argue that flavonoids, which have apoptotic effects in GBM cells, can form a basis for further *in-vitro* and *in-vivo* studies to create new treatment approaches (Pak, & Oztopcu-Vatan, 2019). With this theory, flavonoids, which are determined to have neuroprotective and anti-tumor effects, can shed light on the potential of targeting to reduce chemotherapy-induced side effects and delay or prevent subsequent chemotherapy resistance by reducing the effective doses of chemotherapeutic drugs in general use. Therefore, studies indicate that investigating the anti-cancer effects of flavonoids may increase the potential to discover new therapeutic candidates for GBM treatment. Since signaling pathways such as ZEB1, PI3K, which play a role in the formation of TMZ resistance in GBM cells, are also targeted by flavonoids such as fisetin and berberine, it can be predicted that these flavonoids will be a guide for obtaining positive results in TMZ resistance and improving TMZ activity. In this context, the effects of fisetin and berberine, commonly found in the structure of various therapeutic plants and can also be used as food supplements, on anti-cancer and TMZ resistance in GBM cells were investigated.

2.2.1.1. Fisetin

A flavonoid commonly found in strawberries, apples, onions, wine, and tea, fisetin (3,3′,4′,7-tetrahydroxyflavone) is an anti-oxidant, anti-inflammatory and anti-cancer properties have been revealed (Imran et al., 2020) which means that it can protect healthy cells from the cytotoxicity of chemotherapy drug while combating cancerous ones. In addition to being a phytopharmaceutical that can be taken nutritionally (Figure 26), fisetin can also be purchased in supplement form with health benefits due to its safety profile. The apoptotic, senolytic, anti-migratory, anti-

proliferative, and anti-invasive effects of fisetin have shed light on treating various cancers. It has been shown that fisetin has pleiotropic features due to its ability to target signaling pathways such as ZEB1 in melanoma (Pal et al., 2016), which also plays a role in the formation of TMZ resistance in GBM cells.

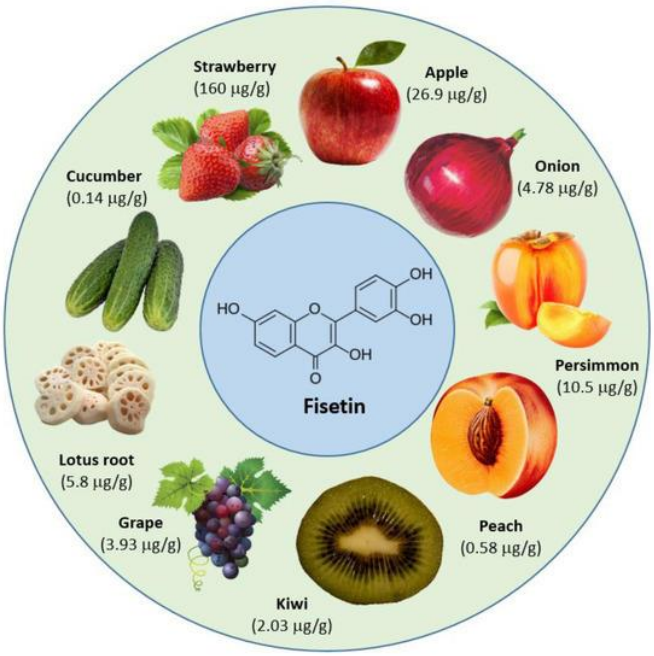

Figure 26. The molecular structure and occurrence of fisetin in nature and in various foods (Rahmani et al., 2022).

In GBM cells, fisetin has been identified to operate on common specific signaling pathways in a way that may also reduce TMZ resistance. It has been shown in laryngeal cancer that fisetin upregulates caspase-3 and downregulates the PI3K/Akt pathway and Mitogen-activated protein kinase 3 (MAPK3), which are important pathways in TMZ resistance, and increases anti-cancer activity (Zhang, & Jia, 2016). Another study found that fisetin affected the MAPK pathway, causing G2/M arrest of cells and inhibiting renal cell carcinoma proliferation and metastasis. (Hsieh et al., 2019).

Fisetin also targets the ZEB1 (Pal et al., 2016), which is linked to the development of drug resistance in GBM and is crucial for the EMT mechanism and metastasis of this kind of cancer. With the crosstalk between these pathways, fisetin can affect the EMT process, and according to one study, fisetin inhibited ZEB1-mediated invasiveness when used with sorafenib in BRAF-mutated melanomas (Pal et

al., 2016). It was also found that fisetin could suppress the EMT process in triple-negative breast cancer, this time targeting the PI3K/PTEN/Akt pathway, increasing epithelial markers (E-cadherin) and decreasing mesenchymal markers (N-cadherin) (Li et al., 2018).

Fisetin has been frequently implicated in repressing tumor aggressiveness in cancer. It can lead the human cervical cancer HeLa cells to apoptosis in Akt dependent manner (Afroze et al., 2022). It is known that fisetin leads to cell death in pancreatic cells by reducing Ki67, which is one of the indicators of cell aggression (Jia et al., 2019). It has been determined that fisetin can direct cancer cells to senescence, with a senolytic effect. In this way, it can prevent the proliferation of cancer cells and direct them to apoptosis (Beltzig, Christmann, & Kaina, 2022). Fisetin-inducted p53 expression also correlates with apoptosis in human renal carcinoma caki cells (Min, Nam, & Kwon, 2017). Again, fisetin is an effective biomolecule in renal cell carcinoma in reducing the number of colonies (Hsieh et al., 2019). In addition, the bioactive molecule can also prevent colony formation in human oral squamous cell carcinoma by targeting p21-Activated kinase 4 (PAK4), which has an essential role in cancer parameters (Li, Jia, & Dai, 2020). This tendency to apoptosis is mediated by increased caspase-3 due to fisetin in hepatocellular carcinoma (Chen et al., 2002). In addition to increasing caspase-3, it has also been found to increase caspase-8 and -9, p53 and decrease the Bax/Bcl2 ratio (Rahmani, Almatroudi, Allemailem, Khan, & Almatroodi, 2022). It is known that induction of apoptosis with fisetin in Bladder cancers is provided by increasing p53 and decreasing Nuclear Factor kappa B (NF-κB) (Rahmani et al., 2022). The effect of fisetin on apoptosis was also demonstrated in GBM, consistent with other types of cancers (Pak, & Vatan, 2019). Moreover, it has been shown that this bioactive molecule can target almost 27 genes in G2/M alone, causing cancer cells to stop in the cell cycle (Kumar et al., 2023). To give an example, this arrest with fisetin in bladder cancer can occur in phases of the cell cycle by targeting p53 and reducing CDK2 and cyclin A, which are involved in the S phase (Li et al., 2011). Activation of p21 due to fisetin-mediated p53 phosphorylation can disrupt cyclin B1 and stop cells at G2/M in uterine leiomyomas (Lee et al., 2020) (Figure 27). Clinically, fisetin supplementation reduced interleukin-8 and metalloproteinase-7 levels in colorectal cancers, thereby reducing inflammation (Rahmani et al., 2022).

The importance of fisetin in DNA repair mechanisms, which also plays a role in therapy resistance mechanisms, has recently attracted significant attention. Recently, fisetin has led to double-strand breaks in breast cancers and reduced radioresistance (Khozooei et al., 2022) and also caused radiosensitization in liver cells by directing cancer cells to apoptosis due to the endoplasmic reticulum (ER) stress (Kim, 2023). Furthermore, fisetin's usability in organs damaged by radiation has been patented (Rahmani et al., 2022). In addition to radioresistance, it has proven the role of fisetin in overcoming drug resistance by sensitizing cisplatin resistance via MAPK and caspases in lung adenocarcinoma (Zhuo, Zhang, Zhu, Zhu, & Chen, 2015). In prostate cancers, fisetin has demonstrated its efficacy in cabazitaxel resistance by reducing the expression of chemotherapy drug efflux pump P-gp (Mukhtar, Adhami, Siddiqui, Verma, & Mukhtar, 2016). Also, various drug delivery methods, such as nanoparticles, are being developed to further increase the effectiveness of fisetin (Kumar et al., 2023).

Last but not least, fisetin can show promise for novel treatment strategies for difficult-to-cure cancers like GBM and sensitize it to chemotherapeutic agents. The signal transduction of fisetin is in quite a wide range, and many features are yet to be discovered. To fully comprehend the pathways targeted by fisetin, further research is needed.

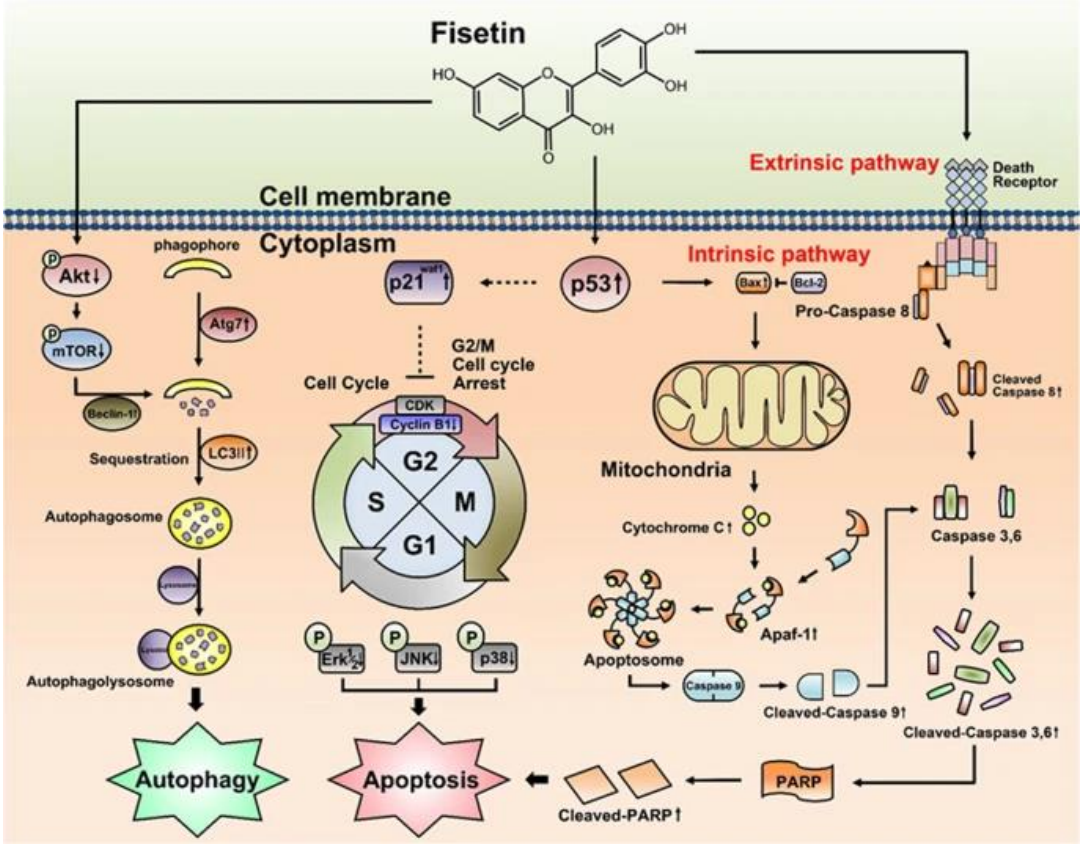

Figure 27. The signal transduction of fisetin in uterine leiomyomas (Lee et al., 2020).

2.2.1.2. Berberine

Berberine (5,6-dihydro-9,10-dimethoxybenzo[g]-1,3-benzodiocolo[5,6-a] quinolizinium) is a natural compound (Figure 28. b) mainly isolated from species of the Berberis genus in the Berberidaceae family (Figure 28. a). Its antidiarrheal effect has been demonstrated clinically, and it has been traditionally used in treating diarrhea in Chinese medicine for hundreds of years (Khin-Maung, Myo, Nyunt, Aye, & Tin, 1985). It is also stated that it is used as a supplement to alleviate the symptoms of some inflammatory diseases (Neag et al., 2018). Berberine is administrated orally; however, there are several methods developed, such as delivery in nanoparticles, to increase its bioavailability (Javed Iqbal et al., 2021).

In addition, berberine is herbal medicine exerting other pharmacological functions. According to that, there are studies demonstrating the anti-oxidant (Kazaz et al., 2020) and anti-tumor (Farooqi et al., 2019) activity of berberine. The anti-tumor of berberine has been demonstrated in various liver, lung, cervical, and gastrointestinal

cancers and leukemia (Wang, Liu, Du, Ma, & Yao, 2020). It has been shown to inhibit cancer malignity parameters such as cell proliferation, invasion, and metastasis.

a) b)

Figure 28. a) The source of berberine (Longevity website) b) The chemical structure of berberine (Neag et al., 2018).

Berberine can disrupt the cell cycle at G2/M by increasing p53, p21, and PI3K in chondrosarcoma cells (Eo, Kim, & Kim, 2014). The berberine-induced increase in this p53 also induces colorectal cancer cells to undergo apoptosis (Piyanuch, Sukhthankar, Wandee, & Baek, 2007). Berberine causes both apoptosis and cell cycle arrest by commonly affecting the Bax/Bcl2 ratio and increasing caspase-3 (Liu, Meng, Wu, Qiu, & Luo, 2019) (Figure 29). Thanks to its feature of increasing p53, it can direct cancerous cells to apoptosis (Liu et al., 2019). Due to its effect on cell cycle checkpoints, it leads to cell cycle arrest, for example, by suppressing cyclin E and increasing cyclin B1 (Liu et al., 2019). In breast cancer, berberine causes S phase arrests and additionally plays a role in reducing resistance to chemotherapy drugs (Gao et al., 2019). It has been shown that berberine can reduce ZEB1 in myofibroblast cells (Huang, Wang, Qi, & Pang, 2020) and HIF-1α (Ai et al., 2021), which are also essential in TMZ resistance.

Berberine also has many tumor-suppressing effects on GBM cells. *In-vitro* and *in-vivo* pioneering studies have shown that berberine effectively reduces migration, invasion, and tumor growth and induces autophagy in GBM (Wang et al., 2016). Furthermore, berberine also reduces tumor metastasis and cell proliferation by affecting various pathways. One of these pathways is suppressing metalloproteinase-

2 and 9 (Liu et al., 2019). By suppressing metalloproteinase-2, berberine has also been proven to have an anti-migratory effect on GBM (Irina et al., 2021).

In addition, using berberine in combination with other substances has recently gained importance. For example, in GBM, combination treatment with curcumin may cause cell death by affecting pathways such as PI3K (Maiti, Plemmons, & Dunbar, 2019). In addition, according to the article in artificial intelligence (AI)-based program that scans for drug interactions (SUPP.AI), the current understanding of the relationship between berberine and TMZ and how berberine increases sensitivity to TMZ is via MAPK3 pathway (Qu et al., 2020).

This bioactive molecule further regulates epigenetic modulations in cancer (Figure 29). In terms of DNA methylation, it has an increasing effect on CDKN1A in multiple myeloma (Liu et al., 2019). Its relationship with histone modifications in reducing HDACs has also been proven in non-small lung cancer (Huang, Liu, Gong, Wu, & Wen, 2017). Berberine is also of great importance in terms of regulating noncoding RNAs in cancer. It has been shown to reduce miR-21, one of the oncogenic miRNAs, in colon cancers (Liu et al., 2019). Interestingly, the role of berberine in overcoming TMZ resistance in gliomas has been demonstrated by increasing CASC-2, a tumor suppressor lncRNA, in combination with TMZ (Duan, Hao, Ren, Xue, & Qiao, 2021).

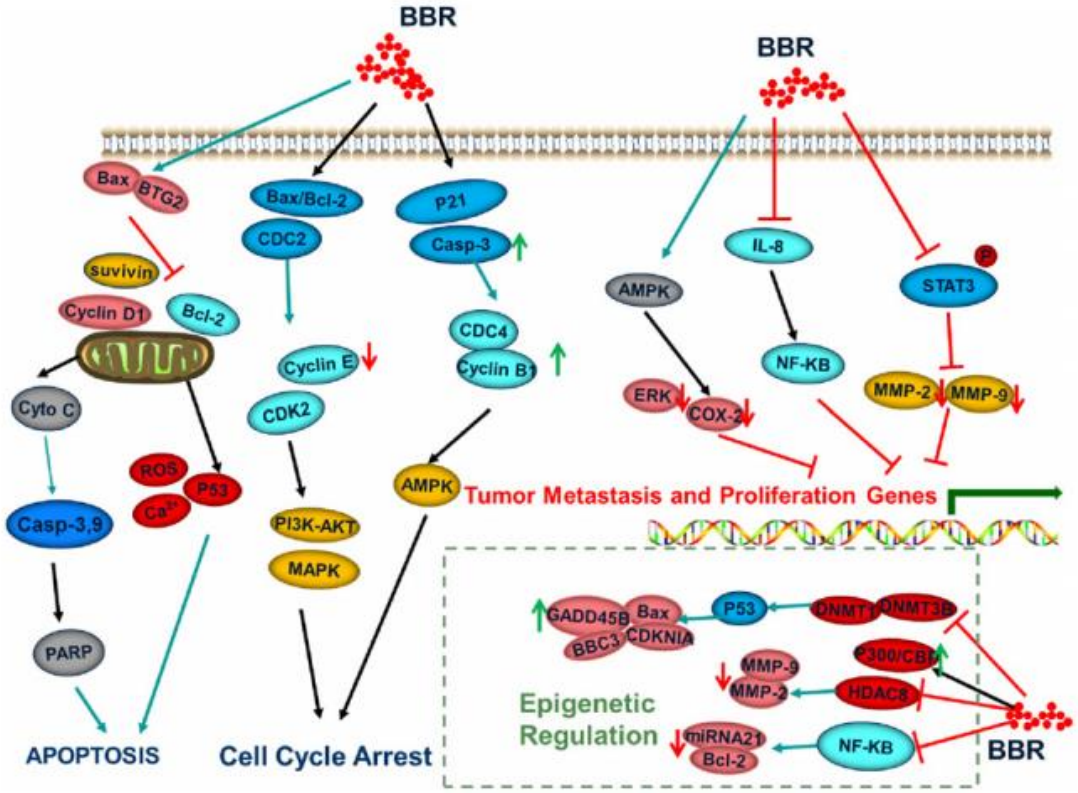

Figure 29. The signal transduction pathways of berberine (Liu et al., 2019).

2.3. *In-vitro* evaluation of the effectiveness of bioactive substances in cancer treatment

Several *in-vitro* methods have been developed to evaluate the effectiveness of bioactive substances in cancer treatment. In particular, an environment has been sought that can reflect the heterogenous tumor microenvironment one step closer in order to develop personalized therapies and better predict patient response. In modern precision medicine, 2D culture, organ-on-a-chip, spheroid and organoid creation in 3D cultures, 3D bioprint, and assembloid methods are developed by parcellating tissues taken from the patient. Since these methods have the characteristics of the tumor taken from the patient, it is foreseen that they protect the genetic background of the parental tumor and can be used in the development of personalized treatment, which is expected to reduce the use of experimental animals.

2.3.1. Two-dimension (2D) *In-vitro* Models

Two-dimension (2D) *in-vitro* techniques including wound healing, colony fomrayion assay and flow cytometric methods to detect apoptosis and cell cycle arrest can provide valuable information about the course of GBM and the response to therapy.

2.3.1.1. Wound Healing Assay

Wound healing (wound scratch) assay is an *in-vitro* method that symbolizes the cell-to-cell interaction, invasion, and migration abilities of cancer cells. What wound scratch assay *in-vitro* experiment provides in terms of cancer is that it allows comparing anti- and pro-migration properties of molecules (Vang Mouritzen, & Jenssen, 2018). In this method, cells seeded on culture plates are dosed according to the relevant experimental groups, and a monolayer scratch is drawn on the plate with a pipette tip. (Figure 30). As a result, the effect of molecules on the invasion and migration ability of cells is observed in an inverted microscope at certain time intervals according to the closure rate of the cell-free area in this scratch, and this area is calculated with the software to show cell migration rate (Bise, Kanade, Yin, & Huh, 2011). Since the control group is metastatic, there should be closure in the wound width, which should be suppressed in the treated group compared to it. There are various regulators, such as EMT, that drive this migration. EMT is a mechanism related to migration that shows epithelial cells gaining mesenchymal characteristics (Yarrow, Totsukawa, Charras, & Mitchison, 2005). By regulating such markers in processes, it is crucial to use anti-migrative compounds to reverse this wound-healing process in cancer.

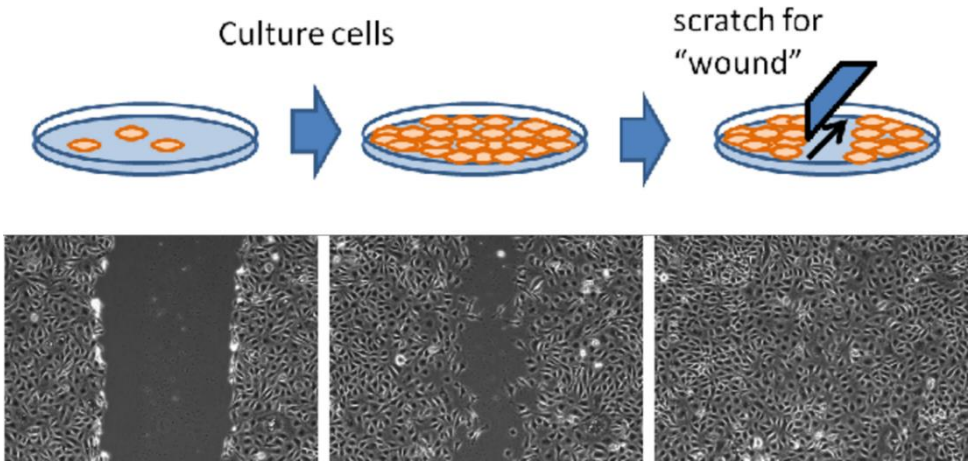

Figure 30. The workflow of wound scratch assay and wound closure over time (Bise et al., 2011).

2.3.1.2. Colony Formation Assay

The most important feature of cancer cells is their ability to divide uncontrollably. Colony formation assay (clonogenic assay) is an *in-vitro* assay based on the ability of a single cell to develop into a colony which is defined as consisting of at least 50 cells (Rajendran, & Jain, 2018). It was first used to assess how radiation affected cancer cell survival (Franken, Rodermond, Stap, Haveman, & van Bree, 2006). Many materials can be used as starting materials, including *in vitro*-derived mammalian cells and *ex-vivo* tissues (Brix, Samaga, Belka, Zitzelsberger, & Lauber, 2021). In *in-vitro* analysis, the dose of the molecule is given to cancer cells to test its adhesion-independent cell proliferation. The effects of the molecules called to suppress the uncontrolled growth of each cell in the population on the colony formation ability are examined with the help of staining (Figure 31). This effect is observed at least 10 days after the cells are seeded in culture plates in experimental groups containing the new agent prior to the staining (Franken et al., 2006). The results are statistically calculated and tablolized compared with the untreated control group. In conclusion, the effects of treatments on the ability of clonal expansion and unlimited proliferation capacity can be observed via colony formation assay.

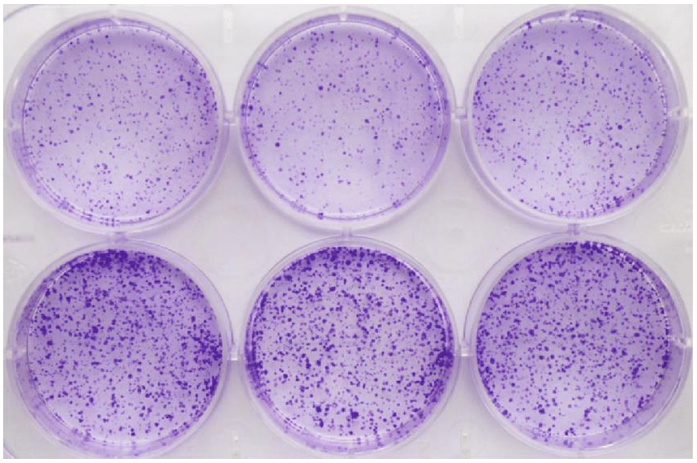

Figure 31. The different number of colonies in both control and treated group (Bai, Zhang, Li, & Zhang, 2017).

2.3.1.3. Apoptosis

It is known that cancer cells can escape the apoptotic pathway (Fernald, & Kurokawa, 2013). As mentioned in 2.1.3.2.3.3, one of the possible ways TMZ acts on cancer cells is via the MMR mechanism. The mismatched thymine created due to TMZ alkylation is detected and removed with a futile MMR cycle. Consequently, cells with strand breaks undergo apoptosis. This mechanism is found to be different in terms of dependency on p53 according to the properties of the cell (p53-WT or p53 mutant). If the cell is p53-WT, the p53-dependent pathway starts with upregulating p53 and casase-8 and continues with caspase-3 activation, eventually resulting in apoptosis (Figure 32). In the case of p3-mutant cells, the pathway is independent of p53 and starts with the downregulation of Bcl2 and Bcl2/Bax. In the further step, caspase-9 is upregulated, and at the end, cancer cells are triggered to undergo apoptosis via activation of caspase-3 as well (Figure 32). Even though cells obtaining different properties may lean on apoptosis in different pathways but end up with the same result, apoptosis (Roos et al., 2007).

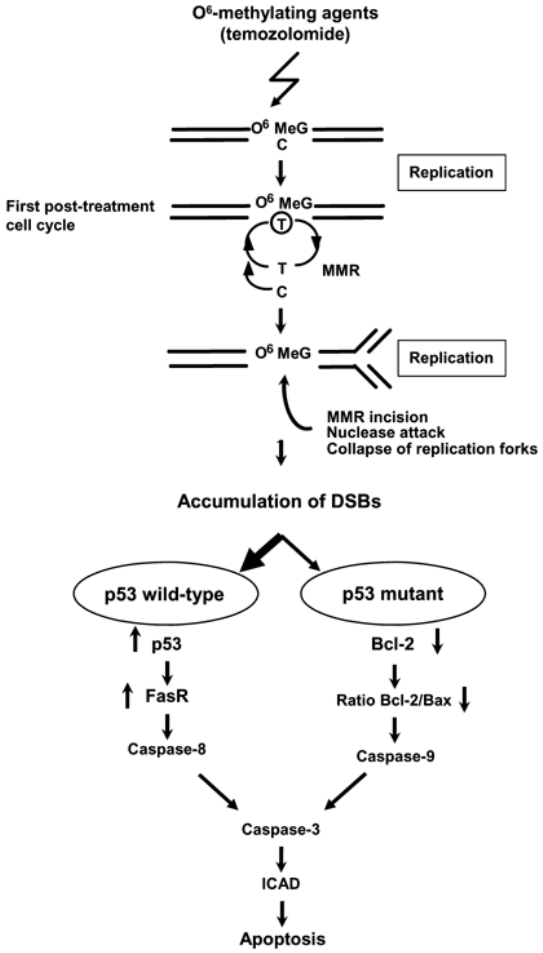

Figure 32. Recognition of the mismatch base created by TMZ by MMR and the tendency of the cell to apoptosis in a p53-dependent or independent way (Roos et al., 2007).

Accordingly, *in-vitro* analysis of cell death is a decisive process in new treatment and drug development studies. The induction of cancer cells by drug therapy to be viable, necrotic, early and late apoptotic (programmed cell death) can be determined morphologically by flow cytometric methods such as "Annexin V" and quantitatively by staining methods such as acridine orange/propidium iodide (AO/PI) (Ismail et al., 2014). However, necrotic deaths, which are not preferred for reasons such as scattering of cell contents, are also inevitable. As a result of the experiment, if the molecule leads to apoptosis, which causes cancer cells to die in a controlled manner without expelling their components, Annexin V binds to phosphatidylserine in outer surface of cells undergoing apoptosis and its fluorescent can be detected by the machine. This technique is a valuable tool for studying the effects of potential cancer treatments, such as natural flavonoids (Fan et al., 2019), cell-penetrating peptides

(Karpel-Massler et al., 2016), and other compounds (Ardi Putra, Setyabudi, Wijayanti, & Indah Budhy, 2022).

Acridine orange is a fluorophore that binds nucleic acid that preferentially stains all nucleated cells. When bound to dsDNA, it generates green fluorescence so does viable cells. On the other hand, propidium iodide binds ssDNA or RNA with poor membrane integrity and nonviable cells to fluoresce red in a rounded shape by binding. It is impermeable to living cells (Hou et al., 2015). Necrotic cells appear orange or red in a rounded shape of the cell, whereas viable cells are brilliant green, and their structure is well protected. Late apoptosis represents greenish-orange color inside the cells, whereas early apoptosis appears green but in horseshoe shape morphology (Ercelik et al., 2023). Based on the shape of the nuclei, AO/PI labeling enables the separation between necrotic and apoptotic cells. While necrotic cells have enlarged and damaged nuclei, apoptotic cells have condensed and disrupted nuclei (Anasamy et al., 2013).

2.3.1.4. Cell Cycle Arrest

The cell cycle method is a flow cytometric approach that is used in order to study proliferation and cell cycle of cancer cells. Flow cytometry determines the DNA content and each cell cycle phase with the help of PI staining. This approach can be used to investigate how different treatments affect cancer cells, such as how flavonoids block cell cycle progression and trigger apoptosis in cancer (Li, Cui, Cai, Wang, & Yao, 2005). The G0 phase is considered the resting phase for cells. The cell increases the number of organelles in the G1 phase, replicates its DNA in the S phase, and rearranges its contents in preparation for division in the G2 phase. After the transition to the M phase, the phase of mitosis and proliferation becomes inevitable (Gousias, Theocharous, & Simon, 2022). There are four checkpoints in cell cycle transitions: G1, intraS-phase, G2M, and spindle assembly (Figure 33). The regulation of transitions here is provided by the controls in the G1 phase, for example, whether the cell has reached a sufficient size and can go to cell division. In addition, controls for DNA damage are made in the G1 and S phases, and if any damage is observed, the cell cycle is stopped at that stage. There are also cyclins and cyclin-dependent kinases (CDKs) that regulate these checkpoints in the cell cycle (Gousias et al., 2022). These

molecules, which are specific to each stage of the cell cycle, work cooperatively and follow the state of the cell in the cycle. In drug development studies, at which stage the new molecule arrests the cell cycle, and its rate at each stage is presented as percentage data in the relevant devices after the experiments with cell cycle kits. To give an example, it can be said that if the drug treatment results in the arrest in the S phase, it may be an effective molecule in stopping the transition of cancer cells to the proliferative phase. In GBM, several clinical trials mainly target these regulatory molecules, CDKs. For instance, a clinical study (ClinicalTrials.gov ID NCT02345824) focused on the effectiveness of ribociclib, a CDK4/6 inhibitor, on GBM patients. Accordingly, it can also give an idea about the possible relationship of the drug with the molecules in a checkpoint control at these stages.

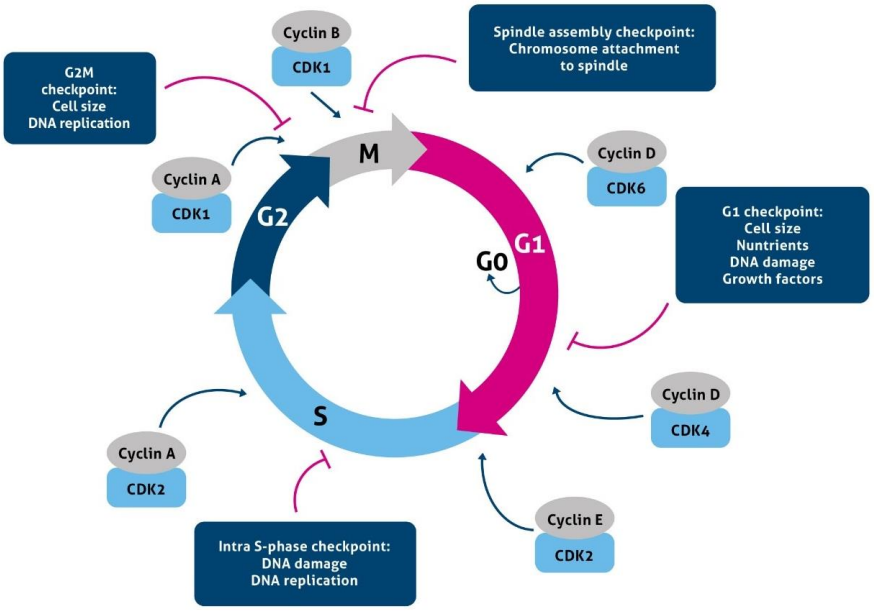

Figure 33. The regulation cell cycle in each phase (Ptglab.com).

2.3.2. Three-dimension (3D) Tumor Sphere Models

Analyses such as cytotoxicity, migration, colony formation, and cell death are fundamental and essential in cancer cells, and they are also methods that can be used in three-dimensional (3D) cultures. The reason why 3D culture models are preferred more than 2D is because they can better reflect the heterogeneous environment of cancer cells and represent the *in-vivo* environment with cell-to-extracellular matrix

interactions (Doh, Kwon, Ku, & Lee, 2019). Therefore, it is foreseen that it can allow the development of personalized, targeted therapies. 3D environment represents stem cell properties (Zhou et al., 2011). Generally, a spheroid comprises a necrotic core, an outer region of proliferating cells, and layers of intermediate layers of quiescent cells. Inside the spheroid has oxygen and food deprivation; for this reason, it better reflects the hypoxia environment as well (Bhattacharya, Calar, Evans, Petrasko, & de la Puente, 2020). 3D sphere or organoid structures can be obtained by using ultra-low attachment plates (Su et al., 2013) that prevent the cell from "adhering" to the bottom of the culture plate or by developing various protocols such as Matrigel (Gibbons et al., 2009) (Figure 34). With these 3D models, the effects of molecules on anti-tumor properties, such as reducing tumor size, can be examined (Al Matari, 2020). A flow-based approach has made it possible to quantify 3D tumor spheroids' mass density, size, and weight simply (Figure 35). It also allows the collection of live 3D tumor spheroids for post-analysis without endangering their viability (Bacchi et al., 2021). These analyzes are the first steps to identify the potential role of new molecules in cancer therapy. It needs to be supported by clinical studies so that it can be developed up to the stage of personalized treatment.

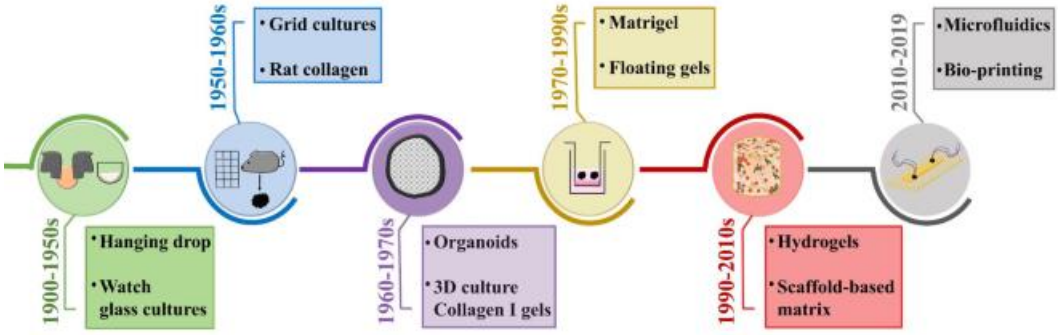

Figure 34. The chronological representation of 3D sphere formation methods over the years (Bhattacharya et al., 2020).

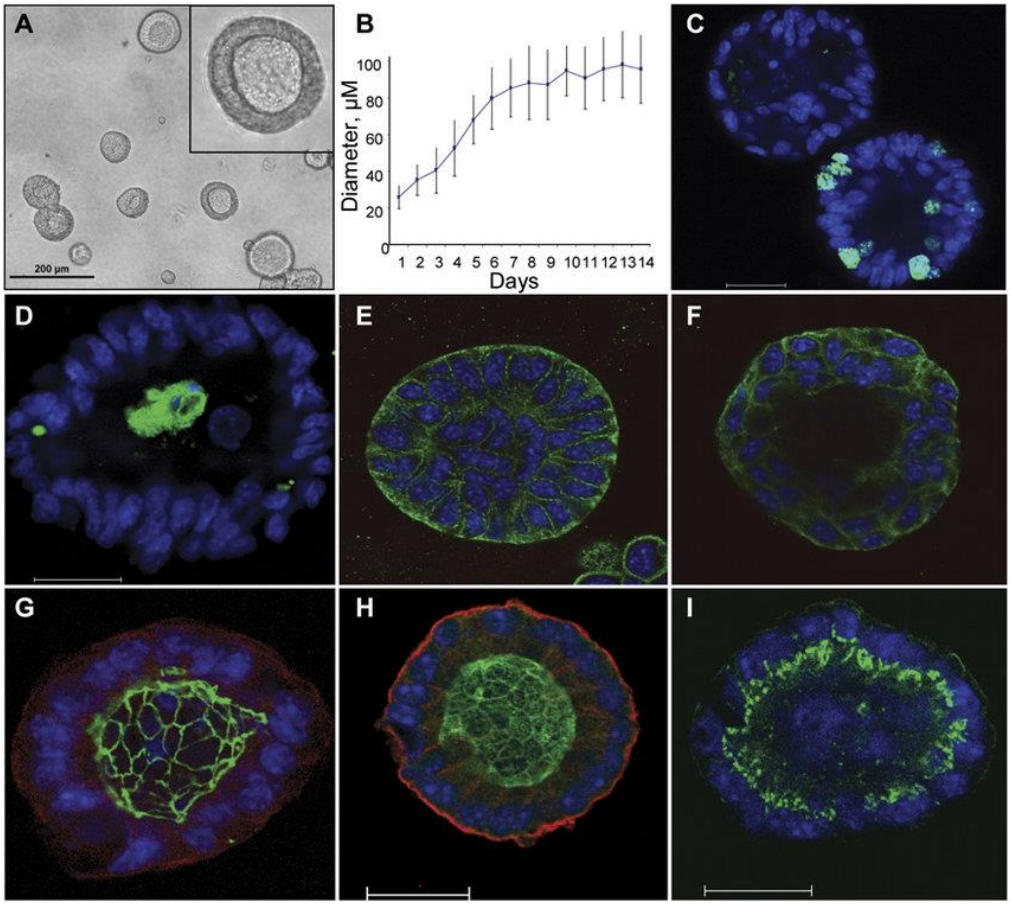

Figure 35. The formation of sphere models over time and the staining analysis of spheroid (Gibbons et al., 2009).

In the current thesis;

It is aimed to examine the effects of flavonoids (fisetin and berberine) in combination with TMZ on suppressing cell viability and reducing proliferation, killing cells apoptotically and arresting the cell cycle, on tumor aggressiveness (invasion, colony formation, and ability to reduce tumor size) under norm/hypoxia conditions in TMZ-resistant and non-resistant GBM cells. In addition, it was aimed to investigate the effects of tumor aggressiveness on invasion in norm/hypoxia conditions and the effects on MMR marker MSH2 and EMT marker MSH2, which have a role in drug resistance mechanisms, in TMZ-resistant T98G, TMZ-sensitive A172 and acquired TMZ-Resistant (A172-R) cell lines with acquired resistance. For this purpose, the effects of flavonoid, which is the most effective combination therapy candidate complementary to TMZ in GBM treatment,

1) on hypoxia-inducible tumor aggressiveness and drug resistance mechanisms,

2) on the presence of ZEB1 markers associated with drug resistance,

3) on the presence of MSH2 gene in MMR mechanism, which is very important in drug resistance,

4) on validation the relevant mechanisms in primary brain tumors.

3. MATERIAL AND METHODS

3.1. Materials

3.1.1. Used Equipment

NGK Class II Biosafety Laminar flow cabinet (Tissue culture hood) (Nükleon, Türkiye)

CO_2 Incubator (Nuve, Türkiye)

xCELLigence system (RTCA DP, Agilent Technologies, Santa Clara, CA, USA)

Centrifuge (Nuve, Türkiye)

Refrigerated Centrifuges (Beckman Coulter, USA)

Refrigerated Centrifuges (Labogene, Denmark)

Microcentrifuges (Cleaver Scientific, England)

Vortex (VELP Scientifica, Italy)

Vortex (Biosan, Lethonia)

-150°C freezer (Panasonic, Japan)

-80°C freezer (Panasonic, Japan)

-80°C freezer (Nuve, Türkiye)

-20°C freezer (Bosch, Türkiye)

-20°C freezer (Ugur, Türkiye)

+4°C freezer (Alaska, Türkiye)

Mr. Frosty™ Freezing Container (Thermo Fisher Scientific, USA)

Thermo-Shaker (Biosan, Latvia)

UV/Vis Spectrophotometer (Beckman Coulter, USA)

Maestro Nano Micro-Volume spectrophotometer (Maestrogen Inc., Las Vegas, NV)

Allegra® X-30 Series Benchtop centrifuge (Beckman Coulter, USA)

Heater Block (Techne, England)

Sensitive weighing machine (AND, Japan)

Profilex PCR System (Thermo Fisher Scientific, USA)

Thermal Cycler (Biorad, USA)

Step One Plus System Real Time PCR (Applied Biosystem, USA)

Light Microscope (Olympus, Japan)

Inverted Microscope (Labomed, USA)

EVOS™ M5000 Cell Imaging System (Thermo Fisher Scientific, USA)

Muse® Cell Analyzer (Merck Millipore, Germany)

C100 Automated Cell Counter (RWD Life Science, USA)

E-plate (Elips, Türkiye)

Cell scraper, handle 220mm, handle 13mm (Genesuz, Türkiye)

Multipipetor (Boeco, Germany)

Pipet Controler (Acumax, India)

0.5-10 µl Pipette (BrandTech Scientific, England)

10-100 µl Pipette (BrandTech Scientific, England)

20-200 µl Pipette (BrandTech Scientific, England)

100-1000 µl Pipette (BrandTech Scientific, England)

3.1.2. Used Materials

Dulbecco's modification of Eagle medium (DMEM-F12) (Sigma Aldrich, USA)

Fetal Bovine Serum (FBS) (Biological Industries, USA)

Phosphate Buffered Saline (PBS) (Sigma Aldrich, USA)

Sodium Pyruvate (Merck Biochom, Germany)

Penicillin-Streptomycin (Gibco, Thermo Fisher Scientific, USA)

Tripsin EDTA (0.25%) (Gibco, Thermo Fisher Scientific, USA)

Temozolomide (Sigma Aldrich, USA)

Fisetin (Tokyo Chemical Industry, USA)

Berberine (Tokyo Chemical Industry, USA)

Dimethyl sulfoxide (DMSO) (Sigma Aldrich, USA)

PerkinElmer CellCarrier Spheroid (Thermo Fisher Scientific, USA)

Annexin V Apoptosis Detection Kit FITC (Invitrogen ™, USA)

CellMAXTM Colonogenic Assay Kit (BioPioneer, USA)

Acridine orange (AO) and Propidium iodide (PI) (Sigma-Aldrich, USA)

95% Ethanol (Sigma Aldrich, USA)

Chloroform (Sigma Aldrich, USA)

Isopropanol (Sigma Aldrich, USA)

Zymo RNA Isolation Kit (Zymo Research, USA)

TRIzol^{TM} Reagent (Invitrogen™, USA)

cDNA Synthesis Kit (ProtoScript, UK)

SYBR Green I Master Mix (GoTaq, USA)

3.2. Methods

3.2.1. Clinical Samples and Ethics Statement

High-grade primary brain tumors to be used in the project were obtained from surgical operations performed by Bursa Uludag University (BUU) Neurosurgery Department. Retrospective evaluations were made in 3 high-grade primary brain tumor cells, which were evaluated by a qualified pathologist and approved with Ethics Committee no: 2023-3/43 by the Ethics Committee of the Faculty of Medicine of the BUU. The proliferation of the clinical samples in the cell culture was successfully optimized, as stated below (3.2.2.1).

3.2.2. Cell Lines Used in the Study

Human GBM cell lines planned to be studied in our project were T98G (TMZ resistant), A172 (TMZ non-resistant), A172-R (A172-R cell line, which had acquired resistance due to long-term TMZ exposure in A172 cell line) and L929 cell line to be used as healthy control. Cell lines obtained from cryotubes kept at -152 ˚C freezer in the stocks of Department of Medical Biology at BUU.

Table 4. Panel of tumor characteristics of two GBM cell lines; A172 and T98G (Modified data obtained from cellosaurus.org and atcc.org)

Name	Tumor Source	Histology	Mutant Gene	Gene Sequence	TMZ
A172	Primary (53-year-old, male patient)	GBM	CDKN2A (ATCC) PTEN (ATCC)	c.1_471del471 c.165_1212del1048	**Sensitive (Lee et al., 2016)**
T98G	Primary (61-year-old, male patient)	GBM	CDKN2A (ATCC) PTEN (Cellosaurus) TP53 (Cellosaurus) MGMT-positive (Wang, Chen, Liu, You, & Mao, 2013)	c.1_471del471 p.Leu42Arg (c.125T>G) p.Met237Ile (c.711G>T)	**Resistant (Lee et al., 2016)**

Cell lines were originally derived from cells arising from primary cell cultures (Table 4). T98G is a multinucleated, round-shaped, adherent GBM cell line with fibroblast-like morphology (Figure 36) obtained from a 61-year-old male patient

(Table 4) (Kiseleva, Kartashev, Vartanyan, Pinevich, & Samoilovich, 2016). T98G is a cell line consistently considered as intrinsic (natural) TMZ-resistant in various studies (Lee et al., 2016). T98G is characterized by parameters such as the upregulation of hypoxia, VEGF and downregulated p53 (Figure 37). T98G is known as p53 mutant, PTEN mutant and MGMT-positive (Wang et al., 2013) and the p53 value is found to help to predict sensitivity status and response to TMZ (Hermisson et al., 2005). The effective dose (IC50) of TMZ in T98G cells varies up to 1,585 μmol/L (Alonso, Gomez-Manzano, Bekele, Yung, & Fueyo, 2007).

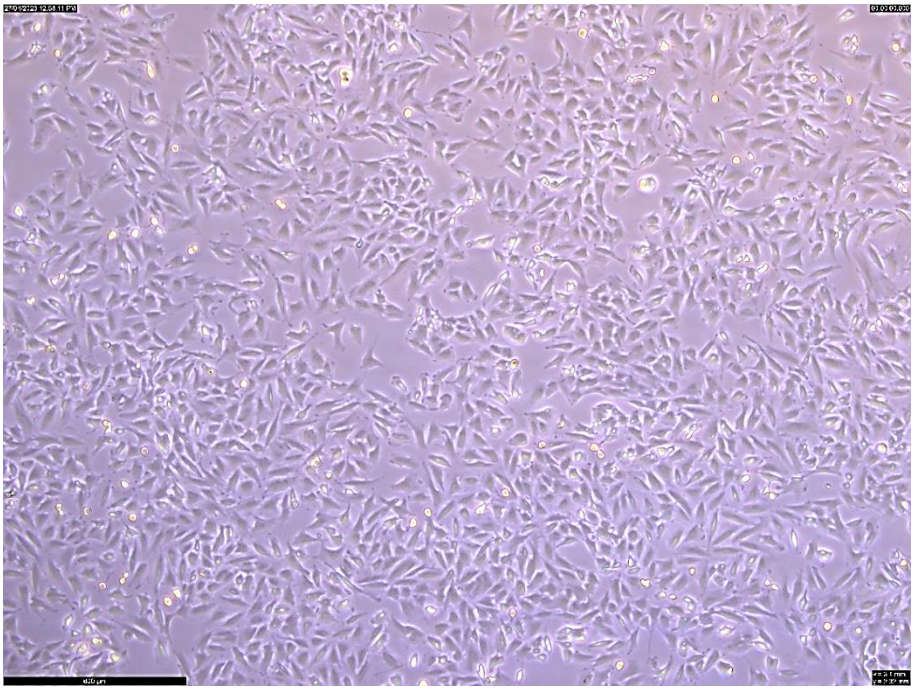

Figure 36. Microscopic representation of the T98G morphology at 4X objective.

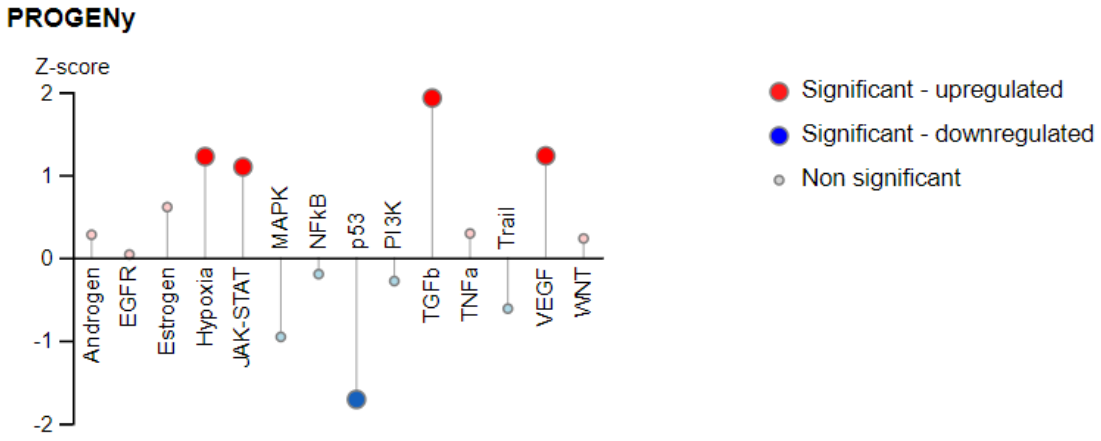

Figure 37. The expression pattern of T98G (Proteinatlas.org).

A172 is multinucleated fibroblast-like but its morphology is more spindle-shaped (Figure 38). Unlike T98G, A172 is bearing wild type p53 while being CDKN2A and PTEN mutated (Table 4). According to ProteinAtlas, A172 has TGF-β upregulation (Figure 39). A172 is also widely used in GBM studies due to its sensitivity to TMZ (Soni, Adhikari, Lin, Sherman, & Keidar, 2022).

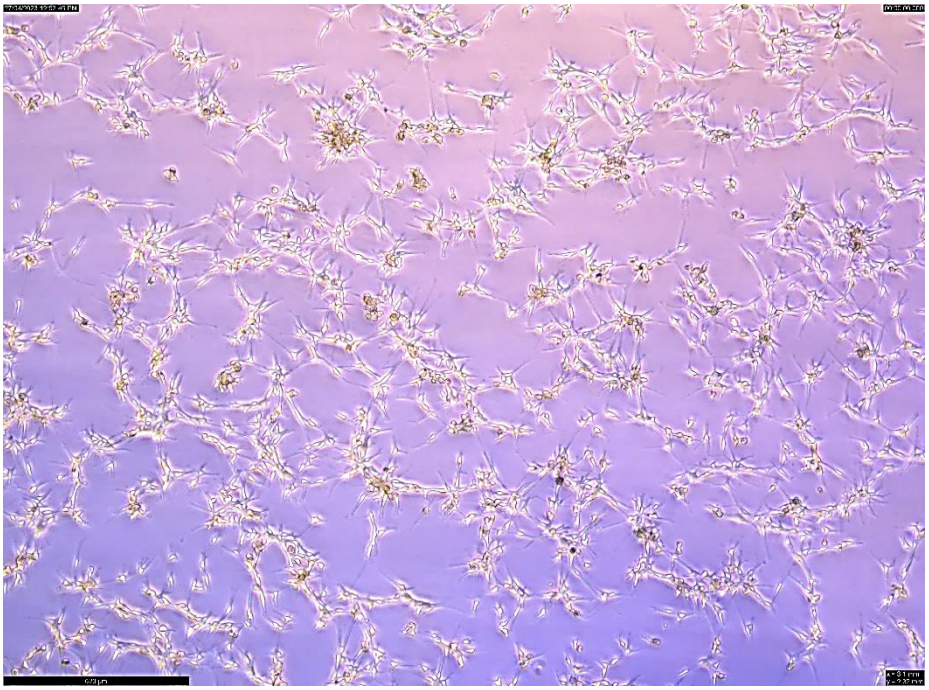

Figure 38. Microscopic representation of the A172 morphology at 4X objective.

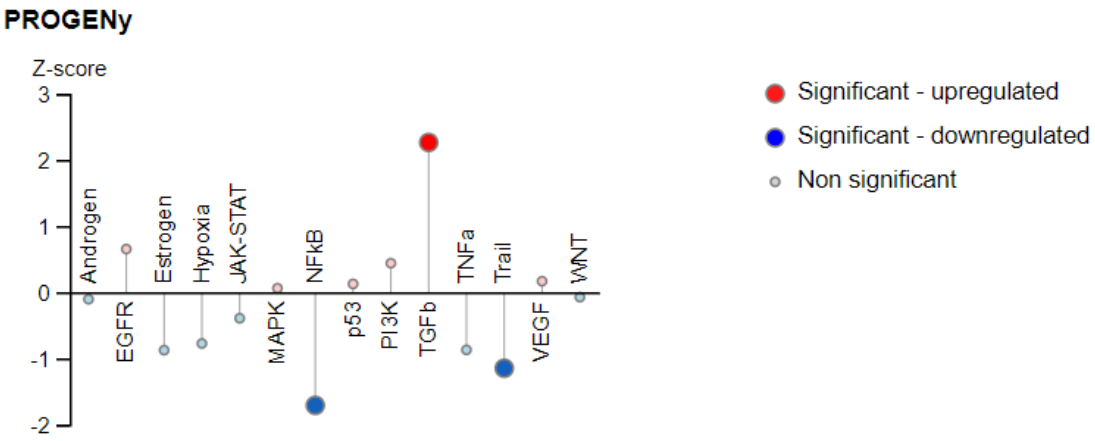

Figure 39. The expression pattern of A172 (Proteinatlas.org).

L929 is an adherent mouse fibroblast cell line (Figure 40). The fibroblast morphology of L929 is similar to A172 and T98G, and it has been determined in the

literature to be biocompatibility with GBM cells as a non-tumorigenic healthy fibroblast cell. Accordingly, U373-MG (Wiranowska et al., 2010) and T98G (Applause, 2022) are used L929 as control in their studies.

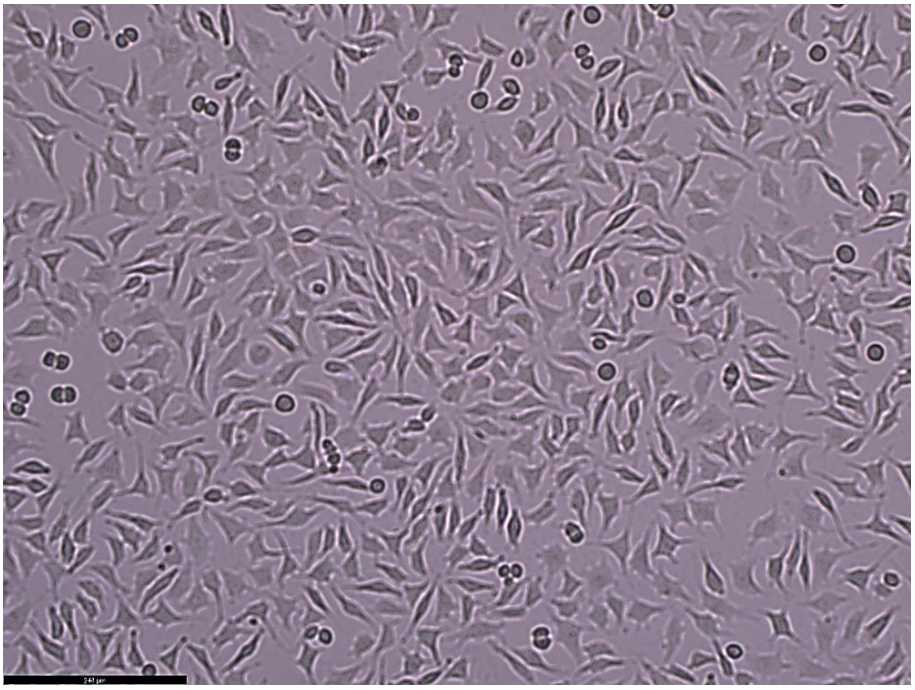

Figure 40. Microscopic representation of the L929 morphology at 4X objective.

3.2.2.1. Cell Culture and Propagation of Cells

Human GBM cell lines (A172, A172-R, T98G and L929) were stored in cell culture medium in an incubator at 37˚C and 5% CO_2 for normoxic conditions. Cell lines were cultured and proliferated in Dulbecco's Modified Eagle's Medium-F12 (DMEM-F12) standard cell culture medium containing 10% fetal bovine serum (FBS), 1% Antibiotic/Antimycotic solution, 1 mM sodium pyruvate and 2 mM L-glutamine. In the experiments, cell stocks of less than 25^{th} passages were used from cell lines stored in the cryotube at -152°C.

Initially, the frozen cells in the cryotube were expected to dissolve well in the 50 mL falcon containing sufficient water. It was agitated gently until thawed. Then, the cells were transferred to 15 mL falcon containing 1000 µL of DMEM-F12 with the help of a sterile pipette and centrifuged at 1200 x g for 5 minutes. After getting rid of the supernatant, 1000 µL DMEM-F12 was added to the pellet and mixed thoroughly. Cells were finally seeded into 25 cm^2 culture plates (T25) with the help of a serological

pipette. Cells grown in culture plates were observed with a microscope at desired times.

3.2.2.2. Passage of Cells

The cells in the culture plates were passaged by changing the medium (approximately every 3 days) if the cell density increased and the plate surface became 70% full. In cases where more cells were required, medium (T75) and large (T175) sized plates were used.

In the first step of passaging, the medium of the cells was removed and washed gently with phosphate-buffered saline (PBS). After getting rid of PBS, the harvesting and detachment of the adherent cells from the flask were achieved by adding 0,25% trypsin. After 5 minutes, DMEM-F12 was added onto trypsin in 2:1 rate (media:trypsin) to stop the trypsinization reaction due to its ability to inhibit the effect of trypsin (For instance, if the volume of the trypsin was 4 mL, the required volume of DMEM-F12 was 8 mL). The cells were transferred to 15- or 50-mL falcon and then, centrifuged at 1200 x g for 5 minutes. The supernatant was subsequently removed. 1000 µL of DMEM-F12 was added into a falcon and mixed properly. The mixture was transferred further to the desired flask to adjust the required cell concentration.

3.2.2.3. Cryopreservation of Cells

In the initial step of cell stocking, the pellet was created using the same method mentioned above (3.2.2.2). However, instead of 1000 µL DMEM-F12, 900 µL DMEM-F12 was added to the cell suspension which was pelleted during the passaging process. Cells were mixed by pipetting up and down and transferred into a cryotube. Later on, 100 µL dimethyl sulfoxide (DMSO) was added to the cryotube. Cells were taken from room temperature to Mr. Frosty™ Freezing Container placed at -80°C freezer which provides graded refrigerating. Cells, then, were taken to a -152°C freezer within one day and stored for the required period of time.

3.2.2.4. Counting of Cells

To begin counting cells, two different methods were used. In both methods, the step was continued from the stage where cell pipetting was done with 1000 µL DMEM-F12 (see 3.2.2.2).

3.2.2.4.1. Thoma Haemocytometer Cell Counting Chamber

Thoma haemocytometer cell counting chamber consists of 16 squares with a center square of 1 mm^2 (Figure 41). 100 µL from the cell in the falcon and 100 µL fresh DMEM-F12 were put into a new cell-free Eppendorf tube. The mixture was pipetted well. Furthermore, 100 µL of the mixture was loaded between the chamber's surface and coverslip by lifting upper coverslip very carefully. The sanitization of the chamber was done by cleaning with alcohol before using and after each counting. The number of cells in the first four grid-lined squares were counted manually in the inverted microscope (Labomed, USA) at 10X objective. This counted number of cells was multiplied by 4 for the total cell number in the 16 wells. The dilution factor was found by the division of final volume and sample volume (200 µL/100 µL) which results in 2. The calculation in order to find total cell number was completed as shown in equation below.

$$\text{Total Cell Number (cells/mL)} = \text{The Counted Cell Number} \times 4 \times 2 \times 10^4$$

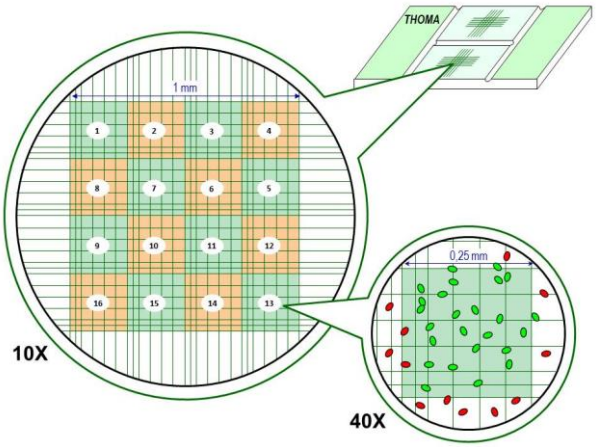

Figure 41. Thoma haemocytometer cell counting chamber and representation of cells in gridlines (Insilico.ehu.eus).

3.2.2.4.2. Automated Cell Counter

At the end of the passage, 10 µL of cells was taken from the falcon to which 1000 µL DMEM-F12 was added, and loaded onto the disposable slide slowly, taking care not to form bubbles, and added to the relevant compartment of the cell counting device. Due to its fluorescence capabilities, the software analyzes cells and recognizes between live and dead cells accurately. In general, the number of live and dead cells was counted but only live cells were taken into account as the total number of cells (Figure 42).

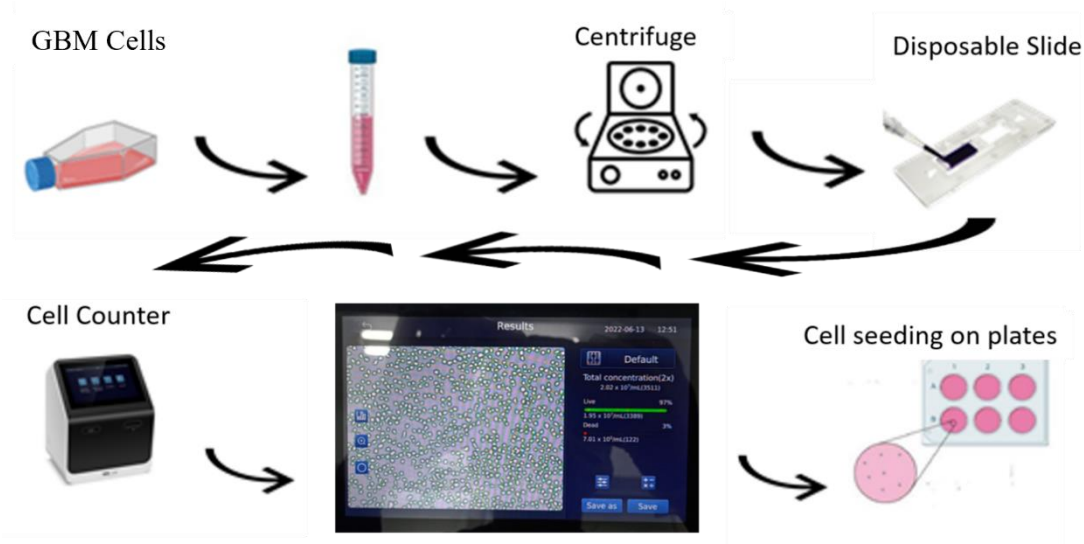

Figure 42. Experimental steps of counting optimized number of cells for the experiment via RWD Cell Counter system.

3.2.3. Preparation of Pharmaceutical Stocks

Temozolomide ($C_6H_6N_6O_2$) (Molecular Weight: 194.15 g/mol) was provided from Sigma-Aldrich in lyophilized form (CAS Registry Number:85622-93-1, Product Number: T2577). It was dissolved in 10 mg/ml DMSO as suggested from the firm. All of the aliquoted stock drug solutions were stored at -20°C until the experiment.

Fisetin (3,3′,4′,7-tetrahydroxyflavone) (Molecular Weight: 286.24 g/mol) was purchased from Tokyo Chemical Industry (TCI) in crystalline solid powder form (CAS Registry Number: 528-48-3, Product Number: T0121). It was dissolved in 57 mg/mL

(199.13 mM) DMSO at 25°C. Solutions were stored at -20°C freezer prior to the experiment.

Berberine (5,6-dihydro-9,10-dimetoksibenzo[g]-1,3-benzodiokolo[5,6-a] quinolizinium) (Molecular Weight: 371.82 g/mol) was purchased from TCI in solid physical state (CAS Registry Number: 141433-60-5, Product Number: B0450). It was dissolved in 22.5 mg/mL (66.89 mM) DMSO 25°C and stored at -20°C freezer. To achieve this dilution from stock solutions, calculations were made in Molarity Calculator section of GraphPad website. All of the intermediate stocks of compounds were diluted with DMEM-F12 with the calculated amounts shown in Figure 43 and kept at -20°C freezer likewise main stocks.

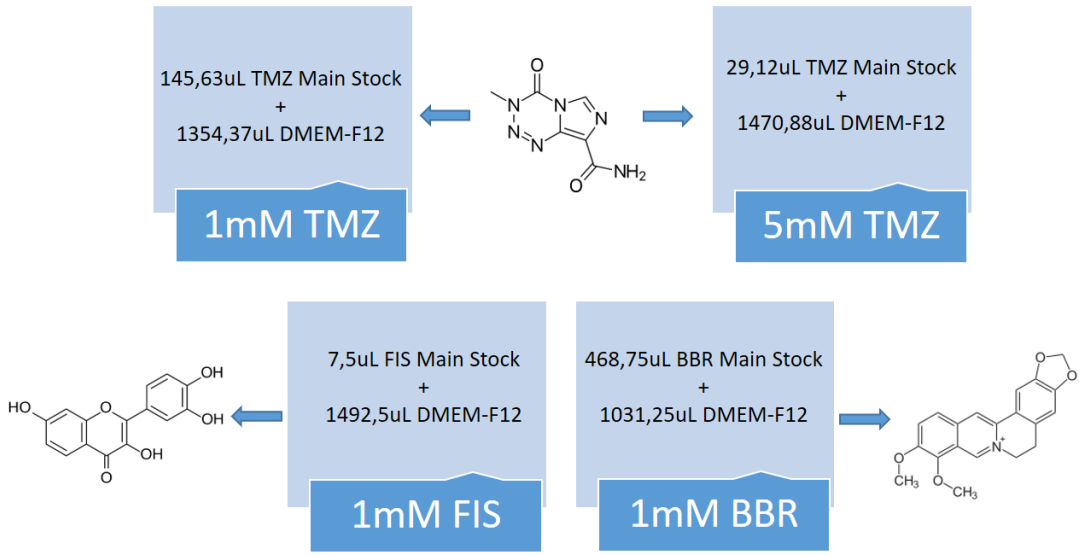

Figure 43. Preparation of drug intermediate stocks of TMZ, Fisetin (FIS) and Berberine (BBR).

3.2.4. Cell Viability

For *in-vitro* cell viability, xCELLigence high-technology with a non-invasive electrical impedance monitoring technique that uses the RTCA (Real Time Cell Analyzer) biosensor system on E-plates was used. Cell proliferation was determined by making real-time measurements with E-plates consists of 1x16-well format with high-density gold electrode arrays on the specially designed base under each well. After the 16-well E-plate layout was created according to experimental design, initially, 100 µL of DMEM-F12 was added per well and E-plate was introduced to the

system by being tareed by placing it in the device connected to the RTCA software on the computer in the incubator. With subsequent calculations (see 3.2.2.4), 100 µL of DMEM-F12 containing $15x10^3$ cells per well was added to the wells. With the xCELLigence system, real-time measurement tracking can be performed at desired intervals (Figure 44). After 24 hours (24h) awaiting cell attachment and log-phase in the curve, appropriate dosing was done according to the experimental setup. Experiments were performed in triplicates for each dose. Then, the change in cell proliferation was established in real-time by measurements made every 5 minutes to evaluate the effective dose of TMZ and flavonoid concentrations during the incubation period determined in the GBM cells xCELLigence system.

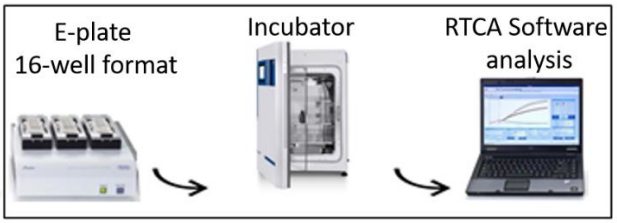

Figure 44. Cell proliferation analysis with the xCELLigence system.

3.2.4.1. Determination of IC50 Doses for TMZ, Fisetin and Berberine

15,000 cells/100 µL GBM cells were seeded into a 16-well E-plate and exposed to increasing dose concentrations of TMZ and flavonoids in 3 replicates in the xCELLigence system. The cell growth curve was obtained by measuring cell growth every 5 minutes for 72h via sensors built into the E-plate bottom layer. Thus, the half-maximal inhibitory concentration (IC50) of the compounds, which reduces cell proliferation by approximately 50%, the effective dose and incubation time were determined. With the results obtained with xCELLigence, the IC50 values were calculated using GraphPad Prism 8.0 software. To sum up, the change in cell proliferation was determined by exposure to different combinations of flavonoids and TMZ concentrations whose effective doses were evaluated by xCELLigence system analysis.

3.2.4.2. Detection of Antagonistic-Synergistic Effects

If the combined effect of two drugs (TMZ and flavonoid) was greater than the sum of the effects when these drugs were used separately, it was considered as "synergistic effect", and if the effect between the two drugs was equal to the effect of using them individually, then, it was considered as "additive effect". However, if the use of the two drugs in combination created less effect than the use of the drugs separately, the effect between these two drugs was considered as antagonist. The synergistic, additive, or antagonistic effects of flavonoids with TMZ were determined using the SynergyFinder web application (version 2.0) (Figure 45). These effects were calculated by the synergy score revealed in the program used. (Synergy score<-10, antagonist; -10< synergy score <10, additive; synergy score>10 represents synergistic effect, respectively). In the SynergyFinder web application, which is used for drug combinations, the model is automatically calculated with the mathematical model by the program, without relying on any additional statistical method (Ianevski, Giri, & Aittokallio, 2022).

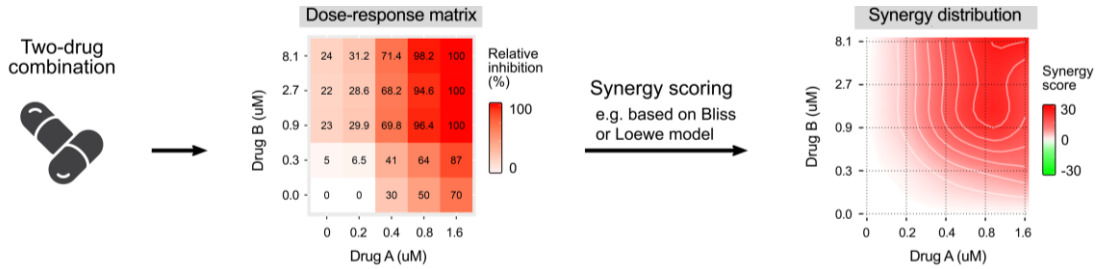

Figure 45. Flow chart of SynergyFinder web application in two-drug combination (Synergyfinder.fimm.fi).

3.2.5. Establishment of acquired TMZ resistance in the TMZ-non-resistant cell line (A172)

The A172 cell line known to be susceptible to TMZ was used to generate acquired TMZ-resistant cell lines (A172-R). In order to establish resistance, two different methodologies were modified (Lee, Ko, Joe, Kang, & Hong, 2011; St-Coeur, Poitras, Cuperlovic-Culf, Touaibia, & Morin, 2015), and adapted taking into account the doses determined in 3.2.4. This study was designed to assess the acquired TMZ

resistance with consecutive TMZ exposure for a long period of time (Figure 46). Observations were made up to the IC50 dose of 900 μmol/L TMZ (Ercelik et al., 2023), which was the IC50 dose in A172 determined by our team in their previous studies, and sensitive cells were allowed to gain resistance to this dose.

In the TMZ dose escalation method for acquired resistance, A172 cells (150,000 cells/well) were seeded into a 6-well plate with 3 replications. It was dosed 24h after seeding, after ensuring the cells adhered to the layer. Cells were initially treated with 100 μmol/L TMZ two days a week for two weeks. The TMZ drug was applied dropwise without damaging the cells on the plate surface and without the pipette tip touching the ground. The plates were shaken manually for one minute to ensure that the applied drug was evenly distributed in the well. One week after every 2-3 weeks of dosing, cells were allowed to proliferate without dosing only on TMZ-free media. When yellowish color was observed in the medium of the cells, fresh medium was provided to the cells approximately every 3 days and observed under an inverted microscope. Afterwards, the TMZ dosage delivered to cells that reach 70% confluence was stepwise increased to 100, 200, 350, 450, 550, 750 and 900 μmol/L every 2-3 weeks (or when cells become resistant to this dosage) (Figure 46). In the end, cells that survive and proliferate during this chronic treatment period were referred to as A172-900-R (A172-R). Cells that did not reach 70% confluence in the plates for 4 weeks were excluded from the experiment.

The response of sublines expressed as A172-R, obtained through experiments during approximately 18 months, to TMZ was studied in real time with the xCELLigence system. The validation of the resistance method, which was planned to be developed in the A172 cell line, was achieved in the cell proliferation test xCELLigence system using 16-well E-plates, and the invasion ability from functional analyzes was achieved by the wound healing method. Acquired resistant cells that were not treated with TMZ were used as a control group.

Initially, cells cultivated in a 6-well plate were inoculated into the E-plate after a long treatment of dose of 350 μmol/L TMZ and 35,000 cells per well. When the effect on this cell death was shown by xCELLigence that the cells did not cause death to the TMZ dose, it was determined as for example, A172-350-R which was resistant to the 350 μmol/L TMZ dose. The same procedure was repeated for each dose

(350, 450, 550, 750 and 900 µmol/L) when mortality was observed to decrease as a result of long-term treatment of the respective TMZ dose. Once the cells were expected to gain resistance at 900 µmol/L TMZ, 70% confluence was achieved. Then the 6-well plate and E-plate were treated with A172 IC50 doses TMZ, Fisetin and TMZ+Fisetin.

In the 6-well plate planned with the number of groups suitable for the experimental setup, the middle of each well of the A172 cell lines, grown in a single layer up to 80% fill for 24h, was drawn vertically with 10 µL pipette tips. After removing the cell debris from the plates with 1XPBS, the cells were incubated by adding 2 mL of the medium. The closure of the gaps that occurred along these scratches represented wound healing and the invasion ability of the cells. After selecting the appropriate areas to take pictures of the scratches, images were taken at desired times (0h, 6h, 24h) under the inverted microscope. It was measured using NIH ImageJ software version 1.52a. The effect of the cell line, which developed resistance in the experiment, to increase the invasion was analyzed via wound scratch assay. Experiments were carried out in 3 repetitions.

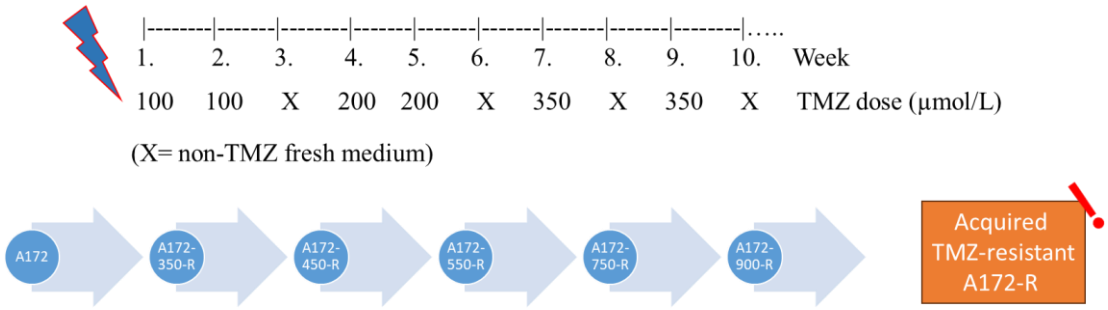

Figure 46. Dose escalation method to develop acquired TMZ resistant cell line from sensitive parental strain (X= non-TMZ fresh medium).

3.2.6. Determination of the Efficacy of Molecules on Cell Biological Behaviors in the GBM Cell Line

The effect of the treatment with IC50 values of TMZ, Fisetin and Berberine on cell biological behaviours including apoptosis and cell cycle were investigated with flow cytometric methods in TMZ-resistant T98G and TMZ -sensitive A172 cell line**.**

3.2.6.1. Investigation of Effects on Apoptosis

Muse™ Annexin V & Dead Cell kit was used to evaluate the effects of complementary therapy on apoptosis and early and late apoptotic rates in T98G cell lines. $1x10^5$ T98G cells/2mL cells were seeded in a 6-well culture plate. When seeding into the culture dish, care was taken to seed the cells equally in each well and ensure that the cells were spaced apart. Cells were expected to adhere to the plate within a 24-hour incubation period in a 37°C incubator containing 5% CO_2. The next day, cells attached to the surface of the culture plate were treated with flavonoids and TMZ for 24h according to plate setup (Figure 47). Muse™ Annexin V & Dead Cell Reagent was kept in the dark at room temperature prior to staining experimentation. After that, at the end of the incubation period, each medium of wells was transferred into its own new 1.5 mL Eppendorf for further analysis. Since it was a cell death experiment, it was essential not to lose the cells that were floating in the media. Cells were scraped off and dislodged from their culture plate via cell scraper by rotating the plate manually. Experimental groups were again inhibited with their own medium collected before and transferred to the same labeled eppendorfs. Centrifugation was done for 5 minutes at 1200 x g in an Allegra® X-30 Series Benchtop centrifuge (Beckman Coulter). Later on, extra attention was paid to the blurry-looking pellet sticking to the bottom corner of Eppendorf due to centrifugal force. In the washing step, the supernatant was withdrawn, 1000 µL of PBS was added to the cells and centrifuged again at the same settings. 100 µL of Muse™ Annexin V & Dead Cell Reagent was added to the cells washed with 100 µL of PBS to provide cell suspension. Then, the mixture was vortexed directly at medium speed for 5 seconds. Cells were incubated for 20 minutes at room temperature in a dark place protected from light. Furthermore, measurements were made in Muse® Cell Analyzer (Merck Millipore, Germany). Each analysis step was performed in at least three repetitions (Figure 48).

a)

Control 2mL DMEM-F12	400µL TMZ + 1600µL DMEM-F12	32,8µL Fisetin + 1967,2µL DMEM-F12
400µL TMZ+ 32,8µL Fisetin+ 1567,2 uL DMEM-F12	Control 2mL DMEM-F12	Control 2mL DMEM-F12

b)

Control 2mL DMEM-F12	400µL TMZ + 1600µL DMEM-F12	227uL Berberine + 1773uL DMEM-F12
400 uL TMZ + 227 uL Berberine + 1373 uL DMEM-F12	Control 2mL DMEM-F12	Control 2mL DMEM-F12

Figure 47. The 6-well culture plate design for Annexin V according to IC50 values of a) TMZ and fisetin b) TMZ and berberine in T98G.

Figure 48. The summary of the Annexin V experiment (Modified from Merckmillipore.com).

3.2.6.2. Morphological Analysis of Cell Viability with Acridine Orange/Propidium Iodide (AO/PI)

T98G and A172 cells were seeded in a 24-well culture dish at $1x10^5$ cells per well and kept for one day in a CO_2 incubator. Later on, experimental groups were treated according to the IC50 values of each compound (Figure 49). After 24 hours, prior to the cell staining, Acridine Orange/Propidium Iodide (AO/PI) mixture was prepared by adding 1XPBS. Then, the DMEM-F12 medium of the cells was withdrawn and 90 µL 1XPBS was added to cells followed by the addition of 10 µL AO/PI dye. After 5 minutes, the photos of morphological changes caused by treatments were taken in EVOS Cell Imaging System (Thermo Fisher Scientific, Waltham, MA) (Figure 50). The quantification analysis of necrotic cells, PI was made via HALO Artificial Intelligence (HALO AI) software (Indica Lab).

A172 Control	A172 TMZ (900µM)	A172 FIS (13,78µM)	A172 TMZ+FIS (900µM+13,78µM)		
T98G Control	T98G TMZ (900µM)	T98G FIS (13,78µM)	T98G TMZ+FIS (900µM+13,78µM)		

Figure 49. Experimental 24-well culture plate design representing experimental groups.

Figure 50. The representation of AO/PI morphological analysis with EVOS Cell Imaging System (Created with Biorender.com).

3.2.6.3. Examining the Effects on Cell Cycle

The Muse Cell Cycle Kit (Millipore) was used to determine the cell cycle arresting effects of flavonoids and TMZ in T98G and A172 cells. Cells were seeded in a 6-well culture dish at $1x10^5$ cells per well and after making sure that the cells were attached within 24h, the medium from the first well was withdrawn first and subsequently continued to treat. The IC50 doses of flavonoids were processed alone or in combination with an effective dose of TMZ according to the plate order below (Figure 51-52). Initially, DMEM-F12s of all wells were withdrawn and 500 µL 0.25% trypsin was added to each. After the cells were kept in an oven for 2 minutes, they were inhibited by placing 1000 µL of DMEM-F12 on them. Cells were transferred to labeled 1.5 mL eppendorfs and centrifuged at 1200 x g for 5 minutes in an Allegra® X-30 Series Benchtop centrifuge (Beckman Coulter). The supernatant was then carefully removed with a pipette. Cells were washed by adding 1000 µL of 1XPBS to each eppendorf. Centrifugation was performed at 300 x g for 3 minutes. Supernatant was discarded again, paying close attention to the pellet. Cells were then washed with 1000 µL of ice-cold 70% ethanol, respectively, and stained according to the protocol. Ethanol-fixed cells, respectively, were centrifuged at 300 x g for 3 minutes, the pellet was washed with 500 µL of 1XPBS and centrifuged again at 300 x g for 3 minutes. In the final step, supernatant was discarded and 200 µL of Muse™ Cell Cycle Reagent was added. Cells were waited for 30 minutes at room temperature in a dark place. Thus, cell cycle analysis of complementary therapy in the indicated cell lines was observed in the Muse® Cell Analyzer (Figure 53).

Control 2mL DMEM-F12	32,8µL Fisetin + 1967,2µL DMEM-F12	400µL TMZ+ 32,8µL Fisetin+ 1567,2µL DMEM-F12
400µL TMZ + 1600µL DMEM-F12	287,4µL Berberine + 1712,6µL DMEM-F12	287,4µL Berberine + 400µL TMZ + 1312,6µL DMEM-F12

Figure 51. The 6-well plate design representing experimental groups for cycle analysis in T98G.

Control 2mL DMEM-F12	27,56µL Fisetin + 1972,44µL DMEM-F12	360µL TMZ+ 27,56µL Fisetin+ 1612,44µL DMEM-F12
360µL TMZ + 1640µL DMEM-F12	227µL Berberine + 1773µL DMEM-F12	227µL Berberine + 360µL TMZ + 1413µL DMEM-F12

Figure 52. Experimental 6-well culture plate design representing groups for cycle analysis in A172.

Figure 53. The experimental setup for flow cytometric cell cycle analysis with Muse® Cell Analyzer (Modified from Merckmillipore.com).

3.2.7. Investigation of Effects of Flavonoids Alone and in Combination with TMZ on Tumor Aggressiveness

Assessment of tumour malignancy and aggressiveness in cell culture could be done through several methods including wound scratch, colony formation assay in 2D, and tumor size observation in the 3D environment. A172 and T98G were used to observe the differences of this parameter in TMZ non-resistant and TMZ-resistant cell lines, respectively.

3.2.7.1. Determination of Effect on Invasion-Migration

In order to observe the cell-to-cell interaction, cell invasion and migration effect of flavonoids alone and in combination with TMZ in GBM cell lines, a wound scratch test was created and this effect was evaluated by wound-healing assay. Wound healing assay was performed in multi-culture plates for flavonoid alone, TMZ alone and flavonoid-TMZ combined version. $12x10^4$ T98G and $15x10^4$ A172 cells seeded in a 6-well culture plate and after making sure that the cells were attached within 24h, the medium from the first well was drawn first. The wells were passed through these stages one by one in terms of not leaving the cells without the medium. With a 10µL pipette tip fixed on a flat surface, three vertical scratches slightly apart from each other were created at the end of the 24-hour cell attachment period. Each well was washed with 1XPBS quickly to get rid of unwanted contamination. Later on, plates were dosed according to plate setup shown in Figure 54-55.

a)

Control 2mL DMEM-F12	400µL TMZ + 1600µL DMEM-F12	32,8µL Fisetin + 1967,2µL DMEM-F12
400µL TMZ+ 32,8µL Fisetin+ 1567,2µL DMEM-F12	Control 2mL DMEM-F12	Control 2mL DMEM-F12

b)

Control 2mL DMEM-F12	400µL TMZ + 1600µL DMEM-F12	287,4µL Berberine + 1712,6µL DMEM-F12
287,4µL Berberine + 400µL TMZ + 1312,6µL DMEM-F12	Control 2mL DMEM-F12	Control 2mL DMEM-F12

Figure 54. The representation of experimental plate design for wound healing assay in T98G for a) fisetin b) berberine.

Control 2mL DMEM-F12	360µL TMZ + 1640µL DMEM-F12	27,56µL Fisetin + 1972,44µL DMEM-F12
360µL TMZ+ 27,56µL Fisetin+ 1612,44µL DMEM-F12		

Figure 55. The 6-well culture plate design for wound scracthing assay according to IC50 values of fisetin in A172.

The closure of the gaps that occured along the scratches represented wound healing and the invasion and migration ability of the cells. When the plates were scratched at the beginning, that initial time was considered the zeroth hour. The wound-gap along the scratch was displayed in inverted microscope at 0, 6,18 and 24h (Figure 56). The width of the gap was measured using the NIH ImageJ software version 1.52a web-based program and supported by manuel measurements made with Microsoft® PowerPoint. At the end of the experiment, the rate of preservation of the gap created by the scratch was compared with untreated control and it was able to indicate the effect of the treatment candidate molecule on reducing the invasion / lowering tumor aggresiveness rate.

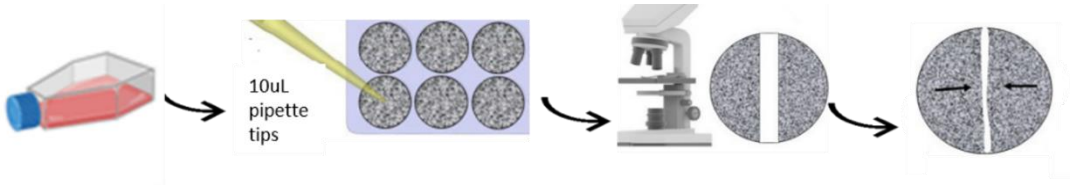

Figure 56. The summary of the wound-healing experimental design (Created with Biorender.com).

3.2.7.2. Determination of Effect on Colony Formation

Cell lines T98G and A172 were treated with either flavonoids alone and TMZ alone or a combination of both. In the colony experiment to be established, the CellMAXTM Colonogenic Assay Kit (BioPioneer, USA) was used to determine the changes upon colony formation. Cells were seeded into 6-well culture plates containing $15x10^4$ cells/2 mL medium, and when they reached 70% density, they were dosed with effective doses of flavonoids and TMZ, either singly or in combination (Figure 57-58). Culture plates were incubated for 24h in a normoxic environment in a CO_2 incubator. On the following day, the cells were dissociated from the surface of

plates by trypsinization, which was later inhibited with DMEM-F12, and then, transferred to a new 1,5 mL eppendorf. Eppendorfs were centrifuged in an Allegra® X-30 Series Benchtop centrifuge (Beckman Coulter). The supernatant was discarded (in the form of a cloud-like pellet) and 1000 µL of DMEM was added and pipetted. Cells were counted according to the heading 3.2.2.4 and inoculated into 6-well cell culture plates as $1x10^3$ cells in each well in triplicates. Colonies were begun to be observed after 10 days. Colonies were checked every 3 days during this period and the medium was changed on the 5th day. On the 10^{th} day, the medium was withdrawn from cells and colonies were washed with 500 µL 1X PBS for 2-3 times. The pouring of solutions was not directly onto the cell surface, it was placed on the plate wall instead. Furthermore, the fixation of cells was done by adding 500 µL of Fix Solution after the colonies were thoroughly purified from the wash buffer. After fixation, colonies were left at room temperature for 10-15 minutes. Then, 500 µL Staining solution was added. Colonies were washed 2 times with 500 µL of 1X PBS. Treated and untreated colonies, which stand for more than 50 cells, stained with visible blue in each well were photographed (Figure 59) and then counted both manually and in the NIH ImageJ program. Data were expressed as percent survival relative to control: ((mean number of treated)/ (mean number of controls)) x100

a)

Control 2mL DMEM-F12	400µL TMZ + 1600µL DMEM-F12	32,8µL Fisetin + 1967,2µL DMEM-F12
400µL TMZ+ 32,8µL Fisetin+ 1567,2µL DMEM-F12	Control 2mL DMEM-F12	Control 2mL DMEM-F12

b)

Control 2mL DMEM-F12	400µL TMZ + 1600µL DMEM-F12	287,4µL Berberine + 1712,6µL DMEM-F12
287,4µL Berberine + 400µL TMZ + 1312,6µL DMEM-F12	Control 2mL DMEM-F12	Control 2mL DMEM-F12

Figure 57. Experimental setup for colony formation assay for T98G with a) fisetin b) berberine.

Control 2mL DMEM-F12	360µL TMZ + 1640µL DMEM-F12	27,56µL Fisetin + 1972,44µL DMEM-F12
360µL TMZ+ 27,56µL Fisetin+ 1612,44µL DMEM-F12		

Figure 58. The 6-well culture plate design for colony formation assay for in A172 with TMZ and fisetin.

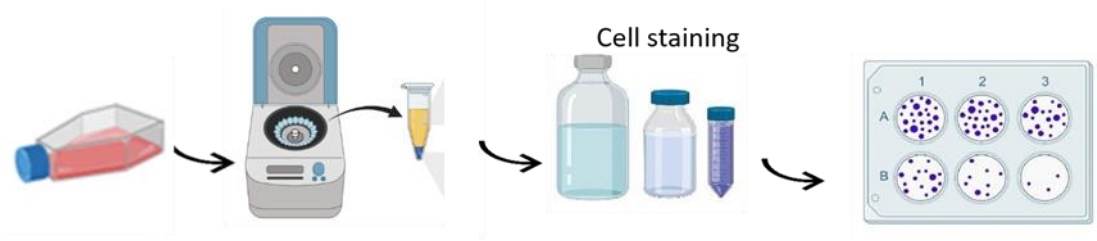

Figure 59. The scheme representing experimental setup for colony formation assay (Modified from Cytosmart.com) (Created with BioRender.com).

3.2.7.3. Effect on Tumor Size Using a Three-dimensional (3D) Culture Model

For the 3D spheroid experiment, PerkinElmer's CellCarrier Spheroid ULA 96-well microplates were used to establish the 3D culture environment for the treatments of cell with flavonoids alone and in combination with TMZ. These microplates were composed of Ultra-Low Attachment (ULA) coated surfaces that enable the formation of spheroids in round shapes in different cells. Surfaces coated with a special add-on provided non-adherent cell properties by preventing cells from adhering to the surface (Total volume of the wells was calculated as 100 µL). T98G cells were seeded into culture dishes with the number of cells (160 cells per well) optimized by our project team and determined as suitable for the experiment.

160 cells per well x 24 total wells = 3840 total cells required.

100 µL total medium volume x 24 total wells = 2400 µL total DMEM-F12 required.

The total number of cells in the T75 flask was 2,000,000. If 2 million cells obtained at 1000 µL DMEM-F12, then 1.7 µL of cell should be drawn for 3840 cells.

Zeroth hour images were taken individually with an inverted microscope before dosing. At 24 hours after culturing cells, wells were treated with calculated IC50 doses of TMZ and flavonoids according to the order shown below (Figure 60). In wells requiring a total dosage of more than 20 µL, the medium was withdrawn from the upper surface without disturbing the spherical structure. Cells without treatment were used as a control. The sphere structure was observed with a microscope at desired times. Within 3h, the convergence between the cells was observed to enhance and cells were begun to form a round sphere structure. In a maximum of 3 days, a complete 3D tumor sphere structure was formed (Figure 61). Sphere wells that formed a hair-like structure attached to the FBS residue were aborted. Imaging was done with the inverted microscope. Measurement of tumor size of 3D spheres was performed with NIH ImageJ software. The effect of targeted complementary therapy on the treated groups in terms of the change in tumor size was found by comparing the untreated groups.

1	2	3	4	5	6	7	8	9	10	11	12
C	C	TMZ	TMZ	FIS	FIS	TMZ+FIS	TMZ+FIS	BBR	BBR	TMZ+BBR	TMZ+BBR

Figure 60. PerkinElmer's CellCarrier Spheroid ULA 96-well microplate experimental setup for T98G (C=Control; TMZ=Temozolomide; FIS=Fisetin; BBR=Berberine).

Figure 61. Summary of the generation of *in-vitro* 3D tumor sphere model with ultra-low attachment plates.

3.2.8. Evaluation of Cells in Hypoxic Environment on the Effects of Drug Resistance Mechanisms

In the T98G, A172 and A172-R cell lines, the analyzes of the selected flavonoid, alone and combined with TMZ, were determined in the hypoxic environment. Why three of the cell lines were used was because of the comparison of the effect of compounds on TMZ non-resistant and TMZ-resistant cell lines. In this process, the appropriate hypoxia environment for cells (37°C, 5% CO_2, ~1% O_2 and

94% N_2) was created using modular incubator chamber (MIC-101; Billups-Rothenberg, Inc., Del Mar, CA). The controlled gas release was provided through regulators connected to the hypoxia chamber while the flow meter, also located in the hypoxia chamber, provided control of the oxygen level (Figure 62). Experiments covering the above-mentioned 3.2.7.1 were repeated in the hypoxic environment with selected flavonoid, which covered the same work packages in parallel with the cell lines in the normoxic environment. Normoxy conditions were created in the CO_2 incubator and hypoxia conditions were achieved successfully by placing the modular incubator chamber in the CO_2 incubator. Experiments were detected in parallel both in the normoxia environment CO_2 incubator and in the modular incubator chamber that provides hypoxia conditions.

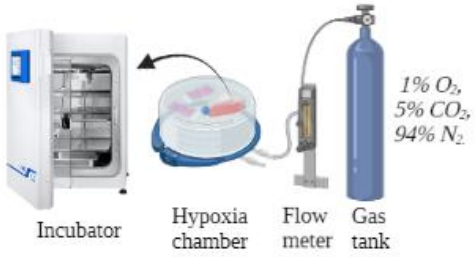

Figure 62. The schematic representation of creation of hypoxia environments in *in-vitro* (Created with Biorender.com).

3.2.9. Determination of the Effect of Flavonoids on Drug Resistance

In the study, the effects of flavonoid and flavonoid-TMZ treatment on drug resistance in GBM cells were comparatively investigated. For this purpose, the effect of TMZ, flavonoid, and TMZ+flavonoid treatment in the GBM cell lines on mRNA expression levels using the genes related to drug resistance, such as the ZEB1 gene and MMR gene MSH2 had been determined by the RT-qPCR method.

3.2.9.1. RNA Isolation

RNA isolation was made in accordance with the protocol with Zymo RNA Isolation Kit (Zymo Research, ABD) and TRIzol™ Reagent (Invitrogen™) from cells obtained from the combination of flavonoid alone and with TMZ and reproduced in a 2D environment. $15x10^4$ cells were planted in 24 well plates for 4 different

experimental groups (Control, TMZ, Fisetin, TMZ+Fisetin) in each cell line and dosed after 24 hours. One day later, the initial step was taken to lyse samples and separate phases. The medium inside of the wells were thrown and wells was washed with ice-cold 1XPBS. The cells were then lysed by adding 450 µL TRIzol™ Reagent in the fume hood (The amount of TRIzol added varies according to the surface of the culture plate rather than the number of cells on the plate. For example, 1 mL TRIzol™ Reagent was added for a diameter of three and a half centimeters. 450 µL TRIzol™ Reagent has been added based on the approximate diameter of 24 well plate). Cells were very well pipetaged and vortexed immediately until they were homogenized. Cells were left 10 minutes at room temperature to to dissociate from the nucleoprotein complex completely.

Later on, 90 µL of chloroform was added and immediately vortexed very well for at least 20 seconds. Cells were waited again for 10 minutes and centrifuged at 12.000 x g for 15 minutes at 4°C. Several phases formed after this step and the upper colorless phase was carefully taken into new nuclease-free eppendorf. RNA, DNA and other protein and lipids were represented respectively in the aqueous phase, interphase and organic phase (Figure 63). Afterwards, 225 µL of isopropanol was added to precipitate the RNA (RNA pellet was often visible when eppendorf was moved up and down several times). Cells were incubated 5 minutes at room temperature, 5 minutes at 4 °C and centrifuged at 12.000 x g for 10 minutes at 4°C. The supernatant was discarded and RNA was shown in the white gel-like pellet. To wash the RNA, cells were suspended again with 450 µL of cold 75% liquid ethanol, slowly pipetting was done. The centrifuge was made at 7,500 x g at 4°C for 5 minutes. This step was repeated two times. The supernatant was pulled thoroughly until no alcohol was left. RNA pellet was left to air dry for 20 minutes. At the last step, 50 µL nuclease-free water was added to solubilize the RNA and waited 5 minutes. The concentration and purity (A260/A280 ratio) of the obtained RNA samples were measured using UV/Vis spectrum (Beckman Coulter DU® 730 Life Science UV/Vis Spectrophotometer) and Maestro Nano Micro-Volume spectrophotometer (Maestrogen Inc., Las Vegas, NV). RNA samples with a ratio of ~1.8-2.0 were selected for cDNA synthesis.

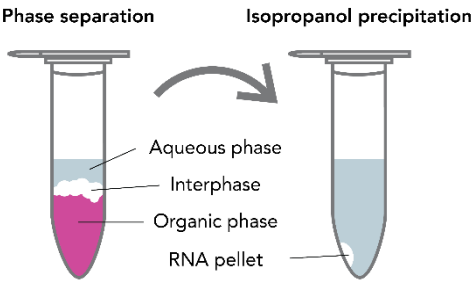

Figure 63. Different phases after phase seperation. Aqueous phase includes RNA, interphase includes DNA, and organic phase includes proteins and lipids (Zymoresearch.eu).

Complementary DNA (cDNA) synthesis was performed from total RNA using a kit based on the Reverse Transcriptase enzyme. 6 µL RNA and 2 µL Random Primer was mixed for each group. The mixture is incubated at 70°C for 5 minutes. Later on, for one sample (1x), 10 µL M-MuLV Reaction Mix and 2 µL M-MuLV Enzyme Mix were added onto the mixture. The total 20 µL cDNA synthesis reaction was first incubated at 25°C for 5 minutes, then at 42°C for 1h and finally at 80°C for 5 minutes for enzyme inactivation. The RT-qPCR experiment was continued with the obtained cDNAs measured in the UV/Vis spectrum and the purity of the cDNAs ~1.8-2.0. The remaining stocks were stored at -20°C.

3.2.9.2. Quantitative Reverse Transcription PCR (RT-qPCR) Analysis

Expression profiles at mRNA levels of ZEB1 and MSH2 genes from synthesized cDNAs in T98G, A172, and A172-R cells were created by Real-Time PCR method based on a SyberGreen probe with primer under appropriate conditions. The β-actin (ACTB) housekeeping gene was used as a control. The details of Forward and Reverse Primer sequences were given in Table 5. Experiments were conducted based on the SYBR Green I Master Mix (GoTaq, USA) protocol, performed in triplicates, and analyzed on the ABI StepOne^{TM} instrument. For the preparation of the mix with the total volume of 18 µL, nuclease-free water, qPCR Master Mix (2x), primers and CXR reference dye were added, respectively (Table 6). The primers were not exposed to light and were briefly spun before use. Afterwards, 2 µL cDNA was loaded to each well. The thermal cycle was revised according to the optimized temperatures of the genes (Table 7). The threshold cycle (Ct) was determined for each RNA expression in

the ABI StepOne™ device and the $2^{-\Delta\Delta Ct}$ method was used to calculate the fold change in gene expression.

Table 5. Forward and reverse primers of genes.

Primer Target	Forward Sequence (5′–3′)	Reverse Sequence (5′–3′)	Reference
β-Actin (ACTB)	GACAGGATGCAGAAGGAGATTACT	TGATCCACATCTGCTGGAAGGT	Pérès et al., 2015
MSH2	GACCGGGGCGACTTCTATAC	GCCCCATGTACTTGATCACC	Tancredi et al., 2022
ZEB1	AGTGTTACCAGGGAGGAGCAGTG	TTTCTTGCCCTTCCTTTCCTGTGTC	Chen et al., 2022

Table 6. The mixture preparation for gene expression of each gene.

ACTB

	Volume (µL)	Concentration
qPCR Master Mix	10	2X
Forward Primer	1,5	200nM
Reverse Primer	2,5	200nM
CXR Reference Dye	0,2	300nM
Nuclease-free water	3,8	
Total volume	18	

MSH2

	Volume (µL)	Concentration
qPCR Master Mix	10	2X
Forward Primer	3	200nM
Reverse Primer	3	200nM
CXR Reference Dye	0,2	300nM
Nuclease-free water	1,8	
Total volume	18	

ZEB1

	Volume (µL)	Concentration
qPCR Master Mix	10	2X
Forward Primer	2	200nM
Reverse Primer	2,5	200nM
CXR Reference Dye	0,2	300nM
Nuclease-free water	3,3	
Total volume	18	

Table 7. The protocol of thermal cycling (*Annealing temperature is 60°C for ACTB and MSH2 and 55°C for ZEB1).

	Cycles	Temperature	Time
Polymerase Activation	1	95	2 minutes
Denaturation		95	15 seconds
Annealing	40	60*	1 minute

3.2.10. Investigation of the Efficacy of Selected Flavonoid to be Effective in Primary Brain Tumor Cells

The first of the tumor tissues taken after surgical resection from patients diagnosed with GBM were histopathologically analyzed by the Department of Pathology of BUU (Figure 64). Then the second one was shredded manually in our department and seeded in culture flasks (Figure 64). Attachment and proliferation of cells to the flask base were observed under the microscope. Cells that reached 70% confluency in the flask were inoculated into cell culture plates. After 24 hours, experimental groups were formed and dosed with TMZ and fisetin, whose IC50s were determined in the GBM cell line. Primary cells were kept in the incubator for 24 hours and RNA and cDNA isolation, RT-qPCR and mRNA analyzes were performed as same as cell line methods, respectively. Overall, the response of each patient to the MSH2 and ZEB1 genes was also validated in primary cultures, both alone and in combination with TMZ and fisetin.

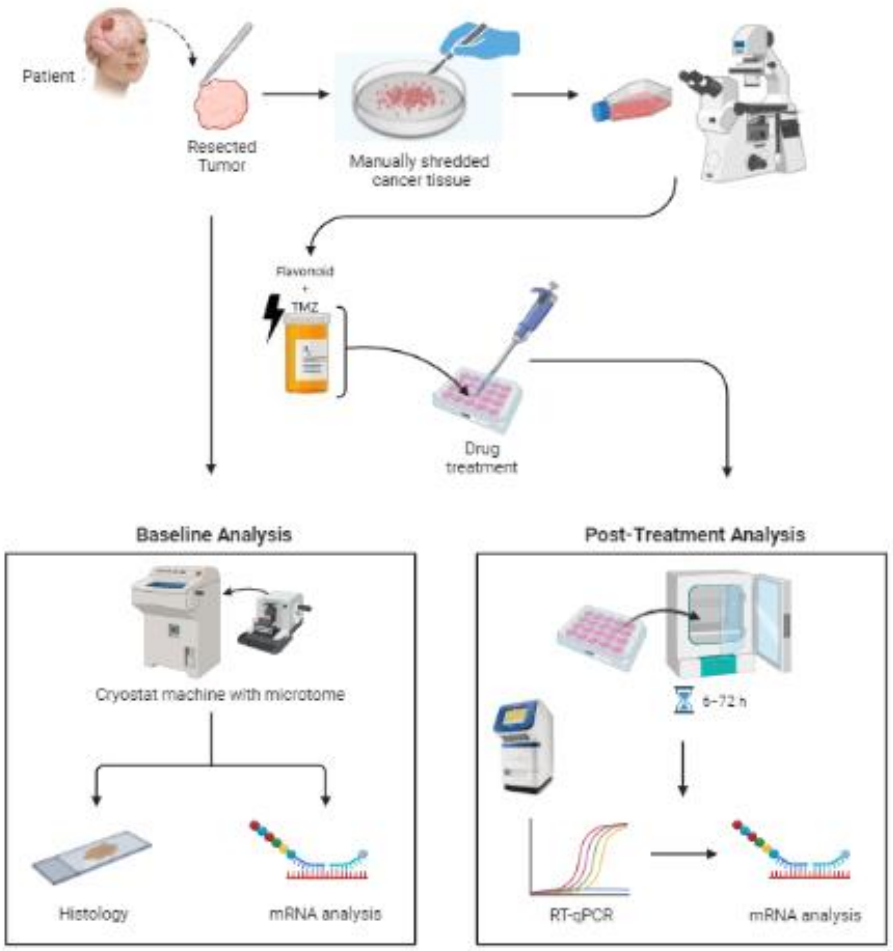

Figure 64. Representation of the experimental steps for primary GBM cells (Created with Biorender.com).

3.2.10.1. Determination of the Characteristics of Drug Resistance and Repair Mechanism in Primary Brain Tumor Cells

In order to determine the characteristics of drug resistance and repair mechanism in 3 high-grade primary brain tumor cells (Ethics Committee no: 2023-3/43) in the stocks of the department, the expression levels of the markers were evaluated with the RT-qPCR method mentioned in the heading 3.2.9.2.

Histopathological analyzes of the tumor were performed by authorized pathologists in the BUU Pathology Department. The frozen section technique was applied to primary brain tumors for rapid freezing to diagnose a histopathologic tissue section. The thin layer of resected tissue was directly placed in a cryostat with a

rotating microtome (Folkerth, 1994). In addition, various immunohistochemical analyzes were performed with section (Figure 64).

3.2.10.2. Evaluation of the Efficacy of Selected Flavonoid in Combination with TMZ in Primary Tumor Cells

Three different primary cultures derived from three different patients were seeded (Figure 65). The effect of the selected flavonoid was analyzed after treating cell with selected flavonoid in primary GBM tumor cells. Primary tumor cells were treated with the active flavonoid alone and simultaneously with TMZ. Similar to the effect of flavonoid on primary cells, mRNA expression levels of ZEB1 and MMR gene MSH2, which were associated with drug resistance, were determined by RT-qPCR (see 3.2.9.2).

a) b) c)

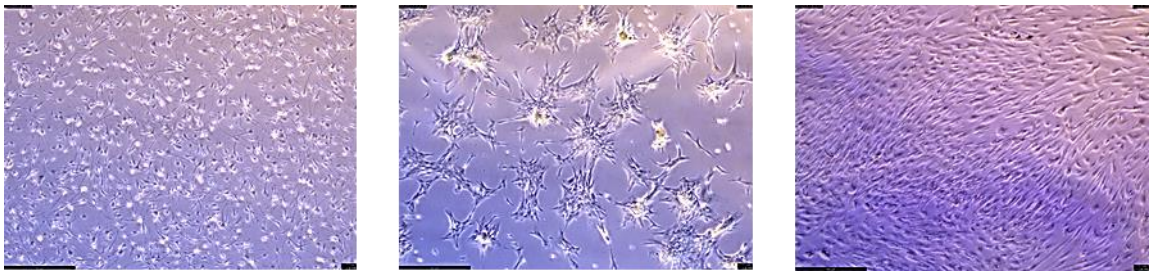

Figure 65. Microscopic representation of the GBM morphology of a) patient 1 b) patient 2) c) patient 3 at 4X objective (scalebar: 620 μm).

3.2.11. Statistical Analysis

The findings obtained from the experimental groups treated with flavonoid and TMZ+flavonoid and the untreated groups (negative control groups) were compared with statistical methods. Complementary statistics of *in-vitro* data are shown as a number, percentage, mean and standard deviation, differences between groups, and cell viability were determined by one-way ANOVA test. Wound healing, annexin V, cell cycle, colony formation, and area calculations in 3D culture was measured with the ImageJ program in *in-vitro* functional analyzes, and the quantitative data obtained were analyzed for statistical significance with the two-way ANOVA test. Statistical

significance in gene expression levels to be performed by RT-qPCR was determined by unpaired t-test from SPSS (20.0) software and GRAPHPAD Prism (8.0) programs. A P value of less than 0.05 at the 95% confidence interval was considered statistically significant (*$p<0.05$, **$p<0.0001$).

4. RESULTS

4.1. Effects of Flavonoids Alone and in Combination with TMZ on Cell Lines

The effects of two different flavonoids, fisetin and berberine, on cell viability in both normal (L929) and GBM cell lines (T98G, A172, A172-R) were determined by the xCELLigence system. Since the desired effect was able to be obtained in IC50 values in 24 hours, IC50 doses for 24 hours were determined as effective for the next experiments.

4.1.1. Determination of the Effect of Fisetin on Cell Proliferation in Control (L929) and GBM Cell Lines

4.1.1.1. Determination of the Effect of Fisetin on Cell Proliferation in T98G

Initially, the cytotoxicity of fisetin on T98G cells was evaluated via a high-tech xCELLigence system (Figure 66. a). T98G cells were treated with 7 different doses of fisetin in Table 8. Due to the dose-dependent inhibition of cell proliferation, the cell index data of fisetin was determined. The effective time of fisetin in T98G cells was the same as the TMZ effective time found in studies in our department and was evaluated as 24h. While 85% viability was observed at the lowest dose of 5 μmol/L in 24h, this rate decreased below 25% at the highest dose of 200 μmol/L (Figure 66. c). The IC50 values calculated after 24-48h of incubation were 16,40 μmol/L and 12,26 μmol/L for T98G, respectively ($p<0,0001$). Consequently, fisetin deters cell proliferation in a dose-dependent manner at 24 and 48h as shown in Figure 66. b.

Table 8. Quantitative values of cell index and cell viability rate after 24h and 48h of fisetin treatment in T98G cell line.

	Cell Index (24h)	***Cell Viability Rate (%) (24h)***	***Cell Index (48h)***	***Cell Viability Rate (%) (48h)***
Control	6.83	100	4,97	100
5 µmol/L	5.84	85,50512	3,99	80,28169
10 µmol/L	5.28	77,306	3,23	64,98994
25 µmol/L	3.46	50,65886	1,87	37,62575
50 µmol/L	1.92	28,11127	0,91	18,30986
75 µmol/L	1.50	21,96193	0,65	13,07847
100 µmol/L	1.39	20,35139	0,67	13,48089
200 µmol/L	1.69	24,74378	1,04	20,92555

a)

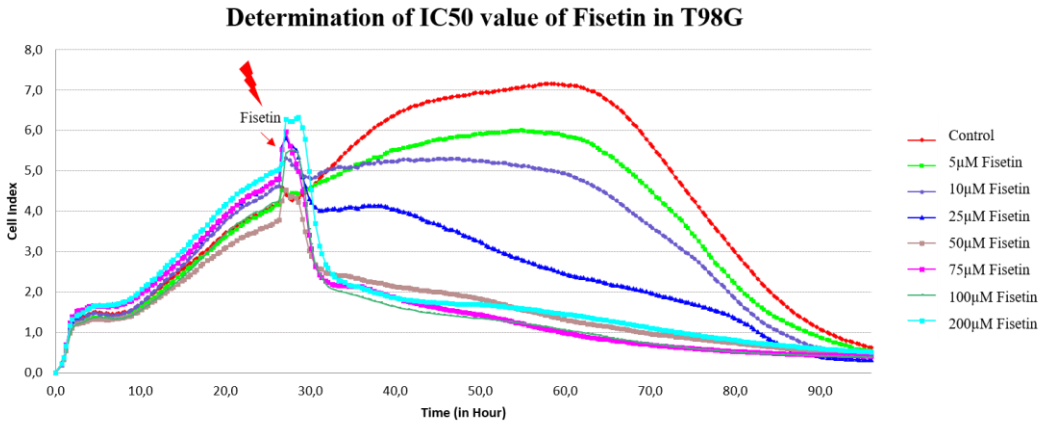

b)

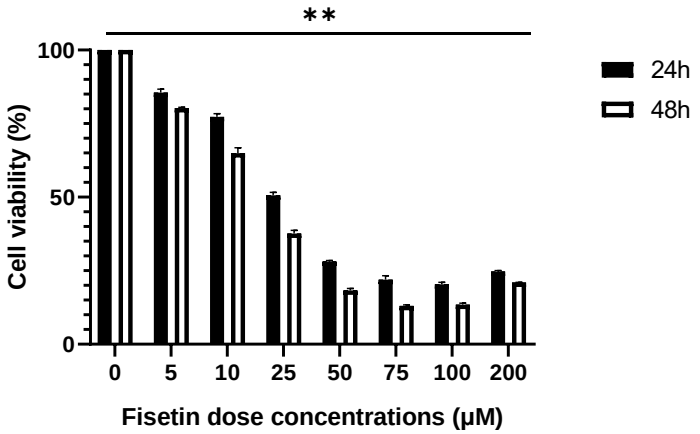

c)

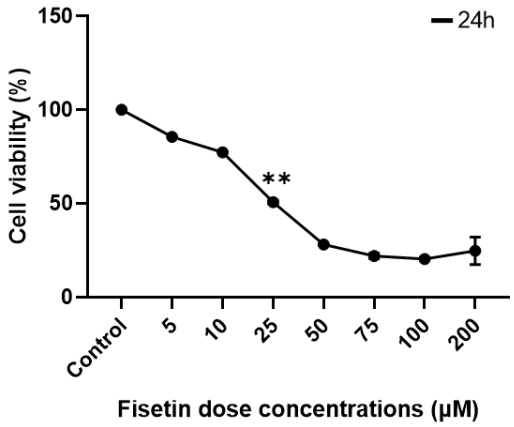

Figure 66. a) Raw data of the effect of fisetin dose concentration on T98G cell proliferation b) Graphical representation of fisetin's effect of cell viability (%) at 24 and 48h on T98G cell line (0 μmol/L (μM) dose means untreated group and represents control group) c) Graphical representation of fisetin dose-dependent cell viability (%) after 24h treatment in T98G cell line (*p<0.05, **p<0.0001). Bars represent mean ± S.D.

4.1.1.2. Determination of the Effect of Fisetin on Cell Proliferation in A172

In order to observe the effect of fisetin on GBM cell lines with different resistance mechanisms, fisetin was tested in TMZ sensitive A172 cell line (see 3.2.2). A172 cells were treated with 7 different doses of fisetin in Figure 67. a to find out cell index data and effective dose. The IC50 values of fisetin over 24 and 48h were detected as 13.78 μmol/L and 10,34 μmol/L in A172 cell line, respectively (p<0,0001) (Figure 67. b). The effective time of fisetin in A172 cells was determined as 24h. Nearly 74% viability was observed at the lowest dose of 5 μmol/L in 24h (Figure 67. c). It has been also found that the lethal effect of fisetin was preserved even at high doses up to 200 μmol/L in 24h (Table 9).

Table 9. Digital data of cell index and cell viability rate after 24h of fisetin treatment in A172 cell line.

	Cell Index (24h)	*Cell Viability Rate (%) (24h)*	*Cell Index (48h)*	*Cell Viability Rate (%) (48h)*
Control	2,25	100	1,53	100
5 µmol/L	1,66	73,77778	1,17	76,47059
10 µmol/L	1,69	75,11111	1,33	86,9281
25 µmol/L	2,5	111,1111	0,79	51,63399
50 µmol/L	2,71	120,4444	1,23	80,39216
75 µmol/L	1,05	46,66667	0,69	45,09804
100 µmol/L	1,22	54,22222	1,26	82,35294
200 µmol/L	1,35	60	1,43	93,46405

a)

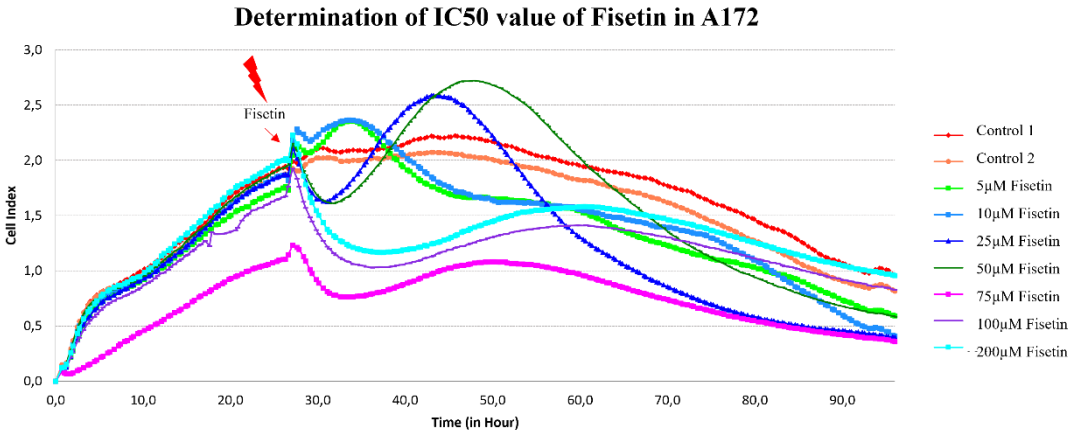

b)

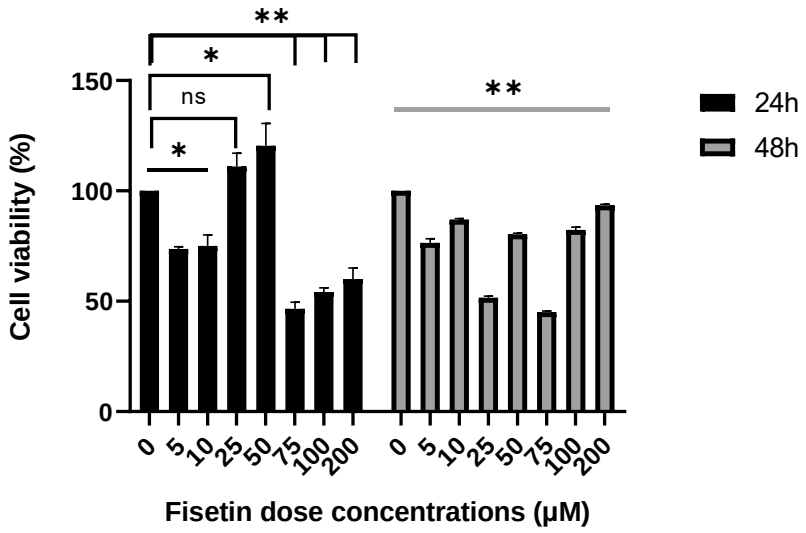

c)

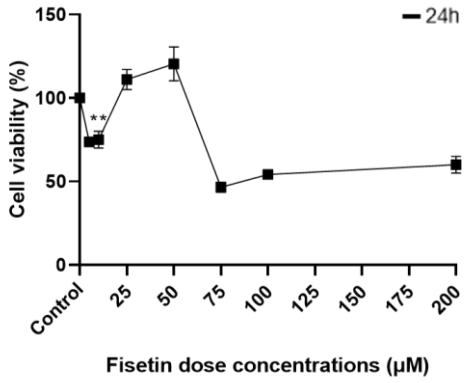

Figure 67. a) Raw data of the effect of fisetin dose concentration on A172 cell proliferation b) Graphical representation of fisetin's effect of cell viability (%) at 24 and 48h on A172 cell line c) Graphical representation of fisetin dose-dependent cell viability (%) at 24h on A172 cell line (*p<0.05, **p<0.0001). Bars represent mean ± S.D.

4.1.1.3. Determination of the Effect of Fisetin on Cell Proliferation in the Control Cell Line (L929)

It had been shown that the fisetin concentrations ranging from 25-75 µmol/L (µM) which include even higher levels of effective IC50 values shown below (ranging from 10-16 µmol/L) were ineffective at 24h after treatment in the fibroblast cell, L929 (Figure 68. a). Since the effective hour of the flavonoid was determined as 24h with the subsequent data, the data of 24h was shown in Table 10. Even when the fisetin concentration increased to 75 µmol/L, cell viability was observed close to 90% proving its usability since it was not cytotoxic to the healthy cells (p<0.0001) (Figure 68. b).

Table 10. Digital data of cell index and cell viability rate after 24h of fisetin treatment on L929 cell line.

	Cell Index (24h)	***Cell Viability Rate (%) (24h)***
Control	0.75	100
25 µmol/L	0.57	76
50 µmol/L	0.71	94
75 µmol/L	0.67	89

a)

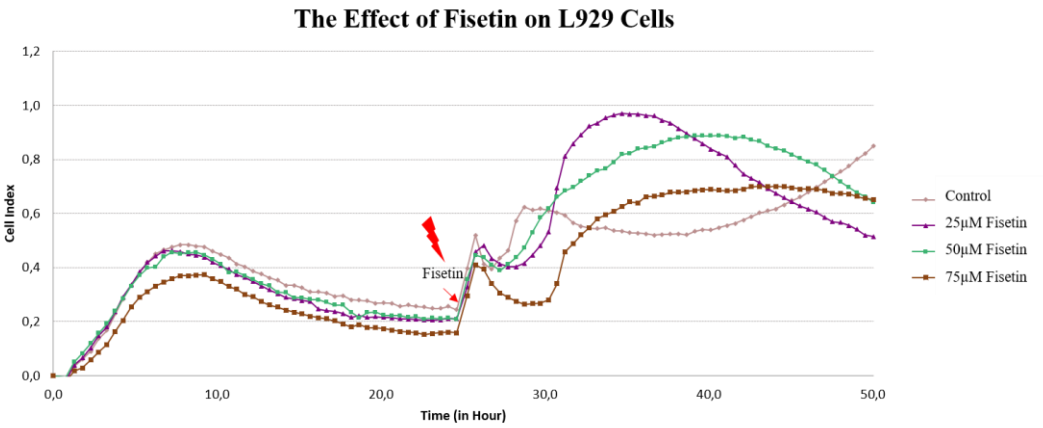

b)

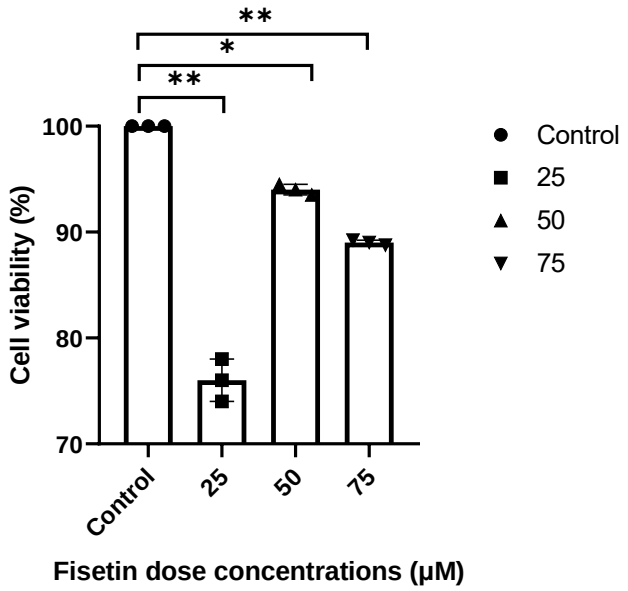

Figure 68. a) Raw data of the effect of fisetin dose concentration on L929 cell proliferation b) Graph of the effect of fisetin doses on L929 cell (*p<0.05, **p<0.0001).

4.1.2. Determination of the Effect of Berberine on Cell Proliferation in Control (L929) and GBM Cell Lines

4.1.2.1. Determination of the Effect of Berberine on Cell Proliferation in T98G

To find the cytotoxicity of berberine on T98G, cells were treated with 5 different doses of berberine in Figure 69. a. With the help of the cell index data of

berberine observed, cell viability rates were calculated (Table 11). Thus, cell viability percentages decreased to 50% at 150 µmol/L and to almost 10% at 200 µmol/L (Table 11). The effective time of berberine in T98G cells was also 24h and effective dose (IC50) was 143,7 µmol/L in 24h ($p<0,0001$) (Figure 69. c). The IC50 value of berberine in 48h was 139,4 µmol/L for T98G ($p<0,0001$) (Figure 69. b).

Table 11. Digital data of cell index and cell viability rate after 24h and 48h of berberine treatment on T98G cell line.

	Cell Index (24h)	***Cell Viability Rate (%) (24h)***	***Cell Index (48h)***	***Cell Viability Rate (%) (48h)***
Control	5,5384	100	7.3424	100
25 µmol/L	5,71	103,09	7.35775	100,21
50 µmol/L	7,1254	128,65	8.2011	11,69
100 µmol/L	5,79135	104,56	6.22925	84,84
150 µmol/L	2,77635	50,13	3.52645	48,03
200 µmol/L	0,6383	11,52	0.5494	7,48

a)

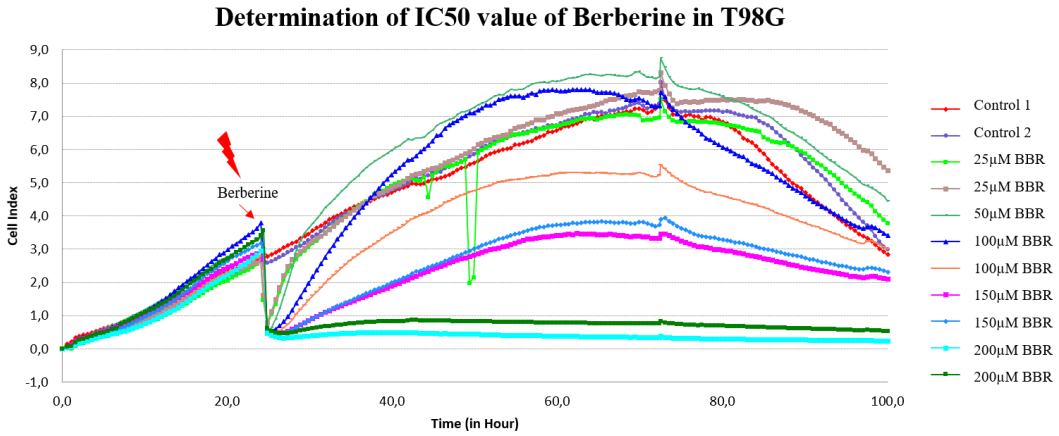

b)

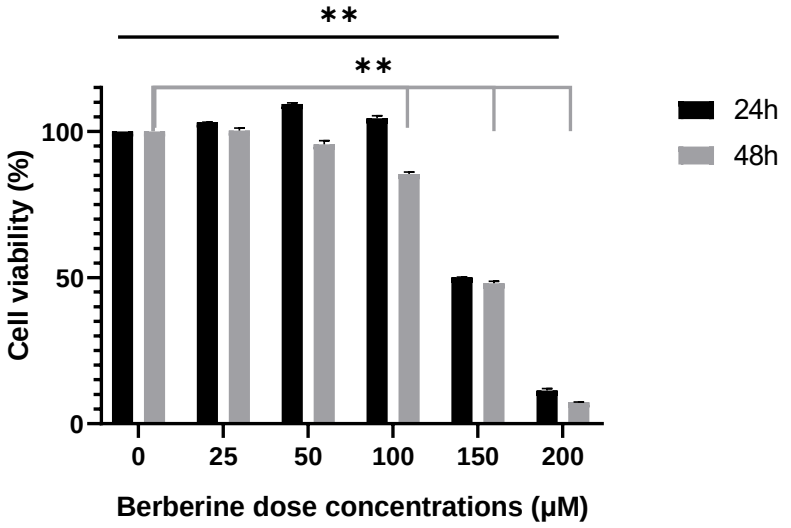

c)

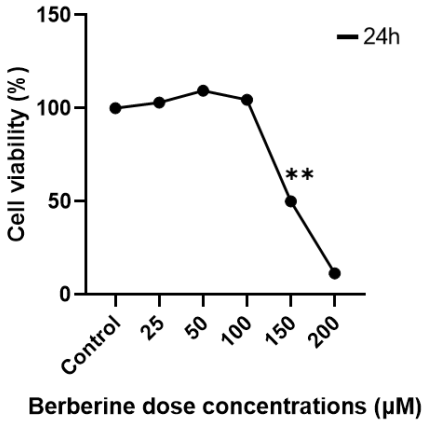

Figure 69. a) Raw data of the effect of berberine dose concentration on T98G cell proliferation b) Graphical representation of the effect of berberine on T98G cell viability (%) at 24 and 48h. c) Graphical representation of berberine dose-dependent cell viability (%) at 24h on T98G cell line (*p<0.05, **p<0.0001).

4.1.2.2. Determination of the Effect of Berberine on Cell Proliferation in A172

The capacity of berberine to inhibit cell viability was investigated in A172 cells treated with 5 different increasing doses of berberine between 25-200 µmol/L (Figure 70. a). The effective time of berberine in A172 was determined as 24h since there was a significant decrease in terms of cell viability shown in Figure 70. c. Thereby,

berberine inhibited cell viability to 23,5% and 10% with 150 µmol/L and 200 µmol/L dose treatment at 24h, respectively (Table 12). In A172, IC50 values of berberine were 113.5 µmol/L for 24h and 72.71 µmol/L for 48h (Figure 70. b).

Table 12. Quantitative values of cell index and cell viability rate after 24h and 48h of berberine treatment in A172 cell line.

	Cell Index (24h)	***Cell Viability Rate (%) (24h)***	***Cell Index (48h)***	***Cell Viability Rate (%) (48h)***
Control	4,20	100	3,67	100
25 µmol/L	5,35	127,381	2,68	73,02452
50 µmol/L	5,69	135,4762	2,45	66,75749
100 µmol/L	4,27	101,6667	2,35	64,0327
150 µmol/L	0,99	23,57143	0,39	10,6267
200 µmol/L	0,45	10,71429	0,12	3,269755

a)

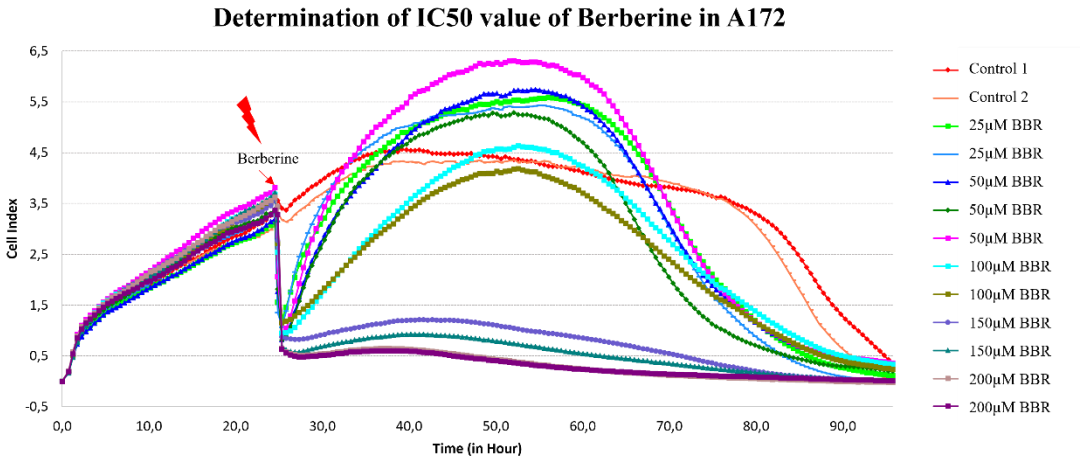

b)

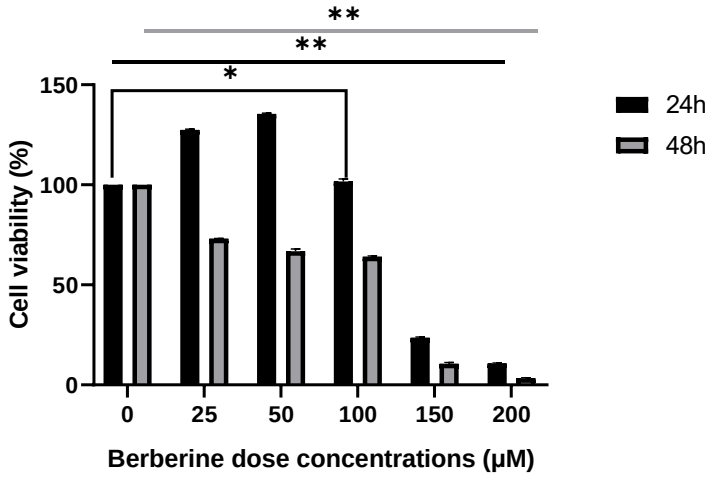

c)

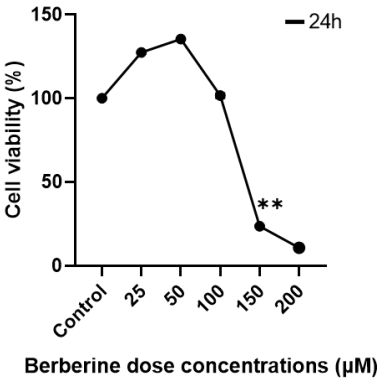

Figure 70. a) Raw data of the effect of berberine dose concentration on A172 cell proliferation b) Graph of the effect of berberine on A172 cell viability (%) at 24 and 48h. d) Graphical representation of berberine dose-dependent cell viability (%) at 24h on A172 (*p<0.05, **p<0.0001).

4.1.2.3. Determination of the Effect of Berberine on Cell Proliferation in the Control Cell Line (L929)

To determine the effect of berberine in control cells, the minimum dose 100 µmol/L and the lowest IC50 value of 113.5 µmol/L (belonging to A172) and high dose 125 µmol/L dose of berberine were tested in L929 cell line (Figure 71. a). In the treatment of 100 µmol/L berberine, L929 cell viability was 57,5%, (p<0,0001) while a direct proportional decrease in viability was observed as the dose increased (Table 13). The alterations in cell viability decreased to 44,27% and 36,14% with the the 113.5 µmol/L and 125 µmol/L dosages of berberine, respectively (p<0,0001) (Figure 71. b).

Table 13. Quantitative values of cell index and cell viability rate after 24h of berberine treatment in L929 cell line.

	Cell Index (24h)	***Cell Viability Rate (%) (24h)***
Control	0,8594	100
100 µmol/L	0,4945	57,54
113,5 µmol/L	0,3805	44,27
125 µmol/L	0,3106	36,14

a)

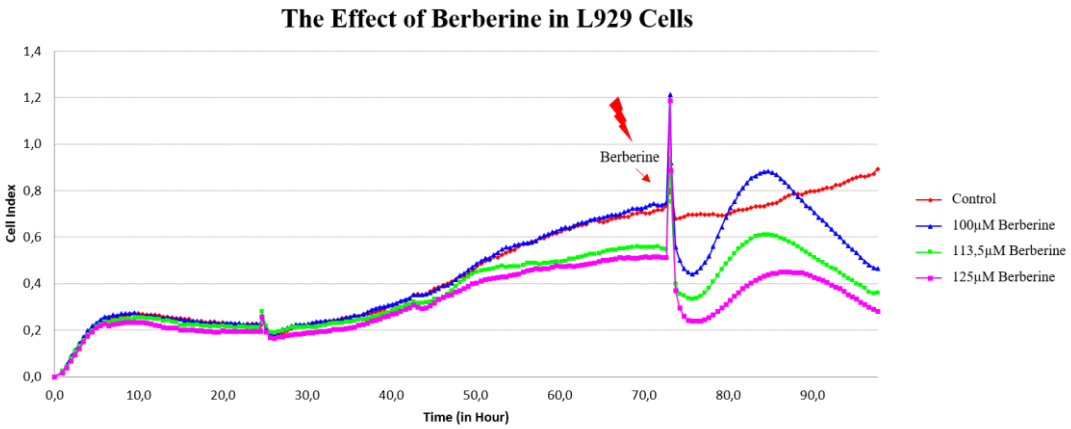

b)

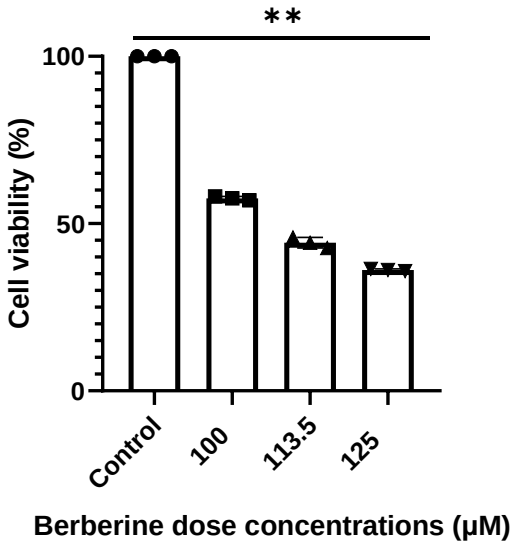

Figure 71. a) Raw data of the effect of berberine dose concentration on L929 cell proliferation b) Graph of the effect of berberine doses on L929 cell line (*p<0.05, **p<0.0001).

4.1.3. Effect of Flavonoids Alone or in Combination with TMZ on Cell Proliferation

In order to investigate the usability of the combined treatment of TMZ and flavonoids in GBM cells, the effect of the effective hours and doses of compounds found in the previous title on cell proliferation was evaluated with the xCELLigence system.

4.1.3.1. Effect of Fisetin Alone or in Combination with TMZ on T98G Cell Proliferation

The effective dose of TMZ in T98G in 24 hours was found to be 1000 µmol/L in earlier findings in our department (Ercelik et al., 2023). The effective dose of fisetin was 16.40 µmol/L (see 4.1.1.1). In combination therapy, both doses were added consecutively. While the T98G cell viability rate was approximately 24% in TMZ treatment, the combined treatment reduced cell proliferation by 35.32% after 24h of treatment ($p<0,0001$) (Table 14). The cell viability difference between TMZ and TMZ+Fisetin was significant ($p<0,0001$). When fisetin alone was used, a significant mortality rate (65,33%) was observed compared to the control cell group ($p<0,0001$) (Figure 72. a). All of the treated groups were statistically significant compared to untreated group (Figure 72. b).

Table 14. Digital data of cell index and cell viability rate of fisetin and combination treatment in T98G.

	Cell Index (24h)	***Cell Viability Rate (%) (24h)***
Control	7,73	100
TMZ	1,84	23,80
Fisetin	5,05	65,33
TMZ+Fisetin	2,73	35,32

a)

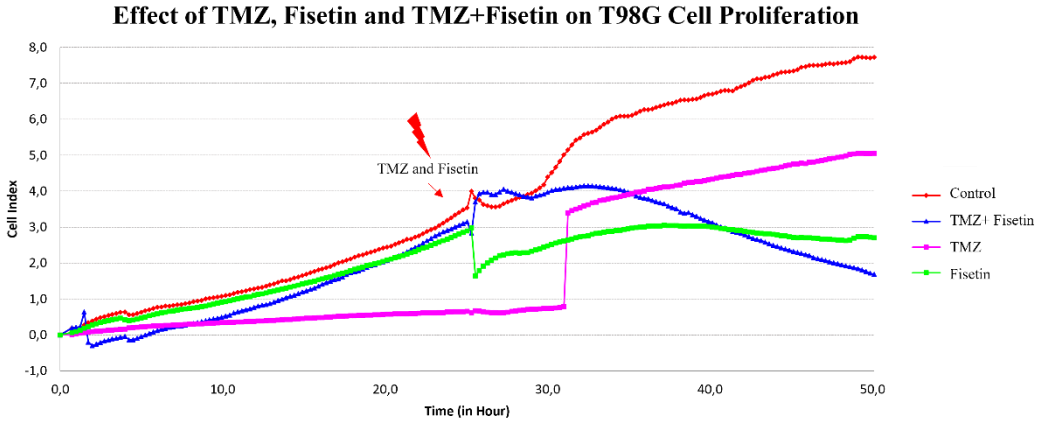

b)

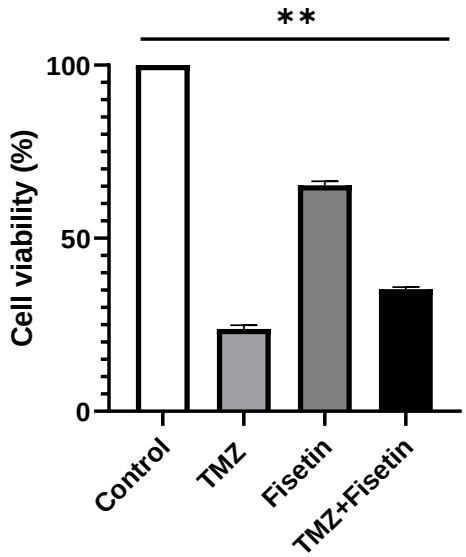

Figure 72. a) Raw data of the effect of TMZ, Fisetin and TMZ+Fisetin on T98G cell proliferation b) Graphical representation of the effects of TMZ, Fisetin and TMZ+Fisetin treatment in T98G.

4.1.3.1.1. Antagonistic-Synergistic Effect of Fisetin with TMZ in T98G

According to the antagonistic-synergistic effect via SyneryFinder web program categorization in section 3.2.4.2, an additive effect of the combination of two drugs named TMZ and fisetin (Figure 73) was found with a synergy value of 1.68 (Table 15).

Table 15. Synergy score between TMZ and fisetin in T98G.

Drug combination	Synergy Score	Most synergistic area score	Method
TMZ+Fisetin	1.68	3.10	ZIP

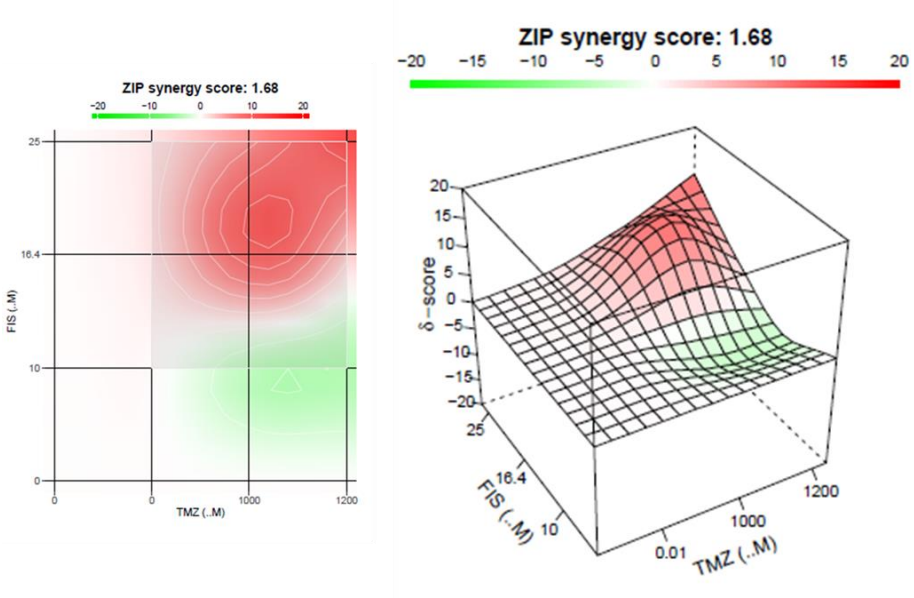

Figure 73. A synergistic score, multisample analysis and consensus synergy for TMZ and fisetin combination in T98G calculated with SynergyFinder web program. (Chosen parameters: Readout: viability; Baseline correction: yes)

4.1.3.2. Effect of Fisetin Alone or in Combination with TMZ on A172 Cell Proliferation

The effective dose of 24h of TMZ in A172 was known as 900 µmol/L in our earlier results (Ercelik et al., 2023). The effective dose of fisetin was 13.78 µmol/L (see 4.1.1.2). Combination therapy was created with the addition of two doses. When using TMZ alone, fisetin alone or the combination therapy, a significant decrease in cell viability was observed compared to the control cell group (Figure 74. a). While TMZ treatment reduced cell viability to 36%, it decreased to 28% with combined treatment in 24h ($p<0,0001$) (Table 16). Cell viability of fisetin-alone group was 15,20% ($p<0,0001$). Percentages of cell viabilities belonging to treated groups were statistically significant compared to control group (Figure 74. b).

Table 16. Average quantitative values of cell index and cell viability rate of fisetin and combination treatment in A172.

	Cell Index (24h)	***Cell Viability Rate (%) (24h)***
Control	5,33	100
TMZ	1,92	36,02
Fisetin	0,81	15,20
TMZ+Fisetin	1,53	28,70

a)

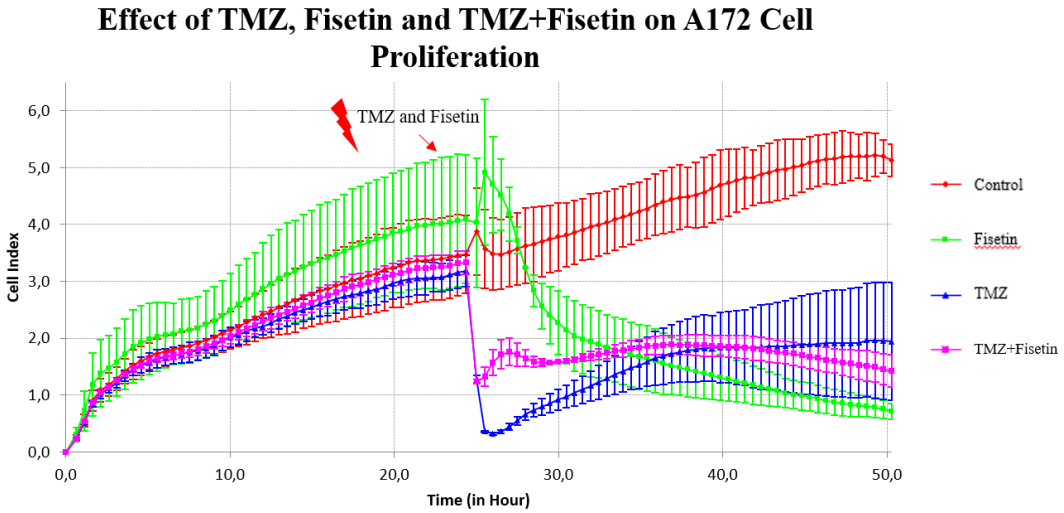

b)

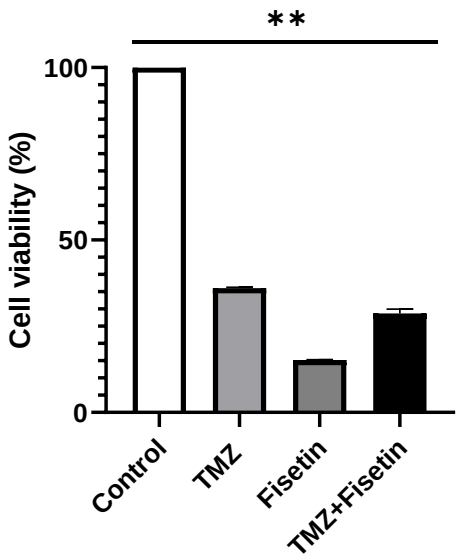

Figure 74. a) Raw data of the effect of TMZ, Fisetin and TMZ+Fisetin on A172 cell proliferation b) Graphical representation of the effects of TMZ, Fisetin and TMZ+Fisetin treatment in A172.

4.1.3.2.1. Antagonistic-Synergistic Effect of Fisetin with TMZ in A172

Considering the synergistic effect detection section in 3.2.4.2, the relationship between TMZ and fisetin in A172 cells was determined as an additive effect. An additive effect similar to T98G findings was found between TMZ and fisetin in A172 cell line (Figure 75) with a synergy score of about 0.1 (Table 17).

Table 17. Synergy score between TMZ and fisetin in A172.

Drug combination	Synergy Score	Most synergistic area score	Method
TMZ+Fisetin	0.10	1.93	ZIP

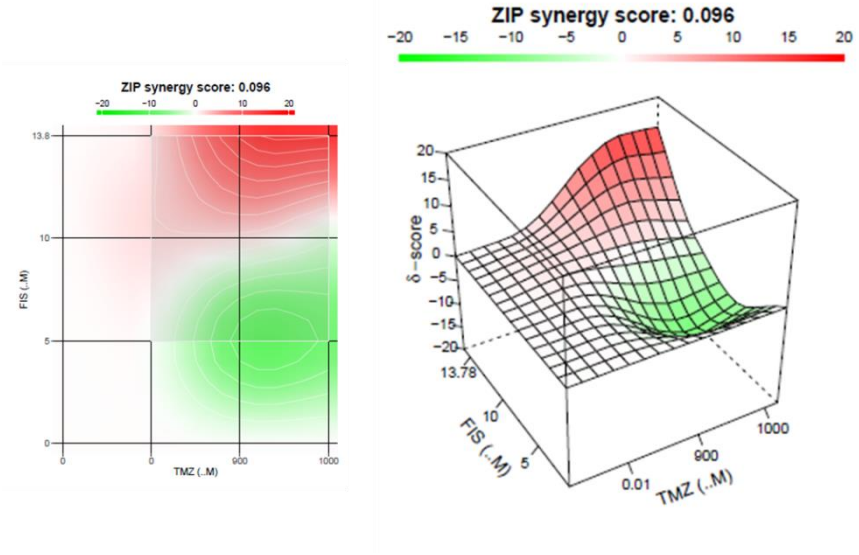

Figure 75. A synergistic score, multisample analysis and consensus synergy for TMZ and fisetin combination in A172 calculated with SynergyFinder web program. (Chosen parameters: Readout: viability; Baseline correction: yes)

4.1.3.3. Effect of Berberine Alone or in Combination with TMZ on T98G Cell Proliferation

Cell index data after 24 hours were obtained as T98G cells were dosed with various doses of TMZ, Berberine and TMZ+Berberine (Figure 76. a). The effect of the IC50 dose of TMZ was determined in T98G as 28,80% (see 4.1.3.1). Cells, when treated with 143,7 µmol/L Berberine-alone, had viability rate at 18,95% (Table 18). With cotreatment of IC50 doses of berberine and TMZ, cell viability was obtained

61,25% (Table 18). All of the average cell viability data of treated groups were significant to untreated control of T98G with p<0,0001 (Figure 76. b).

Table 18. Average digital data of cell index and cell viability rate of berberine and TMZ alone and combination treatment in T98G.

	Cell Index (24h)	**Cell Viability Rate (%) (24h)**
Control	9,6	100
100 µmol/L Berberine	6,09	63,43
143,7 µmol/L Berberine	1,82	18,95
200 µmol/L Berberine	3,09	32,18
100 µmol/L Berberine + 1000 µmol/L TMZ	7,21	75,10
100 µmol/L Berberine + 1200 µmol/L TMZ	7,38	76,87
143,7 µmol/L Berberine + 1000 µmol/L TMZ	5,88	61,25
143,7 µmol/L Berberine + 1200 µmol/L TMZ	4,96	51,66
200 µmol/L Berberine + 1000 µmol/L TMZ	3,87	40,31
200 µmol/L Berberine + 1200 µmol/L TMZ	1,57	16,35

a)

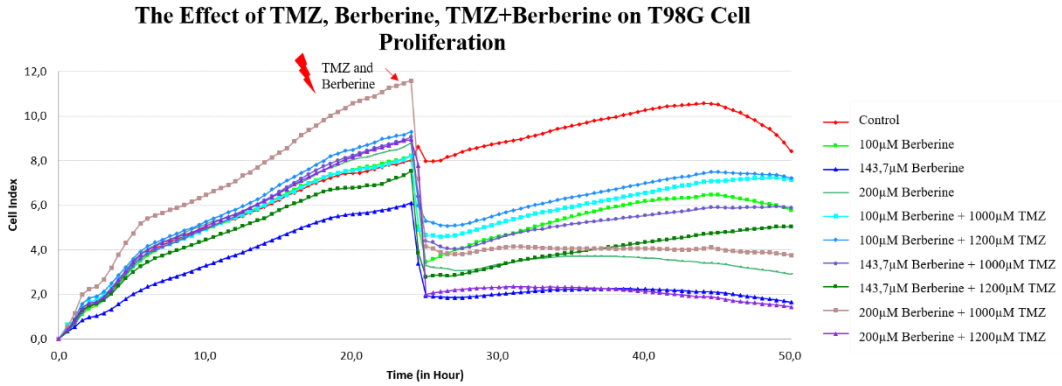

b)

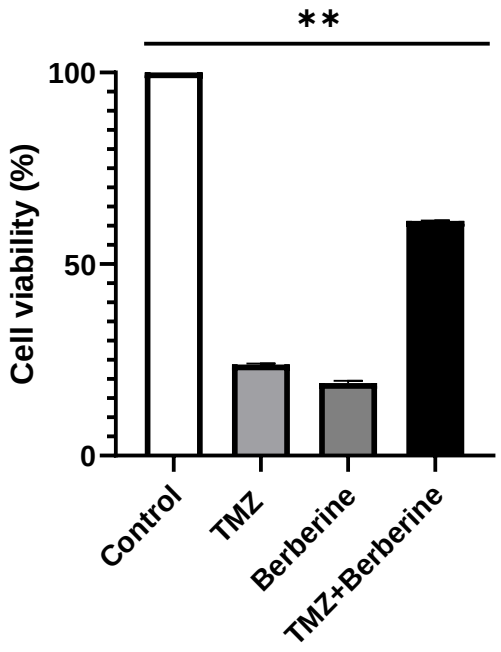

Figure 76. a) Raw data of the effect of TMZ, Berberine and TMZ+ Berberine on T98G cell proliferation b) Graphical representation of the effects of TMZ, Berberine and TMZ+Berberine treatment in T98G.

4.1.3.3.1. Antagonistic-Synergistic Effect of Berberine with TMZ in T98G

When multisample analysis and consensus synergy for TMZ and berberine combination in T98G calculated with SynergyFinder web program (see 3.2.4.2), the relationship between TMZ and berberine was antagonist (Figure 77) with -26,305 ZIP synergistic score in T98G (Table 19).

Table 19. Synergy score between TMZ and berberine in T98G.

Drug combination	Synergy Score	Most synergistic area score	Method
TMZ+Berberine	-26.30	-12.82	ZIP

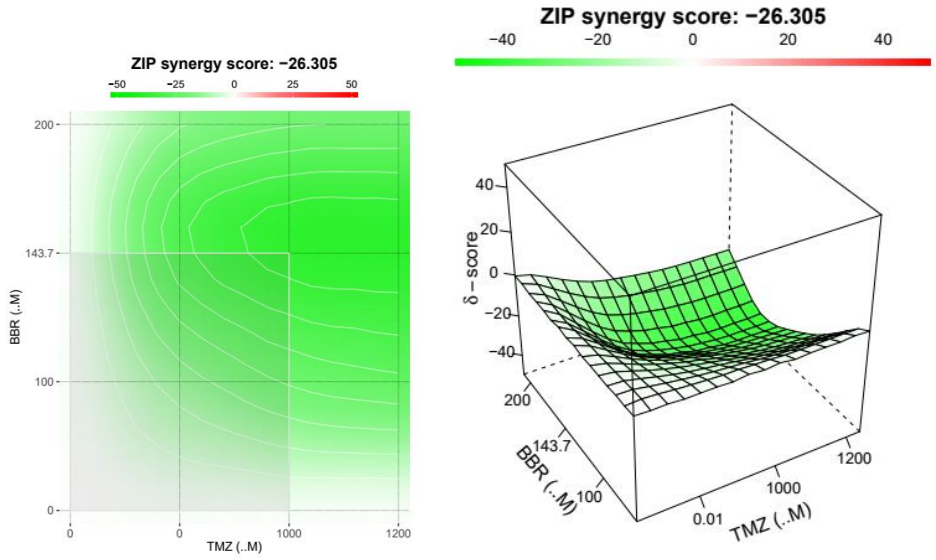

Figure 77. A synergistic score, multisample analysis and consensus synergy for TMZ and berberine combination in T98G calculated with SynergyFinder web program. (Chosen parameters: Readout: viability; Baseline correction: yes)

4.1.3.4. Effect of Berberine Alone or in Combination with TMZ on A172 Cell Proliferation

While A172 cell viability was 9.75% after TMZ treatment, it decreased to 8.06% with TMZ and berberine combined treatment. 36.02% viability was also observed in berberine treatment alone (Table 20) (Figure 78. a). TMZ, Berberine, TMZ+Berberine treated groups were statistically significant compared to untreated group of A172 ($p<0,0001$) and relationship between TMZ and TMZ+Berberine was also significant with p value of 0,0035 in A172 (Figure 78. b).

Table 20. Digital data of cell index and cell viability rate of TMZ, Berberine and TMZ+Berberine in A172.

	Cell Index (24h)	***Cell Viability Rate (%) (24h)***
Control	5,33	100
TMZ	0,52	9,75
Berberine	1,92	36,02
TMZ+Berberine	0,43	8,06

a)

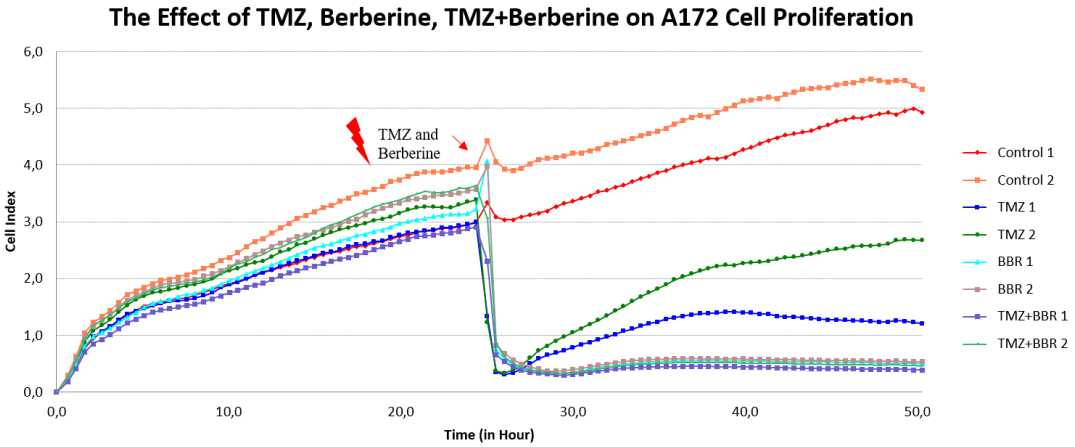

b)

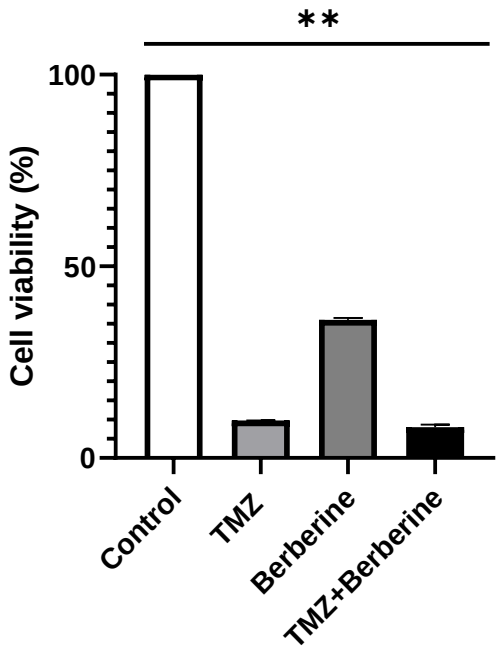

Figure 78. a) Raw data of the effect of TMZ, Berberine and TMZ+ Berberine on A172 cell proliferation b) Graphical representation of the effects of TMZ, Berberine and TMZ+Berberine treatment in A172.

4.1.3.4.1. Antagonistic-Synergistic Effect of Berberine with TMZ in A172

To assess the synergistic effect of the combination of two drugs, the Syngeryfinder web program (see 3.2.4.2), was used and according to the calculations in terms of multisample analysis and consensus synergy, an additive effect was

evaluated between TMZ and berberine (Figure 79) with a ZIP synergy score equivalent to 4.27 in A172 cell line (Table 21).

Table 21. Synergy score between TMZ and Berberine in A172.

Drug combination	Synergy Score	Most synergistic area score	Method
TMZ+Berberine	4.27	5.05	ZIP

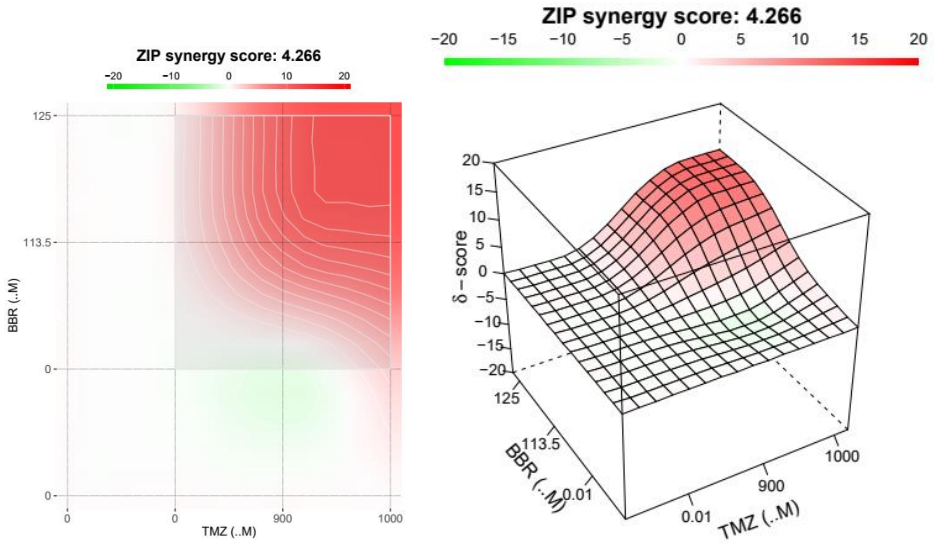

Figure 79. A synergistic score, multisample analysis and consensus synergy for TMZ and berberine combination in A172 calculated with SynergyFinder web program. (Chosen parameters: Readout: viability; Baseline correction: yes)

4.2. Cytotoxic Effects of Increasing TMZ Doses in Acquired TMZ Resistant Cells (A172-R)

The effect of long-term treatment with different escalating doses of TMZ on cell viability has been demonstrated at each stage (350, 450, 550, 750, and 900 µmol/L). Each group was repeated in duplicate and the average values of the data in the program are shown in the graphs. Cells were dosed when they reached sufficient proliferation, and cell index values 24 hours after dosing were taken into account for calculations.

The responses of A172 cells treated with 350µmol/L TMZ for a long time (A172-350-R) and the TMZ-sensitive (A172) cell line to TMZ were compared for cell viability (Figure 80. a). Accordingly, while if viability was accepted as 100% in the

A172 control, this rate decreased significantly below 37% ($p<0,0001$) (Figure 80. b) in A172 treated with 900 µmol/L TMZ (IC50) dose (Table 22). Cell viability of A172-350-R decreased to 19.68% when treated with the IC50 dose of TMZ (900 µmol/L) ($p<0,0001$) (Figure 80. c).

Table 22. Average data of cell index and cell viability rates of A172 and A172-350-R.

	Cell Index (24h)	***Cell Viability Rate (%) (24h)***
A172 Control	5,20	100
A172 900µmol/L TMZ	1,922	36,96
A172-350-R Control	0,437	100
A172-350-R 900µmol/L TMZ	0,086	19,68

a)

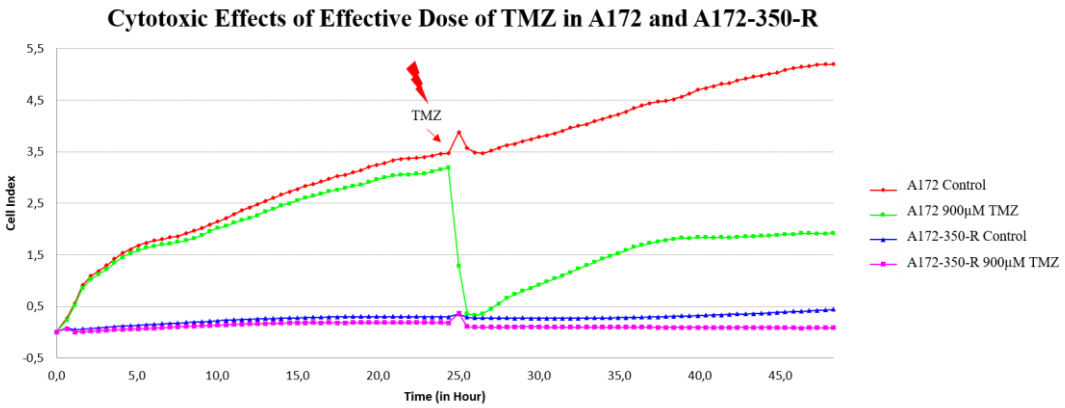

b)

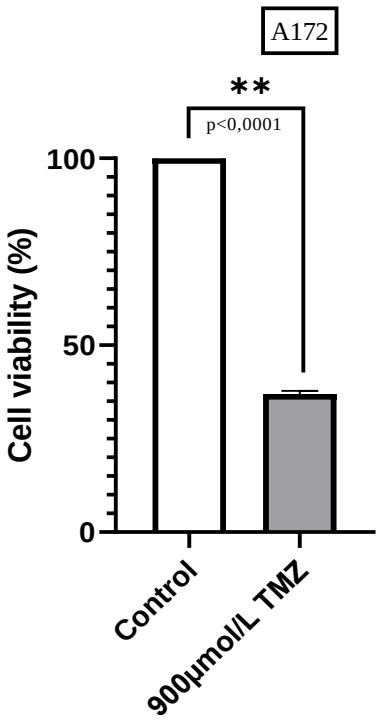

c)

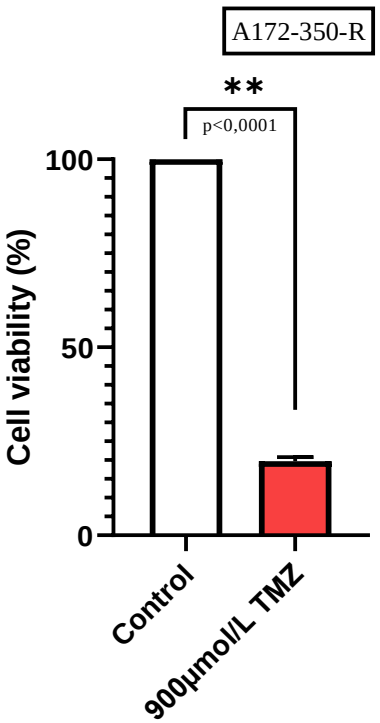

Figure 80. a) Raw data of the effect of TMZ treatment with IC50 dose (900 µmol/L) on A172 and A172-350-R cell proliferation b) Graphical representation of the effect of TMZ on cell index and cell viability rate in A172. c) Graphical representation of the effect of TMZ on cell index and cell viability rate in A172-350-R.

When A172-450-R cells long-treated with a 450 µmol/L dose of TMZ were given an IC50 dose of TMZ (Figure 81. a), they significantly ($p<0,0001$) reduced the viability of the cells ($p<0.0001$) by almost 75% after 24h, compared to the control (Table 23) (Figure 81. b).

Table 23. Average data of cell index and cell viability rates of A172-450-R.

	Cell Index (24h)	***Cell Viability Rate (%) (24h)***
A172-450-R Control	0,5714	100
A172-450-R 900 µmol/L	0,1444	25,27

a)

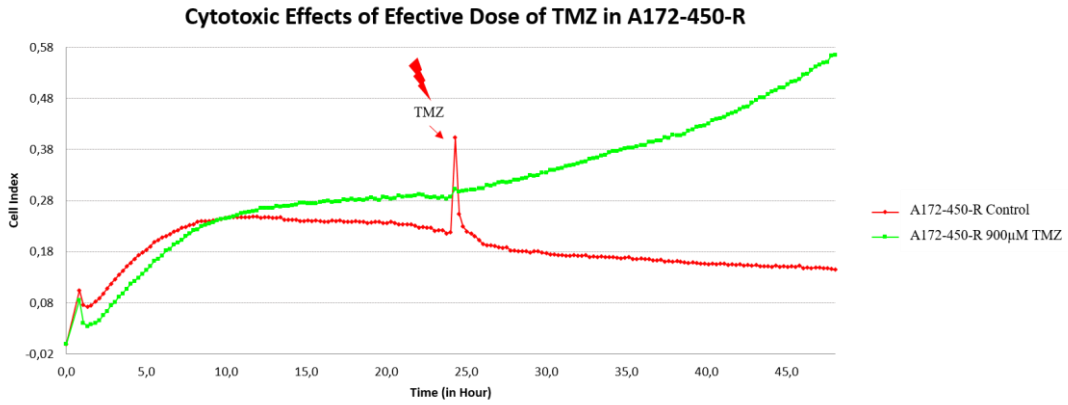

b)

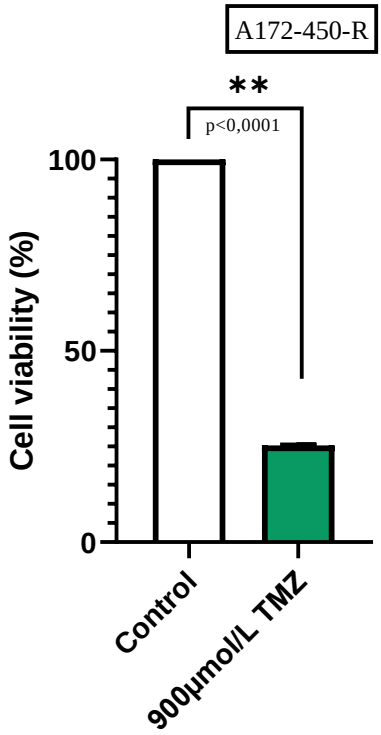

Figure 81. a) Raw data of the effect of TMZ treatment with IC50 dose (900 µmol/L) on A172-450-R cell proliferation b) Graphical representation of the effect of TMZ on cell index and cell viability rate in A172-450-R.

The fact that the A172-550-R cell line, which was expected to gain resistance to 550 µmol/L TMZ dose after long-term treatment of the same dose, had 100.60% cell viability after 24 hours of treatment with 550 µmol/L TMZ which was very similar to the A172-550-R control, proving this hypothesis (Figure 82. a). In addition, even

when treated with the effective dose of TMZ, 900 µmol/L, A172-550-R showed approximately 97% viability (Table 24) (Figure 82. b).

Table 24. Average data of cell index and cell viability rates of A172-550-R after 24h of treatment with 550 µmol/L and 900 µmol/L TMZ doses.

	Cell Index (24h)	***Cell Viability Rate (%) (24h)***
A172-550-R Control	1,66	100
A172-550-R 550 µmol/L	1,67	100,60
A172-550-R 900 µmol/L	1,61	96,98

a)

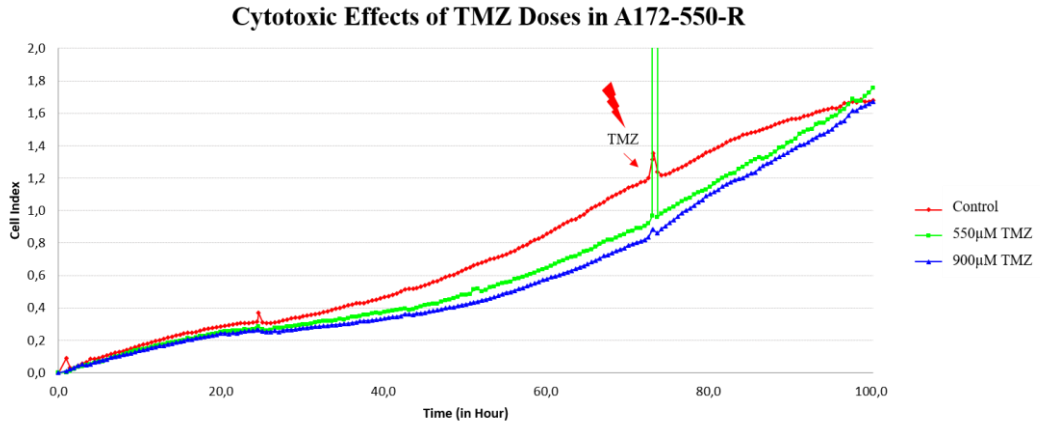

b)

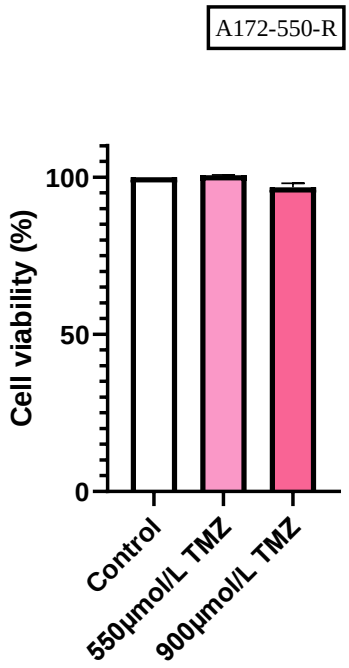

Figure 82. a) Raw data of the effect of TMZ treatment with 550 µmol/L and 900 µmol/L on A172-550-R cell proliferation b) Graphical representation of the effect of TMZ on cell index and cell viability rate in A172-550-R.

A similar effect was seen in A172-750-R when both its own resistant dose of 750 µmol/L and A172 IC50 dose of 900 µmol/L were given (Figure 83. a), and a reduction in the lethality of TMZ was noted by keeping cell viability over 87% in both doses (Table 25) (Figure 83. b).

Table 25. Average data of cell index and cell viability rates of A172-750-R after 24h of treatment with 750 µmol/L and 900 µmol/L TMZ doses.

	Cell Index (24h)	***Cell Viability Rate (%) (24h)***
A172-750-R Control	2,76	100
A172-750-R 750 µmol/L	2,43	88,04
A172-750-R 900 µmol/L	2,41	87,31

a)

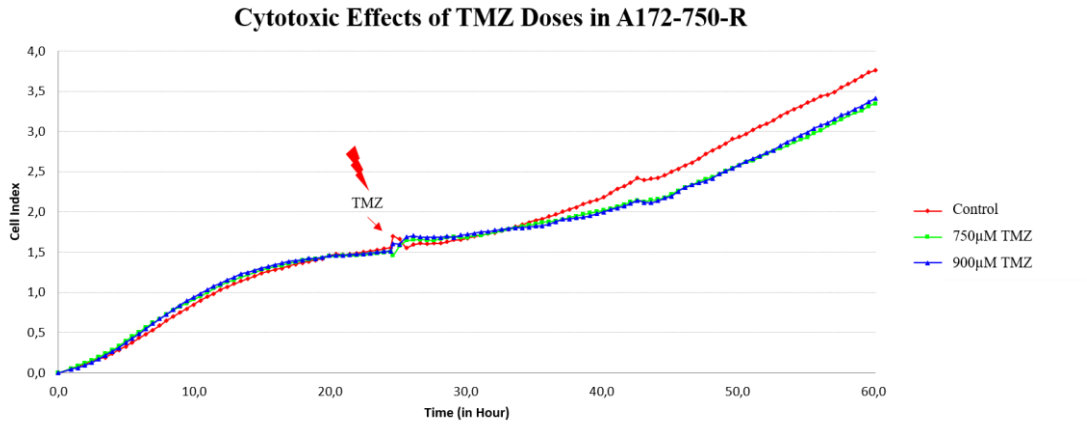

b)

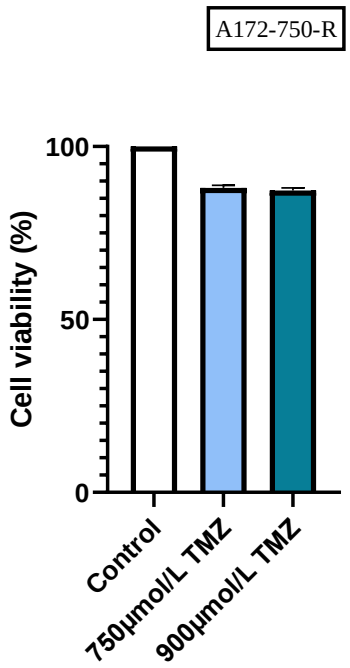

Figure 83. a) Raw data of the effect of TMZ treatment with 750 µmol/L and 900 µmol/L on A172-750-R cell proliferation b) Graphical representation of the effect of TMZ on cell index and cell viability rate in A172-750-R.

With the long-term treatment of A172 with 900 µmol/L (A172-900-R), the cell-to-cell interactions and more aggressive behaviours were clearly observed (Figure 84). The differences between A172 and A172-900-R (A172-R) treated with 900 µmol/L TMZ was statistically significant ($p<0,0001$) meaning that there was a significantly increased cell viability of A172-900-R and decreased TMZ efficiency due to resistance (Figure 85). When A172-900-R cells are dosed with 900 µmol/L

TMZ, the effective IC50 dose of A172 of TMZ, a viability of around 65% was observed which was significant to control of A172-900-R ($p<0,0001$) (Table 26) (Figure 86. b). When treated with 13.78 µmol/L fisetin, the effective IC50 dose of A172 of fisetin, the viability increased to approximately 90% (Table 26) (Figure 86. A). 50.78% viability was obtained when cells exposed to 900 µmol/L TMZ+13.78 µmol/L Fisetin (Table 26) and it was statistically significant from both untreated cells and TMZ-alone treated cells ($p<0,0001$) (Figure 86. b). The present finding showed that fisetin may be useful in breaking acquired resistance.

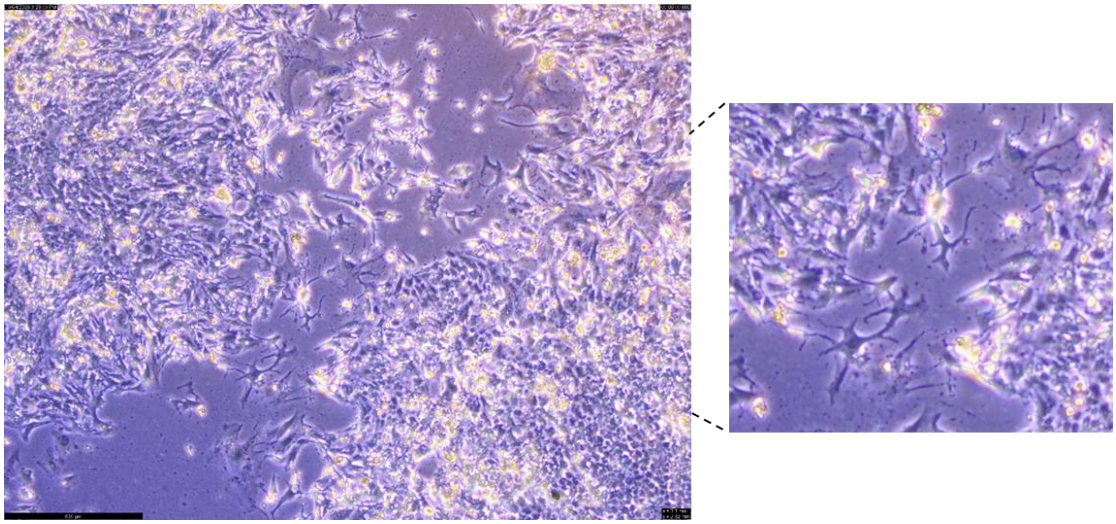

Figure 84. Microscopic representation of the acquired TMZ-resistant A172-900-R morphology and cell-to-cell connections at 4X objective (scalebar: 620 µm).

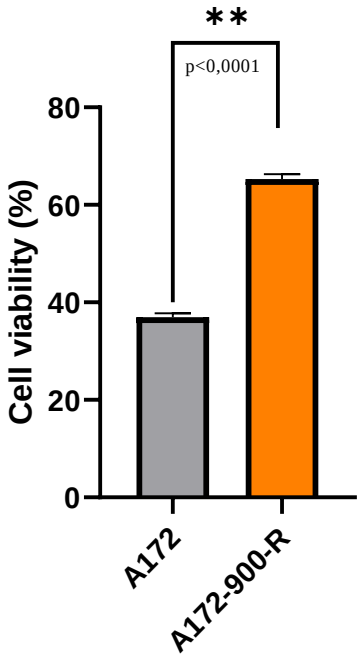

Figure 85. The cell viability difference between A172 and A172-900-R when treated with 900 µmol/L TMZ.

Table 26. Average data of cell index and cell viability rates of A172-900-R after 24h of treatment with IC50 doses of TMZ (900 µmol/L), Fisetin (13.78 µmol/L) and their combination.

	Cell Index (24h)	***Cell Viability Rate (%) (24h)***
Control	3,17255	100
TMZ	2,0754	65,29
Fisetin	2,85855	89,90
TMZ+Fisetin	1,61155	50,78

a)

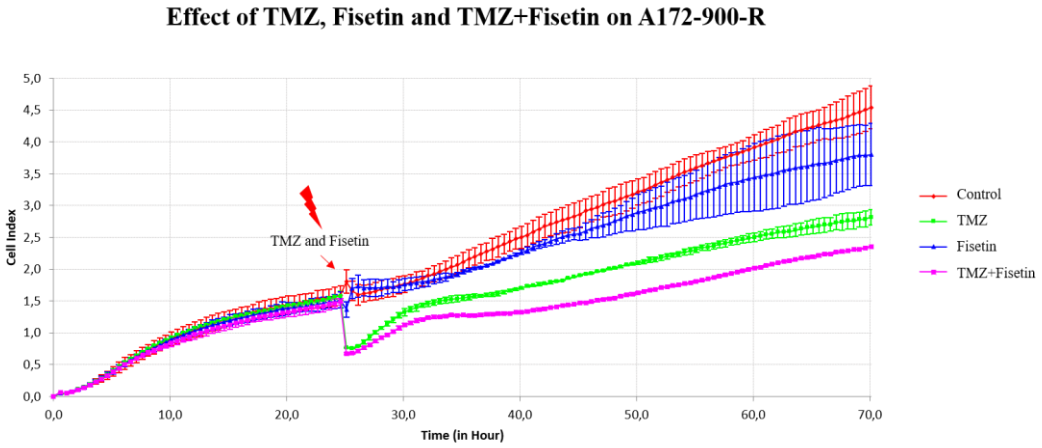

b)

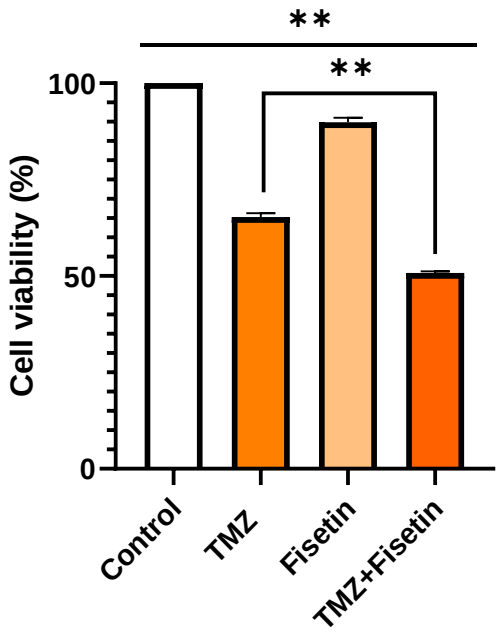

Figure 86. a) Raw data of the effect of TMZ, Fisetin and their cotreatment with 900 µmol/L on A172-900-R cell proliferation b) Graphical representation of the effect of TMZ and fisetin on cell index and cell viability rate in A172-900-R.

4.3. Effects of the Treatment of Flavonoids Alone and in Combination with TMZ on Directing GBM Cells to Apoptosis

4.3.1. Effects of TMZ, Fisetin and TMZ+Fisetin on Apoptosis in T98G

In order to determine the apoptotic effect of TMZ, Fisetin and combination treatment on T98G cells, cells were treated for 24 hours with the effective doses of the compounds. Whilst the number of viable cells was around 85% in the control group, the viabilities for TMZ, Fisetin and TMZ+Fisetin were 19.32%, 29.87% and 19.09%, respectively (Figure 87. a). The percentage of total apoptotic cells was 78.40% in TMZ and increased to 79.85% in the combined group, and also the early apoptotic rate increased compared to TMZ (Figure 87. b). In addition, fisetin alone caused apoptosis of up to 70% significantly ($p<0.0001$) (Figure 87. b). In conclusion, fisetin increased the apoptosis-promoting capacity of TMZ in intrinsic TMZ-resistant T98G cells ($p<0,0001$).

a)

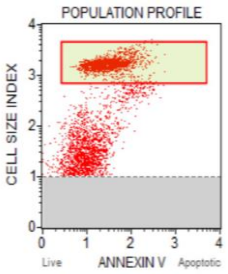

T98G	Apoptosis Profile		Cell Concentration (Cells/mL)	%Gated
Control	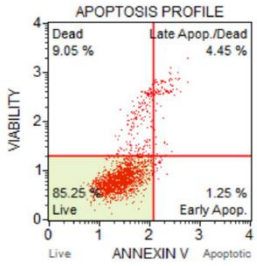	Live (LL) : Early Apoptotic (LR) : Late Apop./ Dead (UR) : Debris (UL) : Total Apoptotic :	1.17E+06 1.71E+04 6.09E+04 1.24E+05 7.79E+04	85.25 % 1.25 % 4.45 % 9.05 % 5.70 %
TMZ	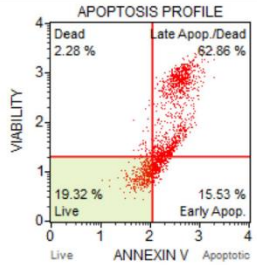	Live (LL) : Early Apoptotic (LR) : Late Apop./ Dead (UR) : Debris (UL) : Total Apoptotic :	1.66E+04 1.34E+04 5.41E+04 1.96E+03 6.75E+04	19.32 % 15.53 % 62.86 % 2.28 % 78.40 %
Fisetin	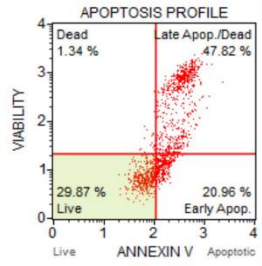	Live (LL) : Early Apoptotic (LR) : Late Apop./ Dead (UR) : Debris (UL) : Total Apoptotic :	1.80E+04 1.26E+04 2.88E+04 8.07E+02 4.14E+04	29.87 % 20.96 % 47.82 % 1.34 % 68.79 %
TMZ+ Fisetin	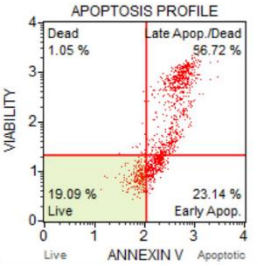	Live (LL) : Early Apoptotic (LR) : Late Apop./ Dead (UR) : Debris (UL) : Total Apoptotic :	1.74E+04 2.11E+04 5.16E+04 9.57E+02 7.27E+04	19.09 % 23.14 % 56.72 % 1.05 % 79.85 %

b)

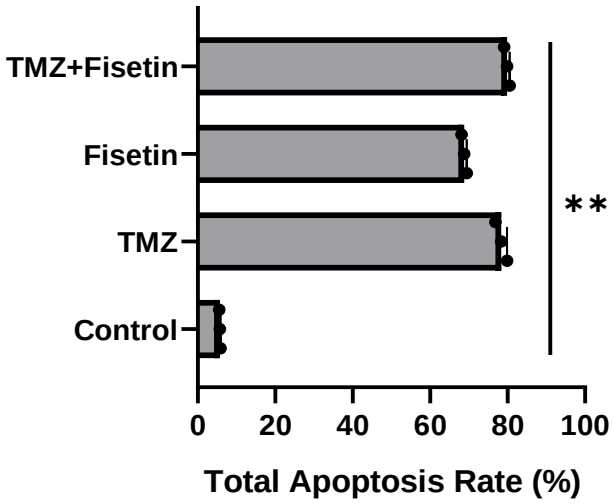

Figure 87. a) Apoptosis profile and number of live and apoptotic cells with the treatment of TMZ, Fisetin and TMZ+Fisetin in T98G using Muse Cell Analyzer. b) Graphical representation of total apoptotis rate (%) with the treatment of TMZ, Fisetin and TMZ+Fisetin in T98G.

4.3.2. Effects of TMZ, Berberine and TMZ+Berberine on Apoptosis in T98G

In the T98G, control (untreated) group, the number of viable cells was around 85% and the total number of apoptotic cells was around 5% (Early Apoptotic, 1.25%; Late Apoptotic/Dead, 4.45%) (Figure 88. a). TMZ treatment reduced the living cell population below 20% levels and caused almost 80% total apoptosis, including early apoptotic 15.53% and late apoptotic/dead 62.86% (Figure 88. a). Berberine alone caused more than 50% total apoptosis, while its combination with TMZ appeared to have increased total apoptosis to approximately 70% (Figure 88. a). All treated groups were significantly different compared to untreated group ($p<0.0001$) (Figure 88. b).

a)

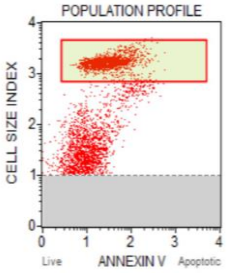

T98G	Apoptosis Profile		Cell Concentration (Cells/mL)	%Gated
Control	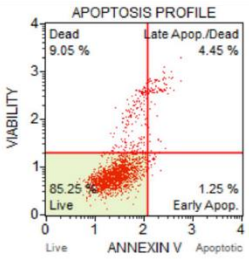	Live (LL) :	1.17E+06	85.25 %
		Early Apoptotic (LR) :	1.71E+04	1.25 %
		Late Apop./ Dead (UR) :	6.09E+04	4.45 %
		Debris (UL) :	1.24E+05	9.05 %
		Total Apoptotic :	7.79E+04	5.70 %
TMZ	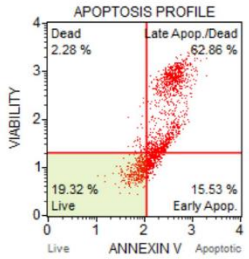	Live (LL) :	1.66E+04	19.32 %
		Early Apoptotic (LR) :	1.34E+04	15.53 %
		Late Apop./ Dead (UR) :	5.41E+04	62.86 %
		Debris (UL) :	1.96E+03	2.28 %
		Total Apoptotic :	6.75E+04	78.40 %
Berberine	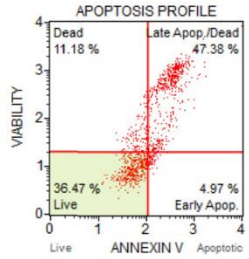	Live (LL) :	1.15E+04	36.47 %
		Early Apoptotic (LR) :	1.57E+03	4.97 %
		Late Apop./ Dead (UR) :	1.49E+04	47.38 %
		Debris (UL) :	3.52E+03	11.18 %
		Total Apoptotic :	1.65E+04	52.35 %
TMZ+ Berberine	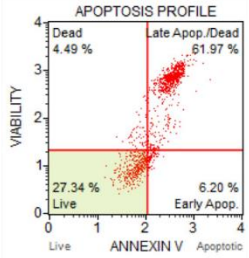	Live (LL) :	9.87E+03	27.34 %
		Early Apoptotic (LR) :	2.24E+03	6.20 %
		Late Apop./ Dead (UR) :	2.24E+04	61.97 %
		Debris (UL) :	1.62E+03	4.49 %
		Total Apoptotic :	2.46E+04	68.16 %

b)

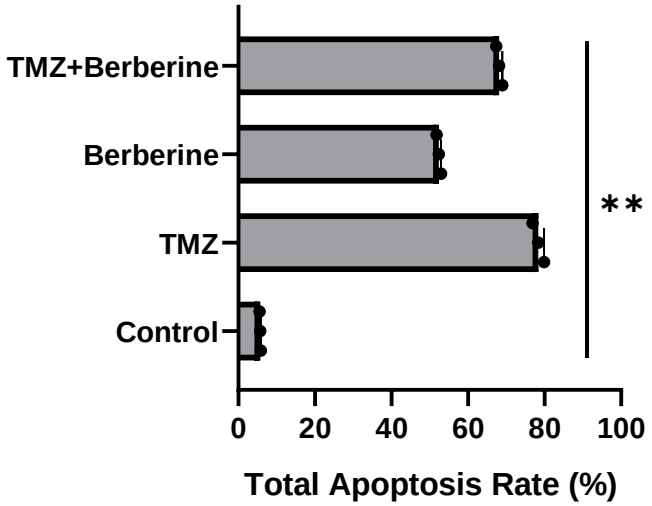

Figure 88. a) Population and apoptosis profile and number of live and apoptotic cells with the treatment of TMZ, Berberine and TMZ+Berberine in T98G. b) Graphical representation of total apoptotis rate (%) with the treatment of TMZ, Berberine and TMZ+Berberine in T98G.

4.3.3. Morphological Assessment of the Effects of TMZ, Fisetin, and TMZ+Fisetin on Apoptosis in T98G with Acridine Orange/Propidium Iodide (AO/PI)

The cell morphology of T98G cells was studied to determine the manner of cell death induced by fisetin therapy. The morphology of T98G cells after fisetin treatment was investigated using AO/PI staining with EVOS™ M5000 Cell Imaging System. Morphological assesment of cell viability showed that Fisetin and TMZ+Fisetin had more of fragmented nuclei in horseshoe-shaped cells which represents apoptosis in T98G (Figure 89. a). While number of necrotic cells were relatively high (33) in fisetin and combination TMZ treated groups, they were decreasing successfully to 1 and 2, respectively (Table 27) (Figure 89. b).

Table 27. Number of total cells and PI positive cells in each experimental group in T98G.

Image Tag	Total Cells	Propidium Iodide Positive Cells
T98G Control	289	2
T98G TMZ	293	33
T98G Fisetin	198	1
T98G TMZ+Fisetin	189	2

a)

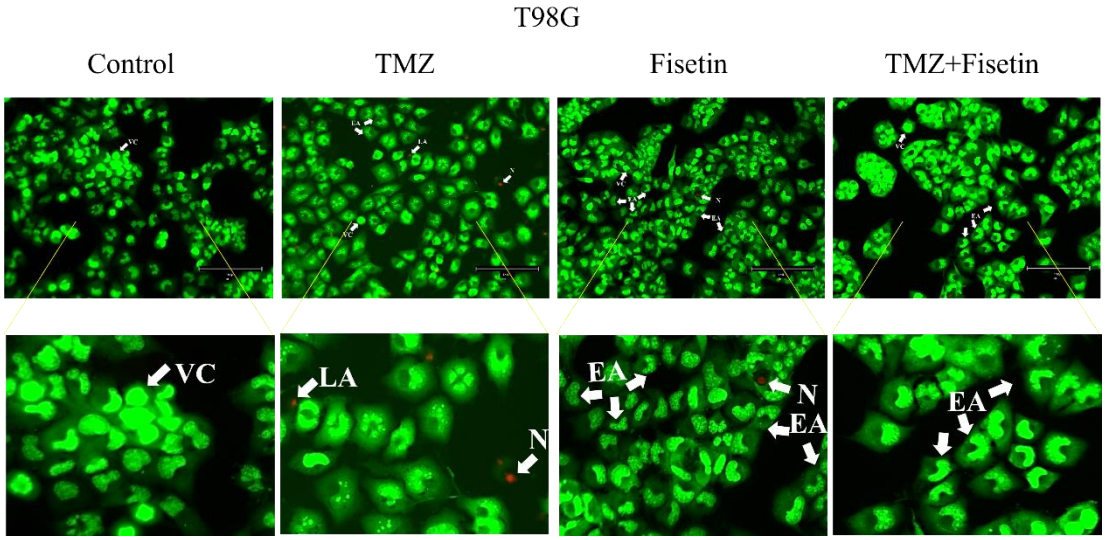

b)

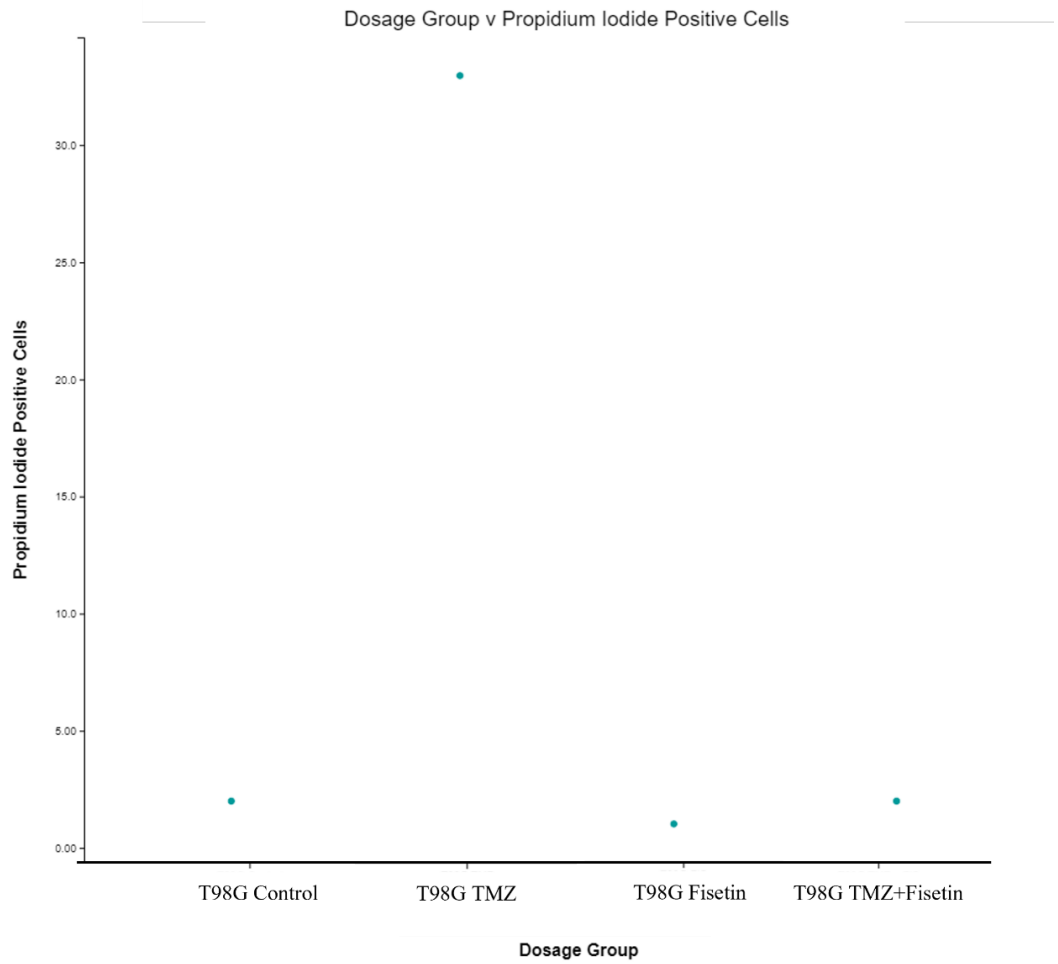

Figure 89. a) Morphological representation of viable, apoptotic and necrotic cells under TMZ, Fisetin and TMZ+Fisetin treatment in T98G (VC: Viable Cells, EA: Early Apoptotic Cells, LA: Late Apoptotic Cells, N: Necrotic Cells) b) Graphical representation of necrotic cells in each group which were detected with PI (The quantification analysis was provided from HALO AI software by Indica Labs).

4.3.4. Morphological Assessment of the Effects of TMZ, Fisetin, and TMZ+Fisetin on Apoptosis in A172 with Acridine Orange/Propidium Iodide (AO/PI)

Cellular morphologies of A172 cells treated with TMZ, Fisetin and TMZ+Fisetin were investigated to identify the mode of fisetin-induced cell death. Fisetin-treated A172 cells had their morphology analyzed by AO/PI staining with EVOS™ M5000 Cell Imaging System. When cell viability was examined morphologically, the difference between healthy and apoptotic cells was visibly demonstrated (Figure 90. a). While TMZ group had more necrotic cells (21), it had been decreased with fisetin (19) and especially, TMZ+Fisetin (4) (Table 28) (Figure 90. b). Additionally, apoptotic cells appearing in horseshoe-shaped morphology were also increasing in fisetin alone and its combination with TMZ (Figure 90. a).

Table 28. Number of total cells and PI positive cells in each experimental group in A172.

Image Tag	Total Cells	Propidium Iodide Positive Cells
A172 Control	414	1
A172 TMZ	466	21
A172 FIS	556	19
A172 TMZ+FIS	395	4

a)

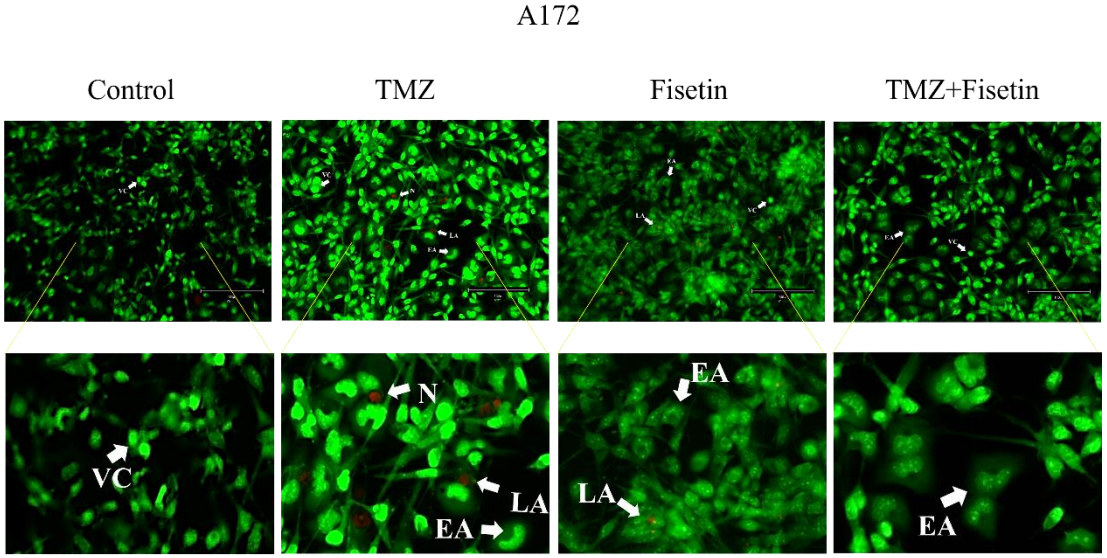

b)

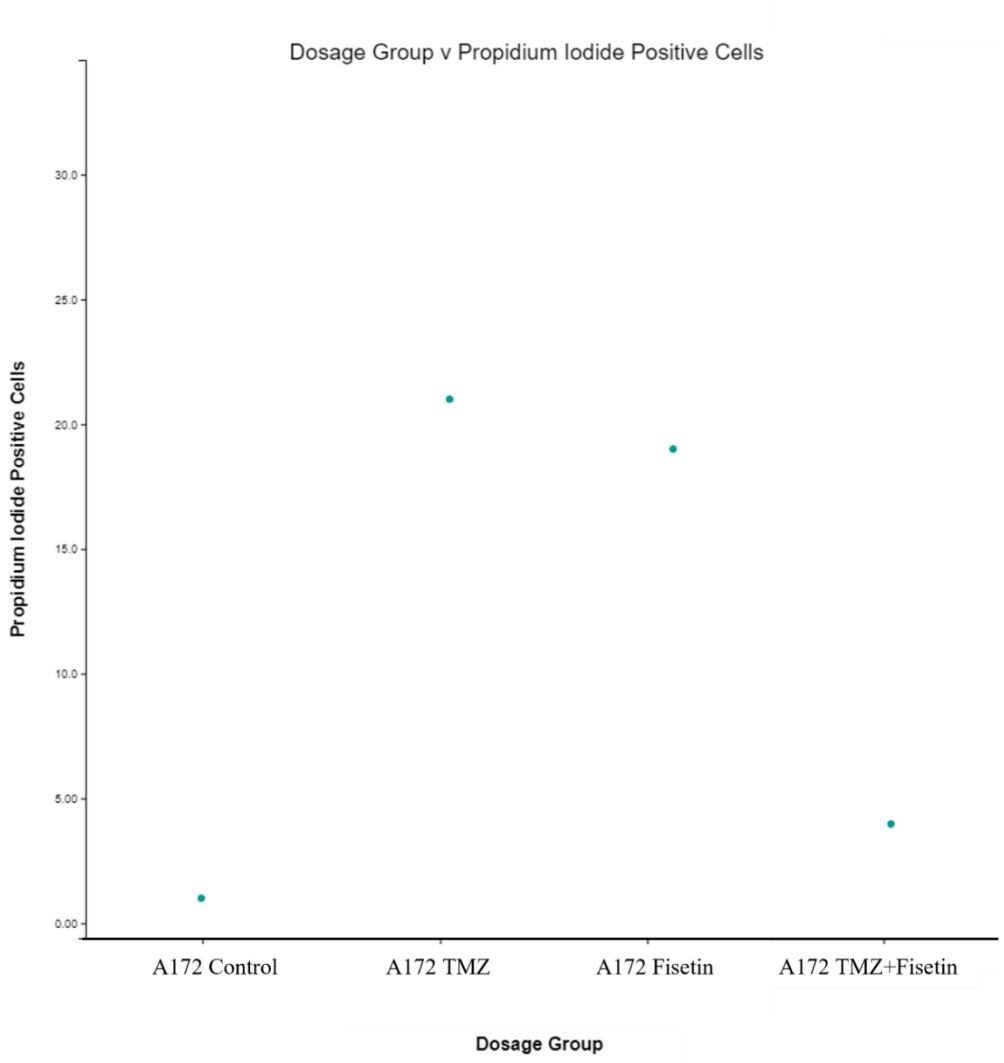

Figure 90. a) Morphological representation of viable, apoptotic and necrotic cells under TMZ, Fisetin and TMZ+Fisetin treatment in A172 (VC: Viable Cells, EA: Early Apoptotic Cells, LA: Late Apoptotic Cells, N: Necrotic Cells) b) Graphical representation of necrotic cells in each group which were detected with PI (The quantification analysis was provided from HALO AI software by Indica Labs).

4.4. Effects of Flavonoids Alone and in Combination with TMZ on Cell Cycle Arrest of GBM Cells

4.4.1. Effects of TMZ, Fisetin and TMZ+Fisetin on the Cell Cycle in T98G

In control cells, the G0/G1 ratio was 46.8, the S ratio was 9.8, and the G2/M ratio was 43.4 (Figure 91. a). In treatment with the effective dose of TMZ, the G0/G1 ratio of T98G cells decreased to 42.1, the ratio in S phase increased to 11.3 and the

G2/M ratio decreased to 37.3. In fisetin treatment, the G0/G1 ratio increased above 50, the S ratio elevated to 11.7, and the G2/M decreased to 37.6. The combination therapy decreased the G0/G1 and S ratio by 2.9 and 1.4, respectively, compared to the control. In contrast, TMZ+Fisetin increased the G2/M ratio by 4.3 (Table 29). There was no significant difference in G0/G1, S and G2/M ratios in TMZ (p=0.7964), Fisetin (p>0.9999) and TMZ+Fisetin (p>0.9999) compared to control cells (Figure 91. b). In summary, Fisetin-only group caused cell cycle arrest in G0/G1 when TMZ+Fisetin caused arrest in G2/M in T98G.

Table 29. Cell cycle distribution data in G0/G1, S, and G2/M phases in T98G.

	G0/G1	**S**	**G2/M**
Control	46,8	9,8	43,4
TMZ	42,1	11,3	37,3
Fisetin	50,7	11,7	37,6
TMZ+Fisetin	43,9	8,4	47,7

a)

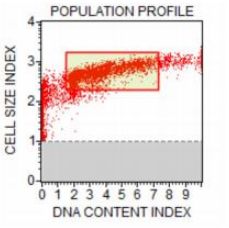

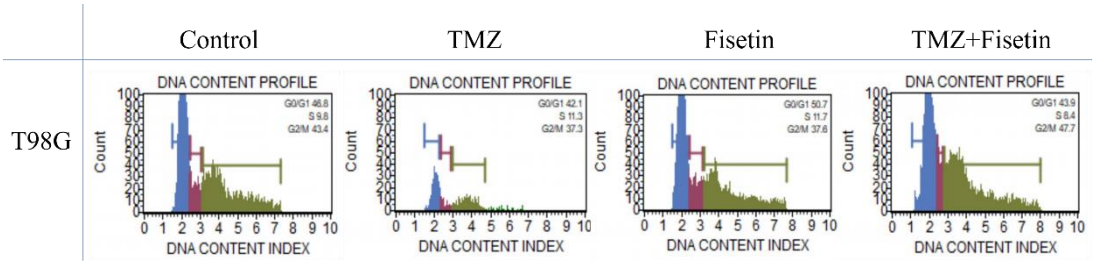

b)

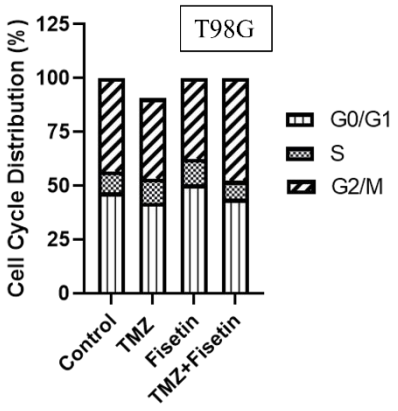

Figure 91. a) Flow cytometric histograms showing population profile of control and DNA content profile of Control, TMZ, Fisetin, TMZ+Fisetin with the use of fluorescence intensity of G0/G1, S, and G2/M phases in T98G using Muse Cell Analyzer. b) Graphical representation of cell cycle distribution percentage of each experimental group.

4.4.2. Effects of TMZ, Fisetin and TMZ+Fisetin on the Cell Cycle in A172

The difference in G0/G1, S and G2/M ratios was not significant in TMZ (p=0.8750), Fisetin (p=0.9773) and TMZ+Fisetin (p=0.9685) when compared with control cells (Figure 92. b). However, in A172, G0/G1 ratios in Control, TMZ, Fisetin and TMZ+Fisetin were determined as 46.5, 45.9, 40.5 and 26.6, respectively. The rates in the S phase were 8.7, 14, 9.3 and 31.4, respectively. G2/M phase was disrupted as 43.3, 15.7, 36.6 and 26.9 (Table 30). It had been observed that all treated groups stopped the cell cycle in S phase, but mostly the combination-mediated induction with 3,6-fold increase compared to untreated group (Figure 92. a).

Table 30. Cell cycle distribution data in each cell cycle phase in A172.

	G0/G1	S	G2/M
Control	46,5	8,7	43,3
TMZ	45,9	14	15,7
Fisetin	40,5	9,3	36,6
TMZ+Fisetin	26,6	31,4	26,9

a)

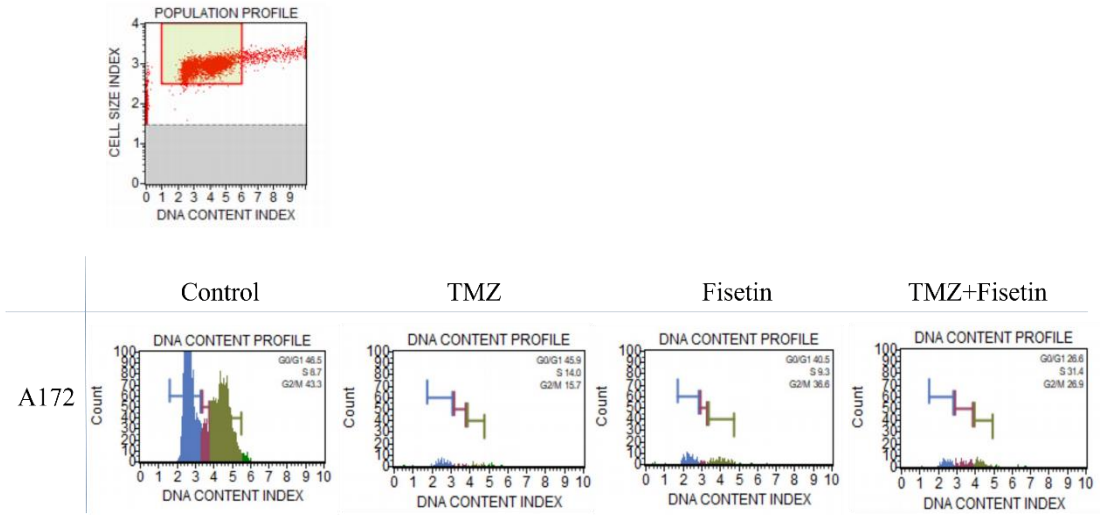

b)

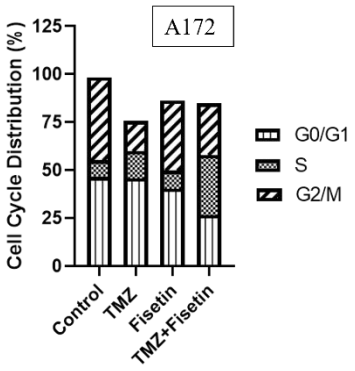

Figure 92. a) Flow cytometric histograms showing population profile of control and DNA content profile of Control, TMZ, Fisetin, TMZ+Fisetin with the use of fluorescence intensity of G0/G1, S, and G2/M in A172. b) Graphical representation of cell cycle distribution percentage of each experimental group.

4.4.3. Effects of TMZ, Berberine and TMZ+Berberine on the Cell Cycle in T98G

In T98G, after 24 hours of TMZ treatment, there was accumulation in the S phase, from 9.8 to 11.3 (Figure 93. a). With berberine treatment, the arrest in the S phase increased from 9.8 to 13.2, and in the G2/M phase from 43.4 to almost 50. In the combined treatment, cell cycle disruption in S phase increased to 13 and G2/M phase arrest exceeded 56 (Table 31). Compared with control cells, there was no significance for TMZ ($p=0.9515$), Berberine ($p>0.9999$) and TMZ+Berberine ($p>0.9999$) in cell cycle phases (Figure 93. b).

Table 31. Cell cycle distribution data in each cell cycle phase in T98G.

	G0/G1	S	G2/M
Control	46,8	9,8	43,4
TMZ	42,1	11,3	37,3
Berberine	37,4	13,2	49
TMZ+Berberine	30,8	13	56,2

a)

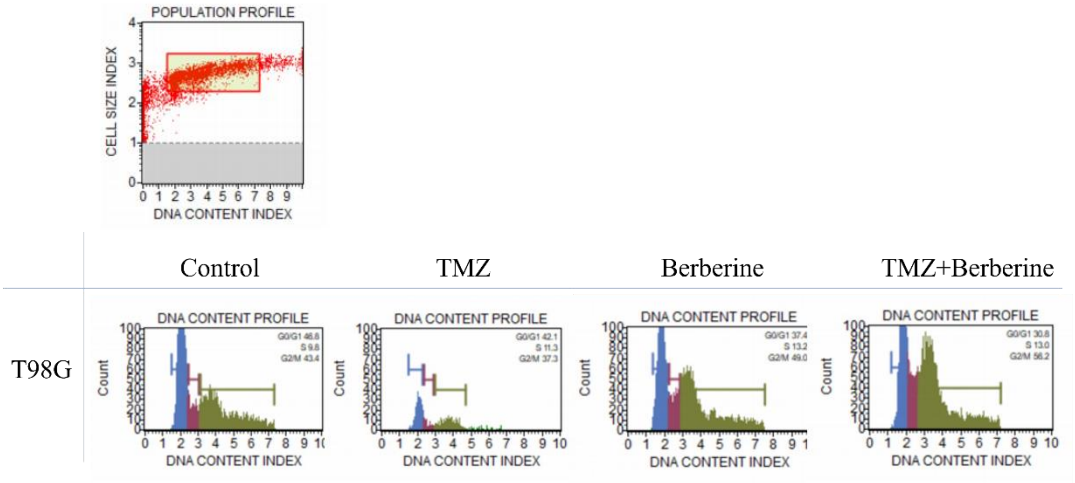

b)

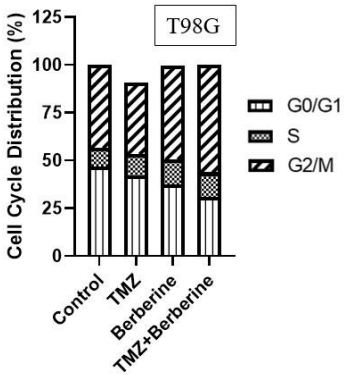

Figure 93. a) Flow cytometric histograms showing DNA content profile of TMZ, Berberine, TMZ+Berberine with the use of fluorescence intensity of cell cycle phases in T98G using Muse Cell Analyzer. b) Graphical representation of cell cycle distribution (%) of each experimental group.

4.5. Effects of Flavonoids Alone and in Combination with TMZ on Wound Healing of GBM Cells

4.5.1. The effects of TMZ, Fisetin and TMZ+Fisetin on Wound Healing in T98G

T98G cells were treated with effective doses of TMZ and fisetin for 24h. Images of the wounded sub-confluent monolayers of T98G cells treated with the effective doses were taken at 4× at 0-6-18-24h (represented) and percentage wound widths were plotted. The number of cells/field was shown in Figure 94. a). Control cells were untreated cells with high metastatic and wound-closure (78,74%) ability after 24h. In the untreated (control) group, it was found that the scratch area gradually closed at 6, 18 and 24 hours, and the width of gap decreased to almost 21% levels at the end of 24h (Figure 94. a). In the treatment of TMZ, this area was closed in a way that kept its borders and the wound area was calculated to be around 72% at the end of the 24h. Surprisingly, fisetin treatment alone successfully increased the wound area to 90,07% (Table 32). This effect was even higher in combination treatment. In addition, the combined treatment resulted in an even better outcome. TMZ+Fisetin resulted not only in the inhibition of wound closure but also increased the wound area (Table 32). Thus, a dispersed morphology with cell borders was observed in the combined treatment, significantly reducing cell invasion and migration. As a result, TMZ+Fisetin treatment increased the anti-invasive effect of TMZ in T98G in normoxia ($p<0.0001$) (Figure 94. b).

Table 32. Digital data of the rates of wound area with TMZ, Fisetin, and TMZ+Fisetin treatment in T98G.

	Control	TMZ	Fisetin	TMZ + Fisetin
0h	100%	100%	100%	100%
24h	21,26%	72,78%	90,07%	101,16%

a)

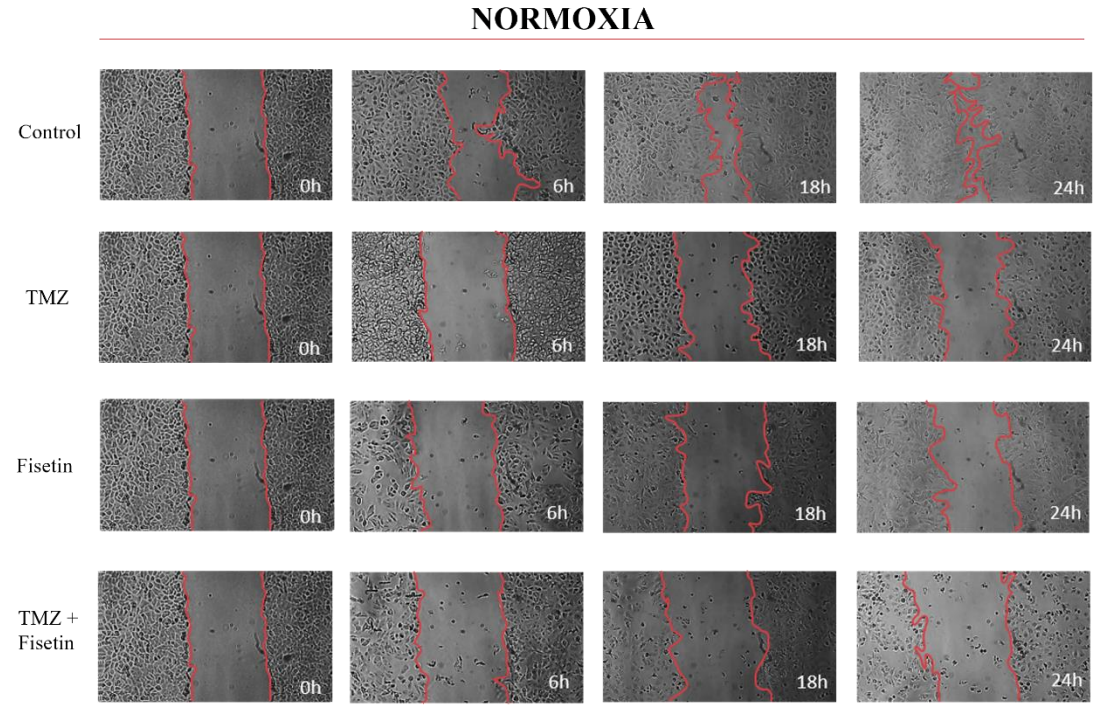

b)

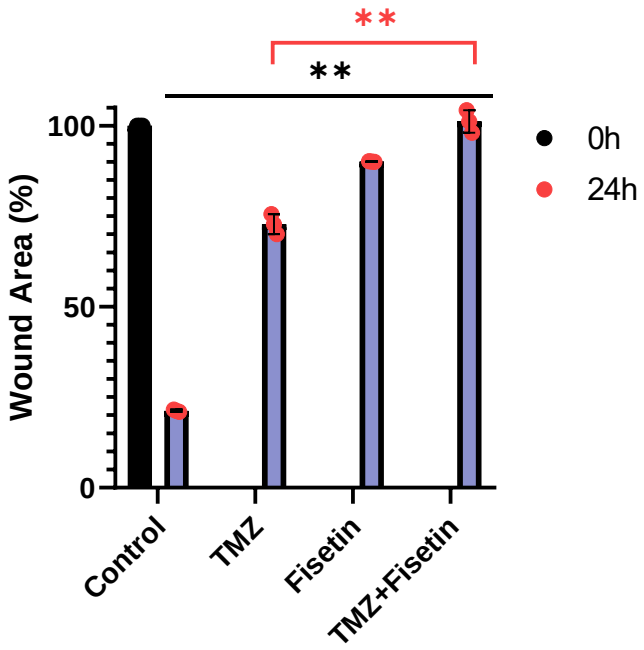

Figure 94. The effect of TMZ, Fisetin, and TMZ+Fisetin on cell invasion and migration with wound healing assay in T98G cell line under normoxic conditions. a) Representative images at 4× at 0, 6, 18, & 24h (scalebar: 620 µm). b) Graphical representation of the percentages of cells in each wound area. The data shown is representative of three independent experiments. Bars represent mean ± S.D.

4.5.2. The effects of TMZ, Fisetin and TMZ+Fisetin on Wound Healing in A172

In A172, almost 73%, 32% ($p<0.0001$), and 27% ($p<0.0001$) of the wound areas were closed 24 hours after dosing in the control, TMZ, and fisetin groups, respectively (Table 33). Fisetin alone showed a similar effect to TMZ. Although wound healing was directly proportional over time in these groups, this was not observed in the combination group (Figure 95. a). Wound area of TMZ+Fisetin treatment resulted in 96,99% which was enhanced compare the TMZ ($p<0.0001$) (Figure 95. b). This finding appeared to enhance the effectiveness of TMZ and it had been found that correlation between TMZ and TMZ+Fisetin was significant ($p<0.0001$) (Figure 95. b). A similar successful anti-invasive and anti-migratory property of TMZ and TMZ+Fisetin therapy was emphasized, with a difference of only 4% between T98G and A172 in both groups (Figure 96).

Table 33. Digital data of the average percentages of wound gap with TMZ, Fisetin, and TMZ+Fisetin treatment in A172.

	Control	TMZ	Fisetin	TMZ + Fisetin
0h	100%	100%	100%	100%
24h	27,03%	68,55%	72,98%	96,99%

a)

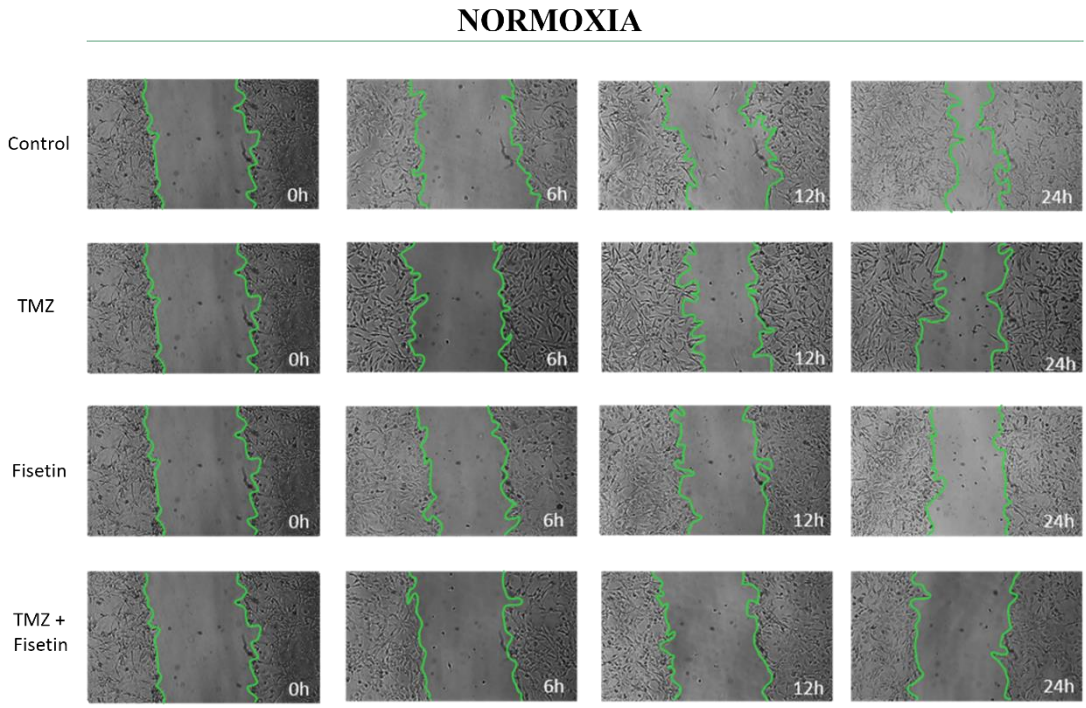

b)

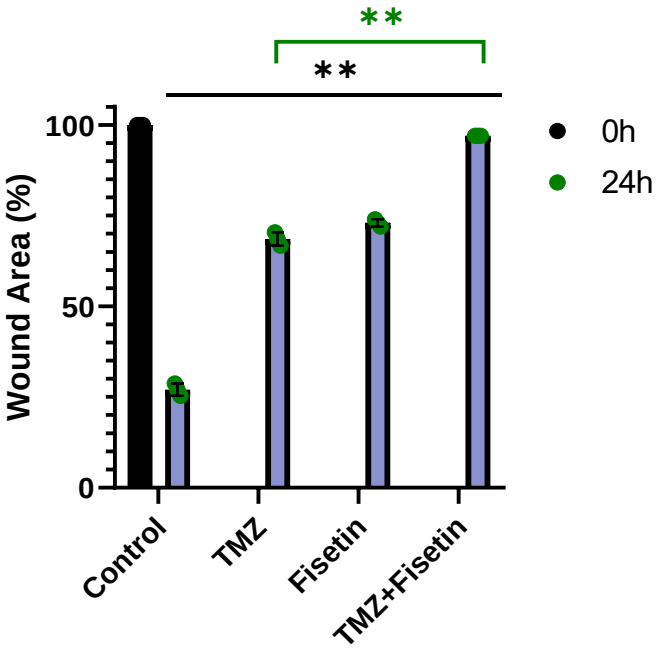

Figure 95. The effect of TMZ, Fisetin, and TMZ+Fisetin on cell invasion and migration with wound healing assay in A172 cell line a) Representative images at 4× at 0, 6, 12, & 24h. b) Graphical representation of the percentages of cells in each wound area. Bars represent mean ± S.D.

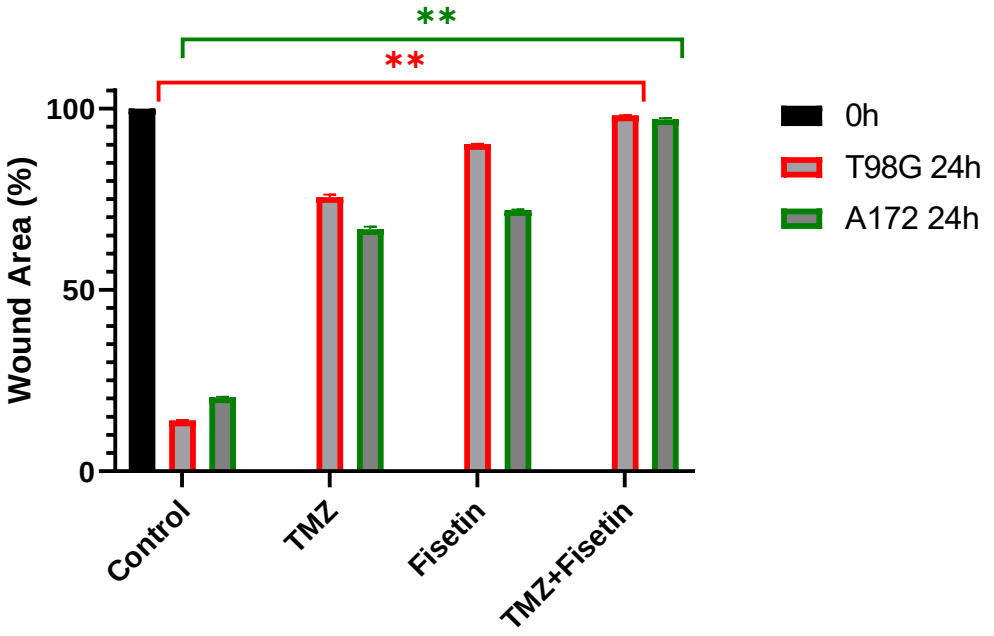

Figure 96. Comparative analysis of the anti-invasive and anti-migrative effect of TMZ, Fisetin, and TMZ+Fisetin treatment in two different GBM cell lines (T98G and A172). Bars represent mean ± S.D.

4.5.3. The effects of TMZ, Fisetin and TMZ+Fisetin on Wound Healing in A172-R

A172-R cells were treated with effective doses of TMZ and fisetin for 24h and images of wounded monolayers were taken at 4× at 0-6-12-24h. The wound widths were shown after subsequent observation of the number of cells/field for required time in Figure 97. a. In untreated cells, closure of wound width was 69.49% at the end 24h of treatment (Table 34). Interestingly, the percentage of wound area in the TMZ alone group was significantly reduced to 39.44% compared to the untreated group, which was higher in the TMZ-sensitive A172 (see 4.5.2). Thus, statistical significance was also obtained when this decrease between TMZ treatment in resistant (A172-R) and non-resistant (A172) cell lines were compared ($p<0,0001$) (Figure 98). Fisetin alone was able to inhibit that wound closure up to 68,46% (Table 34). The wound closure was 13.23% showing strong migration-repressing effect caused by TMZ+Fisetin treatment even in acquired resistant cell line when TMZ was not effective enough and that change was significant ($p<0,0001$) (Figure 97. b). Notingly, there was a visible

intact appearance protecting wound width at the wound line border in the TMZ+Fisetin treatment (Figure 97. a). In summary, Fisetin alone and combination with TMZ enhanced the anti-invasive and migrative ability and improved effect of TMZ under normoxic conditions in A172-R cells ($p<0,0001$) (Figure 97. b).

Table 34. Digital data of the average rates of wound width with TMZ, Fisetin, and TMZ+Fisetin treatment on A172-R.

	Control	TMZ	Fisetin	TMZ + Fisetin
0h	100%	100%	100%	100%
24h	30,51%	39,44%	68,46%	86,77%

a)

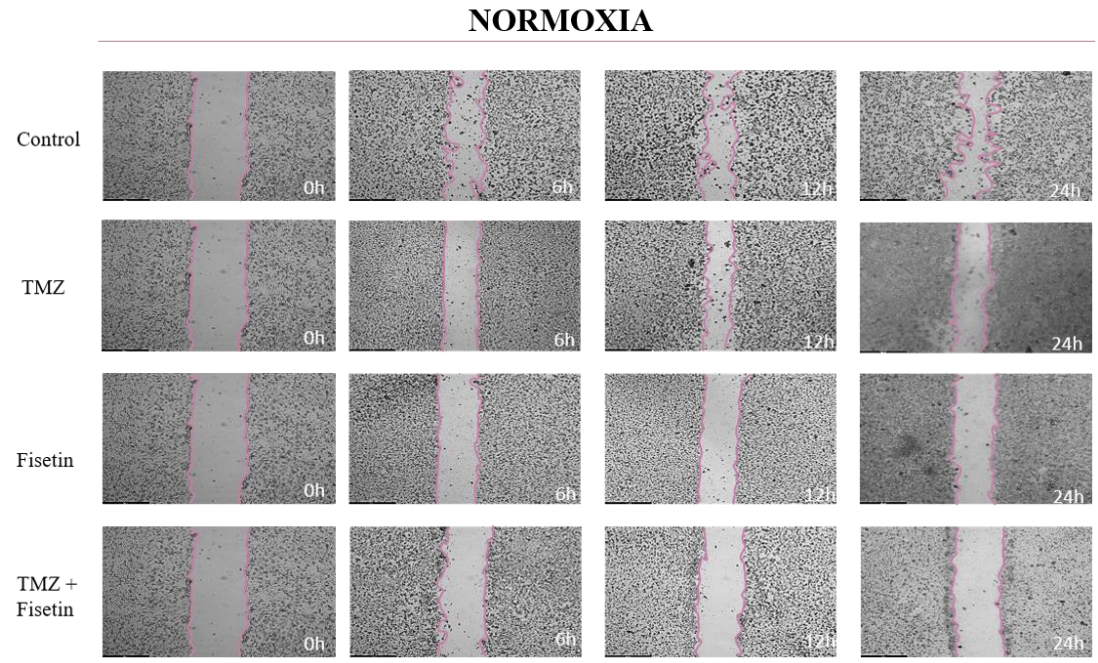

b)

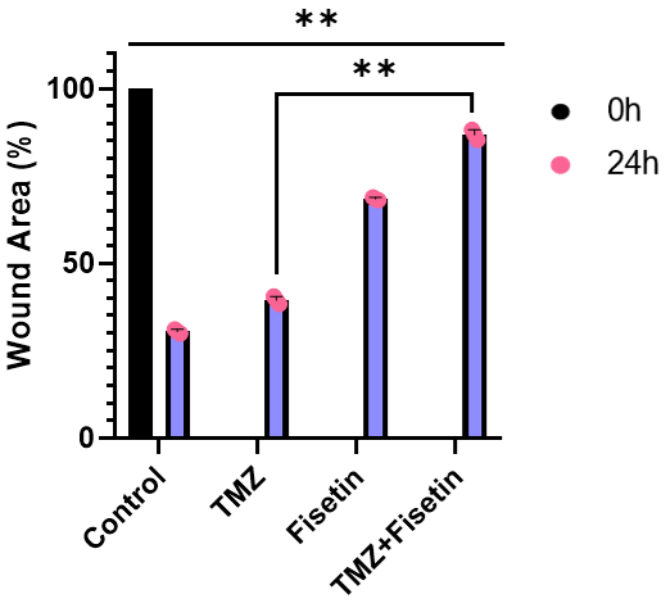

Figure 97. The effect of TMZ, Fisetin, and TMZ+Fisetin on cell invasion and migration with wound healing assay in A172-R cell line a) Representative images taken at 4× at 0, 6, 12, & 24h (scalebar: 620 µm). b) Graphical representation of the percentages of scratch area in each group.

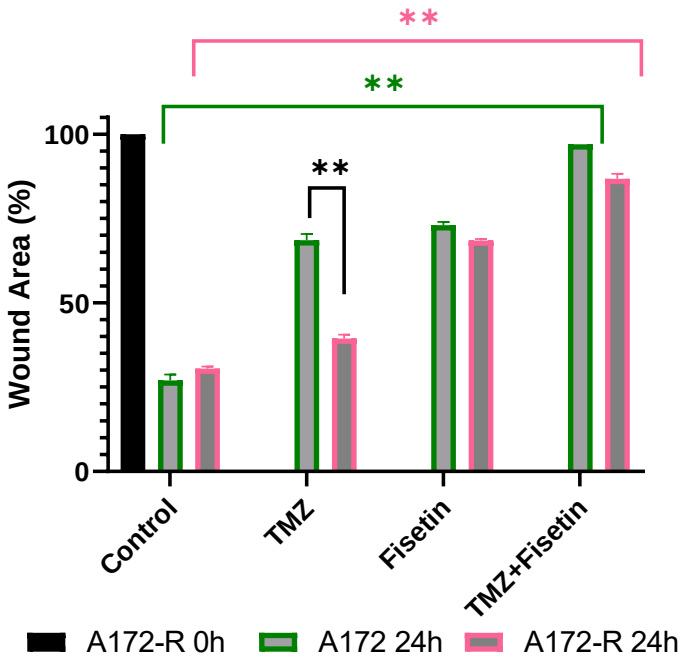

Figure 98. Comparative analysis of TMZ-sensitive A172 and acquired TMZ-resistant A172-R cell line in terms of treatment with TMZ, Fisetin, and TMZ+Fisetin. The data shown is representative of three independent experiments. Bars represent mean ± S.D.

4.5.4. The effects of TMZ, Berberine and TMZ+Berberine on Wound Healing in T98G

In the untreated group, wound width at 24h was observed as 26.37% (Table 35). When treated with IC50 values, at the end of 24h, the open wounded areas in the TMZ-only, Berberine-only, and TMZ+Berberine groups were 71,39%, 101,29%, and 94,18%, respectively (Table 35). The wound width was 101,29% when T98G cells were treated with berberine alone and it proved its anti-migrative ability (Figure 99. a). In addition to this, it meant that only 5,82% of the wounded area was closed for the TMZ+Berberine treatment and it appeared to enhance the effectiveness of TMZ (Figure 99. b). This difference between TMZ and TMZ+Fisetin was appeared to be significant ($p<0,0001$) (Figure 99. b).

Table 35. Digital data of the average rates of wound width with TMZ, Berberine, and TMZ+Berberine treatment in T98G.

	Control	TMZ	Berberine	TMZ + Berberine
0h	100%	100%	100%	100%
24h	26,37%	71,39%	101,29%	94,18%

a)

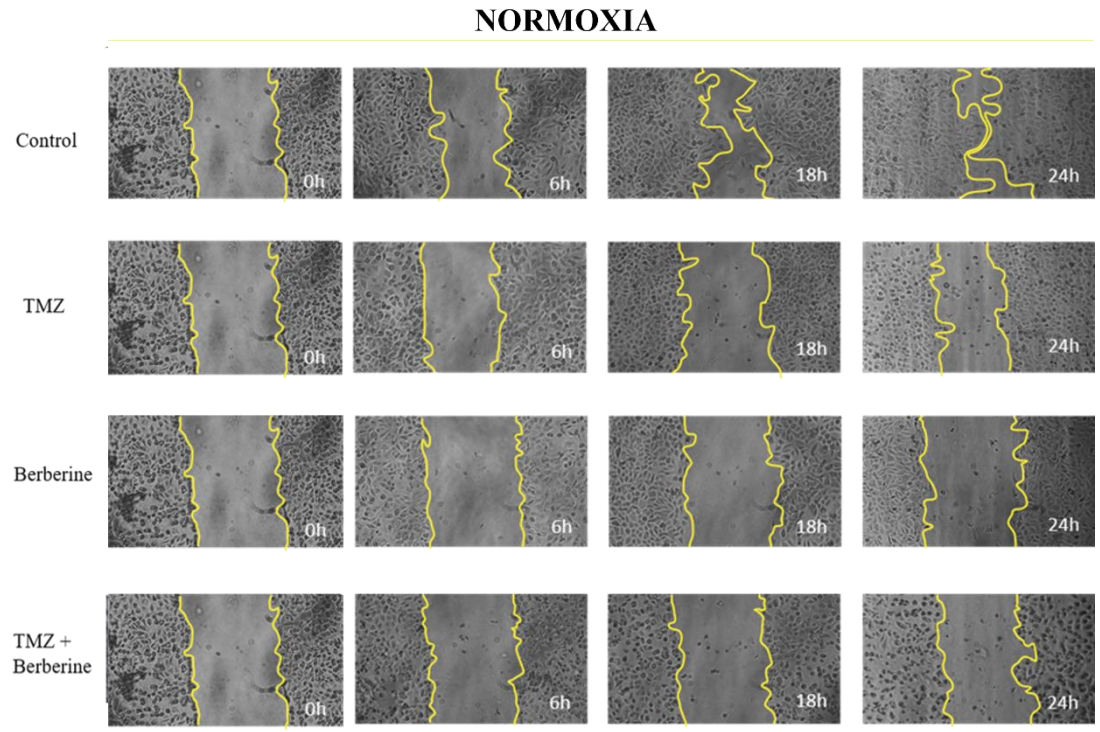

b)

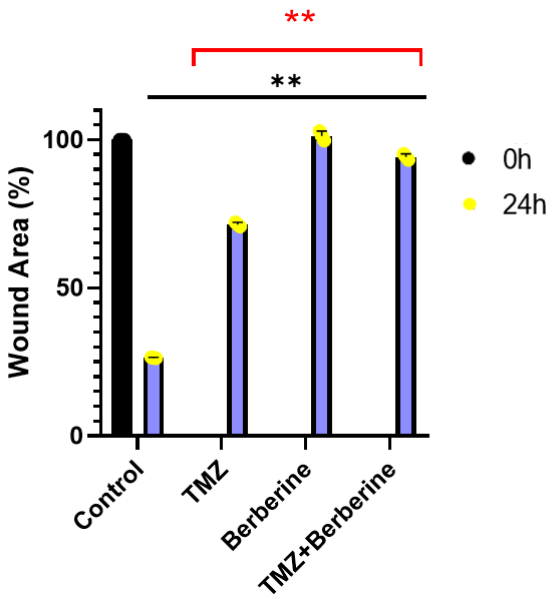

Figure 99. The effect of TMZ, Berberine, and TMZ+Berberine on T98G cell migration and invasiveness via wound healing assay a) Representative images at 4× at 0, 6, 18, & 24h. b) Graphical representation of the percentages of width in each wound area. Bars represent mean ± S.D.

4.6. Effects of Flavonoids Alone and in Combination with TMZ on Colony Formation Ability of GBM Cells

4.6.1. The effects of TMZ, Fisetin and TMZ+Fisetin on Colony Formation in T98G

The effects of effective doses of TMZ, Fisetin and combination treatment on adhesion-independent cell proliferation was tested via colony formation assay. TMZ-alone decreased colony number by 98,73% (78,4-fold) after 24h (Figure 100. a). There were 13,17% of colonies and 7,6-fold inhibition of colonies obtained in fisetin treatment compared to control ($p<0,0001$) (Figure 100. b). On the other hand, the combined therapy inhibited the number of 99,58% colonies formed (235,3-fold more compared to the untreated cells; $p<0,0001$) (Figure 100. a). The number of colonies formed by T98G decreased, and their migration rates slowed upon TMZ+Fisetin compared to untreated and TMZ-only treated cells ($p<0.0001$) (Figure 100. b).

a)

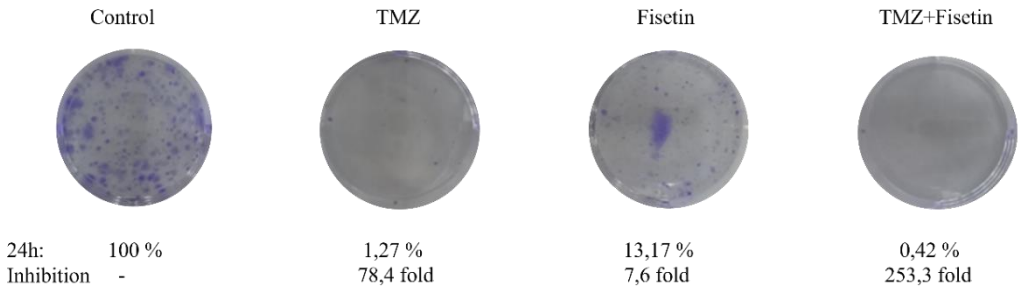

b)

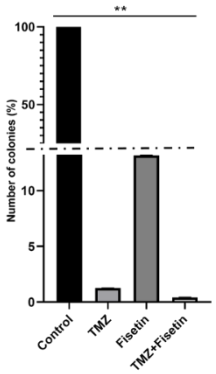

Figure 100. The ability of inhibition of colony formation with TMZ, Fisetin, and TMZ+Fisetin combined treatment in T98G cell line a) Representative colony images b) Graphical representation.

4.6.2. The effects of TMZ, Fisetin and TMZ+Fisetin on Colony Formation in A172

In A172, when cells were treated with TMZ, Fisetin and TMZ+Fisetin for 24h, colony numbers were 3,18%, 22,78% 0,87%, respectively (Figure 101. b). TMZ was able to inhibit colony numbers 31,4-fold ($p<0,0001$) and counted colonies were reduced 4,3-fold ($p<0,0001$) with the fisetin treatment as a result of comparison of untreated group (Figure 101. a). However, TMZ+Fisetin treatment successfully decreased almost 115-fold ($p<0,0001$) colonies formed compared to control (Figure 101. a). When A172 and T98G cells were compared, it was concluded that TMZ+Fisetin treatment produced a significant ($p<0,0001$) response and enhanced the activity of TMZ in both A172 and T98G cell lines (Figure 102).

a)

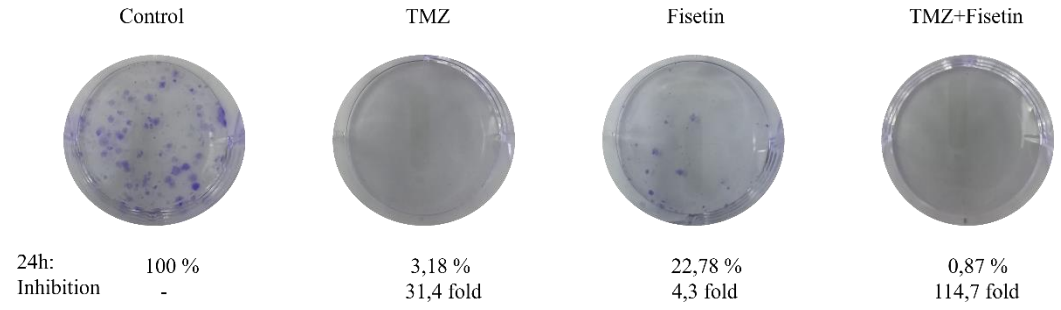

b)

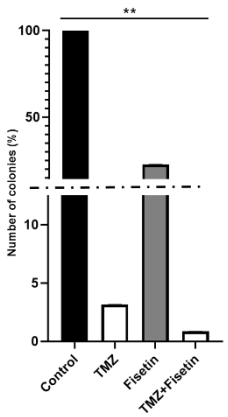

Figure 101. The ability of inhibition of colony formation with TMZ, Fisetin, and TMZ+Fisetin combined treatment in A172 cell line a) Representative colony images b) Graphical representation.

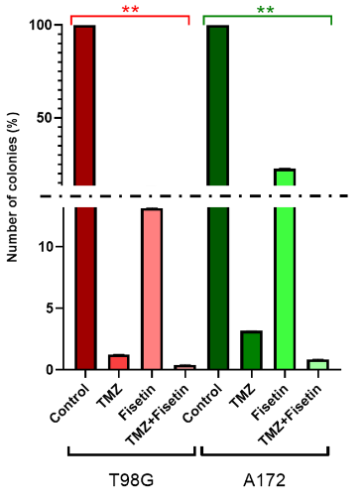

Figure 102. Comparison of the colony formation effect of TMZ, Fisetin, and TMZ+Fisetin treatment in two different GBM cell lines (T98G, A172).

4.6.3. The effects of TMZ, Berberine and TMZ+Berberine on Colony Formation in T98G

Treatments of TMZ, and Berberine alone and in combination were observed for 24h in the colony formation assay. At the end of 24h, the number of colonies in the TMZ group was reduced to less than 3%, and this inhibition was almost 35 times greater than in control cells ($p<0,0001$) (Figure 103. a). Number of colonies counted was 27.87% (3.58-fold; $p<0,0001$) in berberine treatment alone (Figure 103. b). Combination treatment of TMZ and berberine reduced the number of colonies formed to 0.54%, resulting in 183.3-fold colony reduction compared to untreated group ($p<0,0001$) (Figure 103. b).

a)

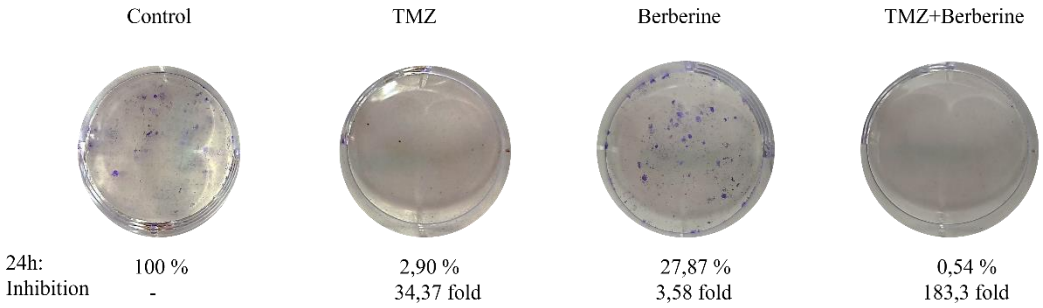

b)

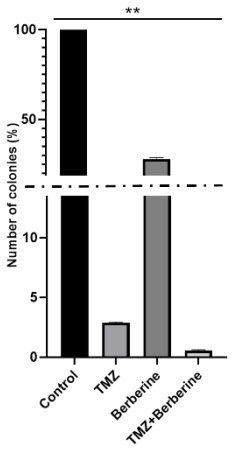

Figure 103. The ability of inhibition of colony formation with TMZ, Berberine, and TMZ+Berberine combined treatment in T98G cell line a) Representative colony images b) Graphical representation.

4.7. Effects of Flavonoids Alone and in Combination with TMZ on Tumor Size in a 3D Culture Model of GBM Cells

4.7.1. Effects of TMZ, Fisetin and TMZ+Fisetin on Tumor Size in a 3D Culture Model of T98G

3D tumor spheres were constructed to assess hypoxic (Bhattacharya et al., 2020) and stemness (Zhou et al., 2011) properties. The tumoroid size of the control group, when considered as 100% at 0h, increased to 201.84% at the end of 24h (Table 36). Tumor size was found to decrease control group by 37.92% corresponding to 24h TMZ treatment. With fisetin treatment, the spheroid size percentage was found to be 59.62%. Reduction of the size by 41.13% was measured which was the highest inhibition rate of all treated groups representing the group of TMZ+Fisetin treatment (Table 36). TMZ, Fisetin and TMZ+Fisetin decreased the size of 3D tumor spheres formed by T98G cells ($p<0.0001$) (Figure 104. b). It was observed that TMZ+Fisetin, and especially fisetin-alone, suppressed the proliferative characteristic of the cells compared to the morphologically scattered and proliferative cells formed by the effect of TMZ (Figure 104. a).

Table 36. The percentages of tumor spheroid sizes of each experimental group (TMZ, Fisetin and TMZ+Fisetin) compared to 0h in T98G.

	Control	TMZ	Fisetin	TMZ + Fisetin
0h	100%	100%	100%	100%
120h	201,84%	62,08%	59,62%	58,87%

a)

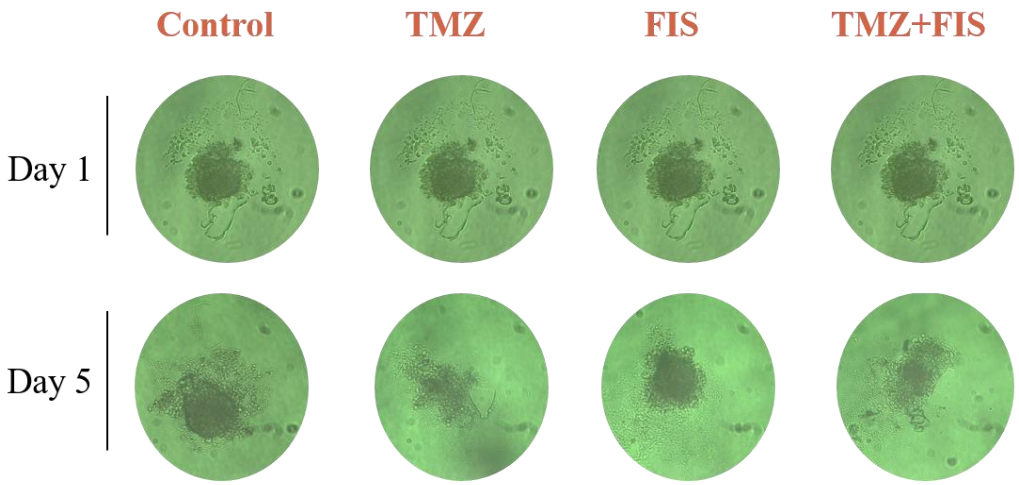

b)

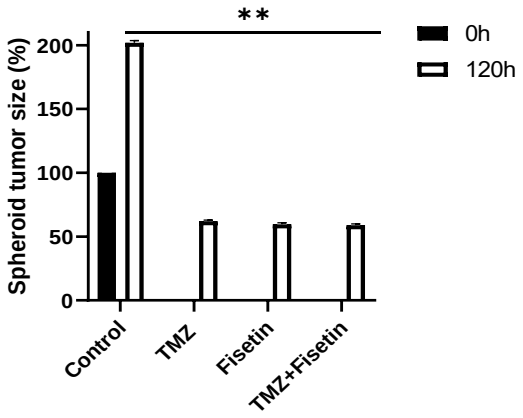

Figure 104. a) 3D tumor sphere generation over time (in 5 days) and tumor size difference in each group b) Graphical representation of the effect of TMZ, Fisetin and TMZ+Fisetin on spheroids.

4.7.2. Effects of TMZ, Berberine and TMZ+Berberine on Tumor Size in a 3D Culture Model of T98G

When the untreated group at 0h was compared with the treated groups at 120h, the obtained data were statistically significant ($p<0,0001$) (Figure 105. b). At the end of 120h, spheroid size increased 2-fold in the control cells, decreased 2.63-fold in the TMZ-treated group, 2.45-fold in the berberine-treated group, and 2.61-fold in the combined group (Table 37). In the Berberine and TMZ+Berberine groups, an appearence that protects the sphere structure and does not disperse was observed, and thanks to this feature, it was concluded that the proliferative interaction of the tumoroid was minimized, similar to fisetin (Figure 105. a).

Table 37. The percentages of spheroid sizes of each experimental group (TMZ, Berberine and TMZ+Berberine) compared to 0h in T98G.

	Control	TMZ	Berberine	TMZ+Berberine
0h	100%	100%	100%	100%
120h	201,84%	62,08%	59,31%	61,75%

a)

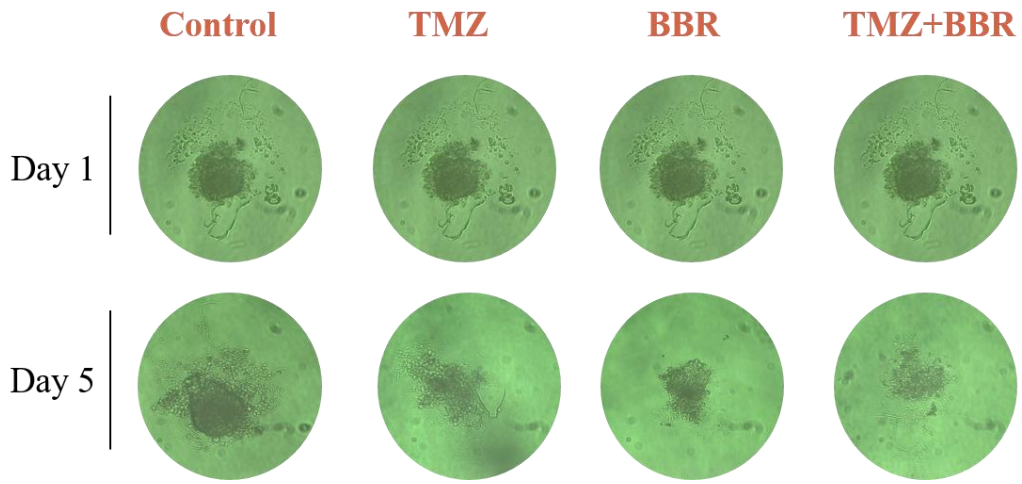

b)

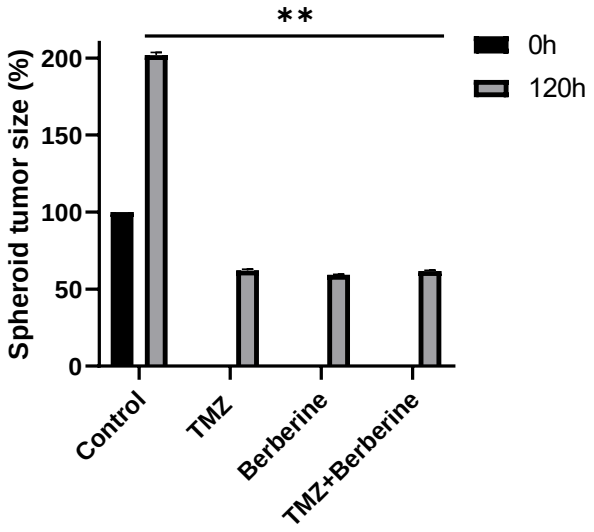

Figure 105. a) 3D tumor sphere generation over time and tumor size difference in each group b) Graphical representation of the effect of TMZ, Berberine and TMZ+Berberine on tumoroids.

4.8. Evaluation of Cells in Hypoxic Environment on the Effects of Drug Resistance Mechanisms

4.8.1. Effects of TMZ, Fisetin and TMZ+Fisetin on Wound Healing in T98G in Hypoxic Environment

The treatment effects were captured under the microscope at 4X at 24h after dosing with TMZ, Fisetin, and TMZ+Fisetin to observe the migration properties of cells in the hypoxic environment (Figure 106. a). Intermediate-hour observations were not photographed to be able to preserve hypoxic conditions as much as possible. In control cells wound area was 15,22% and with TMZ treatment it was increasing to 70,12% (Table 38). The average percentages of wound areas in fisetin and TMZ+Fisetin treatment were 97,35% and 99,87%, respectively (Table 38). Fisetin was more effective to inhibit migratory effect and combination therapy was also preserved its anti-migratory ability in hypoxia (Figure 106. b).

Table 38. Digital data of the average rates of wound width with TMZ, Fisetin, and TMZ+Fisetin treatment in T98G under hypoxia conditions.

	Control	TMZ	Fisetin	TMZ+Fisetin
0h	100%	100%	100%	100%
24h	15,22%	70,12%	97,35%	99,87%

a)

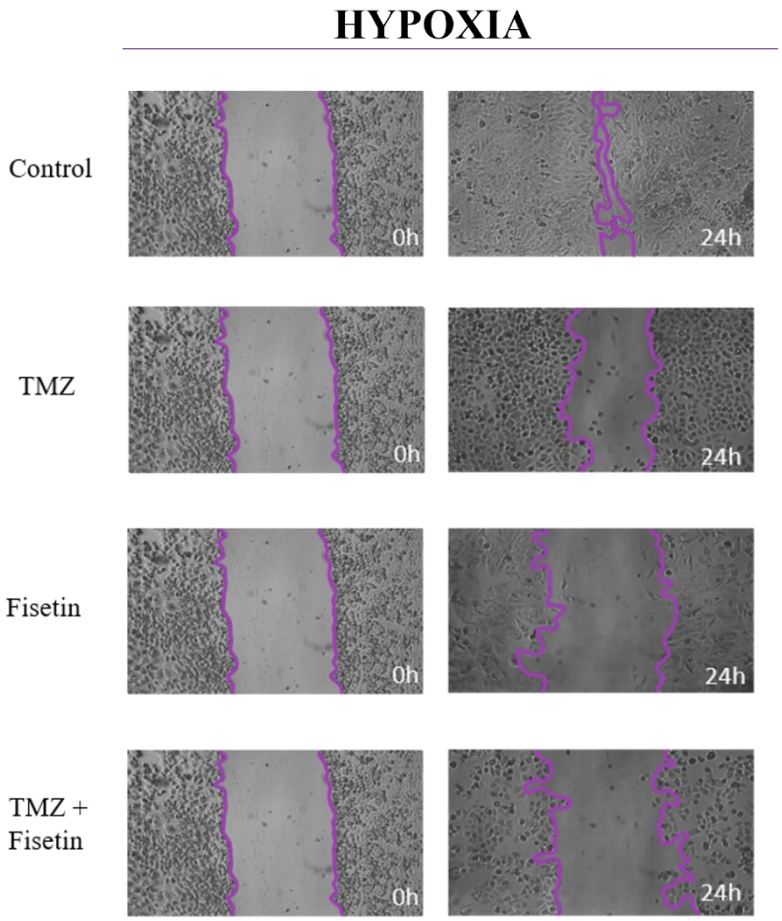

b)

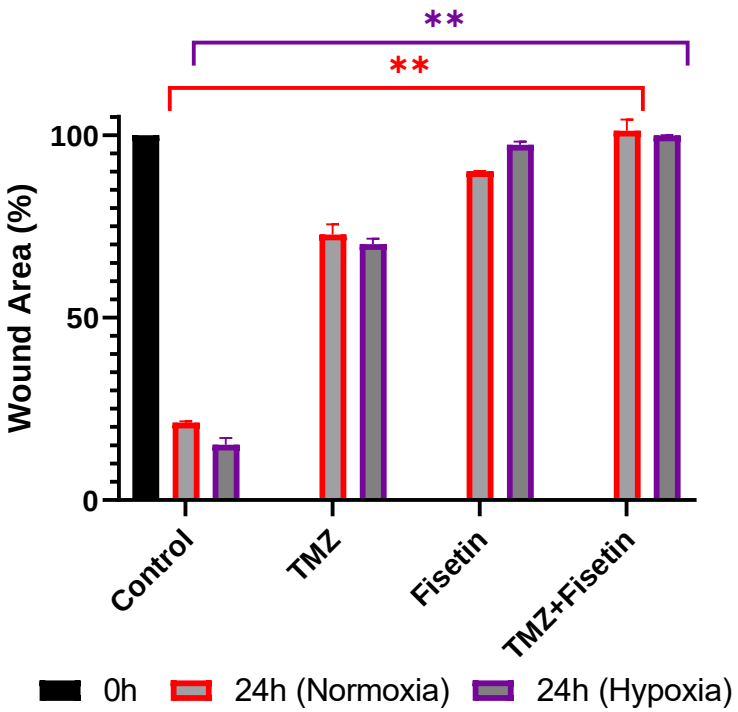

Figure 106. The effect of TMZ, Fisetin, and TMZ+Fisetin on cell invasion and migration with wound healing assay in T98G cell line under hypoxic environment a) Representative images taken in 4× at 0 and 24h (scalebar: 620 µm). b) Graphical representation of the percentages of cells in each wound area. The data shown is representative of three independent experiments. Bars represent mean ± S.D.

4.8.2. Effects of TMZ, Fisetin and TMZ+Fisetin on Wound Healing in A172 in Hypoxic Environment

To investigate the migratory characteristics of A172 cells in the hypoxic environment, the treatment effects were photographed under an inverted microscope at 4X objective at 24 hours after dosing with TMZ, Fisetin, and TMZ+Fisetin (Figure 107. a). The wound area in control cells was 24,27% and after treatment with TMZ, it increased only to 32,89% (Table 39). Fisetin and TMZ+Fisetin treatments had wound area percentages of 54,15% and 44,99%, respectively (Table 39). Combination therapy also kept its anti-migratory activity under hypoxia. Notingly, fisetin alone treatment was more effective at inhibiting the migratory impact among all groups in hypoxic environment. Although there was a serious decrease in the efficacy of TMZ treatment

compared to the normoxia, fisetin and the combined treatment were also successful in increasing the efficacy of TMZ in hypoxia (Figure 107. b).

Table 39. Data of average percentages of wound area of each experimental group in A172 in hypoxia.

	Control	TMZ	Fisetin	TMZ+Fisetin
0h	100%	100%	100%	100%
24h	24,27%	32,89%	54,15%	44,99%

a)

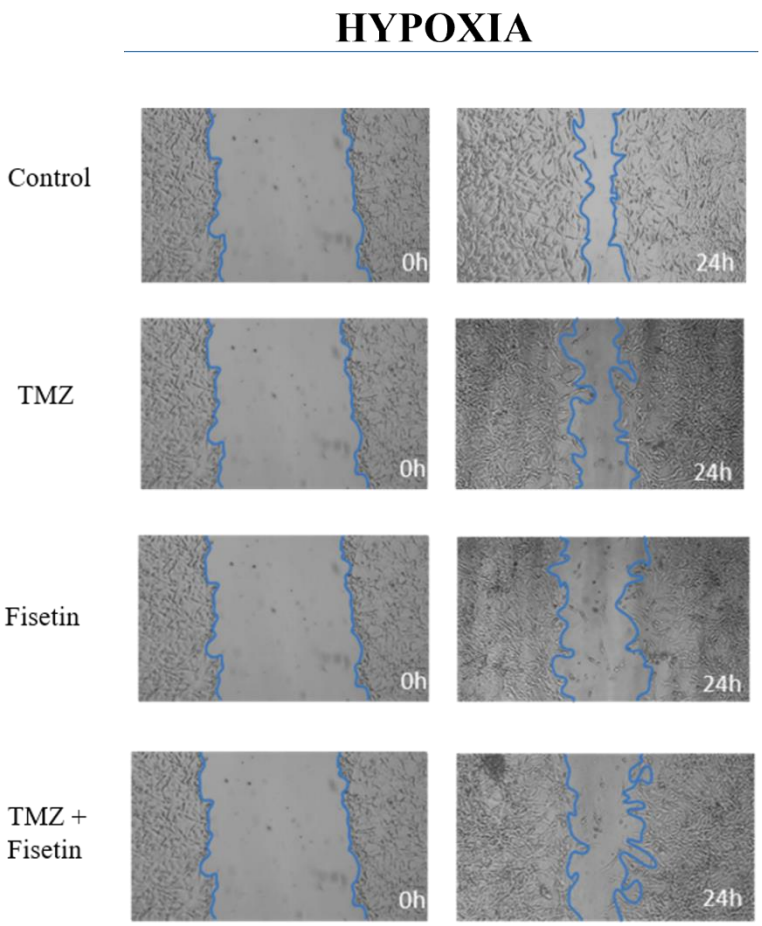

b)

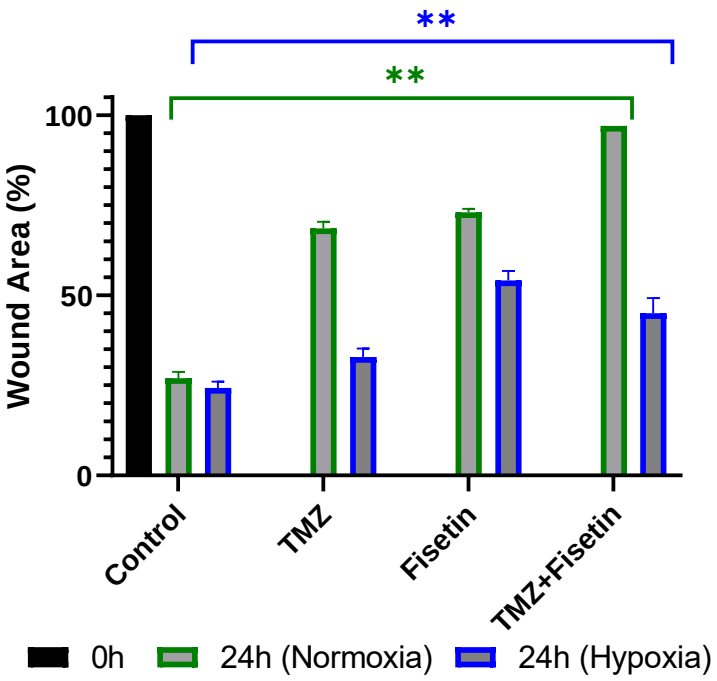

Figure 107. The effect of TMZ, Fisetin, and TMZ+Fisetin on cell invasion and migration with wound healing assay in A172 cell line under hypoxic environment a) Representative images taken in 4× at 0 and 24h (scalebar: 620 μm). b) Graphical representation of the percentages of cells in each wound area. The data shown is representative of three independent experiments. Bars represent mean ± S.D.

4.8.3. Effects of TMZ, Berberine and TMZ+Berberine on Wound Healing in T98G in Hypoxic Environment

The treatment effects were captured using an inverted microscope at 4X objective at 24 hours after dosing with TMZ, Berberine, and TMZ+Berberine in order to examine the migratory features of T98G cells in the hypoxic environment (Figure 108. a). After receiving TMZ treatment, the wound area rose to 70,12% which was 15,22% in control cells (Table 40). Wound width was almost only 3% after berberine alone treatment (Table 40). Wound area percentage for TMZ+Berberine treatment was 93,06%, respectively (Table 40). Under hypoxia, combination treatment maintained its anti-migratory effects. In a hypoxic environment, it should be noted that berberine alone treatment was even more successful at suppressing the migratory impact across all groups (Figure 108. a). Even in hypoxia, berberine and the combined therapy were effective in enhancing TMZ efficacy in comparison to normoxia (Figure 108. b).

Table 40. Digital data of the average rates of wound width with TMZ, Berberine, and TMZ+Berberine treatment in T98G in hypoxia.

	Control	TMZ	Berberine	TMZ+Berberine
0h	100%	100%	100%	100%
24h	15,22%	70,12%	97,06%	93,06%

a)

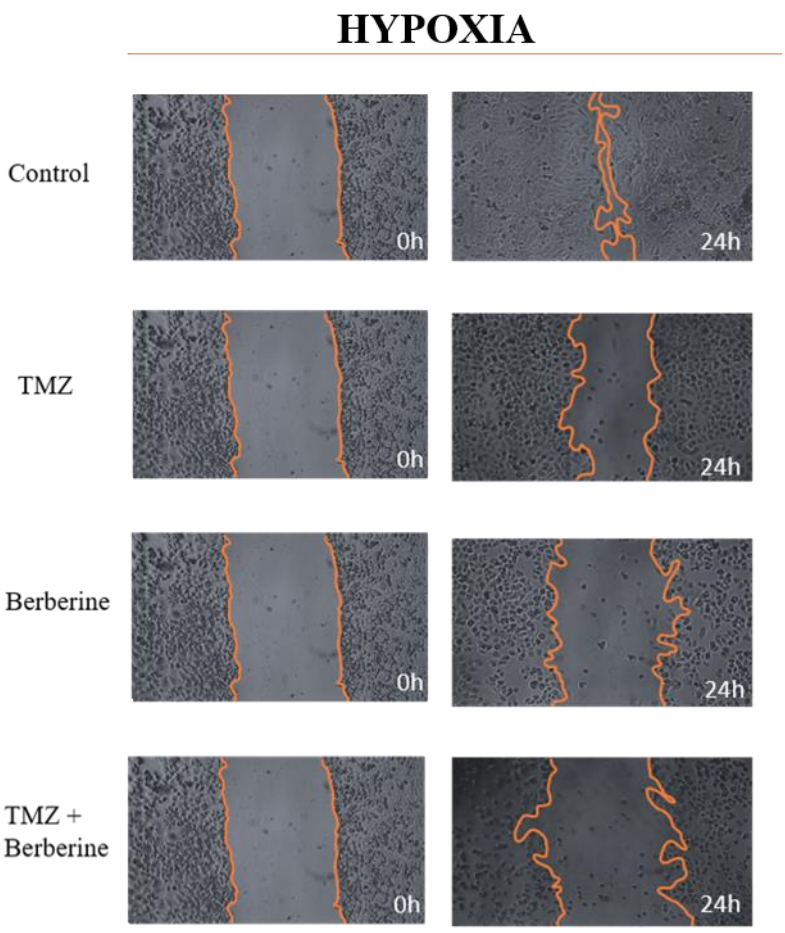

b)

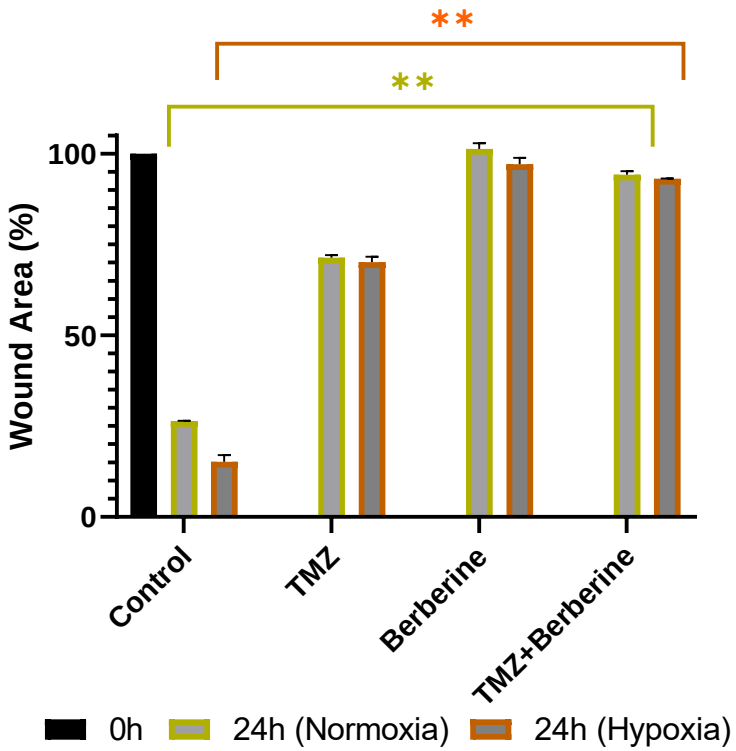

Figure 108. The determined effect of TMZ, Berberine, and TMZ+Berberine on cell invasion-migration with wound healing assay on T98G cell line under hypoxic environment a) Representative images taken in 4× at 0 and 24h (scalebar: 620 µm). b) Graphical representation of the percentages of cells in each wound area. The data shown is representative of three independent experiments. Bars represent mean ± S.D.

The effect of combining fisetin and berberine with TMZ was investigated in the current investigation in GBM. The effective dose of berberine was about ten times that of fisetin, and it also decreased non-tumor cell viability to almost 44% in 24 hours. Berberine failed to elevate TMZ's sole treatment when controlling apoptosis. Additionally, the necrotic cells increased by almost 10-fold compared to fisetin after berberine therapy. According to our findings, fisetin was chosen for the molecular analysis since it could be most effective at the lowest dose in this situation**.**

4.9. Effects of the Selected Flavonoid on the Expression Levels of Drug Resistance-Related Genes in GBM Cells

The effect of treatment of TMZ, Fisetin alone or in combination with TMZ on the mRNA expression levels of two different genes (MSH2 of the MMR mechanism and EMT marker ZEB1), which are of great importance in TMZ drug resistance, were analyzed in T98G, A172, A172-R and statistically detailed for each group.

4.9.1. Determination of the Effect of TMZ and Fisetin Alone and in Combination on MSH2 Expression Levels in GBM Cells

The effects of 24-hour treatment of effective doses of TMZ, Fisetin and TMZ+Fisetin in T98G, A172 and A172-R cell lines on the transcription level of the MSH2 gene were analyzed referring 3.2.9.2 and $2^{-\Delta\Delta Ct}$ values were calculated (Table 41). In the T98G cell line, treatment of TMZ, Fisetin, and TMZ+Fisetin resulted in significant increase in MSH2 mRNA levels of 9.95-fold ($p<0.0001$), 8.59-fold ($p<0.0001$) and 8.58-fold ($p=0,0003$), respectively, compared to control cells (Figure 109. a). When the TMZ and TMZ+Fisetin groups were compared, no significant change was detected ($p=0,1069$) (Figure 109. a). In A172, there was a significant increase in the differences in MSH2 gene expression levels of the TMZ (30.93-fold), Fisetin (3.78-fold) and TMZ+Fisetin (10.04-fold) groups ($p<0,0001$) compared to control (Table 41) and the comparison between TMZ and TMZ+Fisetin showed significant difference (Figure 109. b) ($p<0,0001$). In the cell line with acquired TMZ resistance (A172-R), MSH2 gene expression levels also increased significantly, 4.43-fold in TMZ ($p=0,0249$) and 5,52-fold in TMZ+Fisetin ($p<0,0001$) with comparison of control (Table 41). When the effective dose of fisetin alone was compared with the untreated group, no significant change ($p=0,0521$) was found in the mRNA levels of MSH2 (Figure 109. c). Although no significant difference was observed between TMZ and TMZ+Fisetin ($p= 0,3334$), it was observed that the combination therapy caused the greatest increase in MSH2 among all groups in A172-R (Figure 109. c).

Table 41. Expression levels of MSH2 gene in T98G, A172 and A172-R cells.

		2^–ΔΔCt	p value	T	fold
T98G					
	TMZ	9,949	<0,0001	40,15	9,949
	Fisetin	8,589	<0,0001	29,07	8,589
	TMZ+Fisetin	8,58	0,0003	12,18	8,58
A172					
	TMZ	30,93	<0,0001	88,17	30,93
	Fisetin	3,78	<0,0001	183,4	3,78
	TMZ+Fisetin	10,04	<0,0001	1412	10,04
A172-R					
	TMZ	4,434	0,0249	3,501	4,434
	Fisetin	1,731	0,0521	2,736	1,731
	TMZ+Fisetin	5,526	<0,0001	28,61	5,526

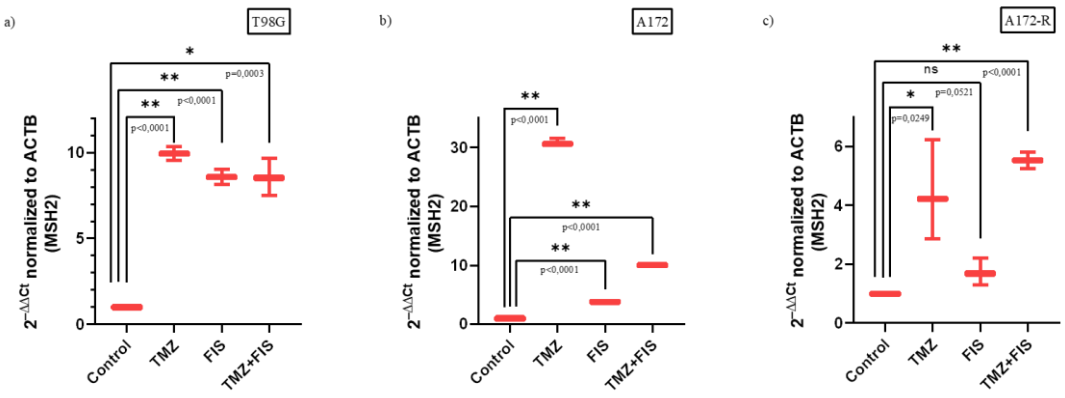

Figure 109. Graphical representation of the effect of TMZ, Fisetin and TMZ+Fisetin combination on MSH2 gene expression levels in a) T98G, b) A172 and c) A172-R cell lines (*p<0,05, **p<0,0001).

4.9.2. Determination of the Effect of TMZ and Fisetin Alone and in Combination on ZEB1 Expression Levels in GBM Cells

As a result of the treatment of effective doses of TMZ, Fisetin and TMZ+Fisetin, it was determined in T98G that the expression levels of the ZEB1 gene were statistically significantly reduced compared to control cells (7,52-fold (p<0,0001); 34,32-fold (p<0,0001); 13,41-fold (p<0,0001), respectively (Table 42). A statistically significant difference emerged as a result of comparison of TMZ alone and combined treatment (p=0,0003) (Figure 110. a). Notingly, the comparison between

TMZ and TMZ+Fisetin was significant due to the 1,78-fold lower ZEB1 expression level in the combination treatment (Figure 110. a). In A172, increased expression of ZEB1 observed in fisetin treatment alone was not significant compared to control ($p<0.4896$) (Figure 110. b). TMZ and TMZ+Fisetin separately significantly reduced ZEB1 levels when compared to the untreated group ($p<0.0001$), and also when compared with each other, this change was not significant ($p=0.359$) (Table 42). Surprisingly, the expression of the ZEB1 gene, which was associated with drug resistance, was significantly increased with TMZ treatment in the A172-R cell line, as if promoting this chemoresistance (p=0,0035) (Figure 110. c). Interestingly, there was a much smaller increase in even fisetin-alone (p=0,2974) and TMZ+Fisetin (p= 0,0698) treatment according to TMZ and these increases were not significant for control. Moreover, a significant 6,75-fold difference was found between TMZ and TMZ+Fisetin treatment (p=0.0362).

Table 42. Expression levels of ZEB1 gene in T98G, A172 and A172-R cells.

		2^–ΔΔCt	p value	T	fold
T98G					
	TMZ	0,1329	<0,0001	150191667	-7,524
	Fisetin	0,02914	<0,0001	62	-34,317
	TMZ+Fisetin	0,07453	<0,0001	182,8	-13,417
A172					
	TMZ	0,02586	<0,0001	526,6	-38,669
	Fisetin	1,462	0,4896	0,7599	1,462
	TMZ+Fisetin	0,02823	<0,0001	720	-35,423
A172-R					
	TMZ	46,86	0,0035	8,474	46,86
	Fisetin	5,141	0,2974	1,258	5,141
	TMZ+Fisetin	6,933	0,0698	2,766	6,933

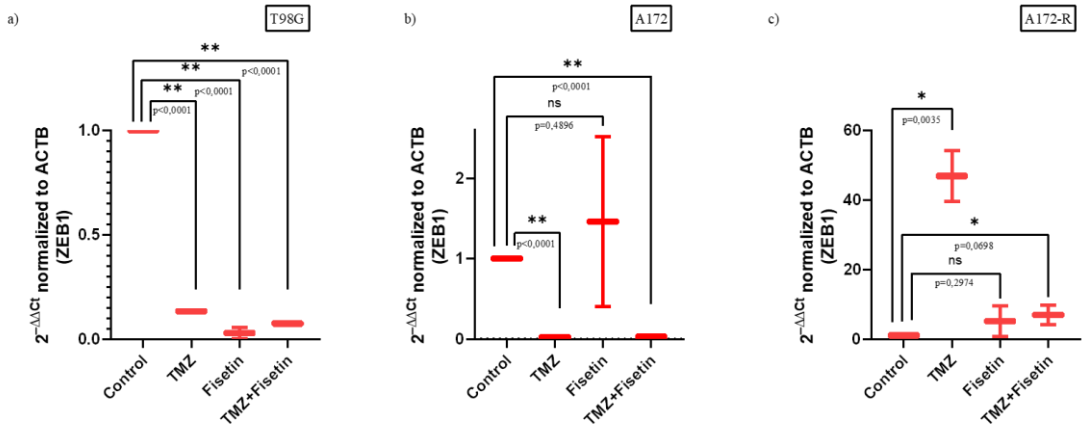

Figure 110. Graphical representation of the effect of TMZ, Fisetin and TMZ+Fisetin combination on ZEB1 gene expression levels in a) T98G, b) A172 and c) A172-R cell lines (*p<0,05, **p<0,0001).

4.10. Validation of data from *in-vitro* analyzes in primary cultures prepared from tumors from GBM patients

In this study, clinical samples taken after surgical resection of three different patients who were diagnosed with primary GBM and did not receive preoperative chemotherapy were included as described in 3.2.1.

4.10.1. Tumor characterization of primary cultured GBM patients

Considering the IHC results, IDH was negative for all GBM patients in the study (Table 43), GBM status was interpreted as elevated aggressiveness group as described before in 2.1.3.1.1. Considering the immunohistochemical results in the GBM patient population, glial fibrillary acidic protein (GFAP), Olig-2 and H3K27me3 were positive in each patient (Table 43). In addition, NFP was positive in neurophil and NeuN was positive in neurons (Table 43). In opposite trend, IDH-1 and ATRX were negative in patients (Table 43). H3K27M status was also negative in two patients but it was unclear whether negative or not for the 3rd patient (Table 43). Ki-67 results were found as 30%, 30% and 25% positive in patients, respectively (Table 43). The p53 values were determined as 30% positive in the first patient, 20% positive in the second patient, and 3% positive in the third patient (Table 43).

Table 43. Reports of patient data and immunohistochemical results of the primary GBM patient population.

	Patient 1	Patient 2	Patient 3
Diagnosis	GBM WHO Grade IV	GBM WHO Grade IV	GBM WHO Grade IV
Sex	Female	Female	Female
Age	49	40	75
IHC Results			
GFAP	Positive	Positive	Positive
Olig-2	Positive	Positive	Positive
IDH-1	Negative	Negative	Negative
ATRX	Negative	Negative	Negative
P53	30% Positive	20% Positive	3% Positive
Ki-67	30% Positive	30% Positive	25% Positive
NFP	positive in neuropil	positive in neuropil	positive in neuropil
NeuN	positive in neurons	positive in neurons	positive in neurons
H3K27M	Negative	Negative	Unknown
H3K27me3	Positive	Positive	Positive

4.10.2. The effects of TMZ, Fisetin and TMZ+Fisetin treatment on the expression levels of genes related to drug resistance in GBM patients

4.10.2.1. The effects of TMZ, Fisetin and TMZ+Fisetin treatment on MSH2 gene expression levels in GBM patients

When TMZ, Fisetin and TMZ+Fisetin treatments were applied to three different patients with GBM diagnoses, the effects on MSH2 gene expression levels were calculated numerically ($2^{-\Delta\Delta Ct}$) (Table 44). As a result, no significant change was found in the mRNA levels of the relevant gene at the effective doses of TMZ, Fisetin, and TMZ+Fisetin compared to control (p=0.1639; p=0.3216; p=0.1529, respectively) (Table 44). However, when all treatment groups were compared, the greatest increase in MSH2 expression levels was achieved in the combined group (Figure 111).

Table 44. Expression levels of MSH2 gene in GBM patient population.

		2^–ΔΔCt	p value	T	fold
Patient Population					
	TMZ	2,094	0,1639	1,703	2,094
	Fisetin	5,358	0,3216	1,13	5,358
	TMZ+Fisetin	7,649	0,1529	1,762	7,649

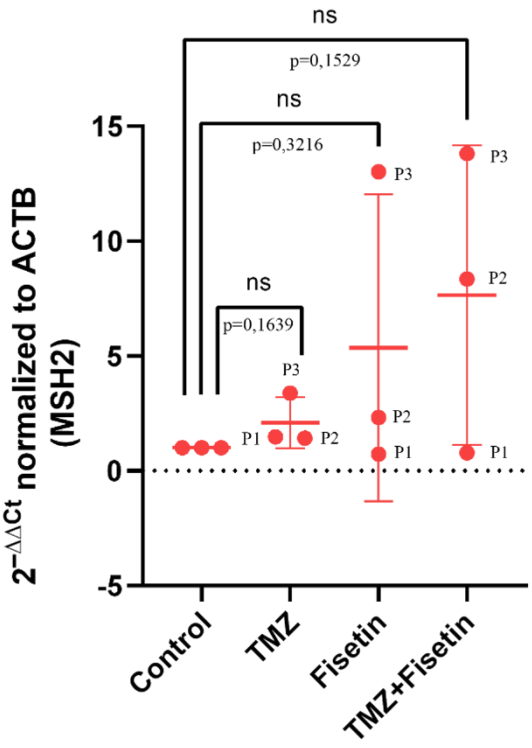

Figure 111. Graphical representation of the effect of TMZ, Fisetin and TMZ+Fisetin combination on MSH2 gene expression levels in GBM patient population. Each round represents different GBM patient.

4.10.2.2. The effects of TMZ, Fisetin and TMZ+Fisetin treatment on ZEB1 gene expression levels in GBM patients

When the ability of three different treatment methods (TMZ, Fisetin, and TMZ+Fisetin) to reduce the expression level of the ZEB1 gene in three different GBM patients was examined, it was determined that the treatment methods did not provide a significant decrease compared to the control (Table 45). Remarkably, a highest reduction in ZEB1 mRNA expression levels was observed with TMZ+Fisetin treatment (Figure 112).

Table 45. Expression levels of ZEB1 gene in GBM patient population.

Patient Population		2^–ΔΔCt	p value	T	fold
	TMZ	1,071	0,9314	0,09156	1,071
	Fisetin	1,403	0,7643	0,3209	1,403
	TMZ+Fisetin	0,3996	0,0594	2,611	-2,502

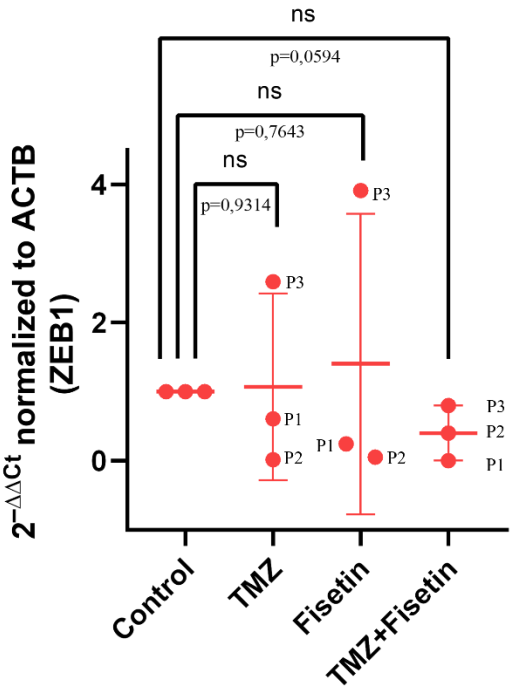

Figure 112. Graphical representation of the effect of TMZ, Fisetin and TMZ+Fisetin combination on ZEB1 gene expression levels in GBM patient population. Each round represents different GBM patient.

5. DISCUSSION AND CONCLUSION

GBM is a brain tumor in stage IV of the whom classification, the most aggressive, the most lethal, and the most limited treatment, which can become resistant to this treatment, and the patient survival is still limited to 12.6 months (Mesfin et al., 2023; Van Gool et al., 2022). Thanks to its advantages, such as crossing the BBB, the response to the chemotherapy drug TMZ, which has been used as standard chemotherapy for years, may vary according to GBM characterization. Due to its different character, GBM patients can resist genetic and epigenetic changes and treatment-related acquired chemotherapy and do not respond well to treatment. Although the methylation status of MGMT was one of the first changes detected in patients' association with TMZ response, it does not constitute a direct link (Hegi et al., 2008). Indeed, there is an urgent need to evaluate new biomarkers in order to be a potential predictive and prognostic biomarker for the patient's response to treatment and resistance (Wick et al., 2014). Accordingly, this study investigated the ability of another DNA repair protein MSH2 and the EMT biomarker ZEB1 in non-resistant, intrinsic, and acquired resistant cell lines and patients. In addition, changes in the mRNA levels of these genes were observed when treated with TMZ and flavonoid alone or in combination with the drug.

The interactions of two natural flavonoids, fisetin, and berberine, which can be taken as a supplement and are present in various fruits, vegetables, and plants, alone and in combination with TMZ in GBM, were investigated. The initial finding was that fisetin did not cause a cytotoxic effect on non-tumor cells (L929) with fibroblast morphology as T98G and A172, even at doses almost 5-fold higher than the effective dose. In addition, in the literature, the cytotoxic effect of fisetin in a healthy lung cell line (BEAS-2B) was found only at a dose much higher than the active dose (270 μmol/L) (Pak, & Oztopcu-Vatan, 2019). TMZ + Fisetin combined treatment in T98G showed a similar cytotoxic effect to TMZ ($p>0,005$). The combination of fisetin with TMZ on T98G cell proliferation was discussed for the first time in the literature. Since the cell viability of GBM cell line T98G declined significantly in a time- and dose-dependent manner by fisetin compared to healthy cells and preserved the lethal effect of fisetin in A172 at high doses indicated that these GBM cells were sensitive to these doses of fisetin. In A172, the capacity of fisetin to inhibit cell viability contributed to

the TMZ-induced anti-proliferative effect with an additive effect, and interestingly, fisetin-alone produced a significant reduction in cell viability. This study provided novel insights into the effect of fisetin alone and in combination with TMZ in A172. Given the results of fisetin and TMZ having an additive effect on each other, showing their usability together with contributing to each other's effects, this may indicate a potential candidacy for fisetin to be used in GBM therapy.

For berberine, non-cancerous L929 cell viability was approximately 45% when dosed with the effective berberine dose of A172 (113,5 μmol/L). Whereas it was found in the literature that cell viability decreased below 40% even at a dose lower than half of this effective dose (50 μmol/L) in a non-cancer human dermal fibroblast (Agnarelli et al., 2018). In both GBM cells (T98G and A172) dosed with 200 μmol/L berberine, berberine caused a much more cytotoxic effect and reduced cell viability to approximately 10% in cancer cells ($p<0.0001$). Although TMZ and berberine had antagonistic effects in T98G in this study, it had been shown that berberine affected the Bax/Bcl2 ratio and activated caspase-3, directing T98G to apoptosis (Eom et al., 2008) and reducing TMZ resistance in TMZ-resistant U87MG-R cells (Qu et al., 2020). Berberine was used to prove that TMZ resistance suppression also via MAPK pathway in the U87MG-R cell line (Qu et al., 2020) and had a migration inhibitory role in T98G, U87MG, and primary culture (Irina et al., 2021) in the literature. However, to our best knowledge, no TMZ and berberine cotreatment examples were found in T98G. In spite of the fact that there was also a lack of involvement in the effects of berberine on A172 cells in the literature, it had been found in this study that TMZ and berberine treatment had additive effects. The two different synergistic scores in two different GBM cell lines may be due to their different features. Berberine, which caused close to 64% cell death even in the treatment alone, increased the anti-proliferative effect of TMZ in A172 and caused more than 91% cell death in the combined treatment.

Because there are significant differences between innately resistant cancer cells and cancer cells that acquire resistance over time, well-characterized chemoresistant cell lines, preferably originating from a standard susceptible parental cell line, need to be developed to achieve the most effective therapeutic results. A previous study generating resistant cell lines and screening for innate resistance colonies in the same

cell line provided new insights into the critical differences in these two cell populations for hepatocellular carcinoma (Meena et al., 2013). Therefore, the current study developed a chemoresistant cell line model to understand the phenomenon of resistance to chemotherapeutics (TMZ) and was often seen as a model of evolution in cancer and a tool for discovering new drugs that may be more effective against cancer. Eventually, the TMZ-resistant (A172-R) cell line was obtained from the TMZ-sensitive (A172) cell line by intermittent exposure to increasing doses of TMZ for approximately one and a half years. During the process, cell viability rates were evaluated, and it was proved that the effective doses of TMZ were killing the A172-350-R and A172-450-R cells, but this phenomenon was changing over time. Upon a time when cells were expected to gain resistance to long-term treatment of TMZ doses, it was consistent with our findings in A172-550-R cell lines. The ability of 550 μmol/L and 900 μmol/L doses of TMZ to inhibit cell viability was not significant compared to the control, and cell viability was 100,60%, and 97%, respectively, which proves this hypothesis. Since A172 was expected to gain resistance up to the TMZ IC50 dose, by increasing the TMZ dose to 750μmol/L, TMZ-induced cell death did not increase above 13% in A172-750-R cells. When cell viability analysis was performed in cells that became resistant to 900μmol/L TMZ dose over time and still had 70% confluence at a given dose, it was observed that TMZ-induced cell death was also at a low level. When the same effective dose of TMZ was given to A172 parental strain, even the highest vitality was over 35%, while 65% viability was observed in A172-900-R, which showed that its sensitivity to TMZ was successfully decreased ($p<0,0001$). The effects of fisetin in cell line that became resistant to the chemotherapeutic agent due to long-term exposure to TMZ (A172-900-R) had been reported for the first time, noting a significant reduction in the lethality of TMZ as resistance gained. Hence, the resultant A172-900-R lines were less sensitive to an effective dose of TMZ compared to its parental strain A172 but when treated with effective doses of TMZ+Fisetin, cell viability of resistant cell lines were decreasing nearly 50%, which may imply the effects of fisetin overcoming TMZ resistance. The potential of fisetin, which has been found to be able to overcome radioresistance with ER stress in liver cells (Kim, 2023) and cisplatin resistance with pathways such as caspase in lung adenocarcinoma (Zhuo et al., 2015), in combination with TMZ and its first-time-mentioned usability

overcoming TMZ resistance in T98G, A172 and A172-R cells can pave a path for the future studies.

Until now, fisetin's senolytic effect on the T98G cell line and its effect on apoptosis (Pak, & Vatan, 2019) had been mentioned, as well as fisetin's effect on GBM senescence in another GBM cell line (Beltzig et al., 2022) but its effects on tumor aggressiveness had not been shown in combination with TMZ. The obtained data on the effect of fisetin causing apoptosis was in agreement with previous studies, which found that fisetin induced apoptosis in GBM cells due to its senolytic effect (Beltzig et al., 2022), and in human cervical cancer, HeLa cells through pathways such as Akt (Afroze et al., 2022). What we found in this study was that fisetin induced apoptosis (70%) and additively affected the apoptosis-promoting capacity of TMZ in TMZ-resistant T98G cells ($p<0,0001$) by increasing total apoptotic cells to almost 80%, mainly early apoptotic ones via Annexin V assay. In morphological analysis to identify the mode of fisetin-induced cell death, horseshoe-shaped cells representing apoptotic cells were in apparent enhancement, and viable cells were in profound distinction with fisetin and TMZ+Fisetin treatment in both T98G and A172 cell lines. Notably, when the same areas were quantifiably evaluated with HALO AI, the results were consistent with Annexin V flow cytometry regarding having fewer necrotic cells than TMZ in TMZ+Fisetin in T98G. Likewise, the quantitative number of necrotic cells, which were not desirable due to several patterns like release of their intracellular contents, were increased during TMZ treatment in T98G and A172 cells, and what was noteworthy was that fisetin and TMZ+Fisetin treatment decreased the number of necrotic cells in both cell lines. Prior research showed that the apoptotic death rate of cisplatin in T98G and A172 cell lines used in our study was explained by p53-WT and mutant status (Park, & Kim, 2002). It had been determined in human renal carcinoma caki cells that fisetin associated with p53 stimulation increased apoptosis (Min et al, 2017). As apoptosis increases with the presence of p53, it may be predicted that the increase in apoptosis may also be triggered by fisetin in GBM. According to the literature, we assumpted that since p53 was related to apoptosis, treatment with fisetin could increase the rate of apoptosis in p53 dependent manner (Min et al., 2017) also in these two GBM cell lines, but more systematic and theoretical analysis is required to demonstrate it.

There may be differences in the presence of p53 in directing TMZ-induced apoptosis (Roos et al., 2007). While apoptosis is directed by decreasing the Bax/Bcl2 ratio and interacting with caspase-3 and 9 in p53 mutant cells, it can be triggered by increasing p53 and interacting with caspase-3 and 8 in p53-WT cells (Roos et al., 2007). In previous studies, fisetin was found to induce p53, reduce the Bax/Bcl2 ratio and activate caspase-3, -8, -9 (Rahmani, Almatroudi, Allemailem, Khan, & Almatroodi, 2022). Fisetin-induced caspase-3 increase in hepatocellular carcinoma led to apoptosis (Chen et al., 2002). Also, DNA damage is an attribution of apoptotic cell death (Eom et al., 2008). Hence, if there are low levels of MSH2, the MMR mechanism and, thus, this apoptosis cascade is disrupted. Defects in MSH2 are also correlated with chemotherapy resistance. Although the T98G and A172 action mechanisms differed, the Fisetin and TMZ+Fisetin treatment resulted in increased apoptosis in both. Consequently, if fisetin may direct apoptosis by increasing the levels of MMR genes such as MSH2 and targeting caspase-3, which is common in the cascade leading to apoptosis in TMZ independently of p53, it may be suitable for use alone or in combination with TMZ regardless of p53 status and support our similar anti-cancer results in T98G (p53-mutant) and A172 (p53-WT). In this study, it was shown that MSH2 levels were increasing in fisetin and a combination of TMZ for the first time, but this enhancement was not higher than TMZ-alone in T98G and A172; however, in acquired TMZ-resistant cells (A172-R), combination therapy was improving the effect of TMZ-alone by increasing the MSH2 levels having highest enhancement (more than 5-fold) among treated groups. It may be hypothesized that TMZ+Fisetin therapy in A172-R could successfully increase the number of MSH2 genes, increase the sensitivity of cells to TMZ and maybe even lead TMZ-resistant GBM cells more to apoptosis. Nevertheless, further analysis is still needed to evaluate the p53 status being changed due to resistance.

Berberine was also found to cause an increase in early apoptotic cells in the U87MG compared to the control (Palma et al., 2020), although berberine was said not to trigger apoptosis but senescence in other GBM cell lines (Liu et al., 2015) and its combination with TMZ was known as increasing apoptosis in glioma cell (Duan et al., 2021). Berberine-induced Bax/Bcl2 ratio change and caspase-3 activation alone were found to direct T98G to apoptosis (Eom et al., 2008). In our findings, although

berberine and its cotreatment with TMZ could not surpass the total apoptosis rate in TMZ-alone treatment in T98G, they, mainly TMZ+Berberine, caused a severe increase in total apoptosis, especially in late apoptosis, compared to the control. Berberine alone caused a more than 10-fold increase in necrotic cells compared to fisetin in T98G.

For cancerous cells, when the cell cycle continues, the cells are resistant to apoptosis and do not respond to chemotherapeutic agents. Previously in the literature, TMZ-induced G2/M cell arrest resulted in U87MG cells (Tai et al., 2021); however, our findings in A172 and T98G were that the TMZ-only group was arrested in the S phase. In T98G, the fisetin-only group inhibited cell cycle progression in G0/G1 phase, while TMZ+Fisetin caused arrest in G2/M. Other investigators had also found that fisetin could interrupt the cell cycle in G0/G1 due to induction p53, which has a significant role in controlling the cell cycle and altering several cell cycle checkpoints in bladder cancer (Li et al., 2011). In previous studies, fisetin had been mentioned for its senolytic effect, as it can direct the cell to senescence and stop its proliferation (Beltzig et al., 2022). Along with this finding, the information in the literature that G2 arrest in gliomas was caused by senescence and autophagy (Agnarelli et al., 2018) may be associated with the fact that TMZ+Fisetin combined treatment increased arrest in the G2/M phase.

Consistent with the literature that showed an increase in S phase when exposed to both 1- and 2-cycle TMZ doses in A172 cells (Perazzoli et al., 2015), our results also concluded an enhancement in S phase arrest with TMZ treatment and disrupting cancer cells to undergo proliferative phase. Although this accumulation of the S phase was relatively less in fisetin treatment, TMZ+Fisetin increased 3.6-fold compared to the control and more than 2-fold compared to TMZ. It was previously shown that fisetin reduced CDK2 and cyclin A, which were involved in the S phase in bladder cancers (Li et al., 2011).

It had been found that the induction of berberine caused arrest in the G1 phase in T98G (Eom et al., 2008) but in our resultants in the same cell line, TMZ blocked the cell cycle in the S phase, while Berberine-only and TMZ+Berberine reduced cells in G0/G1 with an associated increase in both S and G2/M phase. A senescence and autophagy-induced G2 arrest was also previously detected in the U343 glioma cell line (Agnarelli et al., 2018). It had also been investigated that there was an interruption of

the cell cycle in the S phase with the combination of berberine and TMZ in glioma (Duan et al., 2021).

It was not known how the effect of flavonoids (fisetin and berberine) concurrent use with TMZ, the chemotherapy drug, and the nature of the effect (synergistic, additive, or antagonistic) on TMZ, how the difference between normoxic and hypoxic environments affects the effectiveness of these flavonoids on the biological processes targeted and on the aggressiveness of the tumor. Our *in-vitro* data showed that fisetin effectively inhibited the migratory effect of GBM cells alone and with combination therapy under both normoxia and hypoxia. To represent GBM and its microenvironment one step further, wound healing abilities were observed under hypoxic conditions.

It was demonstrated in triple-negative breast cancer that fisetin up-regulated E-cadherin and claudin and down-regulated N-cadherin and vimentin to inhibit the EMTs process (Li et al., 2018). Again, in the same study, it was found that the PI3K/Akt (inhibition) and PTEN (upregulation) pathways, which play an essential role in both EMT and TMZ resistance, were also targeted by fisetin (Li et al., 2018). In another publication about human renal carcinoma caki cells, there was an induction of p53 protein expression by fisetin (Min et al., 2017). There was a finding in the literature that this p53 also weakened the process of EMT in hepatocellular carcinoma by reducing ZEB1 with the help of miRNAs (Kim et al., 2011). It was found that the combined use of sorafenib and fisetin in BRAF-mutated melanoma reduced the expression of ZEB1, an EMT biomarker (Pal et al., 2016).

In the present study, the invasion and migration effects of fisetin and berberine on A172 and T98G cells were investigated by the wound scratch assay. When untreated cancer cells with a high rate of metastasis and wound closure were used as control, a significant decrease in the invasion and migration abilities of T98G and A172 cells treated with effective doses of TMZ, Fisetin, and TMZ+Fisetin was observed ($p<0,0001$). In T98G, in the treatment of TMZ, wound closure was observed in approximately 27% by preserving the wound area boundaries. With the treatment of fisetin-alone, wound closure was reduced to 10%. This GBM cell migration suppressive effect of fisetin may be due to its effect on EMT markers (Li et al., 2018; Pal et al., 2016). It was noteworthy that this outcome was even stronger when

compared to TMZ+Fisetin combination therapy, and it not only prevented wound closure but also resulted in a further increase in wound area with scattered cell border morphology. Consequently, fisetin and, especially, TMZ+Fisetin treatment successfully increased the anti-invasive and migrative effect of TMZ under normoxic conditions in T98G cells ($p<0.0001$). In A172 cells, fisetin alone had a similar effect to TMZ, increasing wound opening to almost 73%, but the scratched wound area in TMZ+Fisetin after 24h was found to maintain nearly the 0h state of control, with only 3% wound closure ($p<0.0001$).

In the current study, ZEB1 gene expression levels were also successfully reduced in T98G and A172 cell lines by combining TMZ and fisetin. Consonantly, the effect of combination therapy on T98G and A172 wound area in a normoxic environment agreed with reducing the EMT process by supporting the effect of TMZ and fisetin alone.

The most exciting finding was that TMZ, in the acquired TMZ-resistant A172-R cells due to long-term drug therapy, did not suppress migration that much compared to previous results of parental strain A172 resulting in significant inhibition of wound area ($p<0,0001$). It was an opposite trend compared to the previous finding in A172, meaning the inhibition of its effectiveness on tumors. In the A172-R cell line, fisetin treatment alone reduced the width of the gap to almost 70%, and with TMZ+Fisetin treatment, this wound width was increased up to 86%. Moreover, this value significantly increased the wound gap compared to TMZ alone ($p<0,0001$). Remarkably, the combination therapy resulted in a visible intact morphology protecting wound width at the wound line boundary, significantly reducing cell invasion, migration, and proliferative property with the contribution of fisetin. These findings may provide insight into the literature about the effects of fisetin on EMT as an anti-migratory agent in TMZ-resistant and non-resistant GBM cells. However, more studies are needed to be evaluated. Consonantly, there was a potent inhibition of invasion and migration abilities of T98G mainly caused by berberine with wound width surpassing 100%. Combination therapy suppressed cell migration and invasion ability, and this suppression was even better in berberine-alone treatment by widening the wound-scratch area ($p<0,0001$). It had been previously shown that berberine-induced metalloproteinase-2 inhibition in T98G suppresses cell migration (Irina et al.,

2021). This study found that berberine-alone and the combination of TMZ could increase the anti-migratory effectiveness of TMZ ($p<0,0001$). In conclusion, there was a significant difference between TMZ and flavonoid-combination treatment in both fisetin and berberine in T98G and A172 cell lines, which would increase TMZ efficacy under normoxia conditions ($p<0.0001$).

Previously, the hypoxia environment, known to reflect the tumor microenvironment better, was compared with the normoxia environment in T98G cells (Macharia et al., 2021). It was found that in a hypoxic environment, its morphology changed compared to a normoxia environment, and it increased various TMZ resistance and GBM-related parameters such as HIF, angiogenesis, stemness, and anti-apoptotic markers. In another GBM cell line, it had been shown that the signaling axis between hypoxia-related HIF and EMT-related ZEB1, both commonly associated with TMZ resistance, may play a role in the more decisive mesenchymal shift in hypoxic conditions (Joseph et al., 2015). Our results also proved that, in T98G, the percentage of wound scratch area in control cells decreased more in a hypoxic environment than normoxia, proving that it further increased the invasive and migrative ability of cancerous cells. Even in hypoxia, where GBM cells became more resistant to chemotherapy, fisetin reduced the excessive migration rate of T98G compared to untreated cells. In accordance with our results, the wound closure rate, invasion, and migration ability of TMZ increased in a hypoxia environment. Additionally, while hypoxia was also correlated with reduced TMZ efficacy, TMZ+Fisetin therapy significantly enhanced the success of TMZ, likewise normoxia, in T98G ($p<0.0001$).

In the A172 cell (TMZ-sensitive), the effect of the hypoxic environment on TMZ was seen very clearly, as it increased the wound healing rate to almost twice compared to normoxia. Combination treatment of fisetin successfully increased TMZ efficacy by further opening the wound area, and the other important effect was that fisetin alone exhibited an even greater anti-migratory effect than treated groups. In the hypoxic environment, albeit slightly, a more invasive wound closure expected in T98G control cells and a low effect on the expected wound closure in TMZ treatment were observed. Berberine both showed a more influential effect than TMZ in the treatment alone and increased the effect of TMZ in combination with TMZ, again supporting normoxia conditions.

Consistent with our results of fisetin, reducing number of colonies was found in renal cell carcinoma (Hsieh et al., 2019). To our best knowledge, the ability of fisetin to reduce colony numbers by enhancing the activity of TMZ has yet to be elaborated in GBM cells. In addition, strong effects of fisetin and berberine were shown to suppress the ability of cancer cells to form colonies (>50 cells). Primarily, in T98G, colony count was reduced by almost 80-fold with TMZ treatment compared to control ($p<0.0001$). Although an almost 8-fold reduction was observed in fisetin alone, this colony-reducing effect was strongly enhanced over 235-fold in combination treatment with fisetin. ($p<0,0001$). The solid decrease in the number of colonies in combination therapy by increasing the efficacy of TMZ-only showed that cell migration rates of cells with TMZ+Fisetin treatment slowed down compared to both control and TMZ treatment alone ($p<0.0001$). In A172, TMZ and fisetin inhibited colony numbers by close to 32% and 5%, respectively. While TMZ+Fisetin treatment reduced the majority of colonies (115-fold more compared to the untreated cells; $p<0,0001$). In comparing A172 and T98G, fisetin treatment combined with TMZ strongly inhibited the number of colonies and produced a significant ($p<0,0001$), effective, and supportive response to TMZ in both cell lines. A study reported that fisetin treatment in human oral squamous cell carcinoma suppressed the colony formation ability by PAK4, a gene associated with cell proliferation and invasion (Li et al., 2020). Prior studies have found that fisetin suppresses Ki-67, associated with tumor aggression, and increases apoptosis in PANC-1 cells (Jia et al., 2019). In the present study, fisetin and its combination with TMZ presented successful results in both cell lines (T98G and A172), both in wound healing and colony formation assay related to tumor aggressiveness and its additive effect on apoptosis.

3D sphere formation assay, since the inside core of spheroids results in relatively less nutrients and oxygen, had been used to represent hypoxia (Bhattacharya et al., 2020) and stem-cell features (Zhou et al., 2011). Musah-Eroje & Watson had been demonstrated a stronger TMZ resistance in 3D sphere model than 2D of GBM and this was triggered by the increase of biomarkers such as CD133 and OCT4 in GBM. This is the first study to demonstrate the effects of fisetin alone and with the combination of TMZ in 3D sphere size, and according to that, it may provide novel insights into the role of fisetin in overcoming TMZ resistance by reducing the size of

the tumoroid and reducing the proliferative interaction of its structure. Compared to control cells which had increased their size more than 2-fold in 120h, TMZ, Fisetin, and TMZ+Fisetin were found to significantly reduce the size of 3D spheroid formed by T98G cells ($p<0.0001$). The study showed that both fisetin alone and TMZ+Fisetin inhibited the proliferative characteristics compared to the morphologically scattered cells of TMZ alone. The effect of TMZ, Berberine, and TMZ+Berberine on tumoroid size reduction in T98G was significant ($p<0.0001$) compared to untreated spheroid after five days. The tumoroid-size inhibitory effect of berberine alone and combined with TMZ was very similar to TMZ alone, and it was found that it almost preserved the intact sphere structure and reduced the proliferative interaction, likewise to the results of fisetin. These findings also support wound healing in the hypoxic environment in terms of suppressing tumor aggressiveness with fisetin and berberine treatment alone and with the combination of TMZ in T98G.

It was worth saying that the ability of fisetin to induce double-strand breaks which was shown in breast cancer (Khozooei et al., 2022), might help us to understand the relation of fisetin in the DNA repair mechanism. An MMR gene MSH2, which had garnered significant research attention, plays a role in fixing errors in DNA replication, and its defect is correlated with chemotherapy drug resistance (Graham, Putnam, & Kolodner, 2018). However, the lack of efficacy of fisetin on MSH2 expression was found in the literature, and based on this, the effects of fisetin treatment on MSH2 gene expression were studied both alone and in combination with TMZ. So, with the TMZ+Fisetin cotreatment, we had the greatest increase among all treated groups in A172-R regarding MSH2 gene expression, which was significant to the untreated group ($p<0,0001$). Remarkably, in T98G, TMZ treatment increased the MSH2 gene expression almost 10-fold. The treatment, even with fisetin alone, had a significant increase in MSH2 levels ($p<0.0001$), and that impact was similar to combination therapy, whose difference was not significantly different from TMZ ($p=0,1069$). In A172, the highest increase in MSH2 was observed in the TMZ group; it may be because of the fact that it was also considered TMZ-sensitive and TMZ was found to successfully increase the MSH2 in *in-vivo* model of Lynch syndrome to be able to combat cancer cells (Wojciechowicz et al., 2014) but the enhancement of MSH2 gene

levels which were lower than TMZ was also significant in fisetin and its combination with TMZ compared to control ($p<0,0001$).

Differences in gene expression levels appear to be a reason for the patient population with diverse characteristics. It was seen that the results were similar to each other in the parameters evaluated in the patients. Since all of the patients we evaluated had aggressive GBM, they were similar to the parameters evaluated. However, there were differences in 3 patients in terms of p53 positiveness, a parameter commonly associated with patient survival (Toraih et al., 2019). To reveal this difference, other parameters we obtained were compared with the expression status of p53.

Defects in MSH2 favor the growth of GBM cells and cause TMZ resistance (McFaline-Figueroa et al., 2015), and we aimed to increase these levels with fisetin treatment. Since the lack of MSH2 transcripts was already associated with the recurrence of the disease and response to TMZ (McFaline-Figueroa et al., 2015), evaluating the effect of fisetin on this parameter was pivotal. In the patient with low p53 status (patient 3), a higher increase in MSH2 levels was detected in the TMZ, Fisetin, and TMZ+Fisetin treatment compared to the others, which was also maximized with the combined treatment. It was determined that fisetin increased the expression of MSH2 more efficiently in the patient with low P53 values. We anticipated that the behavior pattern was similar when the patient with low p53 (patient 3) and the p53-mutant cell line (T98G) were associated. With the expected increase of MSH2 to high levels in patient 3 and T98G, this highest increase can be achieved with the combined treatment of fisetin, which may improve TMZ sensitivity. A similar TMZ response to T98G may be expected in this patient if the patient would be potentially treated with combination therapy. A lower effect of MSH2 in terms of fisetin treatment was found in the cell line with p53-WT (A172) compared to T98G with the p53 mutant, and this finding was also similarly lower in patients with high p53 status (patients 1 and 2) compared to patient 3. According to previously mentioned, the p53-enhancing effect of fisetin may have an enhancing effect on both MSH2 and p53 and may be beneficial for overcoming TMZ resistance. Our patient findings and *in-vitro* functional analyses support the anti-tumor effect of fisetin, and this result may also play an essential role in patient survival.

ZEB1 is also a prominent gene that affects EMT and several other malignancies in cancers. However, the specific role of ZEB1 in the context of the effects of fisetin and TMZ was not explicitly mentioned in the search results. In previous studies, it was shown that fisetin activated p53 in bladder cancer cells (Li et al., 2011). In hepatocellular carcinoma, p53 had also been found to suppress the EMT process resulting from the suppression of ZEB1 (Kim et al., 2011). Accordingly, it is plausible that when p53 was mutant, there may be disruptions in the suppression process of ZEB1, and its suppression could be essential to be able to retain an efficient therapy strategy.

In T98G (p53-mutant) cell, there was a certain decrease after TMZ, but this decrease was significantly increased in combination therapy, especially in fisetin alone ($p<0.0001$). Since resistance to TMZ was acquired in A172-R, treatment of TMZ did not reduce ZEB1 levels but increased it more than 46-fold. However, this increase was successfully reduced by cotreatment with fisetin. The primary culture of patient 3 with 3% p53 positive, which is considered as p53 negative (Roshandel et al., 2019), had increased levels of ZEB1 with TMZ treatment, which was similar to A172-R. However, this situation regressed until it decreased in combination therapy. Although there was an insufficient decrease in ZEB1 after TMZ treatment with fisetin and combination therapy, especially in resistant cell lines, the same situation was also seen in the patient with the lowest (3%) p53 positivity among other patients. This increase was suppressed by fisetin and combination treatment in T98G, A172-R cell lines, and third patient. In fact, there was a significant difference in T98G ($p=0.0003$) and A172-R ($p=0.0362$) when combined therapy was compared with TMZ. In the patient population, the increase in ZEB1 in TMZ successfully decreased in patient with low p53 positivity (patient 3) in combination therapy. In A172 (p53-WT), ZEB1 values are reduced with similar success in TMZ and TMZ+Fisetin treatment. In the treatment of A172, the combined treatment also showed a similar and significant effect ($p<0.0001$) to TMZ in ZEB1 levels compared to the control. The p53 found in 30% and 20% positiveness in p1 and p2, respectively, may be effective in suppressing ZEB1 in the treatment of TMZ. However, this effect was also supported both in fisetin alone and in combination therapy with TMZ. Thus, TMZ+Fisetin cotreatment could be successful enough to increase TMZ efficiency.

Surprisingly, the fact that the ZEB1 gene, whose expression was increased in drug resistance, also had excessive enhancement with TMZ treatment in the cell line that acquired TMZ resistance with long-term drug treatment, proving that drug resistance was successfully triggered. At the same time, the application of fisetin alone, especially the combination of TMZ, significantly reduced this effect, showing that it may be an effective compound for breaking chemoresistance. Both findings in cell lines and patients proved that combination therapy with fisetin may have result in better outcomes by increasing the effectiveness of TMZ.

Although our knowledge of the effects of GBM cells on chemotherapeutic drugs and complementary therapies and their relationship with drug resistance mechanisms is still quite limited, personalized, targeted therapy methods, which are very important for the response of the patient with mutations in specific genes, to treatment should be developed in future studies. Considering that it takes many years for a new drug to be accepted as a standard cancer treatment by revealing its mechanism of action and biosafety, studies that aim to improve the use of currently FDA-approved drugs by increasing their effectiveness with a natural biocompatible molecule are extremely important and necessary for GBM patients with a very short survival time.

In the current study, the effect of the combination of fisetin and berberine with TMZ was examined in GBM. The effective dose of berberine was almost 10 times greater than fisetin and also reduced cell viability to almost 44% in 24h in non-tumor cells. In terms of directing apoptosis, it did not pass the treatment of TMZ alone. Besides, necrotic cells were more than 10-fold after berberine treatment compared to fisetin. In this context, a bioactive molecule, fisetin, that could be most effective at the lowest dose was selected in the molecular analysis.

Intrinsic and acquired drug resistance in cancer can occur with the activation of different mechanisms in cells (Wang, Zhang, & Chen, 2019). The resistance that may develop over time due to the use of TMZ in patients who are predicted not to show TMZ resistance may create a stronger resistance situation than in patients with natural TMZ resistance (Wang et al., 2019). Our findings showed that TMZ treatment was more successful in intrinsic TMZ-resistant T98G cells than acquired resistant A172-R. Additionally, our findings showed that fisetin treatment has the potential to

initiate the ability of cells originating from different mechanisms to overcome TMZ resistance.

To put it in a nutshell, two flavonoids, berberine and especially fisetin, have anti-tumor properties in GBM cells. Since fisetin possesses a more potent anti-cancer effect on GBM cells than berberine, according to our findings, understanding the interrelationship between the regulation of MSH2 and ZEB1 in fisetin and drug resistance could help to tackle anti-TMZ resistance in GBM. The current project can contribute to highlight variable biomarkers in resistance mechanisms to improve both survival rates and quality of life in GBM patients with very short lifespans, and is particularly important for personalized medicine. Combination therapy used to break treatment resistance has been found to be preferable to suppress the harmful effects of a chemotherapy drug and increase its effectiveness at lower doses with natural compounds. To assess this hypothesis, it is worth noting that the conducted *in-vitro* analysis is needed to be expanded, considering that mechanisms can both genetically and epigenetically be modulated and supported by further investigation to fully understand the effects of fisetin and berberine on human health since the success of flavonoids, especially fisetin in both TMZ sensitive and resistant cells can not go unnoticed. In conclusion, our findings showed that dietary natural bioflavonoids, especially fisetin, may be a potential drug candidate as anti-cancer agent, which can both support TMZ and be effective in breaking resistance, even in different mechanisms in GBM.

6. REFERENCES

Afroze, N., Pramodh, S., Shafarin, J., Bajbouj, K., Hamad, M., Sundaram, M. K., … Hussain, A. (2022). Fisetin Deters Cell Proliferation, Induces Apoptosis, Alleviates Oxidative Stress and Inflammation in Human Cancer Cells, HeLa. *International journal of molecular sciences*, 23(3), 1707. https://doi.org/10.3390/ijms23031707

Agnarelli, A., Natali, M., Garcia-Gil, M., Pesi, R., Tozzi, M. G., Ippolito, C., … Marracci, S. (2018). Cell-specific pattern of berberine pleiotropic effects on different human cell lines. *Scientific reports*, 8(1), 10599. https://doi.org/10.1038/s41598-018-28952-3

Ai, X., Yu, P., Peng, L., Luo, L., Liu, J., Li, S., … Meng, X. (2021). Berberine: A Review of its Pharmacokinetics Properties and Therapeutic Potentials in Diverse Vascular Diseases. *Frontiers in pharmacology,* 12, 762654. https://doi.org/10.3389/fphar.2021.762654

Al Matari, N., Deeb, G., Mshiek, H., Sinjab, A., Kadara, H., Abou-Kheir, W., & Mhanna, R. (2020). Anti-Tumor Effects of Biomimetic Sulfated Glycosaminoglycans on Lung Adenocarcinoma Cells in 2D and 3D In Vitro Models. *Molecules (Basel, Switzerland),* 25(11), 2595. https://doi.org/10.3390/molecules25112595

Alkıs, M. E. (2022). Investigation of Treatment Potential of O-Vanillin Containing Schiff Base Ligand and Pd(II) Complex in Glioblastoma Multiforme Cells and Efficiency of Electroporation. *Van Med J.* 29(1): 69-75

Alves, A. L. V., Gomes, I. N. F., Carloni, A. C., Rosa, M. N., da Silva, L. S., Evangelista, A. F… Silva, V. A. O. (2021). Role of glioblastoma stem cells in cancer therapeutic resistance: a perspective on antineoplastic agents from natural sources and chemical derivatives. *Stem Cell Res Ther.* 12, 206. https://doi.org/10.1186/s13287-021-02231-x

Amirpour, Z., Bahari, A., Nafisi, B., Rahmani, K., Taghipour Zahir, S. (2020). Prognosis and Survival Study in Patients with Glioblastoma Multiform and Its Relationship with EGFR Expression. *Iran J Neurosurg.* 6 (3):113-120

Anasamy, T., Abdul, A. B., Sukari, M. A., Abdelwahab, S. I., Mohan, S., Kamalidehghan, B., … Sulaiman Rahman, H. (2013). A Phenylbutenoid Dimer, cis-3-(3',4'-Dimethoxyphenyl)-4-[(E)-3'",4'"-Dimethoxystyryl] Cyclohex-1-ene, Exhibits Apoptogenic Properties in T-Acute Lymphoblastic Leukemia Cells via Induction of p53-Independent Mitochondrial Signalling Pathway. *Evidence-based complementary and alternative medicine : eCAM*, 2013, 939810. https://doi.org/10.1155/2013/939810

Ardi Putra, F., Setyabudi, R., Wijayanti, N., & Indah Budhy, S. (2022). Cytotoxic and apoptotic induction activity of protein isolated from blood clam (Anadara (tegillarca) granosa, Linnaeus 1758) Against breast cancer t47d cell line. *Matrix Science Pharma*, 6, 46 - 51.

Arora, A., & Somasundaram, K. (2019). Glioblastoma vs temozolomide: can the red queen race be won?. *Cancer biology & therapy*, 20(8), 1083–1090. https://doi.org/10.1080/15384047.2019.1599662

Atcc.org website

Bacchi, F., Sargenti, A., Musmeci, F., Pasqua, S., Bonetti, S., Gazzola, D., & Cristaldi, D.A. (2021). A viability study of 3D tumor spheroids after their mass-density characterization via an innovative flow-based biophysical method. *Biomedical Science and Engineering.*

Bae, S. H., Park, M. J., Lee, M. M., Kim, T. M., Lee, S. H., Cho, S. Y., … Kim, C. Y. (2014). Toxicity profile of temozolomide in the treatment of 300 malignant glioma patients in Korea. *Journal of Korean medical science,* 29(7), 980–984. https://doi.org/10.3346/jkms.2014.29.7.980

Bai, J. W., Zhang, Y. Q., Li, Y. C., & Zhang, G. J. (2017). Analysis of Epithelial-Mesenchymal Transition Induced by Overexpression of Twist. *Methods in molecular biology (Clifton, N.J.),* 1652, 259–274. https://doi.org/10.1007/978-1-4939-7219-7_17

Banno, K., Iida, M., Yanokura, M., Kisu, I., Iwata, T., Tominaga, E., … Aoki, D. (2014). MicroRNA in Cervical Cancer: OncomiRs and Tumor Suppressor miRs in Diagnosis and Treatment. *The Scientific World Journal.* https://doi.org/10.1155/2014/178075.

Beltzig, L., Christmann, M., & Kaina, B. (2022). Abrogation of Cellular Senescence Induced by Temozolomide in Glioblastoma Cells: Search for Senolytics. *Cells*, 11(16), 2588. https://doi.org/10.3390/cells11162588

Bernardo, B. C., Ooi, J. Y., Lin, R. C., & McMullen, J. R. (2015) miRNA therapeutics: a new class of drugs with potential therapeutic applications in the heart. *Future Medicinal Chemistry* 7;13.

Bhattacharya, S., Calar, K., Evans, C., Petrasko, M., & de la Puente, P. (2020). Bioengineering the Oxygen-Deprived Tumor Microenvironment Within a Three-Dimensional Platform for Studying Tumor-Immune Interactions. *Frontiers in bioengineering and biotechnology*, *8*, 1040. https://doi.org/10.3389/fbioe.2020.01040

Bilicki, D., Zbrożek, M., Fudalej, M., Deptała, A., & Badowska-Kozakiewicz, A. (2022). Glioblastoma - actual knowledge and future perspectives. *OncoReview*, 12(2), 35-44.

Bise, R., Kanade, T., Yin, Z., & Huh, S. I. (2011). Automatic cell tracking applied to analysis of cell migration in wound healing assay. Annual International Conference of the IEEE Engineering in Medicine and Biology Society. *IEEE Engineering in Medicine and Biology Society. Annual International Conference*, 2011, 6174–6179. https://doi.org/10.1109/IEMBS.2011.6091525

Bonneville-Levard A, Frappaz D, Tredan O, Lavergne E, Corset V, Agrapart V., ... Blay, J. Y. (2021). Molecular profile to guide personalized medicine in adult patients with primary brain tumors: results from the ProfiLER trial. *Med Oncol.* Nov 5;39(1):4. doi: 10.1007/s12032-021-01536-4.

Bouget, D., Pedersen, A., Jakola, A. S., Kavouridis, V., Emblem, K. E., Eijgelaar, R. S., … Reinertsen, I. (2022). Preoperative Brain Tumor Imaging: Models and

Software for Segmentation and Standardized Reporting. *Frontiers in neurology*, 13, 932219. https://doi.org/10.3389/fneur.2022.932219

Brix, N., Samaga, D., Belka, C., Zitzelsberger, H., & Lauber, K. (2021). Analysis of clonogenic growth in vitro. *Nature protocols,* 16(11), 4963–4991. https://doi.org/10.1038/s41596-021-00615-0

Butler, M., Pongor, L., Su, Y. T., Xi, L., Raffeld, M., Quezado, M., … Wu, J. (2020). MGMT Status as a Clinical Biomarker in Glioblastoma. *Trends Cancer.* 6(5):380-391. doi: 10.1016/j.trecan.2020.02.010.

Caccese, M., Ius, T., Simonelli, M., Fassan, M., Cesselli, D., Dipasquale, A., … Lombardi, G. (2020). Mismatch-Repair Protein Expression in High-Grade Gliomas: A Large Retrospective Multicenter Study. *International journal of molecular sciences*, 21(18), 6716. https://doi.org/10.3390/ijms21186716

Cai, J., Chen, J., Zhang, W., Yang, P., Zhang, C., Li, M., … Jiang, T. (2015). Loss of ATRX, associated with DNA methylation pattern of chromosome end, impacted biological behaviors of astrocytic tumors. *Oncotarget*. 6(20):18105-15. doi: 10.18632/oncotarget.3906.

Calin, G. A., Sevignani, C., Dumitru, C. D., Hyslop, T., Noch, E., Yendamuri, S., ... Croce, C. M. (2004). Human microRNA genes are frequently located at fragile sites and genomic regions involved in cancers. *Proc Natl Acad Sci U S A.* 101(9):2999-3004. doi: 10.1073/pnas.0307323101.

Cellosaurus.org website

Cha, G. D., Kang, T., Baik, S., Kim, D., Choi, S. H., Hyeon, T., ... Kim, D. H. (2020). Advances in drug delivery technology for the treatment of glioblastoma multiforme. *Journal of controlled release : official journal of the Controlled Release Society*, 328, 350–367. https://doi.org/10.1016/j.jconrel.2020.09.002.

Chai, C, Song, L-J, Han, S-Y, Li, X-Q, & Li, M. (2018). MicroRNA-21 promotes glioma cell proliferation and inhibits senesence and apoptosis by targeting SPRY1 via PTEN/PI3K/AKT signaling pathway. *CNS Neurosci Ther.* 2018;24: 369-380.

Chan, K. M., Fang, D., Gan, H., Hashizume, R., Yu, C., Schroeder, M., … Zhang, Z. (2013). The histone H3.3K27M mutation in pediatric glioma reprograms H3K27 methylation and gene expression. *Genes Dev*. 27(9):985-90. doi: 10.1101/gad.217778.113.

Chandana, S. R., Movva, S., Arora, M., & Singh, T. (2008). Primary brain tumors in adults. *American family physician*, 77(10), 1423–1430.

Chen, B., Li, X., Wu, L., Zhou, D., Song, Y., Zhang, L., … Zhou, W. (2022). Quercetin Suppresses Human Glioblastoma Migration and Invasion via GSK3β/β-catenin/ZEB1 Signaling Pathway. *Frontiers in pharmacology*, 13, 963614. https://doi.org/10.3389/fphar.2022.963614

Chen, Y. C., Shen, S. C., Lee, W. R., Lin, H. Y., Ko, C. H., Shih, C. M., & Yang, L. L. (2002). Wogonin and fisetin induction of apoptosis through activation of caspase 3 cascade and alternative expression of p21 protein in hepatocellular carcinoma cells SK-HEP-1. *Archives of toxicology,* 76(5-6), 351–359. https://doi.org/10.1007/s00204-002-0346-6

Cheng, S. Y., Huang, H. J., Nagane, M., Ji, X. D., Wang, D., Shih, C. C., … Cavenee, W. K. (1996). Suppression of glioblastoma angiogenicity and tumorigenicity by inhibition of endogenous expression of vascular endothelial growth factor. *Proc Natl Acad Sci U S A.* 1996 Aug 6;93(16):8502-7. doi: 10.1073/pnas.93.16.8502.

Choi, W. I., Kim, M. Y., Jeon, B. N., Koh, D. I., Yun, C.O., Li, Y., ... Hur, M. W. (2014). Role of promyelocytic leukemia zinc finger (PLZF) in cell proliferation and cyclin-dependent kinase inhibitor 1A (p21WAF/CDKN1A) gene repression. *J Biol Chem.* 2014 Jul 4;289(27):18625-40. doi: 10.1074/jbc.M113.538751.

Chu, K., Boley, K. M., Moraes, R., Barsky, S. H., & Robertson, F. M. (2013). The paradox of E-cadherin: role in response to hypoxia in the tumor microenvironment and regulation of energy metabolism. *Oncotarget,* 4(3), 446–462. https://doi.org/10.18632/oncotarget.872

ClinicalTrials.gov ID: NCT01849952 https://clinicaltrials.gov/study/NCT01849952

ClinicalTrials.gov ID: NCT02345824 https://classic.clinicaltrials.gov/ct2/show/NCT02345824

Cragg, G. M., & Newman, D. J. (2005). Plants as a source of anti-cancer agents. *Journal of ethnopharmacology,* 100(1-2), 72–79. https://doi.org/10.1016/j.jep.2005.05.011

Crivii, C. B., Boșca, A. B., Melincovici, C. S., Constantin, A. M., Mărginean, M., Dronca, E., … Șovrea, A. (2022). Glioblastoma Microenvironment and Cellular Interactions. *Cancers*, 14(4), 1092. https://doi.org/10.3390/cancers14041092

Cusabio.com website https://www.cusabio.com/c-20829.html

Cytosmart.com website https://cytosmart.com/resources/resources/clonogenic-assay-what-why-and-how

Debaugnies, M., Rodríguez-Acebes, S., Blondeau, J., Parent, M. A., Zocco, M., Song, Y., … Blanpain, C. (2023). RHOJ controls EMT-associated resistance to chemotherapy. *Nature*, 616(7955), 168–175. https://doi.org/10.1038/s41586-023-05838-7

Deng, J., Wang, Y., Lei, J., Lei, W., & Xiong, J. P. (2017). Insights into the involvement of noncoding RNAs in 5-fluorouracil drug resistance. *Tumour biology : the journal of the International Society for Oncodevelopmental Biology and Medicine,* 39(4), 1010428317697553. https://doi.org/10.1177/1010428317697553

Dhawan, A., Manem, V. S. K., Yeaney, G., Lathia, J. D., & Ahluwalia, M. S. (2023). EGFR Pathway Expression Persists in Recurrent Glioblastoma Independent of Amplification Status. *Cancers (Basel).* 2023 Jan 21;15(3):670. doi: 10.3390/cancers15030670.

Ding, J., Li, X., Khan, S., Zhang, C., Gao, F., Sen, S., ... Alfred Yung, W. K. (2022). EGFR suppresses p53 function by promoting p53 binding to DNA-PKcs: a noncanonical regulatory axis between EGFR and wild-type p53 in glioblastoma. *Neuro Oncol.* 3;24(10):1712-1725. doi: 10.1093/neuonc/noac105.

Do, H., & Kim, W. (2018). Roles of Oncogenic Long Non-coding RNAs in Cancer Development. *Genomics Inform.* 16(4):e18. doi: 10.5808/GI.2018.16.4.e18.

Doh, I., Kwon, Y. J., Ku, B., & Lee, D. W. (2019). Drug Efficacy Comparison of 3D Forming and Preforming Sphere Models with a Micropillar and Microwell Chip Platform. *SLAS discovery : advancing life sciences* R & D, 24(4), 476–483. https://doi.org/10.1177/2472555218821292

Dong, L., Jiang, H., Kang, Z., & Guan, M. (2023). Biomarkers for chemotherapy and drug resistance in the mismatch repair pathway. *Clinica chimica acta; international journal of clinical chemistry*, 544, 117338. https://doi.org/10.1016/j.cca.2023.117338

Drápela, S., Bouchal, J., Jolly, M. K., Culig, Z., & Souček, K. (2020). ZEB1: A Critical Regulator of Cell Plasticity, DNA Damage Response, and Therapy Resistance. *Frontiers in molecular biosciences*, 7, 36. https://doi.org/10.3389/fmolb.2020.00036

Du, B., & Shim, J. S. (2016). Targeting Epithelial-Mesenchymal Transition (EMT) to Overcome Drug Resistance in Cancer. *Molecules* (Basel, Switzerland), 21(7), 965. https://doi.org/10.3390/molecules21070965

Duan, H., Hao, C., Ren, X., Xue, W., & Qiao, X. (2021). Berberine enhances the sensitivity of temozolomide to chemotherapy for glioma. *FASEB*, 35(1). https://doi.org/10.1096/fasebj.2021.35.S1.03375.

Dymova, M. A., Kuligina, E. V., & Richter, V. A. (2021). Molecular Mechanisms of Drug Resistance in Glioblastoma. *International journal of molecular sciences*, 22(12), 6385. https://doi.org/10.3390/ijms22126385

Dymova, M. A., Kuligina, E. V., & Richter, V. A. (2021). Molecular Mechanisms of Drug Resistance in Glioblastoma. *International journal of molecular sciences*, 22(12), 6385. https://doi.org/10.3390/ijms22126385

Eo, S. H., Kim, J. H., & Kim, S. J. (2014). Induction of G_2/M Arrest by Berberine via Activation of PI3K/Akt and p38 in Human Chondrosarcoma Cell Line. *Oncology research*, 22(3), 147–157. https://doi.org/10.3727/096504015X14298122915583

Eom, K. S., Hong, J. M., Youn, M. J., So, H. S., Park, R., Kim, J. M., & Kim, T. Y. (2008). Berberine induces G1 arrest and apoptosis in human glioblastoma T98G cells through mitochondrial/caspases pathway. *Biological & pharmaceutical bulletin*, 31(4), 558–562. https://doi.org/10.1248/bpb.31.558

Ercelik, M., Tekin, C., Tezcan, G., Ak Aksoy, S., Bekar, A., Kocaeli, H., … Tunca, B. (2023). Olea europaea Leaf Phenolics Oleuropein, Hydroxytyrosol, Tyrosol, and Rutin Induce Apoptosis and Additionally Affect Temozolomide against Glioblastoma: In Particular, Oleuropein Inhibits Spheroid Growth by Attenuating Stem-like Cell Phenotype. *Life* (Basel, Switzerland), 13(2), 470. https://doi.org/10.3390/life13020470

Everix, L., Seane, E. N., Ebenhan, T., Goethals, I., & Bolcaen, J. (2023). Introducing HDAC-Targeting Radiopharmaceuticals for Glioblastoma Imaging and Therapy. *Pharmaceuticals (Basel)*. 16(2):227. doi: 10.3390/ph16020227.

Fan, S., Xu, H., Liu, H., Hu, Z., Xiao, J., & Liu, H. (2019). Inhibition of cancer cell growth by Tangeretin flavone in drug-resistant MDA-MB-231 human breast

carcinoma cells is facilitated via targeting cell apoptosis, cell cycle phase distribution, cell invasion and activation of numerous Caspases. *Journal of B.U.ON. : official journal of the Balkan Union of Oncology,* 24(4), 1532–1537.

Fan, X., Aalto, Y., Sanko, S. G., Knuutila, S., Klatzmann, D., & Castresana, J. S. (2002). Genetic profile, PTEN mutation and therapeutic role of PTEN in glioblastomas. *Int J Oncol.* 21(5):1141-50.

Farooqi, A. A., Qureshi, M. Z., Khalid, S., Attar, R., Martinelli, C., Sabitaliyevich, U. Y., … Xu, B. (2019). Regulation of Cell Signaling Pathways by Berberine in Different Cancers: Searching for Missing Pieces of an Incomplete Jig-Saw Puzzle for an Effective Cancer Therapy. *Cancers*, 11(4), 478. https://doi.org/10.3390/cancers11040478

Feng, C., Zhao, Y., Li, Y., Zhang, T., Ma, Y., & Liu, Y. (2019). LncRNA MALAT1 Promotes Lung Cancer Proliferation and Gefitinib Resistance by Acting as a miR-200a Sponge. *Archivos de bronconeumologia,* 55(12), 627–633. https://doi.org/10.1016/j.arbres.2019.03.026

Fernald, K., & Kurokawa, M. (2013). Evading apoptosis in cancer. *Trends in cell biology,* 23(12), 620–633. https://doi.org/10.1016/j.tcb.2013.07.006

Fernandes, S. G., Dsouza, R., Pandya, G., Kirtonia, A., Tergaonkar, V., Lee, S. Y., ... Khattar, E. (2020). Role of Telomeres and Telomeric Proteins in Human Malignancies and Their Therapeutic Potential. *Cancers* (Basel). 12(7):1901. doi: 10.3390/cancers12071901.

Folkerth, R. D. (1994). Smears and frozen sections in the intraoperative diagnosis of central nervous system lesions. *Neurosurgery clinics of North America,* 5(1), 1–18.

Franken, N. A., Rodermond, H. M., Stap, J., Haveman, J., & van Bree, C. (2006). Clonogenic assay of cells in vitro. *Nature protocols,* 1(5), 2315–2319. https://doi.org/10.1038/nprot.2006.339

Gao, X., Wang, J., Li, M., Wang, J., Lv, J., Zhang, L., … Mao, W. (2019). Berberine attenuates XRCC1-mediated base excision repair and sensitizes breast cancer cells to the chemotherapeutic drugs. *Journal of cellular and molecular medicine*, 23(10), 6797–6804. https://doi.org/10.1111/jcmm.14560

Garnier, D., Meehan, B., Kislinger, T., Daniel, P., Sinha, A., Abdulkarim, B., … Rak, J. (2018). Divergent evolution of temozolomide resistance in glioblastoma stem cells is reflected in extracellular vesicles and coupled with radiosensitization. *Neuro-oncology*, 20(2), 236–248. https://doi.org/10.1093/neuonc/nox142

Ghaffarian Zirak, R., Tajik, H., Asadi, J., Hashemian, P., & Javid, H. (2022). The Role of Micro RNAs in Regulating PI3K/AKT Signaling Pathways in Glioblastoma. *Iran J Pathol.* 17(2):122-136. doi: 10.30699/IJP.2022.539029.2726.

Ghosh, D., Nandi, S., & Bhattacharjee, S. (2018). Combination therapy to checkmate Glioblastoma: clinical challenges and advances. *Clinical and translational medicine*, 7(1), 33. https://doi.org/10.1186/s40169-018-0211-8

Gibbons, D. L., Lin, W., Creighton, C. J., Rizvi, Z. H., Gregory, P. A., Goodall, G. J., … Kurie, J. M. (2009). Contextual extracellular cues promote tumor cell EMT

and metastasis by regulating miR-200 family expression. *Genes & development,* 23(18), 2140–2151. https://doi.org/10.1101/gad.1820209

Girardi, F., Matz, M., Stiller, C., You, H., Marcos Gragera, R., Valkov, M. Y., … CONCORD Working Group. (2023). Global survival trends for brain tumors, by histology: analysis of individual records for 556,237 adults diagnosed in 59 countries during 2000–2014 (CONCORD-3), *Neuro-Oncology*, Volume 25, Issue 3, March 2023, Pages 580–592, https://doi.org/10.1093/neuonc/noac217

Globocan, 2021. https://gco.iarc.fr/today/data/factsheets/populations/792-turkey-fact-sheets.pdf

Gousias, K., Theocharous, T., & Simon, M. (2022). Mechanisms of Cell Cycle Arrest and Apoptosis in Glioblastoma. *Biomedicines,* 10(3), 564. https://doi.org/10.3390/biomedicines10030564

Graham, V. W. J., Putnam, C. D., & Kolodner, R. D. (2018). DNA Mismatch Repair: Mechanisms and Cancer Genetics, *Encyclopedia of Cancer (Third Edition), Academic Press,* 2019, Pages 530-538, https://doi.org/10.1016/B978-0-12-801238-3.96130-0).

Grube, S., Freitag, D., Kalff, R., Ewald, C., & Walter, J. (2021). Characterization of adherent primary cell lines from fresh human glioblastoma tissue, defining glial fibrillary acidic protein as a reliable marker in establishment of glioblastoma cell culture. *Cancer reports (Hoboken, N.J.),* 4(2), e1324. https://doi.org/10.1002/cnr2.1324

Guo, C. F., Zhuang, Y., Chen, Y., Chen, S., Peng, H., & Zhou, S. (2020). Significance of tumor protein p53 mutation in cellular process and drug selection in brain lower grade (WHO grades II and III) glioma. *Biomark Med.* 2020 Aug;14(12):1139-1150. doi: 10.2217/bmm-2020-0331.

Happold, C., Roth, P., Wick, W., Schmidt, N., Florea, A.-M., Silginer, M., … Weller, M. (2012). Distinct molecular mechanisms of acquired resistance to temozolomide in glioblastoma cells. *Journal of Neurochemistry*, 122: 444-455. https://doi.org/10.1111/j.1471-4159.2012.07781.x

Harutyunyan, A. S., Chen, H., Lu, T., Horth, C., Nikbakht, H., Krug, B., … Majewski, J. (2020). H3K27M in Gliomas Causes a One-Step Decrease in H3K27 Methylation and Reduced Spreading within the Constraints of H3K36 Methylation. *Cell Rep*. 33(7):108390. doi: 10.1016/j.celrep.2020.108390.

Hashemi, M., Etemad, S., Rezaei, S., Ziaolhagh, S., Rajabi, R., Rahmanian, P., … Hushmandi, K. (2023). Progress in targeting PTEN/PI3K/Akt axis in glioblastoma therapy: Revisiting molecular interactions. *Biomed Pharmacother.* 158:114204. doi: 10.1016/j.biopha.2022.114204.

Hegi, M. E., Diserens, A. C., Godard, S., Dietrich, P. Y., Regli, L., Ostermann, S., … Stupp, R. (2004). Clinical trial substantiates the predictive value of O-6-methylguanine-DNA methyltransferase promoter methylation in glioblastoma patients treated with temozolomide. *Clinical cancer research : an official journal of the American Association for Cancer Research,* 10(6), 1871–1874. https://doi.org/10.1158/1078-0432.ccr-03-0384

Hegi, M. E., Liu, L., Herman, J. G., Stupp, R., Wick, W., Weller, M., … Gilbert, M. R. (2008). Correlation of O6-methylguanine methyltransferase (MGMT)

promoter methylation with clinical outcomes in glioblastoma and clinical strategies to modulate MGMT activity. *Journal of clinical oncology : official journal of the American Society of Clinical Oncology,* 26(25), 4189–4199. https://doi.org/10.1200/JCO.2007.11.5964

Hermisson, M., Klumpp, A., Wick, W., Wischhusen, J., Nagel, G., Roos, W., … Weller, M. (2006). O6-methylguanine DNA methyltransferase and p53 status predict temozolomide sensitivity in human malignant glioma cells. *Journal of neurochemistry*, 96(3), 766–776. https://doi.org/10.1111/j.1471-4159.2005.03583.x

Hollman, P. C., & Katan, M. B. (1999). Health effects and bioavailability of dietary flavonols. *Free radical research*, 31 Suppl, S75–S80. https://doi.org/10.1080/10715769900301351

Hou, Z., Imam, M. U., Ismail, M., Azmi, N. H., Ismail, N., Ideris, A., & Mahmud, R. (2015). Lactoferrin and ovotransferrin contribute toward antioxidative effects of Edible Bird's Nest against hydrogen peroxide-induced oxidative stress in human SH-SY5Y cells. *Bioscience, biotechnology, and biochemistry,* 79(10), 1570–1578. https://doi.org/10.1080/09168451.2015.1050989

Hsieh, M. H., Tsai, J. P., Yang, S. F., Chiou, H. L., Lin, C. L., Hsieh, Y. H., & Chang, H. R. (2019). Fisetin Suppresses the Proliferation and Metastasis of Renal Cell Carcinoma through Upregulation of MEK/ERK-Targeting CTSS and ADAM9. *Cells,* 8(9), 948. https://doi.org/10.3390/cells8090948

Huang, C., Liu, H., Gong, X. L., Wu, L. Y., & Wen, B. (2017). Effect of evodiamine and berberine on the interaction between DNMTs and target microRNAs during malignant transformation of the colon by TGF-β1. *Oncology reports,* 37(3), 1637–1645. https://doi.org/10.3892/or.2017.5379

Huang, C., Wang, X. L., Qi, F. F., & Pang, Z. L. (2020). Berberine inhibits epithelial-mesenchymal transition and promotes apoptosis of tumour-associated fibroblast-induced colonic epithelial cells through regulation of TGF-β signalling. *Journal of cell communication and signaling*, 14(1), 53–66. https://doi.org/10.1007/s12079-019-00525-7

Huarte, M. (2015). The emerging role of lncRNAs in cancer. *Nat Med* 21, 253-1261 https://doi.org/10.1038/nm.3981

Hutchings, K. R., Pridham, K. J., Liu, M., & Sheng, Z. (2022). DDDR-19. NEXT-GENERATION PI3K INHIBITOR FOR GLIOBLASTOMA TREATMENT. *Neuro-Oncology*.

Ianevski, A., Giri, A. K., & Aittokallio, T. (2022). SynergyFinder 3.0: an interactive analysis and consensus interpretation of multi-drug synergies across multiple samples. *Nucleic acids research*, 50(W1), W739–W743. https://doi.org/10.1093/nar/gkac382

Imran, M., Saeed, F., Gilani, S. A., Shariati, M. A., Imran, A., Afzaal, M., … Anjum, F. M. (2020). Fisetin: An anticancer perspective. *Food science & nutrition*, 9(1), 3–16. https://doi.org/10.1002/fsn3.1872

Insilico.ehu.eus http://insilico.ehu.eus/counting_chamber/thoma.php

Irina, M., Filippova, S., Timofeeva, S., Sitkovskaya, A., Shamova, T., Enin, Y., … Kit, O. (2021). Antimigratory effect of berberine in T98G, U87MG and primary

glioma cell culture.. *Journal of Clinical Oncology.* 39. e15045-e15045. 10.1200/JCO.2021.39.15_suppl.e15045.

Ismail, N., Ismail, M., Imam, M. U., Azmi, N. H., Fathy, S. F., Foo, J. B., & Abu Bakar, M. F. (2014). Mechanistic basis for protection of differentiated SH-SY5Y cells by oryzanol-rich fraction against hydrogen peroxide-induced neurotoxicity. *BMC complementary and alternative medicine,* 14, 467. https://doi.org/10.1186/1472-6882-14-467

Jain, K. K. (2018). A Critical Overview of Targeted Therapies for Glioblastoma. *Frontiers in oncology*, 8, 419. https://doi.org/10.3389/fonc.2018.00419

Javed Iqbal, M., Quispe, C., Javed, Z., Sadia, H., Qadri, Q. R., Raza, S., … Sharifi-Rad, J. (2021). Nanotechnology-Based Strategies for Berberine Delivery System in Cancer Treatment: Pulling Strings to Keep Berberine in Power. *Frontiers in molecular biosciences,* 7, 624494. https://doi.org/10.3389/fmolb.2020.624494

Jia, S., Xu, X., Zhou, S., Chen, Y., Ding, G., & Cao, L. (2019). Fisetin induces autophagy in pancreatic cancer cells via endoplasmic reticulum stress- and mitochondrial stress-dependent pathways. *Cell death & disease*, 10(2), 142. https://doi.org/10.1038/s41419-019-1366-y

Jiapaer, S., Furuta, T., Tanaka, S., Kitabayashi, T., & Nakada, M. (2018). Potential Strategies Overcoming the Temozolomide Resistance for Glioblastoma. *Neurologia medico-chirurgica*, 58(10), 405–421. https://doi.org/10.2176/nmc.ra.2018-0141

Joseph, J. V., Conroy, S., Pavlov, K., Sontakke, P., Tomar, T., Eggens-Meijer, E., … Kruyt, F. A. (2015). Hypoxia enhances migration and invasion in glioblastoma by promoting a mesenchymal shift mediated by the HIF1α-ZEB1 axis. *Cancer letters*, 359(1), 107–116. https://doi.org/10.1016/j.canlet.2015.01.010

Kammerud, S. C., Metge, B. J., Elhamamsy, A. R., Weeks, S. E., Alsheikh, H. A., Mattheyses, A. L., … Samant, R. S. (2021). Novel role of the dietary flavonoid fisetin in suppressing rRNA biogenesis. *Laboratory investigation; a journal of technical methods and pathology*, 101(11), 1439–1448. https://doi.org/10.1038/s41374-021-00642-1

Karpel-Massler, G., Horst, B. A., Shu, C., Chau, L., Tsujiuchi, T., Bruce, J. N., … Siegelin, M. D. (2016). A Synthetic Cell-Penetrating Dominant-Negative ATF5 Peptide Exerts Anticancer Activity against a Broad Spectrum of Treatment-Resistant Cancers. *Clinical cancer research : an official journal of the American Association for Cancer Research,* 22(18), 4698–4711. https://doi.org/10.1158/1078-0432.CCR-15-2827

Kazaz, I. O., Mentese, A., Demir, S., Kerimoglu, G., Colak, F., Bodur, A., … Turedi, S. (2020). Berberine inhibits the ischemia-reperfusion induced testicular injury through decreasing oxidative stress. *The American journal of emergency medicine,* 38(1), 33–37. https://doi.org/10.1016/j.ajem.2019.04.001

Khin-Maung, U., Myo, K., Nyunt, N. W., Aye, K., & Tin, U. (1985). Clinical trial of berberine in acute watery diarrhoea. *British medical journal (Clinical research ed.),* 291(6509), 1601–1605. https://doi.org/10.1136/bmj.291.6509.1601

Khozooei, S., Lettau, K., Barletta, F., Jost, T., Rebholz, S., Veerappan, S., … Toulany, M. (2022). Fisetin induces DNA double-strand break and interferes with the repair of radiation-induced damage to radiosensitize triple negative breast cancer cells. *Journal of experimental & clinical cancer research : CR*, 41(1), 256. https://doi.org/10.1186/s13046-022-02442-x

Kil, W. J., Cerna, D., Burgan, W. E., Beam, K., Carter, D., Steeg, P. S., … Camphausen, K. (2008). In vitro and in vivo radiosensitization induced by the DNA methylating agent temozolomide. *Clinical cancer research : an official journal of the American Association for Cancer Research,* 14(3), 931–938. https://doi.org/10.1158/1078-0432.CCR-07-1856

Killela, P. J., Reitman, Z. J., Jiao, Y., Bettegowda, C., Agrawal, N., Diaz, L. A., … Yan, H. (2013). TERT promoter mutations occur frequently in gliomas and a subset of tumors derived from cells with low rates of self-renewal. *Proc Natl Acad Sci U S A.* 110(15):6021-6. doi: 10.1073/pnas.1303607110.

Kim, T. W. (2023). Fisetin, an Anti-Inflammatory Agent, Overcomes Radioresistance by Activating the PERK-ATF4-CHOP Axis in Liver Cancer. International Journal of Molecular Sciences, 24(10), 9076. MDPI AG. *Retrieved from* http://dx.doi.org/10.3390/ijms24109076

Kim, T., Veronese, A., Pichiorri, F., Lee, T. J., Jeon, Y. J., Volinia, S., … Croce, C. M. (2011). p53 regulates epithelial-mesenchymal transition through microRNAs targeting ZEB1 and ZEB2. *The Journal of experimental medicine*, 208(5), 875–883. https://doi.org/10.1084/jem.20110235

Kiseleva, L. N., Kartashev, A. V., Vartanyan, N. L., Pinevich, A. A., & Samoilovich, M. P. (2016). CHARACTERISTICS OF A172 AND T98G CELL LINES. *Tsitologiia*, 58(5), 349–355.

Kleihues, P., Louis, D. N., Scheithauer, B. W., Rorke, L. B., Reifenberger, G., Burger, P. C., & Cavenee, W. K. (2002). The WHO Classification of Tumors of the Nervous System, *Journal of Neuropathology & Experimental Neurology*, Volume 61, Issue 3, March 2002, Pages 215–225, https://doi.org/10.1093/jnen/61.3.215

Koehler, A., Karve, A., Desai, P., Arbiser, J., Plas, D. R., Qi, X., … Sengupta, S. (2021). Reuse of Molecules for Glioblastoma Therapy. *Pharmaceuticals* (Basel, Switzerland), 14(2), 99. https://doi.org/10.3390/ph14020099

Koschmann, C., Lowenstein, P. R., & Castro, M. G. (2016). ATRX mutations and glioblastoma: Impaired DNA damage repair, alternative lengthening of telomeres, and genetic instability. *Mol Cell Oncol*. 3(3):e1167158. doi: 10.1080/23723556.2016.1167158.

Kuang, L., Wang, Y., & Zhou, X. (2013). Base excision repair and antineoplastic drug resistance. *Tumori,* 33, 294-298.

Kumar, R. M., Kumar, H., Bhatt, T., Jain, R., Panchal, K., Chaurasiya, A., & Jain, V. (2023). Fisetin in Cancer: Attributes, Developmental Aspects, and Nanotherapeutics. *Pharmaceuticals,* 16(2), 196. MDPI AG. Retrieved from http://dx.doi.org/10.3390/ph16020196

Lamouille, S., Xu, J., & Derynck, R. (2014). Molecular mechanisms of epithelial-mesenchymal transition. *Nature reviews*. *Molecular cell biology,* 15(3), 178–196. https://doi.org/10.1038/nrm3758

Lee S. Y. (2016). Temozolomide resistance in glioblastoma multiforme. *Genes & diseases*, 3(3), 198–210. https://doi.org/10.1016/j.gendis.2016.04.007

Lee, E. S., Ko, K. K., Joe, Y. A., Kang, S. G., & Hong, Y. K. (2011). Inhibition of STAT3 reverses drug resistance acquired in temozolomide-resistant human glioma cells. *Oncology letters,* 2(1), 115–121. https://doi.org/10.3892/ol.2010.210

Lee, J. W., Choi, H. J., Kim, E. J., Hwang, W. Y., Jung, M. H., & Kim, K. S. (2020). Fisetin induces apoptosis in uterine leiomyomas through multiple pathways. *Scientific reports*, 10(1), 7993. https://doi.org/10.1038/s41598-020-64871-y

Lee, Y. J., Seo, H. W., Baek, J. H., Lim, S. H., Hwang S. G., & Kim E. H. (2020). Gene expression profiling of glioblastoma cell lines depending on TP53 status after tumor-treating fields (TTFields) treatment. *Sci Rep* 10, 12272 https://doi.org/10.1038/s41598-020-68473-6

Leece, R., Xu, J., Ostrom, Q. T., Chen, Y., Kruchko, C., & Barnholtz-Sloan, J. S. (2017). Global incidence of malignant brain and other central nervous system tumors by histology, 2003-2007. *Neuro-oncology*, 19(11), 1553–1564. https://doi.org/10.1093/neuonc/nox091

Li, J., Cheng, Y., Qu, W., Sun, Y., Wang, Z., Wang, H., & Tian, B. (2011). Fisetin, a dietary flavonoid, induces cell cycle arrest and apoptosis through activation of p53 and inhibition of NF-kappa B pathways in bladder cancer cells. *Basic & clinical pharmacology & toxicology*, 108(2), 84–93. https://doi.org/10.1111/j.1742-7843.2010.00613.x

Li, J., Gong, X., Jiang, R., Lin, D., Zhou, T., Zhang, A., … Li, H. (2018). Fisetin Inhibited Growth and Metastasis of Triple-Negative Breast Cancer by Reversing Epithelial-to-Mesenchymal Transition via PTEN/Akt/GSK3β Signal Pathway. *Frontiers in pharmacology*, 9, 772. https://doi.org/10.3389/fphar.2018.00772

Li, J., Liu, H., Ramachandran, S., Waypa, G. B., Yin, J. J., Li, C. Q., … Shao, Z. H. (2010). Grape seed proanthocyanidins ameliorate Doxorubicin-induced cardiotoxicity. *The American journal of Chinese medicine*, 38(3), 569–584. https://doi.org/10.1142/S0192415X10008068

Li, W. X., Cui, C. B., Cai, B., Wang, H. Y., & Yao, X. S. (2005). Flavonoids from Vitex trifolia L. inhibit cell cycle progression at G2/M phase and induce apoptosis in mammalian cancer cells. *Journal of Asian natural products research,* 7(4), 615–626. https://doi.org/10.1080/10286020310001625085

Li, Y., Jia, S., & Dai, W. (2020). Fisetin Modulates Human Oral Squamous Cell Carcinoma Proliferation by Blocking PAK4 Signaling Pathways. *Drug design, development and therapy*, 14, 773–782. https://doi.org/10.2147/DDDT.S229270

Li, Z., Pearlman, A. H., & Hsieh, P. (2016). DNA mismatch repair and the DNA damage response. *DNA repair,* 38, 94–101. https://doi.org/10.1016/j.dnarep.2015.11.019

Liang, Q., Zhuo, Y., Wu, X., Zheng, S., Zhuang, J., Wang, K., & Chen, S. (2023). Curcumin combining temozolomide formed localized nanogel for inhibition of postsurgical chemoresistant glioblastoma. *Nanomedicine (London, England),* 10.2217/nnm-2023-0058. Advance online publication. https://doi.org/10.2217/nnm-2023-0058

Liu, D., Meng, X., Wu, D., Qiu, Z., & Luo, H. (2019). A Natural Isoquinoline Alkaloid With Antitumor Activity: Studies of the Biological Activities of Berberine. *Frontiers in pharmacology*, 10, 9. https://doi.org/10.3389/fphar.2019.00009

Liu, G., Yuan, X., Zeng, Z., Tunici, P., Ng, H., Abdulkadir, I. R., … Yu, J. S. (2006). Analysis of gene expression and chemoresistance of CD133+ cancer stem cells in glioblastoma. *Molecular cancer,* 5, 67. https://doi.org/10.1186/1476-4598-5-67

Liu, Q., Xu, X., Zhao, M., Wei, Z., Li, X., Zhang, X., … Shao, C. (2015). Berberine induces senescence of human glioblastoma cells by downregulating the EGFR-MEK-ERK signaling pathway. *Molecular cancer therapeutics*, 14(2), 355–363. https://doi.org/10.1158/1535-7163.MCT-14-0634

Longevity website https://longevity.technology/lifestyle/how-long-does-it-take-for-berberine-to-work/

Louis, D. N., Perry, A., Wesseling, P., Brat, D. J., Cree, I. A., Figarella-Branger, D., … Ellison, D. W. (2021). The 2021 WHO Classification of Tumors of the Central Nervous System: a summary. *Neuro Oncol.* 2021 Aug 2;23(8):1231-1251.

Luo, F., Wei, H., Guo, H., Li, Y., Feng, Y., Bian, Q., & Wang, Y. (2019). LncRNA MALAT1, an lncRNA acting via the miR-204/ZEB1 pathway, mediates the EMT induced by organic extract of PM2.5 in lung bronchial epithelial cells. *American journal of physiology. Lung cellular and molecular physiology,* 317(1), L87–L98. https://doi.org/10.1152/ajplung.00073.2019

Ma, Z., Zhou, H., Chang, Q., & Xue, X. (2019). MicroRNA-based chemoresistance in glioblastoma. *Glioma* [serial online] 2019;2:83-7. https://doi.org/10.4103/glioma.glioma_4_19

Macharia, L. W., Muriithi, W., Heming, C. P., Nyaga, D. K., Aran, V., Mureithi, M. W., … Moura-Neto, V. (2021). The genotypic and phenotypic impact of hypoxia microenvironment on glioblastoma cell lines. *BMC cancer*, 21(1), 1248. https://doi.org/10.1186/s12885-021-08978-z

Maier, H. J., Wirth, T., & Beug, H. (2010). Epithelial-Mesenchymal Transition in Pancreatic Carcinoma. *Cancers*, 2(4), 2058–2083. MDPI AG. Retrieved from http://dx.doi.org/10.3390/cancers2042058

Maiti, P., Plemmons, A., & Dunbar, G. L. (2019). Combination treatment of berberine and solid lipid curcumin particles increased cell death and inhibited PI3K/Akt/mTOR pathway of human cultured glioblastoma cells more effectively than did individual treatments. *PloS one*, 14(12), e0225660. https://doi.org/10.1371/journal.pone.0225660

Marchiq, I., & Pouysségur, J. (2016). Hypoxia, cancer metabolism and the therapeutic benefit of targeting lactate/H(+) symporters. *Journal of molecular medicine (Berlin, Germany),* 94(2), 155–171. https://doi.org/10.1007/s00109-015-1307-x

Mathew, L. K., Skuli, N., Mucaj, V., Lee, S. S., Zinn, P. O., Sathyan, P., … Simon, M. C. (2014). miR-218 opposes a critical RTK-HIF pathway in mesenchymal glioblastoma. *Proceedings of the National Academy of Sciences of the United States of America,* 111(1), 291–296. https://doi.org/10.1073/pnas.1314341111

Matsuzaki, J., & Suzuki, H. (2014). MicroRNAs in Barrett's esophagus: future prospects. *Frontiers in Genetics.* https://doi.org/10.3389/fgene.2014.00069.

McDermott, A. M., Heneghan, H. M., Miller, N., & Kerin, M. J. (2011). The Therapeutic Potential of MicroRNAs: Disease Modulators and Drug Targets. *Pharmaceutical Research* 28(12):3016-29

McDonald, K. L., Aw, G., & Kleihues, P. (2013). Role of Biomarkers in the Clinical Management of Glioblastomas: What are the Barriers and How Can We Overcome Them?. *Frontiers in neurology,* https://scite.ai/reports/10.3389/fneur.2012.00188

McFaline-Figueroa, J. L., Braun, C. J., Stanciu, M., Nagel, Z. D., Mazzucato, P., Sangaraju, D., … Samson, L. D. (2015). Minor Changes in Expression of the Mismatch Repair Protein MSH2 Exert a Major Impact on Glioblastoma Response to Temozolomide. *Cancer research*, 75(15), 3127–3138. https://doi.org/10.1158/0008-5472.CAN-14-3616).

McLendon, R. E.., & Halperin, E. C. (2003). Is the long-term survival of patients with i

Meena, A. S., Sharma, A., Kumari, R., Mohammad, N., Singh, S. V., & Bhat, M. K. (2013). Inherent and acquired resistance to paclitaxel in hepatocellular carcinoma: molecular events involved. *PloS one,* 8(4), e61524. https://doi.org/10.1371/journal.pone.0061524

Merckmillipore.com website https://www.merckmillipore.com/TR/tr/20151006_191750

Mesfin, a F. B., & Al-Dhahir, M. A. (2023). Gliomas. In StatPearls. *StatPearls Publishing.*

Mihaylova, V. T., Bindra, R. S., Yuan, J., Campisi, D., Narayanan, L., Jensen, R., … Glazer, P. M. (2003). Decreased expression of the DNA mismatch repair gene Mlh1 under hypoxic stress in mammalian cells. *Molecular and cellular biology,* 23(9), 3265–3273. https://doi.org/10.1128/MCB.23.9.3265-3273.2003

Min, K. J., Nam, J. O., & Kwon, T. K. (2017). Fisetin Induces Apoptosis Through p53-Mediated Up-Regulation of DR5 Expression in Human Renal Carcinoma Caki Cells. *Molecules (Basel, Switzerland),* 22(8), 1285. https://doi.org/10.3390/molecules22081285

Mishra, V. S., Kumar, N., Raza, M., & Sehrawat, S. (2020). Amalgamation of PI3K and EZH2 blockade synergistically regulates invasion and angiogenesis: combination therapy for glioblastoma multiforme. *Oncotarget.* 11(51):4754-4769. doi: 10.18632/oncotarget.27842.

Mladinich, M., Ruan, D., & Chan, C. H. (2016). Tackling Cancer Stem Cells via Inhibition of EMT Transcription Factors. *Stem cells international,* 2016, 5285892. https://doi.org/10.1155/2016/5285892

Mukhtar, E., Adhami, V. M., Siddiqui, I. A., Verma, A. K., & Mukhtar, H. (2016). Fisetin Enhances Chemotherapeutic Effect of Cabazitaxel against Human Prostate Cancer Cells. *Molecular cancer therapeutics*, 15(12), 2863–2874. https://doi.org/10.1158/1535-7163.MCT-16-0515

Musah-Eroje, A., & Watson, S. (2019). A novel 3D in vitro model of glioblastoma reveals resistance to temozolomide which was potentiated by hypoxia. *Journal of neuro-oncology*, 142(2), 231–240. https://doi.org/10.1007/s11060-019-03107-0

Musah-Eroje, A., & Watson, S. (2019). Adaptive Changes of Glioblastoma Cells Following Exposure to Hypoxic (1% Oxygen) Tumour Microenvironment. *International journal of molecular sciences*, 20(9), 2091. https://doi.org/10.3390/ijms20092091

Neag, M. A., Mocan, A., Echeverría, J., Pop, R. M., Bocsan, C. I., Crişan, G., & Buzoianu, A. D. (2018). Berberine: Botanical Occurrence, Traditional Uses, Extraction Methods, and Relevance in Cardiovascular, Metabolic, Hepatic, and Renal Disorders. *Frontiers in pharmacology,* 9, 557. https://doi.org/10.3389/fphar.2018.00557

Ohgaki, H., & Kleihues, P. (2012). The Definition of Primary and Secondary Glioblastoma. *Clinical Cancer Research*, 19, 764 - 772.

Ortiz, R., Perazzoli, G., Cabeza, L., Jiménez-Luna, C., Luque, R., Prados, J., & Melguizo, C. (2021). Temozolomide: An Updated Overview of Resistance Mechanisms, Nanotechnology Advances and Clinical Applications. *Current neuropharmacology*, 19(4), 513–537. https://doi.org/10.2174/1570159X18666200626204005

Pak, F., & Oztopcu-Vatan, P. (2019). Fisetin effects on cell proliferation and apoptosis in glioma cells. Zeitschrift fur Naturforschung. *C, Journal of biosciences*, 74(11-12), 295–302. https://doi.org/10.1515/znc-2019-0098

Pal, H. C., Diamond, A. C., Strickland, L. R., Kappes, J. C., Katiyar, S. K., Elmets, C. A., … Afaq, F. (2016). Fisetin, a dietary flavonoid, augments the anti-invasive and anti-metastatic potential of sorafenib in melanoma. *Oncotarget,* 7(2), 1227–1241. https://doi.org/10.18632/oncotarget.6237

Palma, T. V., Lenz, L. S., Bottari, N. B., Pereira, A., Schetinger, M. R. C., Morsch, V. M., … de Andrade, C. M. (2020). Berberine induces apoptosis in glioblastoma multiforme U87MG cells via oxidative stress and independent of AMPK activity. *Molecular biology reports*, 47(6), 4393–4400. https://doi.org/10.1007/s11033-020-05500-9

Pan, F., Mao, H., Deng, L., Li, G., & Geng, P. (2014). Prognostic and clinicopathological significance of microRNA-21 overexpression in breast cancer: a meta-analysis.. *International journal of clinical and experimental pathology*.

Panche, A. N., Diwan, A. D., & Chandra, S. R. (2016). Flavonoids: an overview. *Journal of nutritional science,* 5, e47. https://doi.org/10.1017/jns.2016.41

Park, J. T. & Kim, T. Y. (2002). Cisplatin-Induced Apoptosis by Cisplatin in Human Glioblastoma Cell Line. *J Korean Neurosurg Soc.* 2002;31 (6): 574-584.

Pearson, J. R. D., & Regad, T. (2017). Targeting cellular pathways in glioblastoma multiforme. *Signal transduction and targeted therapy*, 2, 17040. https://doi.org/10.1038/sigtrans.2017.40

Perazzoli, G., Prados, J., Ortiz, R., Caba, O., Cabeza, L., Berdasco, M., … Melguizo, C. (2015). Temozolomide Resistance in Glioblastoma Cell Lines: Implication of MGMT, MMR, P-Glycoprotein and CD133 Expression. *PloS one*, 10(10), e0140131. https://doi.org/10.1371/journal.pone.0140131

Pérès, E. A., Gérault, A. N., Valable, S., Roussel, S., Toutain, J., Divoux, D., … Petit, E. (2015). Silencing erythropoietin receptor on glioma cells reinforces efficacy of temozolomide and X-rays through senescence and mitotic catastrophe. *Oncotarget*, 6(4), 2101–2119. https://doi.org/10.18632/oncotarget.2937

Pérez, G., López-Moncada, F., Indo, S., Torres, M. J., Castellón, E. A., & Contreras, H. R. (2021). Knockdown of ZEB1 reverses cancer stem cell properties in prostate cancer cells. *Oncology reports*, 45(5), 58. https://doi.org/10.3892/or.2021.8009

Piyanuch, R., Sukhthankar, M., Wandee, G., & Baek, S. J. (2007). Berberine, a natural isoquinoline alkaloid, induces NAG-1 and ATF3 expression in human colorectal cancer cells. *Cancer letters,* 258(2), 230–240. https://doi.org/10.1016/j.canlet.2007.09.007

Pritchard, C. C., Cheng, H. H., & Tewari, M. (2012). MicroRNA profiling: approaches and considerations. *Nat Rev Genet.* 13(5):358-69. doi: 10.1038/nrg3198.

Proteinatlas.org website https://www.proteinatlas.org/humanproteome/cell+line/brain+cancer

Ptglab.com website https://www.ptglab.com/products/featured-products/cell-cycle-and-checkpoint-controls/

Qin, T., Mullan, B., Ravindran, R., Messinger, D., Siada, R., Cummings, J. R., ... Koschmann, C. (2022). ATRX loss in glioma results in dysregulation of cell-cycle phase transition and ATM inhibitor radio-sensitization. *Cell Rep.* 38(2):110216. doi: 10.1016/j.celrep.2021.110216.

Qu, H., Song, X., Song, Z., Jiang, X., Gao, X., Bai, L., … Yao, Z. (2020). Berberine reduces temozolomide resistance by inducing autophagy via the ERK1/2 signaling pathway in glioblastoma. *Cancer cell international*, 20(1), 592. https://doi.org/10.1186/s12935-020-01693-y

Rahmani, A. H., Almatroudi, A., Allemailem, K. S., Khan, A. A., & Almatroodi, S. A. (2022). The Potential Role of Fisetin, a Flavonoid in Cancer Prevention and Treatment. *Molecules (Basel, Switzerland),* 27(24), 9009. https://doi.org/10.3390/molecules27249009

Rai, R., Banerjee, M., Wong, D. H., McCullagh, E., Gupta, A., Tripathi, S., … Chakravarty, S. (2016). Temozolomide analogs with improved brain/plasma ratios - Exploring the possibility of enhancing the therapeutic index of temozolomide. *Bioorganic & medicinal chemistry letters*, 26(20), 5103–5109. https://doi.org/10.1016/j.bmcl.2016.08.064

Rajendran, V., & Jain, M. V. (2018). In Vitro Tumorigenic Assay: Colony Forming Assay for Cancer Stem Cells. *Methods in molecular biology (Clifton, N.J.),* 1692, 89–95. https://doi.org/10.1007/978-1-4939-7401-6_8

Rajesh, Y., Pal, I., Banik, P., Chakraborty, S., Borkar, S. A., Dey, G., … Mandal, M. (2017). Insights into molecular therapy of glioma: current challenges and next generation blueprint. *Acta pharmacologica Sinica*, 38(5), 591–613. https://doi.org/10.1038/aps.2016.167

Ranganathan, K., & Sivasankar, V. (2014). MicroRNAs - Biology and clinical applications. J Oral *Maxillofac Pathol.* 18(2):229-34. doi: 10.4103/0973-029X.140762.

Ratnakumar, K., & Bernstein, E. (2013). ATRX: the case of a peculiar chromatin remodeler.. *Epigenetics*. https://doi.org/10.4161/epi.23271.

Reardon, D. A., Turner, S., Peters, K. B., Desjardins, A., Gururangan, S., Sampson, J. H., ... Friedman, H. S. (2011). A review of VEGF/VEGFR-targeted therapeutics for recurrent glioblastoma. *J Natl Compr Canc Netw*. 9(4):414-27. doi: 10.6004/jnccn.2011.0038.

Rezaei, O., Tamizkar, K. H., Sharifi, G., Taheri, M., & Ghafouri-Fard, S. (2021). Emerging Role of Long Non-Coding RNAs in the Pathobiology of Glioblastoma. *Frontiers in oncology,* 10, 625884. https://doi.org/10.3389/fonc.2020.625884

Rocha, M. R., & Morgado-Diaz, J. A. (2021). Epithelial-Mesenchymal Transition in colorectal cancer: Annexin A2 is caught in the crosshairs. *Journal of cellular and molecular medicine*, 25(22), 10774–10777. https://doi.org/10.1111/jcmm.16962

Rong, L., Li, N., & Zhang, Z. (2022). Emerging therapies for glioblastoma: current state and future directions. *Journal of experimental & clinical cancer research: CR*, 41(1), 142. https://doi.org/10.1186/s13046-022-02349-7

Roos, W. P., Batista, L. F., Naumann, S. C., Wick, W., Weller, M., Menck, C. F., & Kaina, B. (2007). Apoptosis in malignant glioma cells triggered by the temozolomide-induced DNA lesion O6-methylguanine. *Oncogene*, 26(2), 186–197. https://doi.org/10.1038/sj.onc.1209785

Roshandel, A. K., Busch, C. M., Mullekom, J. V., Cuoco, J. A., Rogers, C. M., Apfel, L. S., … Umans, R. A. (2019). The predictive capability of immunohistochemistry and DNA sequencing for determining TP53 functional mutation status: a comparative study of 41 glioblastoma patients. *Oncotarget*, 10(58), 6204–6218. https://doi.org/10.18632/oncotarget.27252

Russo, A. L., Kwon, H. C., Burgan, W. E., Carter, D., Beam, K., Weizheng, X., … Camphausen, K. (2009). In vitro and in vivo radiosensitization of glioblastoma cells by the poly (ADP-ribose) polymerase inhibitor E7016. *Clinical cancer research : an official journal of the American Association for Cancer Research*, 15(2), 607–612. https://doi.org/10.1158/1078-0432.CCR-08-2079

Saccà, C., Gorini, F., Ambrosio, S., Amente, S., Faicchia, D., Matarese, G., … Majello, B. (2019). Inhibition of lysine-specific demethylase LSD1 induces senescence in Glioblastoma cells through a HIF-1α-dependent pathway.. Biochimica et biophysica acta. *Gene regulatory mechanisms.* https://doi.org/10.1016/j.bbagrm.2019.03.004.

Salehi, S., Taheri, M. N., Azarpira, N., Zare, A., & Behzad-Behbahani, A. (2017). State of The Art Technologies Used to Explore Long Non-coding RNAs in Cancer Disease. *Cellular and Molecular of Medicine* DOI:10.1111/jcmm.13238

Sami, A., & Karsy, M. (2013). Targeting the PI3K/AKT/mTOR signaling pathway in glioblastoma: novel therapeutic agents and advances in understanding. *Tumour Biol.* 34(4):1991-2002. doi: 10.1007/s13277-013-0800-5.

Schreck, K. C., & Grossman, S. A. (2018) Role of Temozolomide in the Treatment of Cancers Involving the Central Nervous System. *Oncology (Williston Park).* 32(11):555-60, 569.

Semenza, G. L. (2010). Vascular responses to hypoxia and ischemia. *Arteriosclerosis, thrombosis, and vascular biology,* 30(4), 648–652. https://doi.org/10.1161/ATVBAHA.108.181644

Seyedmirzaei, H., Shobeiri, P., Turgut, M., Hanaei, S. & Rezaei, N. (2021). VEGF levels in patients with glioma: a systematic review and meta-analysis. *Reviews in the Neurosciences,* 32(2), 191-202. https://doi.org/10.1515/revneuro-2020-0062

Shih, C. H., Chuang, L. L., Tsai, M. H., Chen, L. H., Chuang, E. Y., Lu, T. P., & Lai, L. C. (2021). Hypoxia-Induced MALAT1 Promotes the Proliferation and Migration of Breast Cancer Cells by Sponging MiR-3064-5p. *Frontiers in oncology,* 11, 658151. https://doi.org/10.3389/fonc.2021.658151

Siebzehnrubl, F. A., Silver, D. J., Tugertimur, B., Deleyrolle, L. P., Siebzehnrubl, D., Sarkisian, M. R., … Steindler, D. A. (2013). The ZEB1 pathway links glioblastoma initiation, invasion and chemoresistance. *EMBO molecular medicine,* 5(8), 1196–1212. https://doi.org/10.1002/emmm.201302827

Singh, N., Miner, A., Hennis, L., & Mittal, S. (2021). Mechanisms of temozolomide resistance in glioblastoma - a comprehensive review. *Cancer drug resistance (Alhambra, Calif.),* 4(1), 17–43. https://doi.org/10.20517/cdr.2020.79

Soni, V., Adhikari, M., Lin, L., Sherman, J. H., & Keidar, M. (2022). Theranostic Potential of Adaptive Cold Atmospheric Plasma with Temozolomide to Checkmate Glioblastoma: An In Vitro Study. *Cancers,* 14(13), 3116. https://doi.org/10.3390/cancers14133116

Sorribes, I. C., Handelman, S. K., & Jain, H. V. (2020). Mitigating temozolomide resistance in glioblastoma via DNA damage-repair inhibition. *Journal of the Royal Society, Interface*, 17(162), 20190722. https://doi.org/10.1098/rsif.2019.0722

Spiegl-Kreinecker, S., Pirker, C., Filipits, M., Lötsch, D., Buchroithner, J., Pichler, J., … Berger, W. (2010). O6-Methylguanine DNA methyltransferase protein expression in tumor cells predicts outcome of temozolomide therapy in glioblastoma patients. *Neuro-oncology*, 12(1), 28–36. https://doi.org/10.1093/neuonc/nop003

Spill, F., Reynolds, D. S., Kamm, R. D., & Zaman, M. H. (2016). Impact of the physical microenvironment on tumor progression and metastasis. *Current opinion in biotechnology*, 40, 41–48. https://doi.org/10.1016/j.copbio.2016.02.007

St-Coeur, P. D., Poitras, J. J., Cuperlovic-Culf, M., Touaibia, M., & Morin, P., Jr (2015). Investigating a signature of temozolomide resistance in GBM cell lines using metabolomics. *Journal of neuro-oncology,* 125(1), 91–102. https://doi.org/10.1007/s11060-015-1899-6

Stupp, R., Hegi, M. E., Mason, W. P., van den Bent, M. J., Taphoorn, M. J., Janzer, R. C., … Mirimanoff, R-O. (2009). Effects of radiotherapy with concomitant and adjuvant temozolomide versus radiotherapy alone on survival in glioblastoma in a randomised phase III study: 5-year analysis of the EORTC-NCIC trial. The Lancet. *Oncology*, 10(5), 459–466. https://doi.org/10.1016/S1470-2045(09)70025-7

Stupp, R., Taillibert, S., Kanner, A., Read, W., Steinberg, D., Lhermitte, B., … Ram, Z. (2017). Effect of Tumor-Treating Fields Plus Maintenance Temozolomide vs Maintenance Temozolomide Alone on Survival in Patients With Glioblastoma: A Randomized Clinical Trial. *JAMA*, 318(23), 2306–2316. https://doi.org/10.1001/jama.2017.18718

Su, G., Zhao, Y., Wei, J., Han, J., Chen, L., Xiao, Z., … Dai, J. (2013). The effect of forced growth of cells into 3D spheres using low attachment surfaces on the acquisition of stemness properties. *Biomaterials,* 34(13), 3215–3222. https://doi.org/10.1016/j.biomaterials.2013.01.044

Sun, X., Lv, X., Yan, Y., Zhao, Y., Ma, R., He, M., & Wei, M. (2020). Hypoxia-mediated cancer stem cell resistance and targeted therapy. *Biomedicine & pharmacotherapy = Biomedecine & pharmacotherapie*, 130, 110623. https://doi.org/10.1016/j.biopha.2020.110623

Sung, H., Ferlay, J., Siegel, R. L., Laversanne, M., Soerjomataram, I., Jemal, A., & Bray, F. (2021). Global Cancer Statistics 2020: GLOBOCAN estimates of incidence and mortality worldwide for 36 cancers in 185 countries. *CA Cancer J Clin* 2021;71:209–49. https://doi.org/10.3322/caac.21660

SUPP.AI website https://supp.ai/i/berberine-temozolomide/C0005117-C0076080

Synergyfinder.fimm.fi website https://synergyfinder.fimm.fi/synergy/synfin_docs/

Tai, S. H., Lin, Y. W., Huang, T. Y., Chang, C. C., Chao, L. C., Wu, T. S., & Lee, E. J. (2021). Cinnamophilin enhances temozolomide-induced cytotoxicity against malignant glioma: the roles of ROS and cell cycle arrest. *Translational cancer research*, 10(9), 3906–3920. https://doi.org/10.21037/tcr-20-3426

Tancredi, A., Gusyatiner, O., Bady, P., Buri, M. C., Lomazzi, R., Chiesi, D., … Hegi, M. E. (2022). BET protein inhibition sensitizes glioblastoma cells to temozolomide treatment by attenuating MGMT expression. *Cell death & disease*, 13(12), 1037. https://doi.org/10.1038/s41419-022-05497-y

Tang, H., Zhao, J., Zhang, L., Zhao, J., Zhuang, Y., & Liang, P. (2016). SRPX2 Enhances the Epithelial-Mesenchymal Transition and Temozolomide Resistance in Glioblastoma Cells. *Cellular and molecular neurobiology,* 36(7), 1067–1076. https://doi.org/10.1007/s10571-015-0300-9

Tini, P., Cerase, A., Cevenini, G., Carbone, S. F., Miracco, C., & Pirtoli, L. (2015). Epidermal Growth Factor Receptor Expression May Correlate with Survival Through Clinical and Radiological Features of Aggressiveness in Glioblastoma Treated with Radiochemotherapy. *Anticancer Res.* 35(7):4117-24.

Toraih, E. A., El-Wazir, A., Hussein, M. H., Khashana, M. S., Matter, A., Fawzy, M. S., & Hosny, S. (2019). Expression of long intergenic non-coding RNA, regulator of reprogramming, and its prognostic value in patients with glioblastoma. *The International journal of biological markers*, 34(1), 69–79. https://doi.org/10.1177/1724600818814459

Van Gool, S., Makalowski, J., Schirrmacher, V., & Stuecker, W. (2021). Synergy between TMZ and individualized multimodal immunotherapy to improve overall survival of IDH1 wild-type MGMT promoter-unmethylated GBM patients. *Genes Immun* 23, 255–259 (2022). https://doi.org/10.1038/s41435-022-00162-y

Vang Mouritzen, M., & Jenssen, H. (2018). Optimized Scratch Assay for In Vitro Testing of Cell Migration with an Automated Optical Camera. *Journal of visualized experiments : JoVE,* (138), 57691. https://doi.org/10.3791/57691

Venkataramani, V, Yang, Y., Schubert, M.C., Reyhan, E., Tetzlaffi S. K., Wißmann, N., ... Winkler, F. (2022) Glioblastoma hijacks neuronal mechanisms for brain invasion. *Cell.* 4;185(16):2899-2917.e31. doi: 10.1016/j.cell.2022.06.054.

Vuong, H. G., Nguyen, T. Q., Ngo, T. N. M., Nguyen, H. C., Fung, K. M., & Dunn, I. F. (2020) The interaction between TERT promoter mutation and MGMT promoter methylation on overall survival of glioma patients: a meta-analysis. *BMC Cancer.* 20, 897. https://doi.org/10.1186/s12885-020-07364-5

Wagle, N., Nguyen, M., Carrillo, J., Truong, J., Dobrawa, L., & Kesari, S. (2020). Characterization of molecular pathways for targeting therapy in glioblastoma. *Chin Clin Oncol.* 9(6):77. doi: 10.21037/cco-20-124.

Wang, G., Wang, J. J., To, T. S., Zhao, H. F., & Wang, J. (2015). Role of SIRT1-mediated mitochondrial and Akt pathways in glioblastoma cell death induced by Cotinus coggygria flavonoid nanoliposomes. *Int J Nanomedicine.* 4;10:5005-23. doi: 10.2147/IJN.S82282.

Wang, J., Qi, Q., Feng, Z., Zhang, X., Huang, B., Chen, A., … Wang, J. (2016). Berberine induces autophagy in glioblastoma by targeting the AMPK/mTOR/ULK1-pathway. *Oncotarget,* 7(41), 66944–66958. https://doi.org/10.18632/oncotarget.11396

Wang, X., Chen, J. X., Liu, Y. H., You, C., & Mao, Q. (2013). Mutant TP53 enhances the resistance of glioblastoma cells to temozolomide by up-regulating O(6)-methylguanine DNA-methyltransferase. *Neurological sciences : official journal of the Italian Neurological Society and of the Italian Society of Clinical Neurophysiology,* 34(8), 1421–1428. https://doi.org/10.1007/s10072-012-1257-9

Wang, X., Zhang, H., & Chen, X. (2019). Drug resistance and combating drug resistance in cancer. *Cancer drug resistance (Alhambra, Calif.),* 2(2), 141–160. https://doi.org/10.20517/cdr.2019.10

Wang, Y., Liu, Y., Du, X., Ma, H., & Yao, J. (2020). The Anti-Cancer Mechanisms of Berberine: A Review. *Cancer management and research*, 12, 695–702. https://doi.org/10.2147/CMAR.S242329

Wen, P. Y., & Kesari, S. (2008). Malignant gliomas in adults. *N. Engl. J. Med.* 359, 492–507. doi: 10.1056/NEJMra0708126

Weng, X., Liu, H., Ruan, J., Du, M., Wang, L., Mao, J. … Shan, J. (2022). HOTAIR/miR-1277-5p/ZEB1 axis mediates hypoxia-induced oxaliplatin resistance via regulating epithelial-mesenchymal transition in colorectal cancer. *Cell Death Discov*. 8, 310. https://doi.org/10.1038/s41420-022-01096-0.

Wick, W., Weller, M., van den Bent, M., Sanson, M., Weiler, M., von Deimling, A., … Reifenberger, G. (2014). MGMT testing--the challenges for biomarker-based glioma treatment. Nature reviews. *Neurology*, 10(7), 372–385. https://doi.org/10.1038/nrneurol.2014.100

Willey, C., Yang, EH., & Bonner, J. (2016) Interaction of Chemotherapy and Radiation. *Clinical Radiation Oncology.* 2016: 63–79.e4, doi: 10.1016/b978-0-323- 24098-7.00004-6

Williams, T. M., Moolten, D., Burlein, J., Romano, J., Bhaerman, R., Godillot, A., … Kant, J. A. (1991). Identification of a zinc finger protein that inhibits IL-2 gene expression. *Science (New York, N.Y.),* 254(5039), 1791–1794. https://doi.org/10.1126/science.1840704

Wiranowska, M., Ladd, S., Moscinski, L. C., Hill, B., Haller, E., Mikecz, K., & Plaas, A. (2010). Modulation of hyaluronan production by CD44 positive glioma cells. International journal of cancer, 127(3), 532–542. https://doi.org/10.1002/ijc.25085

Wojciechowicz, K., Cantelli, E., Van Gerwen, B., Plug, M., Van Der Wal, A., Delzenne-Goette, E., … Te Riele, H. (2014). Temozolomide increases the number of mismatch repair-deficient intestinal crypts and accelerates tumorigenesis in a mouse model of Lynch syndrome. *Gastroenterology*, 147(5), 1064–72.e5. https://doi.org/10.1053/j.gastro.2014.07.052

Wrensch, M. R., Minn, Y. A., Chew, T., Bondy, M. L., & Berger, M. S. (2002). Epidemiology of primary brain tumors: current concepts and review of the literature. *Neuro-oncology*, 4 4, 278-99.

Wu, K., Fan, J., Zhang, L., Ning, Z., Zeng, J., Zhou, J., … He, D. (2012). PI3K/Akt to GSK3β/β-catenin signaling cascade coordinates cell colonization for bladder cancer bone metastasis through regulating ZEB1 transcription. *Cellular signalling,* 24(12), 2273–2282. https://doi.org/10.1016/j.cellsig.2012.08.004

Yamashiro, K., Nakao, K., Ohba, S., & Hirose, Y. (2020). Human Glioma Cells Acquire Temozolomide Resistance After Repeated Drug Exposure Via DNA Mismatch Repair Dysfunction. *Anticancer research,* 40(3), 1315–1323. https://doi.org/10.21873/anticanres.14073

Yang, H., Ye, D., Guan, K. L., & Xiong, Y. (2012). IDH1 and IDH2 mutations in tumorigenesis: mechanistic insights and clinical perspectives. *Clin Cancer Res.* 15;18(20):5562-71. doi: 10.1158/1078-0432.CCR-12-1773.

Yarrow, J. C., Totsukawa, G., Charras, G. T., & Mitchison, T. J. (2005). Screening for cell migration inhibitors via automated microscopy reveals a Rho-kinase inhibitor. *Chemistry & biology,* 12(3), 385–395. https://doi.org/10.1016/j.chembiol.2005.01.015

Yoshimoto, K., Mizoguchi, M., Hata, N., Murata, H., Hatae, R., Amano, T., … Sasaki, T. (2012). Complex DNA repair pathways as possible therapeutic targets to

overcome temozolomide resistance in glioblastoma. *Frontiers in oncology*, 2, 186. https://doi.org/10.3389/fonc.2012.00186

Zadeh, G., Bhat, K. P., & Aldape, K. (2013). EGFR and EGFRvIII in glioblastoma: partners in crime. *Cancer Cell.* 2013 Oct 14;24(4):403-4. doi: 10.1016/j.ccr.2013.09.017.

Zhang, Y., Dube, C., Gibert, M. Jr., Cruickshanks, N., Wang, B., Coughlan, M., … Abounader, R. (2018). The p53 Pathway in Glioblastoma. *Cancers* (Basel). 1;10(9):297. doi: 10.3390/cancers10090297.

Zhang, J., Stevens, M. F., & Bradshaw, T. D. (2012). Temozolomide: mechanisms of action, repair and resistance. *Current molecular pharmacology,* 5(1), 102–114. https://doi.org/10.2174/1874467211205010102

Zhang, W., Shi, X., Peng, Y., Wu, M., Zhang, P., Xie, R., … Wang, J. (2015). HIF-1α Promotes Epithelial-Mesenchymal Transition and Metastasis through Direct Regulation of ZEB1 in Colorectal Cancer. *PloS one,* 10(6), e0129603. https://doi.org/10.1371/journal.pone.0129603

Zhang, X. J., & Jia, S. S. (2016). Fisetin inhibits laryngeal carcinoma through regulation of AKT/NF-κB/mTOR and ERK1/2 signaling pathways. *Biomedicine & pharmacotherapy = Biomedecine & pharmacotherapie,* 83, 1164–1174. https://doi.org/10.1016/j.biopha.2016.08.035

Zhang, Y., Cruickshanks, N., Pahuski, M., Yuan, F., Dutta, A., Schiff, D., … Abounader, R. (2017). Noncoding RNAs in Glioblastoma. In: De Vleeschouwer S, editor. *Glioblastoma* [Internet]. Brisbane (AU): Codon Publications; Chapter 6.

Zhao, Z., Liu, M., Long, W., Yuan, J., Li, H., Zhang, C., … Liu, Q. (2021). Knockdown lncRNA CRNDE enhances temozolomide chemosensitivity by regulating autophagy in glioblastoma. *Cancer Cell Int* 21, 456 (2021). https://doi.org/10.1186/s12935-021-02153-x

Zhen, L., Yun-Hui, L., Hong-Yu, D., Jun, M., & Yi-Long, Y. (2016). Long noncoding RNA NEAT1 promotes glioma pathogenesis by regulating miR-449b-5p/c-Met axis. *Tumour biology : the journal of the International Society for Oncodevelopmental Biology and Medicine*, 37(1), 673–683. https://doi.org/10.1007/s13277-015-3843-y

Zhou, C., Jiang, H., Zhang, Z., Zhang, G., Wang, H., Zhang, Q., … Yang, S. (2017). ZEB1 confers stem cell-like properties in breast cancer by targeting neurogenin-3. *Oncotarget*, 8(33), 54388–54401. https://doi.org/10.18632/oncotarget.17077

Zhou, Y., Zhou, Y., Shingu, T., Feng, L., Chen, Z., Ogasawara, M., … Huang, P. (2011). Metabolic alterations in highly tumorigenic glioblastoma cells: preference for hypoxia and high dependency on glycolysis. *The Journal of biological chemistry*, 286(37), 32843–32853. https://doi.org/10.1074/jbc.M111.260935

Zhuo, W., Zhang, L., Zhu, Y., Zhu, B., & Chen, Z. (2015). Fisetin, a dietary bioflavonoid, reverses acquired Cisplatin-resistance of lung adenocarcinoma cells through MAPK/Survivin/Caspase pathway. *American journal of translational research,* 7(10), 2045–2052.

Zymoresearch.eu website https://zymoresearch.eu/pages/what-is-trizol

7. ABBREVIATIONS

2D: Two-dimensional
2–HG: 2-hydroxyglutarate
3D: Three-dimensional
A172-R: Acquired A172-Resistant, A172-900-R
ACTB: β-actin
AIC: 5-amino-imidazole-4-methyl Amide
ATRX: α-thalassemia/mental-retardation-syndrome-X-linked gene
BBB: Blood-brain barrier
BBR: Berberine
BER: Base Excision Repair
BUU: Bursa Uludag University
C: Control
CCF-NLs: Cotinus coggygria flavonoid nanoliposomes
CDKN2A/B: Cyclin-dependent kinase inhibitor 2A/B
cDNA: Complementary DNA
circRNAs: Circular RNAs
CNS: Central nervous systems
CRNDE: Colorectal Neoplasia Differentially Expressed
CSC: Cancer Stem Cells
CSIC: Spanish Council for Scientific Research
DMEM-F12: Dulbecco's Modified Eagle's Medium-F12
DMSO: Dimethyl sulfoxide
DNA-PKcs: DNA-dependent protein kinase catalytic subunit
EACR: Avrupa Kanser Araştırmaları Derneği
EGFR: Epidermal growth factor receptor
EGFRvIII: The epidermal growth factor receptor variant III
EMT: Epithelial-Mesenchymal Transition
ENCODE: Encyclopedia of DNA Elements
ER: Endoplasmic reticulum
EZH2: Enhancer of zeste homolog 2
FBS: Fetal bovine serum
FDA: The Food and Drug Administration
FIS: Fisetin
GBM: Glioblastoma
GFAP: Glial fibrillary acidic protein
GSC: Glioma stem cells
h: Hours
H3K27me: Methylation of lysine 27 on histone 3
HDAC: Histone deacetylase
HDACi: HDAC inhibitor
HIF-1: Hypoxia-inducible factor 1
HOTAIR: HOX transcript antisense RNA
IC50: The half-maximal inhibitory concentration
IDH: Isocitrate dehydrogenase
IHC: Immunohistochemical

IIBB: Biomedical Research Institute of Barcelona
IL-2: Interleukin-2
lncRNAs: Long noncoding RNAs
LSD1: Histone lysine-specific demethylase
MALAT1: Metastasis Associated Lung Adenocarcinoma Transcript 1
MAPK3: Mitogen-Activated Protein Kinase 3
MET: Mesenchymal-epithelial transition
MGMT: O^6-Methylguanine-DNA Methyltransferase
miRNAs: microRNAs
MITC: 5-(3-methyltriazol-1-yl)imidazole-4-carboxamide
MMR: Mismatch Repair
MRI: Magnetic Resonance Image
MSH: MutS homologs
N3MA: N3 methyl adenine
N7MG: N7 methylguanine
NEAT1: Nuclear Paraspeckle Assembly Transcript 1
O6MG: O6 methylguanine
Oncomirs: Oncogenic miRNAs
p1: Patient 1
p2: Patient 2
p3: Patient 3
PAK4: p21-Activated kinase 4
PBS: Phosphate buffered saline
P-gp1: P-glycoprotein 1
PI3K: Phosphoinositide 3-kinase
PLZF: Promyelocytic leukemia zinc finger
PMS1: Post-meiotic segregation increased 1
PTEN: Phosphatase and tensin homolog
RTCA: Real Time Cell Analyzer
RT-qPCR: Real-Time Quantitative Reverse Transcription PCR
siRNA: Small interfering RNA
SNP: Single nucleotide polymorphism
TCGA: The Tumor Cancer Genome Atlas
TCI: Tokyo Chemical Industry
TERT: Telomerase reverse transcriptase
TGF-β: Transforming growth factor-beta
TMZ: Temozolomide
TP53: Tumor protein 53
TUSC7: Tumor Suppressor Candidate 7
ULA: Ultra-Low Attachment
VEGF: Vascular endothelial growth factor
WHO: World Health Organization
WT: Wild type
ZEB1: Zinc-finger E-box-binding homeobox factor 1
α-KG: α-ketoglutarate

8. ACKNOWLEDGMENTS

Öncelikle yüksek lisans sürecimde gerek ders gerek tez dönemimde, özellikle proje yazımı gibi konularda değerli bilgilerini paylaşan ve diğer birçok konuda öğretici olan saygıdeğer tez danışmanım Prof. Dr. Berrin TUNCA'ya ve, bizlere değerli bilgilerini ve deneyimlerini sunarak yol gösterici olan başta bölüm başkanımız Prof. Dr. Ünal EGELİ olmak üzere değerli hocalarım Prof. Dr. Gülşah ÇEÇENER ve Dr. Öğr. Üyesi Işıl Ezgi ERYILMAZLAR'a,

Başımız sıkıştığında imdadımıza koşan ve bir çok konuda akıl danışabildiğimiz ikinci danışmanımız gibi olan emektar kıymetli hocam Doç. Dr. Gülçin TEZCAN'a, deneysel ve istatistiksel süreçlerde yardım eden ekibimin doktora öğrencileri Çağla TEKİN ve Melis ERÇELİK'e ve yüksek lisans öğrencisi Melisa GÜRBÜZ'e,

Primer hasta dokularının sağlanmasında desteği olan Beyin Cerrahisi anabilimdalı hocalarımız Prof. Dr. Ahmet BEKAR, Prof. Dr. Hasan KOCAELİ ve Prof. Dr. Mevlüt Özgür TAŞKAPILIOĞLU'na,

Yüksek lisans hayatımda tanıdığım ve yıllardır tanışıyormuşcasına konuşup gülebildiğim, gerek *in-vitro* gerek *in-vivo* deneylerinde hiç düşünmeden birbirimizin yanıbaşında olduğumuz ekip arkadaşım, akademi bahçemde açan çiçeğim, ekürim, yüksek lisans öğrencisi Mine ÇAMLIBEL'e,

Tıbbi Biyoloji Anabilim dalımızda bir güler yüzüyle, hoşsohbetleriyle, sarılmalarıyla ve destekleriyle bana motive olan tüm öğrencilere ve çalışanlara,

Birbirimizi çok iyi tanıdığımız ve bir kere bile kavga etmediğimiz, en güzel dostluğu ve kardeşliği yıllardır bana yaşatan, her şeyimi paylaşabildiğim, moral ve motivasyon kaynağım, canım sırdaşım, Dilara Nur KUVVET'e,

O sıcacık aile ortamını ve beni hala daha gülümseten bir çok anımı bana sunan mutluluk kaynaklarım, yengem ve kuzenlerime,

Her ne kadar dışarıdan bakıldığında kolay gibi görülse de aslında bol stresli olabilen ve çokca sabır gerektiren bu dönemde koşullar ne olursa olsun bana olan inancını, sevgisini ve desteğini yitirmeyip sadece varlığıyla bile beni motive ederek huzurlandırabilen, zorluklarla savaşmakta benim ilham kaynağım, ying'imin yang'ı, erkek arkadaşım Altay AYKOL'a,

Hayatım boyunca, beni, kendilerinden bile feragat edip destekleyebilen, bana her koşulda azmettiğim işleri başaracak kadar güçlü ve sabırlı olduğumu hatırlatan, beni sadece ben olduğum için sevip her türlü zamanımda bana destek olan, hayatımdaki en büyük şanslarımdan olan benim genetiğim, epigenetiğim ve her şeyim olan biricik annem ve babam, Sabahat FERAH ve Hüseyin FERAH'a çok teşekkür ediyor, saygılarımı sunuyor ve tezimin, akademi dünyasında kendilerini mutsuz ve yalnız hissedip motivasyon arayan, çaresiz ama bir o kadar da güçlü akademisyenlere ilham olmasını diliyorum.

Türkiye Bilimsel ve Teknolojik Araştırma Kurumu TÜBİTAK'a 2224-A kapsamında yüksek lisans tezimin bir bölümünü İtalya'da Avrupa Kanser Araştırmaları Derneği (EACR) kongresinde sunabilme fırsatı ve maddi destekten dolayı ve Bursa Uludağ Üniversitesi Bilimsel Araştırma Proje Koordinasyonu Birimi BAP'a THIZ-2021-747 ve TYL-2023-1365 nolu iki proje için verdiği maddi destekten dolayı teşekkür ediyorum.

Yüksek lisans tezimi yıllar önce bu dünyaya gözlerini kapamış fakat hala benimle gurur duyduklarını hissettiğim anneannem Nebahat PORTAKAL'a ve dayım Ali PORTAKAL'a ithaf ediyorum.

9. CURRICULUM VITAE

Sena FERAH studied primary school in Bursa Mithatpaşa Primary School and high school in Bursa Süleyman Çelebi Anatolian High School. She successfully completed her undergraduate education in Çanakkale Onsekiz Mart University, Department of Molecular Biology and Genetics (100% English). During her bachelor's degree, she participated in two Erasmus+ study mobilities, the first of which was at Czechia Ostrava University, the second at Universitat Autònoma de Barcelona, and she did a voluntary internship in the field of Neuropharmacology at the Biomedical Research Institute of Barcelona (IIBB), affiliated with the Spanish Council for Scientific Research (CSIC). In August 2021, she started her ongoing master's program in Bursa Uludag University Faculty of Medicine, Department of Medical Biology.